Department of Precision and Microsystems Engineering

# Development of a High-Temperature Industrial Heat Pump Model with a Novel Compressor Technology

Vincent Alexander Bashandy

Report no : 2024.009
Coach : Dr.ir. J.W.R. Peeters
Professor : Dr.ir. J.W.R. Peeters
Specialisation : Energy, Flow & Process Technology
Type of report : Master Thesis
Date : January 29, 2024

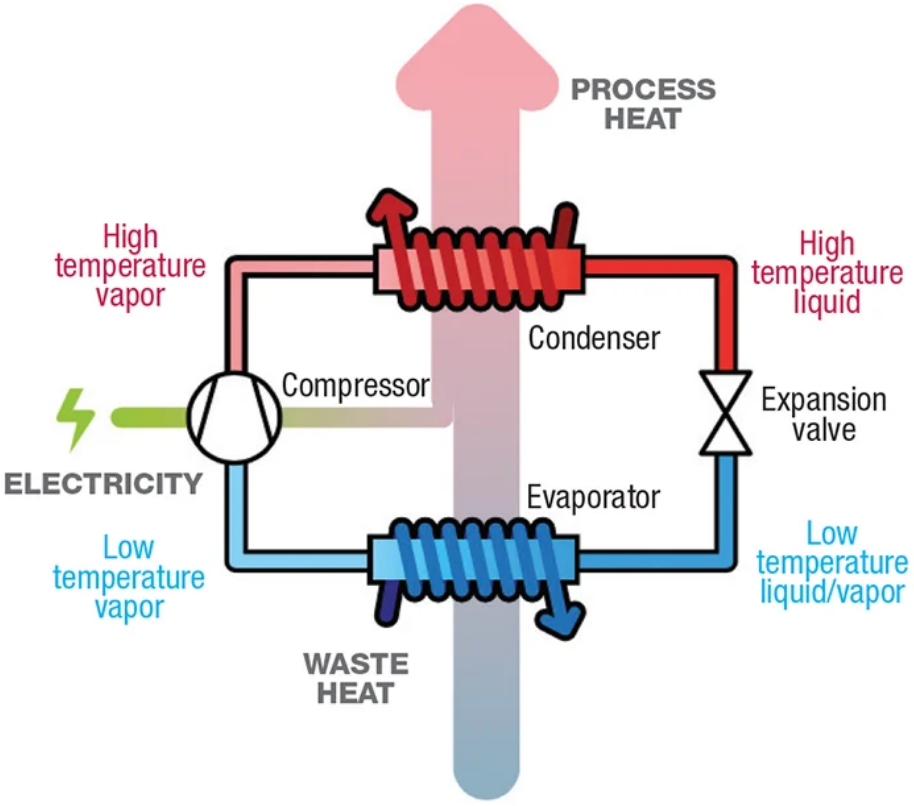


TU Delft Delft University of Technology

Challenge the future

# Development of a High-Temperature Industrial Heat Pump Model with a Novel Compressor Technology

by

**Vincent Alexander Bashandy**

to obtain the degree of Master of Science in
**Mechanical Engineering**

Delft University of Technology
Department of Process & Energy
The Netherlands
January 29, 2024

| | |
|---|---|
| Source of title page image: | Ondrey, G. (2021) [38] |
| Student number: | 4714989 |
| Project duration: | March, 2023 - February, 2024 |
| Date of defense: | Thursday February 8, 2024 |
| Graduation committee: | Dr.ir. J.W.R. Peeters |
| | PhD. A. Zhao |
| | Prof. dr. ir. K. Hooman |
| | Dr. Ir. J.F.L. Goosen |

**Abstract**

The current global environmental crisis has resulted in increased efforts towards more efficient and sustainable industrial processes. High-temperature heat between 150 °C & 400 °C accounts for a major part of the energy demand in industrial processes. At the same time, large quantities of waste heat are unutilised at temperatures up to 200 °C. A heat pump could upgrade this waste heat to cover a part of the demand, resulting in considerable savings both for the planet and the operator. Nevertheless, heat pumps have seen little development in heat delivery temperatures above about 150 °C. This research aims to assess the current technological potential and limitations of high-temperature heat pumps. Subsequently, solutions and recommendations are developed.

Focussing on mechanical vapour compression heat pumps, a thorough understanding of such cycles is gained first. The performance of a heat pump is highly dependent on the choice of cycle setup and working fluid, with the compressor posing the largest limitations for higher temperatures. To assess these, this project develops a heat pump model which simulates many different working fluids for different component configurations. The model was subjected to two temperature domains, covering waste heats of 100 °C & 200 °C and process heat temperatures in the range of 150 °C to 400 °C. Results were obtained for all fluids incorporated in RefProp 9.0 and showed that multistage compression with intercooling and superheating considerably improved the performance of nearly all fluids. By comparing fluids based on efficiencies, capacities, temperatures and pressures, benzene and propylcyclohexane showed the best performance for the lower and higher part of process heat temperatures, respectively. The results however also showed the potential superiority of water as it has the best efficiencies and the largest applicability range, which combines with the hazard-free & environmentally friendly nature, low cost and wide availability. The main downside of water appeared to be the persistent, unacceptably high compression temperatures, combined with large pressures and pressure ratios.

It was subsequently investigated how the disadvantages of water could be handled. A solution was found in the usage of Liquid Piston Gas Compression (LPGC), in which a rising liquid column, supplied by a pump, acts as a reciprocating piston in a compression chamber. This setup conveniently allows for liquid spray injection to cool the steam upon compression and alleviates limitations on the pressure ratio. By using the same water as the liquid in the LPGC, any temperature rise is compensated by the evaporation of liquid, resulting in more steam with a lower temperature.

A numerical model of this type of compressor was made in which dynamics were modelled down to individual droplets. This simplified approach provided insight into the compression path with such liquid injection and allowed the approximate determination of the required amount of spray. Results showed that the injection could cool the vapour adequately even for high temperature lifts. The LPGC was subsequently incorporated into a single-stage heat pump cycle and compared the results for other fluids using ordinary compressors. These results showed large CoP improvements of 15-25 % CoP and low discharge temperature. With that, it was shown that an environmentally friendly fluid could be used in a simple single-stage configuration and still provide the best performance compared to any other fluid.

# Contents

# Nomenclature

**Abbreviations**

| | |
|---|---|
| CFC | ChloroFluoroCarbon |
| CoP | Coefficient of Performance |
| DCHX | Direct-Contact Heat Exchanger |
| FC | Flash Chamber |
| GWP | Global Warming Potential |
| HC | HydroCarbon |
| HCFC | HydroChloroFluoroCarbon |
| HCFO | HydroChloroFluoroOlefin |
| HFC | HydroFluoroCarbon |
| HFO | HydroFluoroOlefin |
| HTHP | High-Temperature Heat Pump |
| IC | InterCooling |
| ICHX | Indirect-Contact Heat Exchanger |
| LPGC | Liquid Piston Gas Compression |
| ODP | Ozone Depletion Potential |
| VCHP | Vapour Compression Heat Pump |
| VHC | Volumetric Heating Capacity |
| WC | Wet Compression |

**Constants**

| | |
|---|---|
| $g$ | Gravitational acceleration |

**Parameters**

| | |
|---|---|
| $\Delta$ | Difference |
| $\eta$ | Efficiency |
| $\tau$ | Characteristic response time |
| $A$ | Area |
| $C$ | Coefficient/constant |
| $D$ | Diameter |
| $F$ | Force |
| $f$ | Fraction |
| $m$ | Mass |
| $N$ | Number of steps |
| $n$ | Number of stages |
| $t$ | Time |
| $u$ | Gas velocity |
| $V$ | Volume |
| $v$ | Droplet elocity |
| $w$ | Relative velocity |
| $r$ | (Pressure) Ratio |
| Re | Reynolds number |

**Subscripts**

| | |
|---|---|
| 0 | Reference/environment/dead state |
| $e$ | Outlet property |
| $i$ | Inlet property |
| $j$ | Discrete instant |
| $k$ | Index of layer/Index of compressor |
| $x$ | Location |
| area | Area-based |
| C | Cold/evaporator/source property |
| c | Controlling stream |
| CD | Condenser |
| cl | Clearance |
| com | Compressopm |
| CP | Compressor |
| CV | Control volume |
| cycle | Total of the cycle |
| D | Drag |
| d | Destruction/droplet |
| eq | Equilibrium state |
| EV | Evaporator |
| evap | Evaporated |
| ex | Exergetic |
| exp | Expanson |

| | |
|---|---|
| f | Indication of flow exergy |
| H | Hot/condenser/sink property |
| HX | Heat exchanger |
| L | Liquid |
| LC | Liquid column |
| LS | Liquid spray |
| mass | Mass-based |
| max | Maximum value |
| min | Minimum value |
| open | Instant of discharge opening |
| P | Process stream |
| PU | Pump |
| r | Reacting stream |
| s | Isentropic/Surface |
| sat | Saturated state |
| SC | Supercooling |
| SH | Superheating |
| T | Total layer property |
| V | Vapour |
| W | Waste stream |
| XP | Expander |
| XV | Expansion valve |

**Thermodynamic properties**

| | |
|---|---|
| $\kappa$ | Polytropic coefficient/Specific heat capacity ratio |
| $\mu$ | Dynamic viscosity |
| $\overline{T}$ | Thermodynamically averaged temperature |
| $\rho$ | Density |
| $c$ | Specific heat capacity |
| $E$ | Exergy |
| $e$ | Specific exergy |
| $h$ | Specific enthalpy |
| $p$ | Pressure |
| $Q$ | Heat |
| $q$ | Specific heat |
| $s$ | Specific entropy |
| $T$ | Temperature |
| $U$ | Overall heat transfer coefficient |
| $W$ | Work |
| $w$ | Specific work |
| $x$ | Vapour quality (fraction) |

# List of Figures

# List of Tables

# Chapter 1

# Introduction

Since the Industrial Revolution, the primary source of heat for both industrial and residential purposes has been the combustion of fossil fuels. However, with climate change becoming an ever-increasing problem, alternative methods need to be found to enable sustainable heating. A viable solution is to employ electric heating using renewable electricity. Technologies that can be used are, amongst others, direct electric heating, by generating and burning hydrogen or by using a heat pump. Heat pumps play a major role as one of the possible solutions due to their ability to transfer significantly more heat energy than the electric energy required to power them. Heat pumps have already found widespread use in building space heating, where heat is transferred from the air or the ground into the building. The temperature difference is small and therefore the efficiency can be high.

Industries could also benefit from using heat pumps. According to Kosmakadis (2019), 70 % of the EU industrial energy consumption is related to heating. Many industrial processes however need heat at much higher temperatures than space heating. Heat consumption temperatures can range from 0 °C to over 1000 °C. About 25 % of heat consumption falls in the range of 100 °C to 500 °C [29]. A heat pump that transfers heat from ambient air to that temperature level will likely not give much gain in efficiency compared to direct electric heating, the latter being much cheaper than a heat pump. However, in all industrial processes where heat is used, waste heat is also discarded. These waste heat streams are often still at considerable temperature levels. According to Papepetrou et al. (2018), the largest part of the waste heat potential in the EU exists in the 100-200 °C range. Indeed, this has been recognised and many industrial heat pumps already exist. Mainstream commercial industrial installations currently however only go up to about 90 °C of heat delivery temperature. Various products exist that can reach higher temperatures up to about 150 °C [29], while some experimental setups and extensive simulation studies have been performed for temperatures up to 200 °C [33, 3]. A considerable portion of industrial heat demand is however at even higher temperatures.

This report therefore investigates the possibility of implementing a high-temperature heat pump (HTHP) between the process heat demand and waste heat supply for heat delivery temperatures between 150 °C and 400 °C. Waste heat temperatures in the range of 100 °C to 200 °C are considered. The main research question therefore is:

*How can a high-temperature heat pump be developed for upgrading industrial waste heat in the range of* 100-200 °C *to process heat in the range of* 150-400 °C*?*

The temperature ranges that are investigated are divided into two domains:

1. Domain 1: a waste heat temperature of 100 °C with process heat temperatures ranging from 150 °C to 300 °C.
2. Domain 2: a waste heat temperature of 200 °C with process heat temperatures ranging from 250 °C to 400 °C.

To support this research question, five subquestions are defined:

- *What is the potential for HTHPs in the current industrial market?*

- *What are the limitations to why HTHPs have not yet been widely implemented in industries at these temperature ranges?*
- *What are the best components configurations and fluid combinations for HTHPs?*
- *What performance can be achieved with conventional heat pumps operating within the stated temperature ranges and what factors prevent improvements?*
- *How can the heat pump be improved to overcome the factors preventing performance improvements?*

To answer these questions, the following approach is taken. First, in Chapter 2 the fundamental technology of heat pumps will be discussed, along with the different types, configurations, components and fluids. Then in Chapter 3, the state-of-the-art of HTHPs are presented together with the potential that exists for industrial heat pumps at higher temperatures and the limitations that prevent this potential from being reached. With this knowledge, a heat pump model is developed. The model structure, inputs, assumptions and calculations are discussed in Chapter 4. Moreover, the procession of this model into heat pump cycles and a design tool is shown here. Using this model, different heat pump cycles are simulated for multiple fluids over multiple temperature ranges. The results are shown and discussed in Chapter 5. The conclusion to these results is given in Chapter 6, which also explains why the decision was made to develop a dedicated compressor model. This model simulates a liquid piston gas compressor (LPGC). Its structure, the inputs and assumptions, the calculations and boundary conditions are explained in Chapter 7. This model is first simulated for an example case to show the intrinsic results. Subsequently, the LPGC model is implemented in a cycle of the heat pump model. This cycle is subjected to the same inputs as the other heat pump cycles. The results are displayed and discussed in Chapter 8. The conclusion to these results is joint with the general conclusion to the report in Chapter 9.

# Chapter 2

# Heat Pump Technology & Types

This section aims to discuss the technology behind heat pumps and their different aspects. First, in Section 2.1, the fundamental working principle of heat pumps together with the underlying thermodynamics is described. After that, in Section 2.2, the different types of heat pump cycles are discussed and differences in the way that the system can be set up are identified. Subsequently, in Section 2.3, the advantages and disadvantages of different types of components found in heat pumps are discussed. Finally, in Section 2.4, the topic of heat pump fluids is elaborated, with the different aspects that are involved in the selection of a suitable substance.

The heat pump fluid is commonly referred to as refrigerant or coolant [35]. Because this project is mainly concerned with heating, it is more appropriate to refer to it as working fluid.

## 2.1 Thermodynamics of heat pumps

Using the definitions from [28], a heat pump/refrigeration cycle transfers heat from a low-temperature heat source to a high-temperature heat sink using a work input, as in Figure 2.1. While the working principle is the same, the purpose of a heat pump cycle is to deliver heat to the sink while the purpose of a refrigeration cycle is to take away heat from the source. Since this report concerns heat pumps, the convention is used where there is a heat demand at the sink and a waste heat supply at the source. Both are heat exchangers where heat is transferred to or from the working fluid. At the source, the waste heat supply comes from a fluid called the waste fluid. The sink demand is usually required for a fluid that is used in a certain process, so it is called the process fluid. Heat transfer from a source is indicated with 'C' for cold ($\dot{Q}_{\mathrm{C}}$) while heat flow to a sink is indicated with 'H' for hot. Work is done on the working fluid to increase the pressure of the working fluid. This work adds to the heat supplied to the sink, so $\dot{Q}_{\mathrm{H}} = \dot{Q}_{\mathrm{C}} + \dot{W}$.

Depending on the operating conditions of the heat pump, there can be different temperature profiles in the source and sink heat exchanger. The heat transfer can take place at constant temperature in case both fluids are changing phase. When this situation applies to both the source and sink, they can be taken as constant temperatures $T_{\mathrm{W}}$ (for waste) & $T_{\mathrm{P}}$ (for process), as shown in Figure 2.1a. However, in many cases, fluids are not changing phase (or are mixtures changing phase) and the temperature profiles are inclined, called a temperature glide. A combination of constant and inclined temperature profiles is also possible. If that applies to both the source and sink, the inlet and outlet temperatures of the waste and process fluid have to be taken into account. This is shown in Figure 2.1b, where $i$ signifies inlet and $e$ the outlet (exit).

Figure 2.2 shows different possibilities for the temperature profiles of the process, waste and working fluids. In all cases, there is a temperature difference between fluids in the heat exchangers. In the source heat exchanger, the working fluid is colder than the waste fluid, such that heat can be extracted from the latter. The temperature difference is $\Delta T_{\mathrm{C},x} = T_{\mathrm{W},x} - T_{\mathrm{C},x}$, where $x$ indicates any location along the heat exchanger ranging from $i$ to $e$. In the sink heat exchanger, the working fluid is hotter than the process fluid, such that heat can be supplied to the latter. The temperature difference is $\Delta T_{\mathrm{H},x} = T_{\mathrm{H},x} - T_{\mathrm{P},x}$. This temperature difference is required to make heat transfer possible. The smaller this difference is, the lower the heat transfer driving force and the larger the heat exchanger needs to be [28]. A minimum temperature difference $\Delta T_{min}$ is often set in the design

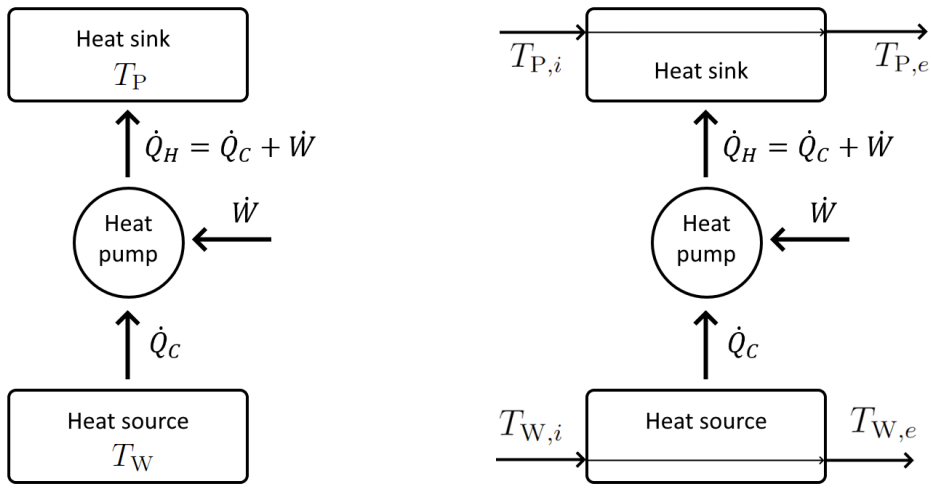


**(a)** Constant temperature source and sink

**(b)** Source and sink with fluid streams fluids

**Figure 2.1:** General energy flow diagram for any type of heat pump. The source and sink can either be at constant temperature or exhibit temperature glides.

of heat pumps to define how close the temperature of the working fluid is allowed to get to that of the waste and process fluids. The constraint is then for any $x$:

$$\min\left(\Delta T_{\mathrm{C},x}\right) > \Delta T_{min} \qquad \min\left(\Delta T_{\mathrm{H},x}\right) > \Delta T_{min} \tag{2.1}$$

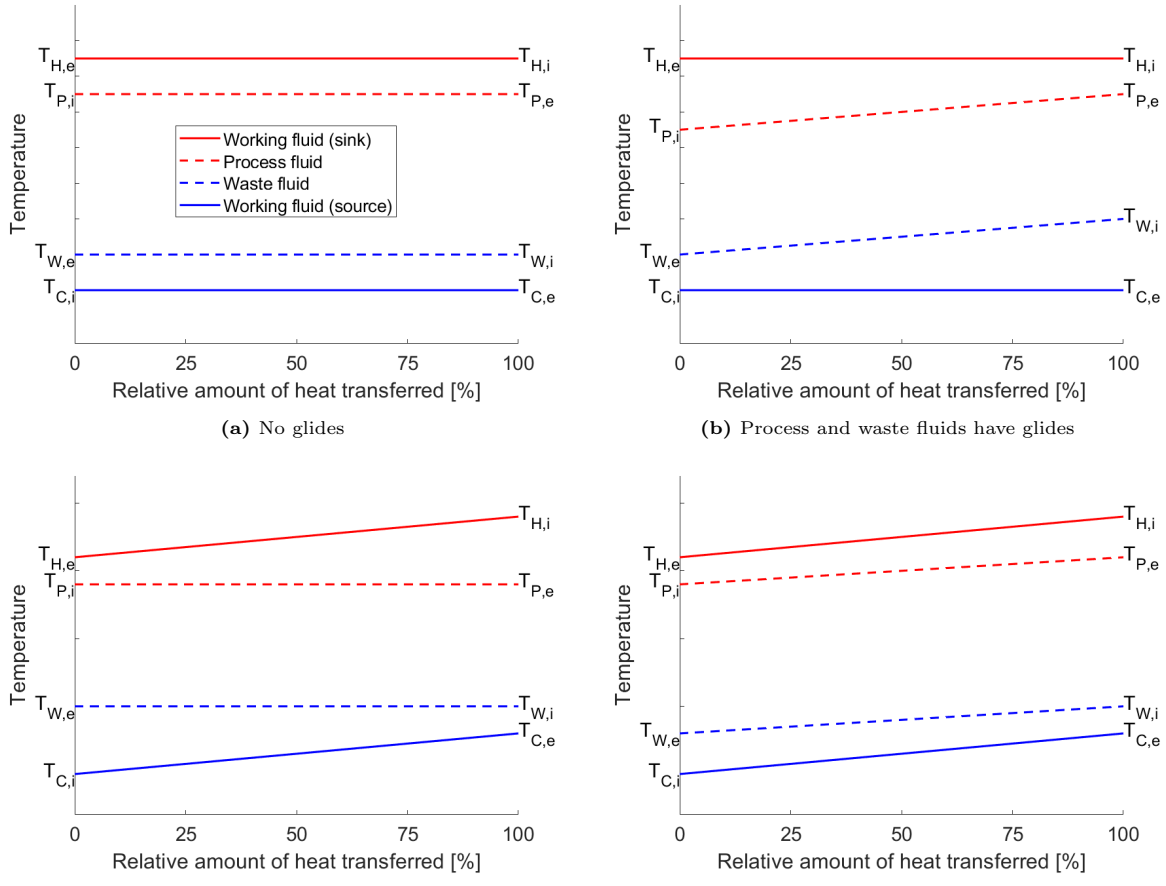


**(a)** No glides

**(b)** Process and waste fluids have glides

**(c)** Working fluid has glides

**(d)** All fluids have glides

**Figure 2.2:** Different temperature profiles for process and working fluids at the source and sink.

The temperature lift of the heat pump is defined as the difference between the thermodynamically

averaged temperatures of the process and waste fluids:

$$\Delta T = \overline{T}_{\mathrm{P}} - \overline{T}_{\mathrm{W}} \tag{2.2}$$

where $\overline{T}_{\mathrm{P}}$ & $\overline{T}_{\mathrm{W}}$ are the temperatures for which the entropy change is equivalent to the temperature glide. They can be calculated with [28]:

$$\overline{T}_{\mathrm{W}} = \frac{T_{\mathrm{W},e} - T_{\mathrm{W},i}}{\ln \frac{T_{\mathrm{W},e}}{T_{\mathrm{W},i}}} \qquad \overline{T}_{\mathrm{P}} = \frac{T_{\mathrm{P},e} - T_{\mathrm{P},i}}{\ln \frac{T_{\mathrm{P},e}}{T_{\mathrm{P},i}}}. \tag{2.3}$$

If there are no temperature glides like in Figure 2.2a and Figure 2.2c, then $T_{\mathrm{W},i} = T_{\mathrm{W},e} = T_{\mathrm{W}}$ and $T_{\mathrm{P},i} = T_{\mathrm{P},e} = T_{\mathrm{P}}$. In that case, Equation (2.3) does not apply, instead:

$$\overline{T}_{\mathrm{W}} = T_{\mathrm{W}} \qquad \overline{T}_{\mathrm{P}} = T_{\mathrm{P}}. \tag{2.4}$$

Besides temperature lift, a widely used way to indicate the performance of a heat pump is the Coefficient of Performance (CoP), which is the amount of heat delivered to the sink per unit of work input necessary to accomplish this. It is calculated with [28]:

$$\mathrm{CoP} = \frac{\dot{Q}_{\mathrm{H}}}{\dot{W}}. \tag{2.5}$$

Since $\dot{Q}_{\mathrm{H}} = \dot{Q}_{\mathrm{C}} + \dot{W}$ and $\dot{Q}_{\mathrm{C}}$ is positive, the CoP of mechanical heat pumps is inherently larger than 1. This implies that the heat pump can transfer more heat than the electrical energy that it consumes. Therefore, a heat pump is always a more energy-efficient way of heating than direct electric heating, which has a CoP of 1.

The theoretical maximum achievable CoP is that which corresponds to the ideal Lorenz cycle [28, 48, 3]:

$$\mathrm{CoP}_{\max} = \frac{\overline{T}_{\mathrm{H}}}{\overline{T}_{\mathrm{H}} - \overline{T}_{\mathrm{C}}}. \tag{2.6}$$

In case there are no temperature glides, this equation and the calculated maximum CoP become equivalent to the Carnot CoP [3].

From these equations, it appears that the larger the average difference between the source and sink temperatures of the working fluid, the smaller the CoP is. At the same time, the temperature lift of the heat pump is the average difference between the process and waste temperatures. That implies that the theoretical best heat pump performance is attained when the temperature differences between the working fluid and the waste/process fluids in the source and sink heat exchangers are kept to a minimum [28].

The degree to which the actual CoP reaches the maximum CoP is signified by the exergy efficiency, which is calculated with [28]:

$$\eta_{\mathrm{ex}} = \frac{\mathrm{CoP}}{\mathrm{CoP}_{\max}}. \tag{2.7}$$

As already said, the working fluid can change phase in the source and/or sink heat exchangers. If this happens on the source side, the working fluid would evaporate from a liquid into a vapour since it has to take up heat from the waste fluid. The source heat exchanger is then called an evaporator. It could however be that the working fluid does not change phase, but merely heats up. In vapour compression heat pumps, however, this is rarely the case. Therefore, the source heat exchanger is always called the evaporator, even if nothing is evaporating. Likewise, if the working fluid changes phase on the sink side, it condenses from vapour to liquid since it has to give up heat to the process fluid. The sink heat exchanger is then called a condenser. It is however also possible that the working fluid just cools down as a vapour but does not change phase. Despite this, it will still be called a condenser in this report for consistency.

If the working fluid changes phase in both the evaporator and the condenser, the heat pump cycle is called a subcritical cycle. This is possible if the working fluid remains in subcritical states, i.e. below the critical point. It is however also possible that the working fluid is at a subcritical state in the evaporator, but is at a supercritical state in the condenser. The heat pump cycle is then called transcritical. Lastly, the fluid may be at supercritical states in both the evaporator and condenser.

The heat pump cycle is then called supercritical, also commonly referred to as *gas cycle* or *reverse Brayton cycle* [35].

The mechanism by which most heat pumps work is to bring the working fluid from the level of the evaporator to the level of the condenser by increasing its pressure level. In mechanical heat pumps, this is achieved by mechanical compression. Ideally, this compression is executed without heat loss to the environment, i.e. adiabatically. The first law of thermodynamics then dictates that the internal energy of the fluid must increase. In other words, the temperature level increases with the pressure level. To return the fluid to the lower pressure level after it has given up its heat to the sink, it needs to be expanded again. By the same law, the temperature of the fluid decreases, allowing it to take up heat from the source again [35].

The simplest heat pump cycle is the reversed Carnot cycle, which is shown in Figure 2.3. It works by adiabatic & isentropic compression and expansion processes, for which a compressor and turbine are used. The evaporation and condensation happen entirely at constant temperatures. Since all processes are reversible, this cycle represents the ideal case. The reversed Carnot cycle is however

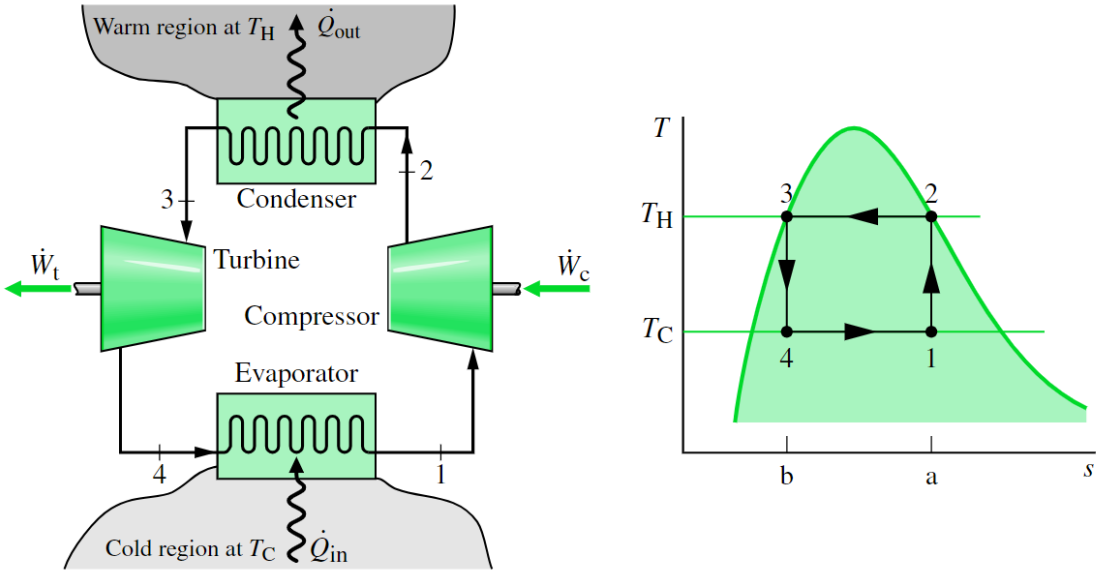


**Figure 2.3:** A reversed Carnot cycle, which is the ideal cycle with only reversible processes [35].

not realistic nor practical due to the following reasons [35]:

- The compression and expansion processes happen in the two-phase region, also called wet compression/expansion. This implies liquid droplets in turbomachinery which are very susceptible to damage from small particles. Therefore, practical cycles are usually limited to dry compression.
- Real turbomachinery does not have a perfect isentropic efficiency but induces an increase in entropy during the process.
- The available work to be extracted by the turbine is usually small compared to the compression work. Instead, an expansion valve is generally used, which simply throttles the flow. The expansion process then becomes isenthalpic, implying unavoidable entropy production. Wet expansion is however not an issue.
- Heat exchangers normally induce a pressure drop between the inlet and outlet, resulting in a temperature glide. In this research, however, it is assumed that this effect can be neglected.
- No component is truly adiabatic, since perfect isolation is not possible. In this research, however, it is assumed that the heat loss is negligible compared to the heat flow rates in heat pumps.

A more realistic subcritical cycle is shown in Figure 2.4. This shows that the evaporator outlet is slightly hotter than the saturation temperature (state 1). This superheat prevents liquid droplets in the compressor. The divergence from the ideal isentropic compression process is described by the

isentropic compressor efficiency, $\eta_{\text{CP}}$:

$$\eta_{\text{CP}} = \frac{h_{2s} - h_1}{h_2 - h_1}. \tag{2.8}$$

The value of the isentropic efficiency depends on the type of compressor and the operating conditions. The compressor outlet (state 2) is highly superheated, implying that vapour enters the condenser at a temperature much larger than the saturation temperature. At the same time, the condenser outlet temperature is slightly below the saturation temperature, thus it emits subcooled liquid (state 3). Therefore, the temperature profile of the working fluid in the condenser is the line from state 2 to state 3. Due to the angles in this profile, it is difficult to match it to a process fluid which does not have this exact profile, without a very large $T_{\text{H}}$. The process from state 3 to state 4 involves an expansion valve with the associated increase in entropy.

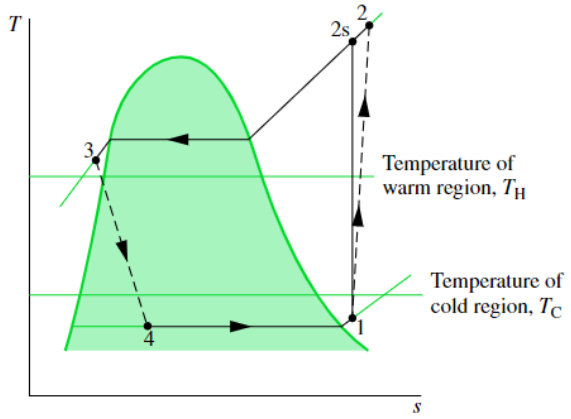


**Figure 2.4:** An actual vapour compression cycle with dry compression from a superheated state. The divergence of the compression process due to the isentropic efficiency is also shown. The condenser emits subcooled liquid [35].

The angular profile in the condenser becomes straighter if the fluid is in a supercritical state, like in transcritical and supercritical cycles. Figure 2.5 shows a temperature-entropy (T-s) and pressure-enthalpy (p-h) diagram of methanol with a subcritical, transcritical and supercritical cycle of a vapour compression heat pump. The temperature profile in the condenser is from state 2 to state 3 in each case. As can be seen, the subcritical cycle has an angular profile, the transcritical cycle a curvy profile and the supercritical cycle a near-straight profile. In the latter cycle, the evaporator also has a temperature glide as the working fluid remains outside the two-phase region. Since wet expansion is avoided, the implementation of a turbine is not as difficult. Moreover, the amount of work that can be extracted from a turbine in supercritical cycles is not small compared to the compressor work. Nevertheless, the achievable CoP of supercritical cycles is generally low since relatively large pressures and volume flow rates are needed [35].

Using the first law of thermodynamics, the heat transfer rate and power of the components in a heat pump can be related to the enthalpy differences over the components. Using the cycles of Figure 2.5, this gives [35]:

$$\text{Evaporator:} \qquad \dot{Q}_{\text{C}} = \dot{m}\,(h_1 - h_4) \tag{2.9}$$

$$\text{Compressor:} \qquad \dot{W}_{\text{CP}} = \dot{m}\,(h_1 - h_2) \tag{2.10}$$

$$\text{Condenser:} \qquad \dot{Q}_{\text{H}} = \dot{m}\,(h_3 - h_2) \tag{2.11}$$

$$\text{Expanion valve:} \qquad h_1 = h_2 \tag{2.12}$$

This analysis assumed steady-state operation and neglected kinetic and potential energy. Since the mass flow rate is constant, the CoP can then be expressed in terms of the enthalpy differences as well. Using Equation (2.5):

$$\text{CoP} = \frac{h_3 - h_2}{h_1 - h_2}. \tag{2.13}$$

Optimising the CoP therefore involves maximizing the specific enthalpy difference over the condenser relative to the specific enthalpy difference over the compressor.

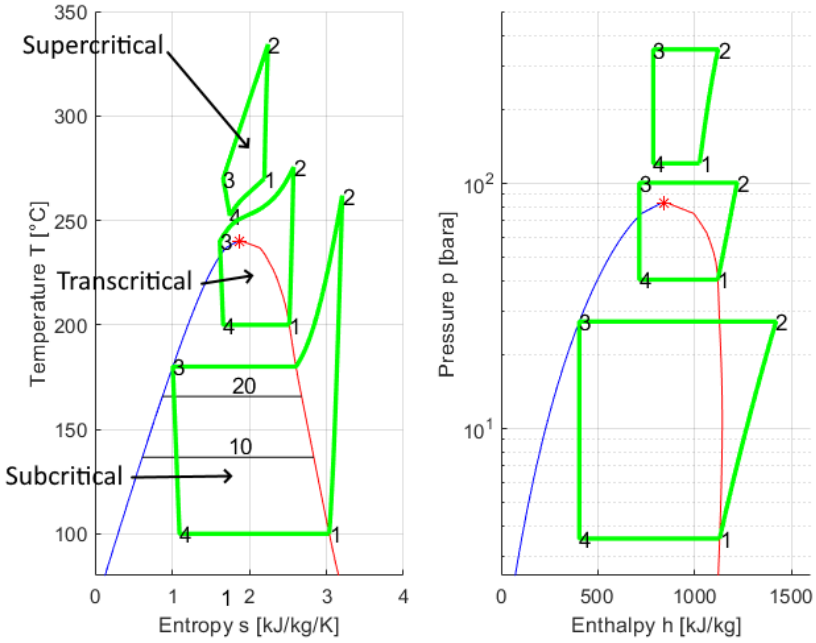


**Figure 2.5:** A subcritical, transcritical and supercritical cycle of a vapour compression heat pump cycle using methanol as working fluid. Properties evaluated with RefProp 9.0 [20].

A distinction can be made between fluids in terms of the shape of the vapour-liquid regions in the T-s diagram. As can be seen in Figure 2.6, a fluid can be classified as wet, isentropic or dry. The terminology originates from Rankine cycles theory and is determined based on whether a fluid becomes wetter or dryer upon isentropic expansion from a saturated vapour. A wet fluid therefore has a negative slope of the saturated vapour line in the T-s diagram. Water is an example but also methanol, as can be seen in Figure 2.5. If the slope of the saturated vapour line is positive, the fluid is said to be dry. Most organic fluids are dry. The degree of overhang generally has a positive correlation with molecular weight and complexity. That is, the larger the molecular weight, the dryer it becomes when it expands. Edge cases where the saturated vapour line is approximately vertical (near-infinite slope) are called isentropic fluids. These remain approximately a saturated vapour upon isentropic expansion [6]. Dry fluids are advantageous in Rankine cycles since they do

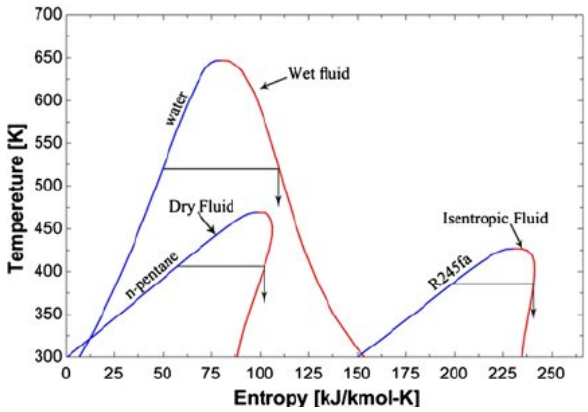


**Figure 2.6:** The T-s diagram of different fluids, showing the different shapes of the vapour liquid dome [6].

not need superheating to avoid liquid in the turbomachinery [15]. The opposite is however true in heat pumps, where they become wet upon isentropic compression. The terminology of wet and dry is unfortunate for heat pumps since the cycle and the effects are reversed. Therefore, from this point in this report, the terms are reversed as well. Fluids like water are thus called **dry** and fluids like n-pentane are called **wet**.

Wet compression can lead to severe damage to a centrifugal compressor due to erosion of the blades [45, 22]. Despite that, wet compression can also be a way of improving the performance of a

heat pump for dry fluids. It could improve the CoP and also prevent the compressor discharge temperature from being excessively high since the temperature during compression is fixed to the saturation temperature. On top of that, it keeps the specific work of the compression as low as possible by maintaining a high gas density [22]. There exists an optimum compressor inlet quality for which the heat pump is most efficient. This is usually around the quality which makes the compressor outlet just saturated vapour [56]. For water, the CoP improvement could be significant, for other dry fluids only marginal. For wet fluids, wet compression has a negative effect on CoP [22].

## 2.2 More advanced vapour compression heat pump cycles

By adding extra components, several advancements can be made to the standard cycle shown in Figure 2.3 (though with an expansion valve instead of the turbine). These improvements can have different purposes like increasing CoP, increasing temperature lift or decreasing compressor discharge temperature. Improvements could also be added together to combine the benefits The elementary improvements are discussed here, and are displayed with T-s and p-h diagrams of the cycle applied to a dry fluid for subcritical conditions. For completeness, the standard cycle is shown in Figure 2.7. This is referred to as a single-stage cycle, due to the single compressor. There are thus two pressure levels in the system, that of the evaporator and that of the condenser.

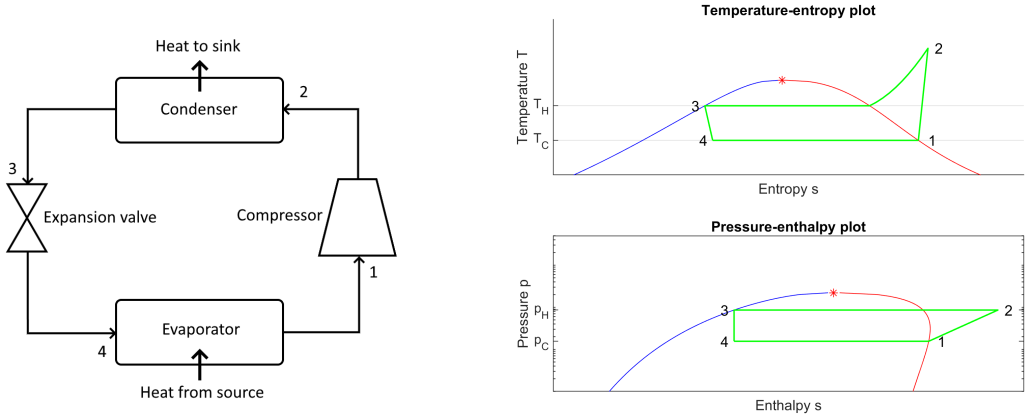


**Figure 2.7:** Diagram of a single-stage vapour compression heat pump in its simplest form with the corresponding cycle shown in property diagrams.

**Internal superheating** Looking at the T-s diagram Figure 2.7, it is noticed that the condenser outlet (point 3) is a high-temperature and pressure liquid, which is throttled to a lower temperature and pressure. The internal energy is used to evaporate part of the liquid. The evaporator inlet is therefore two-phase vapour-liquid mixture. The amount of heat that can be taken up in the evaporator from the waste fluid is smaller than if a saturated liquid enters the evaporator. To use the energy in the condenser outlet more efficiently, an indirect-contact heat exchanger (where fluid streams do not come into contact) can be used to heat the outlet of the evaporator (point 1), as shown in Figure 2.8. This allows the compressor to receive superheated vapour (point 2). For wet fluids, this superheating could be used to avoid wet compression. At the same time, the liquid from the condenser is subcooled from point 4 to point 5 [28, 45].

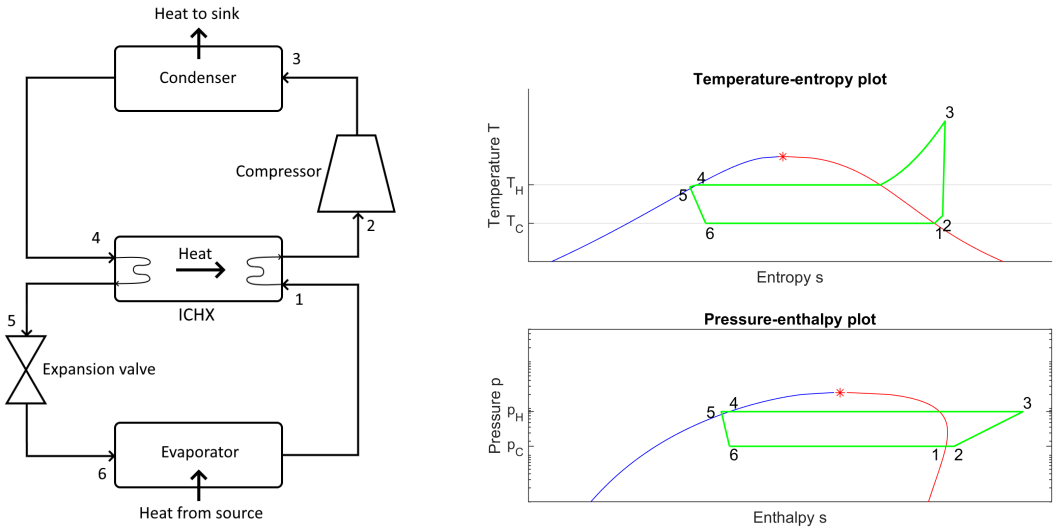


**Figure 2.8:** Diagram of vapour compression heat pump with an internal superheater with the corresponding cycle shown in property diagrams.

By sizing the heat exchanger, the degree of superheating can be set. The maximum superheat possible is the temperature difference between the evaporator and condenser outlet minus the minimum allowed temperature difference. The amount of superheating needed to avoid wet compression depends on the working fluid and process conditions but can vary from 0 to 35 K [3]. For certain working fluids, the CoP decreases compared to an un-superheated system. For others, there exists an optimum degree of superheat [2].

**Flash chamber** A flash chamber is a compartment with a large volume which allows a two-phase stream to settle and separate. Due to the large volume, the velocity of the stream is reduced and droplets are not entrained anymore in the vapour. Due to the density difference, the droplets gather in the bottom of the chamber while the vapour gathers in the top. A connection at the bottom can therefore draw saturated liquid and a connection at the top can draw saturated vapour [35]. Such a flash chamber ensures that components receive a single phase if required.

**Ejector** An ejector uses a high-pressure (motive) stream to entrain a low-pressure stream (suction), resulting in an intermediate-pressure stream (discharge). Due to the different pressure levels in the heat pump, (part of) the high-pressure stream can be used to increase the pressure of the low-pressure stream. Thereby, the pressure ratio over the compressor and with that the compressor work is reduced [16, 24]. This improves the CoP of the heat pump while the compressor can be smaller. There are multiple ways in which an ejector can be applied in a heat pump. A simple cycle with an ejector is displayed in Figure 2.9. Here, the condenser outlet is used as the motive stream to entrain the evaporator outlet (suction stream). The discharge is a two-phase stream at intermediate pressure. A flash chamber is used to separate the stream into saturated liquid and saturated vapour. The vapour enters the compressor, while the liquid is expanded to the evaporator pressure level with an expansion valve. This cycle was used in [52], [46], [16] (with addition internal heat exchanger. The ejector thereby recovers some of the expansion energy that an expander could have recovered. An ejector is however simple, cheap and available compared to an expander [28]. Despite that, according to Adamson et al. (2022), an ejector is very susceptible to small deviations in operating conditions from the design point and therefore difficult to design.

**Multistage expansion with parallel compression** As could be seen in Figure 2.7, the expansion over the valve resulted in a two-phase mixture (point 4). The vapour fraction of this mixture is not needed in the evaporator since only the liquid needs to be evaporated. However, the vapour does need to be compressed again from the pressure of the evaporator to that of the condenser. A way to partly avoid this is by splitting the expansion into multiple stages. Figure 2.10 shows a setup where two expansion valves are used and an intermediate two-phase state is created at point 4. A flash chamber is used to separate the vapour from the liquid. The vapour enters a second compressor at point 7 and is compressed back into the condenser. The pressure ratio is smaller than the pressure

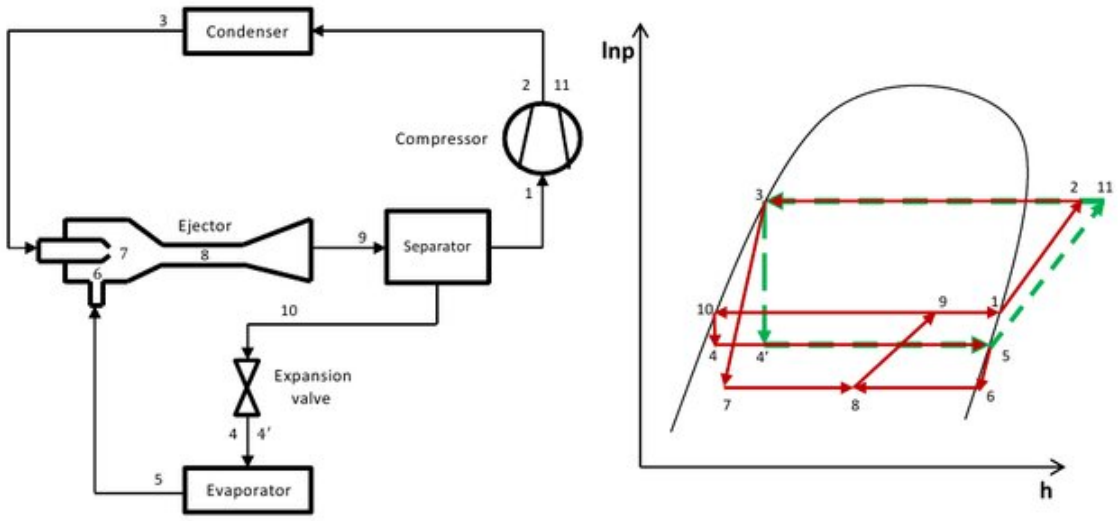


**Figure 2.9:** Diagram of a single-stage cycle with an ejector to increase the suction pressure before the compressor [50].

ratio of the main compressor and thus the amount of compression work is lower [2] The saturated liquid at point 5 is expanded to the evaporator pressure.

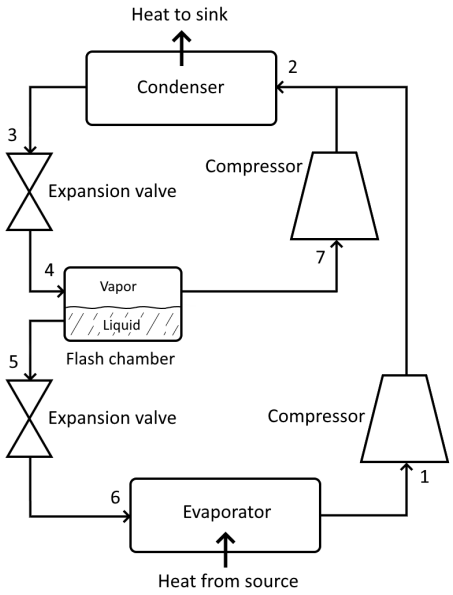


**Figure 2.10:** Diagram of a single-stage cycle with multistage expansion and parallel compression [50].

**Mutlistage compression with intercooling** It could be that the required temperature lift requires a compression ratio which cannot be delivered by one compressor [2]. This is partly due to compressors being unable to cope with very large pressure differentials. Another big issue is that the fluid may reach compressor discharge temperatures that are too high for the equipment [31]. To overcome these issues, the compression process can be divided into multiple separate compression stages. The large discharge temperature issue can be addressed by intercooling the discharge from one compressor before it enters the next compressor. It can also improve the CoP [2]. Intercooling can be done in several ways. One way is to use an indirect-contact heat exchanger (ICHX) as shown in Figure 2.11.

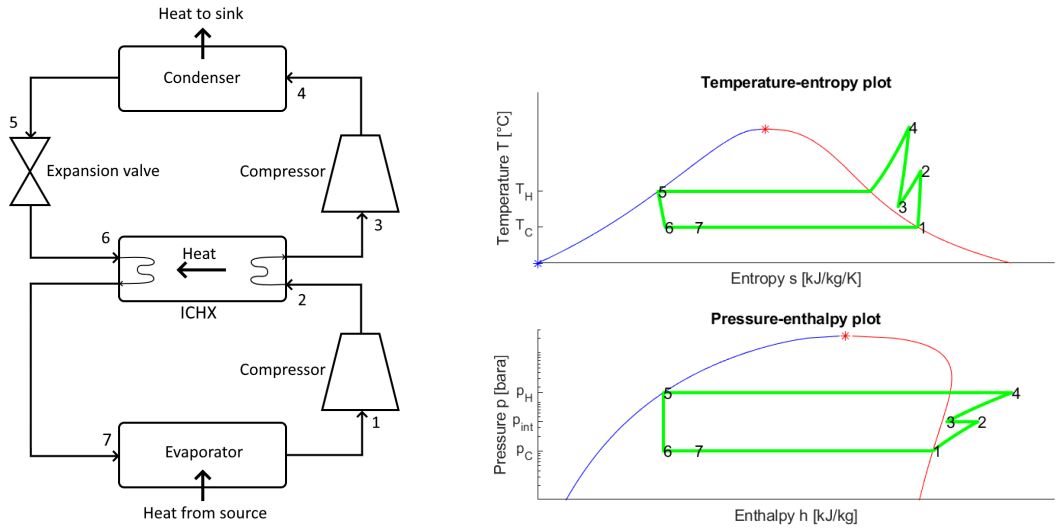


**Figure 2.11:** Diagram of a dual-stage heat pump with intercooling using an indirect-contact heat exchanger.

After the condenser outlet is expanded over the expansion valve (point 6), it is colder than the discharge from the first compressor (point 2). This temperature difference cools the compressor discharge down before entering the second compressor (point 3) and preheats the two-phase mixture at point 6 before entering the evaporator [59].

Another way of intercooling is shown in Figure 2.12. Here, the expansion is also dual-staged. After the first expansion valve, the fluid enters a flash chamber at point 6. The saturated liquid enters the second expansion valve (point 7) before going to the evaporator (point 8). The first compressor discharges at point 2 into a direct-contact heat exchanger (DCHX), into which also the saturated vapour enters at point 9. In a DCHX, two fluid streams come into contact, mix and exchange heat, resulting in a single discharge. The pressures of the two streams need to be equal, dictating that the saturated vapour is cooler than the compressor discharge. The fluid therefore enters the second compressor (point 3) at a lower temperature than at point 2, as can also be seen in Figure 2.12. The mass flow rates through both compressors are different [35].

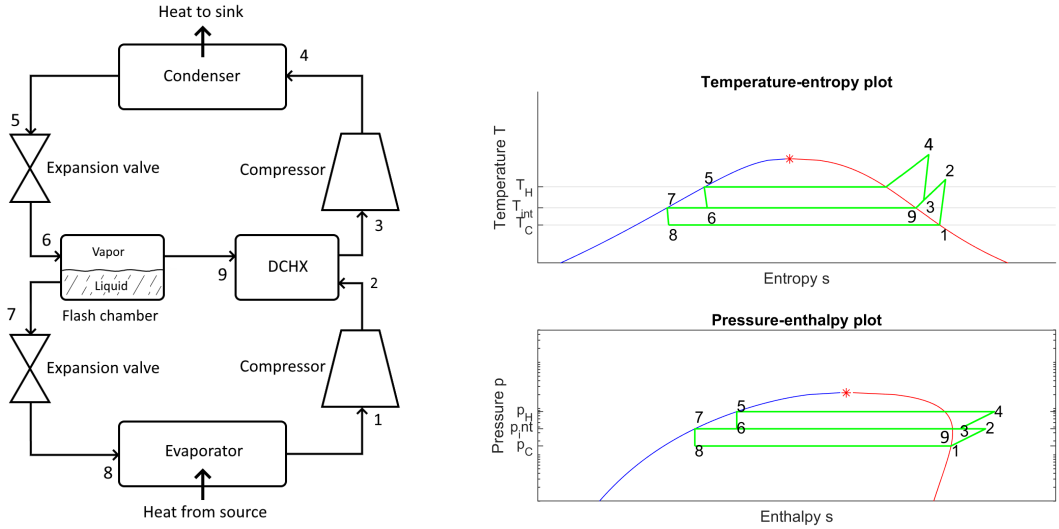


**Figure 2.12:** Diagram of a dual-stage heat pump with intercooling using a direct-contact heat exchanger with saturated vapour from a flash chamber.

The DCHX can also be combined with a flash chamber. In that way, the discharge of the first compressor can be fully cooled down to saturated vapour by evaporating some of the liquid. This reduces the mass flow rate through the first compressor and with that the required compression work, increasing the CoP of the heat pump [28]. A setup of a dual-stage cycle with intercooling using a DCHX combined with a flash chamber can be seen in Figure 2.13. Despite the increased CoP, it

can also be a disadvantage to supply saturated vapour the the compressor since liquid entrainment is risked. The intercooling of Figure 2.11 & Figure 2.12 can be designed to retain a small degree of superheating to avoid this risk [45].

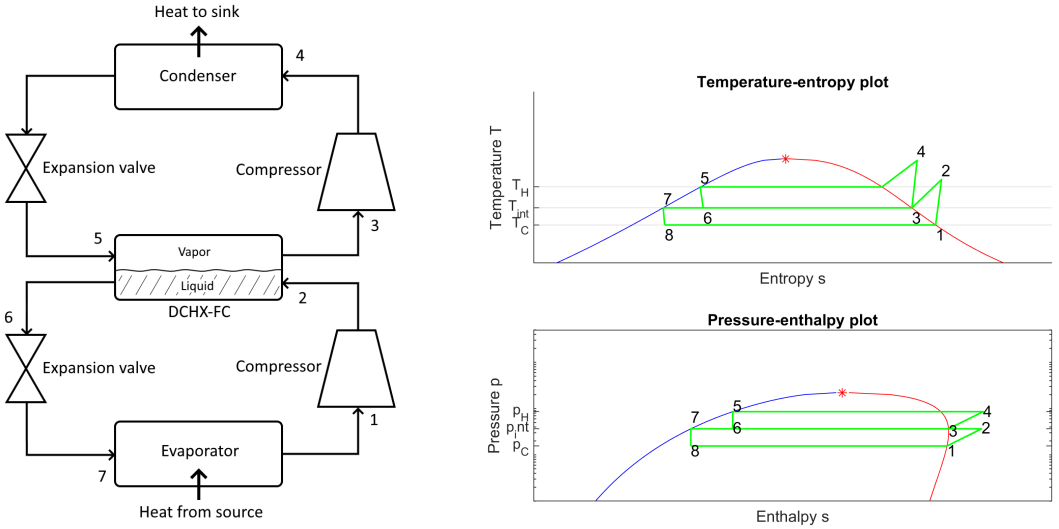


**Figure 2.13:** Diagram of a dual-stage heat pump with intercooling using a direct-contact heat exchanger combined with flash chamber.

Cao et al. (2014) compared, amongst others, the multistage intercooling cycles of Figure 2.12 and Figure 2.13 to the standard cycle of Figure 2.7. It appeared that the intercooling cycles were about 25 % to 35 % more efficient.

**Mechanical Vapor Recompression heat pump** In certain cases, it is possible to use waste fluid directly in a heat pump [28]. This fluid is then directly compressed and condensed. After the condenser, the liquid can still be used for additional superheating or intercooling before being expanded to ambient conditions and discarded. A diagram of this process, which is called Mechanical Vapor Recompression (MVR), is shown in Figure 2.14. The advantages are that a separate working

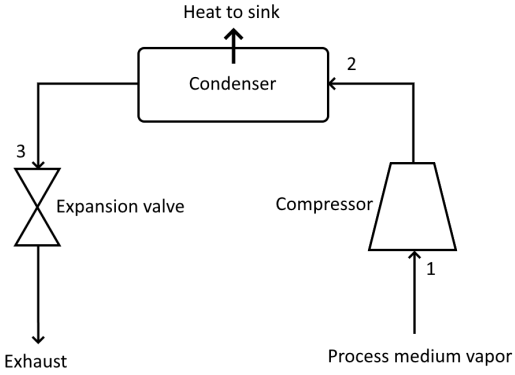


**Figure 2.14:** Diagram of a Mechanical Vapor Recompression heat pump.

fluid is not required, one heat exchanger can be saved and the efficiency can be larger because the minimum temperature difference on the source side is no longer needed. It does however limit the working conditions of the heat pump to those dictated by the source process medium, since it became, in effect, the working fluid [28].

**Cascaded heat pump** In some cases, the desired temperature lift cannot be handled by a single working fluid. It could be that the absolute pressure becomes too high on the sink side, or the cycle becomes transcritical when this is not desired. A solution in these cases is to use a cascaded heat pump, which consists of multiple heat pumps in series, where the condenser of the previous heat pump cycle gives up heat to the evaporator of the next heat pump cycle. A diagram of this

setup is shown in Figure 2.15. The upper and lower cycles are fully disconnected and can therefore

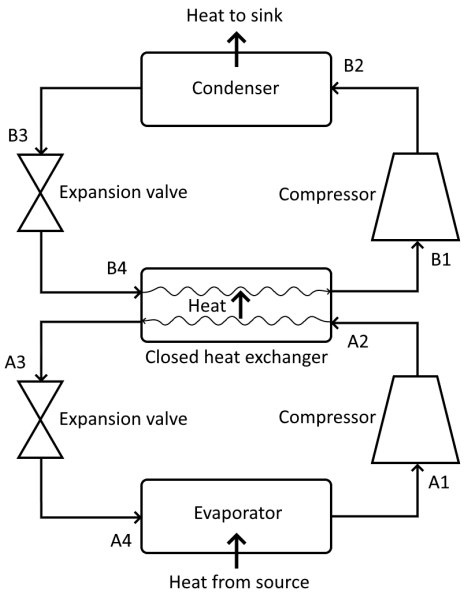


**Figure 2.15:** Process flow diagram of a cascaded heat pump.

have different working fluids. A disadvantage of this setup is that there needs to be a minimum temperature difference in the closed heat exchanger, inherently reducing efficiency [28].

Up to now, only mechanical heat pumps have been considered. Instead of mechanical work, however, heat pumps can also be driven by heat or chemical reactions. Moreover, combinations of these are possible. As the focus of this research is on mechanical heat pumps, these alternative types are only briefly discussed.

**Thermal Vapor (Re)Compression heat pump** Instead of using a compressor to achieve the pressure rise, an ejector can be used. The evaporator outlet is then the suction stream. A high-pressure motive fluid entrains the fluid from the evaporator and discharges it at higher pressure to the condenser. The motive fluid can be obtained by heating a fluid under pressure in a boiler. Part of the liquid from the condenser is pumped to be the fluid supply of the boiler. As such, the use of an expensive mechanical compressor is avoided and it is thus called a thermal vapor compression heat pump or an ejector heat pump. If a supply of pressurised vapour is already present at a plant, it can be used as motive fluid instead. In that case, it would be a thermal vapour recompression heat pump [28].

**Compression Resorption Heat Pump** Another method to use temperature glides is by using a compression resorption heat pump. This works with the cycle of Figure 2.7 but uses a mixture of different substances as the working fluid instead of a pure fluid. The mixture consists of two substances A and B where A can be absorbed in B. The condenser now becomes the absorber. The absorption process is exothermic and thereby releases heat, which makes the temperature drop. The fluid now leaves the condenser as a saturated liquid solution and is then expanded to the lower pressure level. Due to the internal heat, part of A is vaporised out of the solution. It then enters the evaporator, which has now become a desorber. Heat is taken from the heat source to liberate the remaining A as vapours while substance B remains a liquid. Now wet compression can be used to increase the pressure level of the solution. Alternatively, the vapour and liquid can be separated and routed to a compressor and pump respectively, which pump the substances to a higher pressure. This is then called an Osenbrück cycle [28]. Due to the involvement of both absorption and compression, it is sometimes also called a hybrid heat pump [2].

**Absorption heat pump** The absorption heat pump functions on the same principle as a compression resorption heat pump, only here the mechanical compressor is replaced by a 'thermal compressor'. In the evaporator, the fluid (mainly substance A) is vaporised. The vapours are subsequently absorbed by a liquid substance B in the absorber. This is an exothermic reaction, so it releases heat. The solution is now a liquid and can easily be pumped up to a higher pressure level

by a pump using little energy. Subsequently, a high-temperature heat source liberates substance A as vapours from the solution in the desorber. The vapors, now at the higher pressure level, are condensed in the condenser where they give up their heat to the sink. The liquid remaining after the condenser is routed back to the evaporator via an expansion valve. Most of substance B remains in the desorber and is routed back to the absorber via another expansion valve [28].

The CoP of such a heat pump is usually low (often even lower than 1) and it is generally only used in places where a high-temperature heat source is available as waste heat [54] [2].

## 2.3 Components of heat pumps

This section describes the individual components of the heat pump in more detail. This provides insight into the different types of these components and their advantages. It also shows the limits and constraints that each component poses and therefore helps in the component selection in the modelling part of this project.

### 2.3.1 Heat exchangers

Heat exchangers make heat transfer between two fluids at different temperatures possible. They can be direct-contact or indirect-coontact. In a direct-contact heat exchanger, two fluids are allowed to mix and equalise at an intermediate temperature. In an indirect-contact heat exchanger, two fluid streams always remain separated. The temperature difference between the fluids is the driving force of heat transfer. Other important parameters in a closed heat exchanger are the surface area $A$ and the overall heat transfer coefficient $U$. The amount of heat transferred can then be calculated with:

$$Q = UA\Delta T. \tag{2.14}$$

Smaller temperature differences will reduce irreversibilities (entropy production), however, increase heat exchanger size for the same capacity [2].

The condensers and evaporators are usually of the closed type, as process medium and working fluid should not be mixed. The most common closed type is the shell and tube heat exchanger consisting of a tube bundle in a shell. One fluid stream passes through the tubes, while the other flows in the shell around the tubes. Its construction is easy and well-established. The tube side fluid can have very high pressures and they are easily cleaned [47]. A related type is the finned tube bundle, where the tubes have fins to increase the surface area.

Another common closed type is the plate and frame heat exchanger, which consists of a large number of thin plates spaced apart by a small distance. Every plate has one fluid on one side of the plate, and the other fluid on the other side. They are compact and have high heat transfer efficiency. They allow easy disassembly for maintenance like cleaning or resealing. Adjusting its heat transfer capability is easily done by adding or removing plates. These are however not suited for very high pressures [13].

A third common closed type is the plate-fin heat exchanger in which fluids flow in cross-flow on either side of a plate, where the plate has fins attached.

Heat exchangers are usually made of materials that conduct heat well, like copper and steel. Care has to be taken to prevent fouling, which is the accumulation of contaminants on the heat transfer surfaces, reducing the amount of heat transfer [13].

### 2.3.2 Compression devices

The purpose of a compressor is to increase the pressure of a gas. Compressors can be classified as positive displacement or dynamic. Positive displacement compressors draw gas into a chamber and then reduce the volume of this chamber. At constant speed, they thus provide a constant volumetric flow rate. The outlet opens when the required pressure has been reached. Dynamic compressors on the other hand work by imparting the velocity to the gas and then slowing it down to turn the velocity head into pressure. At constant speed, they provide constant pressure. Heat pumps mainly use the positive displacement type compressor. Compressors can be further classified as reciprocating or rotating. Reciprocating compressors are exclusively of the positive displacement type while rotating compressors can be both dynamic and positive displacement. Compared to

reciprocating compressors, rotating types can be smaller, more efficient, more silent, less vibrant, provide non-pulsating flow and are easy to control [13].

According to the International Energy Agency [21], four types of compressors are used in vapour compression heat pumps: scroll, reciprocating piston, screw and centrifugal compressors. The first three are positive displacement types.

**Scroll compressor** The scroll compressor consists of two meshing spiral scrolls of which one makes a circular movement inside the other. It thereby progressively advances a chamber of gas towards the discharge and is thus classified as a positive displacement type. They are of simple construction, work reliably and entrained liquid droplets are not an issue [52]. Their use is however limited to low pressures and small pressure ratios. Furthermore, they use oil for lubrication and sealing. They are mainly used in smaller heat pumps up to about 100 kW [14].

**Reciprocating compressor** The reciprocating piston compressor consists of a piston-cylinder assembly. Discharge and admission valves are needed to control the flow of gas. As positive-displacement machines, the piston moves up and down, thereby forcing gas through the discharge. They are suitable for higher pressures and they hold their efficiency for increasing pressure ratios relatively well, yet their suction and discharge valves cause them to have a lower efficiency compared to other compressors [13]. Also, they inevitably have some clearance volume which lowers their efficiency [14]. Furthermore, they have a complex structure and multiple moving parts that lead to higher maintenance costs and they require oil for lubrication. Entrained liquid droplets are however no issue. They are used up to about 500 kW of heating power [21].

Alternative to a solid piston, a liquid piston can be used. In that case, a compression chamber is filled with liquid from a pump. The liquid gathers in the bottom of the chamber and forms a rising liquid column with a gas-liquid surface. This method makes the usage of oil superfluous as lubrication is not necessary and sealing is taken over by the liquid [30, 57].

**Screw compressors** Screw compressors consist of one or two rotating screw(s) which trap a pocket of fluid and progressively force it to the discharge. They are therefore of the positive-displacement type. They can achieve moderate pressure ratios but low volume flow rates. Entrained liquid droplets are not an issue [14, 19]. Oil is not needed for lubrication, however, it is often employed as a seal between the screw and the housing, and between both screws in the case of a twin screw. Operation without oil is possible but leads to low volumetric efficiencies [14].

**Centrifugal compressors** Centrifugal compressors, also called turbo compressors, consist of fast-spinning blades that impart velocity to the gas, which is subsequently turned into pressure. They are therefore of the dynamic type. Due to the fast-spinning blades, they are susceptible to liquid droplets [22]. They can provide a high volume flow rate for compact design and are therefore often used with water vapour compression systems, compensating for the low vapour density [3]. They can however only provide a low pressure ratio for a single stage. They are used above 2 MW up to about 5 MW with oil-free variants available from 250 kW [21].

The compression process would ideally be done adiabatically and reversibly so that it is an isentropic process. Any real compressor, however, has an isentropic efficiency less than 100 % [35]. Another deviation from the ideal process is signified by the volumetric efficiency, which accounts for leakage. If the compressor increases the pressure from $p_1$ to $p_2$, pressure ratio is:

$$r_{\text{com}} = \frac{p_2}{p_1}. \tag{2.15}$$

According to Kiss and Ferreira (2017), with multistage compression, the optimal pressure levels are those which result in the same pressure ratio in each compressor. The isentropic efficiency depends on the operating conditions, mainly the pressure ratio, as can be seen in Figure 2.16. The maximum isentropic efficiency of about 70 % is reached for pressure ratios of about 3 to 4 for each compression. The piston compressor retains this efficiency for higher pressure ratios.

Figure 2.17 shows operating regions for screw and centrifugal compressors. As can be seen, the screw compressor is suitable for pressure ratios up to about 9, but has a lower flow rate capacity compared to the centrifugal compressor. The latter is therefore suited for fluids with small densities but it can only achieve a pressure ratio of about 2.5. Reciprocating compressors are more suited for

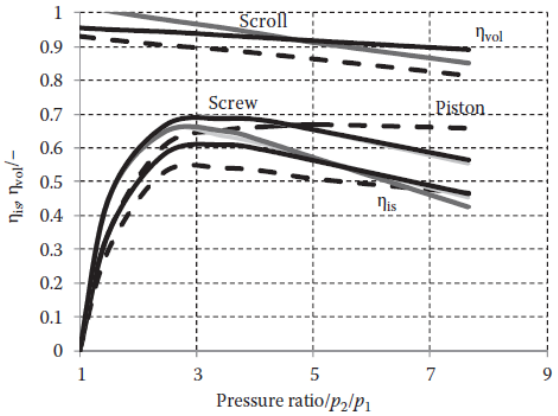


**Figure 2.16:** The influence of the pressure ratio on multiple compressor types' isentropic and volumetric efficiencies. The grey line belongs to scroll compressors, the black line to screw compressors and the dashed line to piston compressors [28].

large pressure ratios and large density fluids [35]. According to Adamson et al., (2022) a pressure ratio of about 8 is the current commercial maximum.

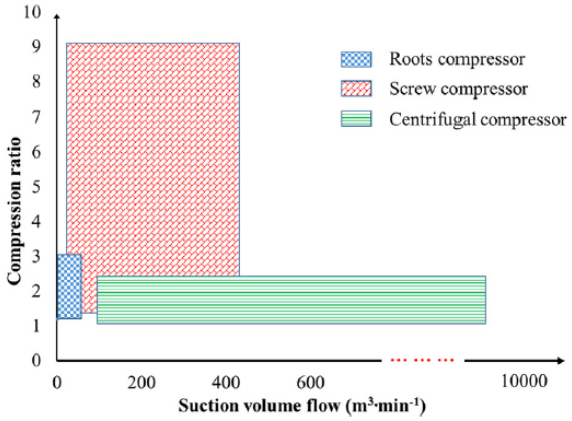


**Figure 2.17:** The operating regions of centrifugal and screw compressors in terms of pressure ratio and volume flow rate [19].

**Lubrication oils** Many compressors require oil for their operation to provide lubrication and/or sealing. The type of lubrication oil is usually dictated by the choice of the working fluid. The oil needs to be compatible in terms of viscosity and thermal stability at high temperatures, which includes coking [3, 21]. When compressing a dry fluid, the discharge temperature however quickly becomes too large for most types of oils. At high temperatures, oil decomposes leading to damage to the compressor. According to Kiss and Ferreira (2017), most oils chemically change at temperatures between 160 °C & 200 °C and contaminate the working fluid. Working fluids might then decompose at high temperatures and material properties could change leading to failure susceptibility.

The practical limit was stated to be 130 °C to 150 °C. A maximum temperature limit of 180 °C was set by [37] to avoid thermal degradation of the lubricant. A slightly more conservative limit of 150 °C was set by [3]. These temperatures practically exclude the use of oil in HTHPs for the temperature ranges considered in this project. Another disadvantage of oil is that it vaporises and travels with the working fluid to the heat exchangers where it will cause fouling [56].

### 2.3.3 Expansion devices

Expansion devices reduce the pressure of the incoming flow of liquid or gas. This is either done by posing a resistance to the flow or by extracting work from it. Expanders can extract work from the flow, which can supplement the compressor for a higher efficiency. Expanders usually are of the centrifugal or screw type. The same drawbacks however apply here in terms of lubrication as was the case with compressors. Apart from that, the expansion device usually receives a saturated

or subcooled liquid flow from the condenser. The exergy of such a liquid flow is relatively low and therefore the energy that an expander would be able to recuperate is significantly lower than the energy it costs to drive the compressor, rendering the expander uneconomical. Furthermore, expansion usually takes place in the two-phase region, which complicates the design. Nevertheless, two-phase expanders have been receiving more attention and have started to show some potential [28].

Most often, simple expansion valves are used. They purely waste energy as heat, but do this by simply throttling the flow [45]. The generated heat will go into evaporating part of the fluid. The expansion valve is often an active device which can adjust its resistance to the flow, thereby taking part in control and accounting for load variations, maintaining the correct pressure ratio in this way [13].

## 2.4 Working fluids

The choice of working fluid has a strong influence on the heat pump performance, due to their different thermodynamic properties. This leads to differences in efficiency and capacity. Furthermore, their thermal suitability, environmental compatibility and safety are important factors in their selection. The main selection criteria are further elaborated here.

**Thermal suitability** The most important requirement is that it has to comply with the source and sink temperatures, $T_{\mathrm{C}}$ and $T_{\mathrm{H}}$ respectively, in a desirable way. This means that the temperature difference between the waste/process fluids and the working fluid should be as close to the minimum temperature difference as possible over the whole length of the heat exchanger. When both waste and process fluids have no glides, a subcritical cycle gives the best fit. When the process fluid has a glide but the waste fluid does not, a transcritical cycle could result in the best fit. If both source and sink have glides, then both a supercritical cycle or a subcritical cycle with a mixture as a working fluid can suit these glides. The properties of the fluid determine what pressure levels are required for these types of cycles. The pressure levels and the pressure ratio between the two pressure levels should be small to avoid costly compressor systems. At the same time, the smallest pressures in the system should ideally be above atmospheric pressure to prevent the infiltration of air or the application of advanced sealing methods [2]. Furthermore, a small adiabatic index is favourable such that compressor discharge temperatures remain limited [24].

**Efficiency** The efficiency of a working fluid is described by the coefficient of performance (CoP) of the heat pump. This value indicates how much heat energy can be delivered to the sink per unit of necessary compression power (Equation (2.5)). For subcritical cycles, the latent heat of vaporization at the operating pressures should ideally be large (thus not too close to the critical point) to have a high CoP [61].

**Capacity** As working fluids have different densities, the capacity of the heat pump in which they are used can differ widely. This property is indicated by the volumetric heating capacity (VHC), which describes the amount of heat energy that can be delivered to the sink per unit of volume of working fluid. It therefore serves as a compressor size indication and a higher VHC means a smaller compressor. The VHC is therefore not so much a technical limitation, but rather an economic one. It is defined as the amount of heat supplied to the sink per unit of volumetric flow rate before the compressor [3]:

$$\mathrm{VHC} = \frac{\dot{Q}_{\mathrm{H}}}{\dot{V}_{\mathrm{CP},i}}. \tag{2.16}$$

In common applications of heat pumps, the VHC is in the range of 3-6 MJ. A lower threshold of about 1 MJ defines the practical limit [3].

**Environmental compatibility** Properties that characterise the environmental impact that working fluids have are important considerations in selecting a working fluid. The most important are the global warming potential and ozone-depletion potential. The global warming potential (GWP) quantifies the impact of the working fluid on global warming compared to $CO_2$. According to [3] a threshold value of a maximum GWP of 10 should be considered. The ozone depletion potential (ODP) quantifies the degree of ozone layer destruction the working fluid has compared to Trichlorofluoromethane, also known as R-11. The ODP should be 0 for all cases.

**Safety** Working fluids can also be compared based on several safety-related factors, such as flammability, explosivity, irritation, health hazards and acute toxicity. These come into effect in cases where the fluid leaves the heat pump in some way, which can be either by a leak of the system or when purposely opening the system for maintenance purposes. The American Society of Heating, Refrigerating and Air-Conditioning Engineers has derived a standard for the classification of the flammability and toxicity of working fluids. This can be seen in Figure 2.18 [4].

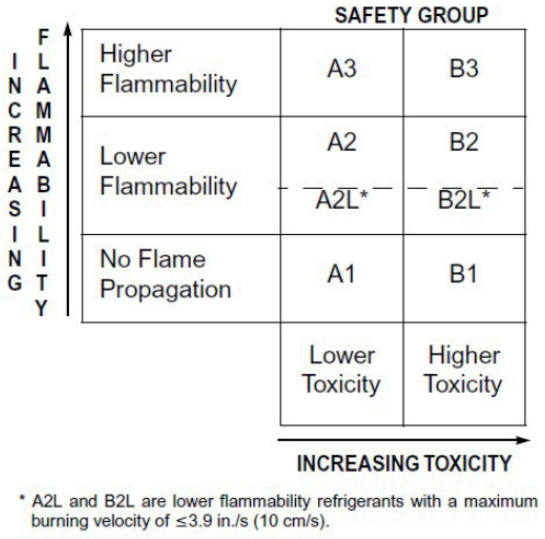


**Figure 2.18:** Safety class allocation indicating the flammability and toxicity of substances used in heat pumps [4].

**Availability** The working fluid should ideally be cheap and already available on the market.

**Other factors** Other factors that make working fluids good contestants are solubility in oil (taking compressor lubrication oil into account) and thermal stability of the working fluid-oil mixture. Since oil is however largely inapplicable to HTHPs, these subjects are not relevant. Instead, good lubrication properties of its own and material compatibility with metals used in the components are desirable [3].

Working fluids can be any suitable natural or synthetic substance or mixture. Many of them are organic compounds, consisting of simple or halogenated hydrocarbons. They can be naturally occurring, like $H_2O$ or $CO_2$ or synthesised in a chemical factory. Furthermore, inorganic compounds are also used like $NH_4$ (ammonia). Most working fluids however consist of different combinations of carbon, hydrogen, fluorine and chlorine atoms. Depending on what atoms are present in a certain substance, different classes of fluids can be categorized. These are for example chlorofluorocarbons (CFCs, consisting of chlorine, fluorine and carbon atoms), hydrofluorocarbons (HFCs, consisting of hydrogen, fluorine and carbon atoms) and hydrochlorofluorocarbons (HCFCs). It was found that the chlorine atom catalyses the depletion of the earth's ozone layer. To counteract this, the use of CFCs is fully banned while HCFCs are being phased out [24]. The replacement for these are chlorine-free hydrocarbons like HFCs, which have zero ozone depletion. However, many fluorinated hydrocarbons have a large impact on global warming. Therefore, increased research in the use of simple hydrocarbons, hydrofluoroolefins (HFOs) and hydrochlorofluoroolefins (HCFOs) is being done with the prospect of HFCs also being banned [3].

Simple hydrocarbons (HCs) are suitable working fluids because of their good thermodynamic performance and lower environmental impact. The larger the number of atoms in HCs, the higher the boiling point. Octane is the smallest HC for which the boiling point is larger than water. They are therefore also suited for high-temperature applications. A drawback is however the high flammability, making certain large-scale applications impossible [24].

Natural substances should be ideal working fluids as their existence in nature implies that they are low on environmental hazards. Water is a competitive working fluid for applications with temperatures above 150 °C. It has a very large latent heat leading to high efficiencies. Due to its thermody-

namic properties, it can also work with relatively low pressures. However, water inherently has high compression ratios and a large adiabatic index, meaning that compressor outlet temperatures can get very high. The small vapor density moreover requires very large compressors [24]. Ammonia is another natural substance that has good properties to be used as a working fluid. It has zero GWP and zero ODP, yet it is classified as highly toxic. It has a high VHC so compressors can be small. The sink temperature using Ammonia is however inherently limited to about 110 °C due to the high pressures necessary [24]. Another popular natural working fluid is $CO_2$. It has zero ODP, a GWP of 1 and is not toxic. Due to the high vapour density, heat pump systems can be very small in size. It does however require large pressures to reach useful temperatures. Due to the small system size, larger pressures are handled more easily, yet the maximum temperature is limited to about 90 °C [24].

# Chapter 3

# HTHP State-of-the-Art & Potential

This section takes a look at the current industrial practices regarding HTHPs. First, Section 3.1 lists some industries which use heat pumps together with an overview of the types of cycles and CoP used. Then, Section 3.2 identifies the potential that currently exists for heat pumps to deliver heat at higher temperatures. The limits that prevented heat pumps from achieving this potential are listed in Section 3.3. Finally, in Section 3.4 some suggestions were identified that could obviate these limits.

## 3.1 Current industrial applications of HTHPs

Currently, heat pumps which have sink temperatures of about 90 °C are on the market [16]. Commercial products are rare above this temperature, with only demonstration products for temperatures up to about 160 °C. For the higher temperatures of 160-200 °C, a limited number of simulations studies and experimental setups exist [33].

A major application area for high-temperature heat pumps is distillation. Distillation is the most used technique to separate substances and accounts for more than 40 % of the total energy consumption of chemical plants. A heat pump is often used to upgrade heat from the condenser of a distillation column so that it can be used to heat the reboiler of the same column [28].

Another large application field is drying. Many products in the food, paper and chemical industry need to be dried at some point in their production. This drying is usually accomplished by using steam or another gas to heat dry air which is then blown over the product. It entrains moisture from the product and therefore the humidity increases. Heat is used to evaporate the water and therefore the discharged humid air has a lower temperature. A heat pump utilises the waste heat contained in this humid air and upgrades it to heat the dry air. Simultaneously, the air is dehumidified so that it can be used as the dry air input [28].

In general, many industries need steam at temperatures of 100-200 °C. The common way of producing this steam is in a boiler fired by fossil fuels. Heat pumps exist which use some industrial waste heat and upgrade it for use as the heat source in the boiler [29].

Jiang et al. (2022) performed a study on what types of HTHPs have been applied in industry. They identified the type of system, type of working fluid CoP, type of compressor, source and sink temperatures and heating capacity. An overview of the results can be seen in Figure 3.1. As seen from Figure 3.1a, the largest sink temperatures encountered are about 150 °C, with CoPs of 2 to 3. In Figure 3.1b, it can be seen that the largest exergy efficiency reached is about 60 %. Furthermore, most heat pumps are developed for temperature lifts below 70 °C with the largest lifts achieved by cascaded cycles. Apart from that, no decisive distinctions could be made between the performances of different cycle configurations. These heat pumps are used in the food, dyeing, medicine & chemical industries and various drying processes.

In another study by Hamid et al. [16], 12 cases of experimental heat pumps (both real setups and simulations) were identified that have sink temperatures above 120 °C. One of them reaches

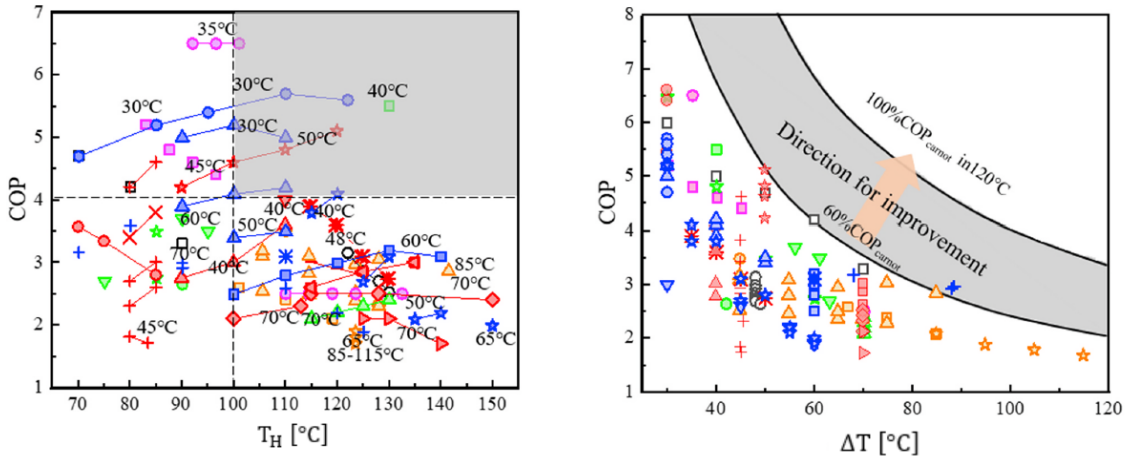


(a) (b)

**Figure 3.1:** CoP of different HTHPs against the sink temperature and the temperature lift. In the left figure, also the temperature lift is indicated. The colour coding is as follows: Single-stage (red), Single stage with improvement (blue), Dual-stage (green), Cascade (orange), Parallel (magenta), Ejector (black) [24].

sink temperatures of 120-200 °C [60] while another goes up to 170-240 °C [23]. Both of these are simulations of a hybrid heat pump, i.e. a compression-resorption cycle.

A study by Arpagus et al. [3] investigated current commercial installations for high-temperature heat pumps and listed the results in the table shown in Figure 3.2.

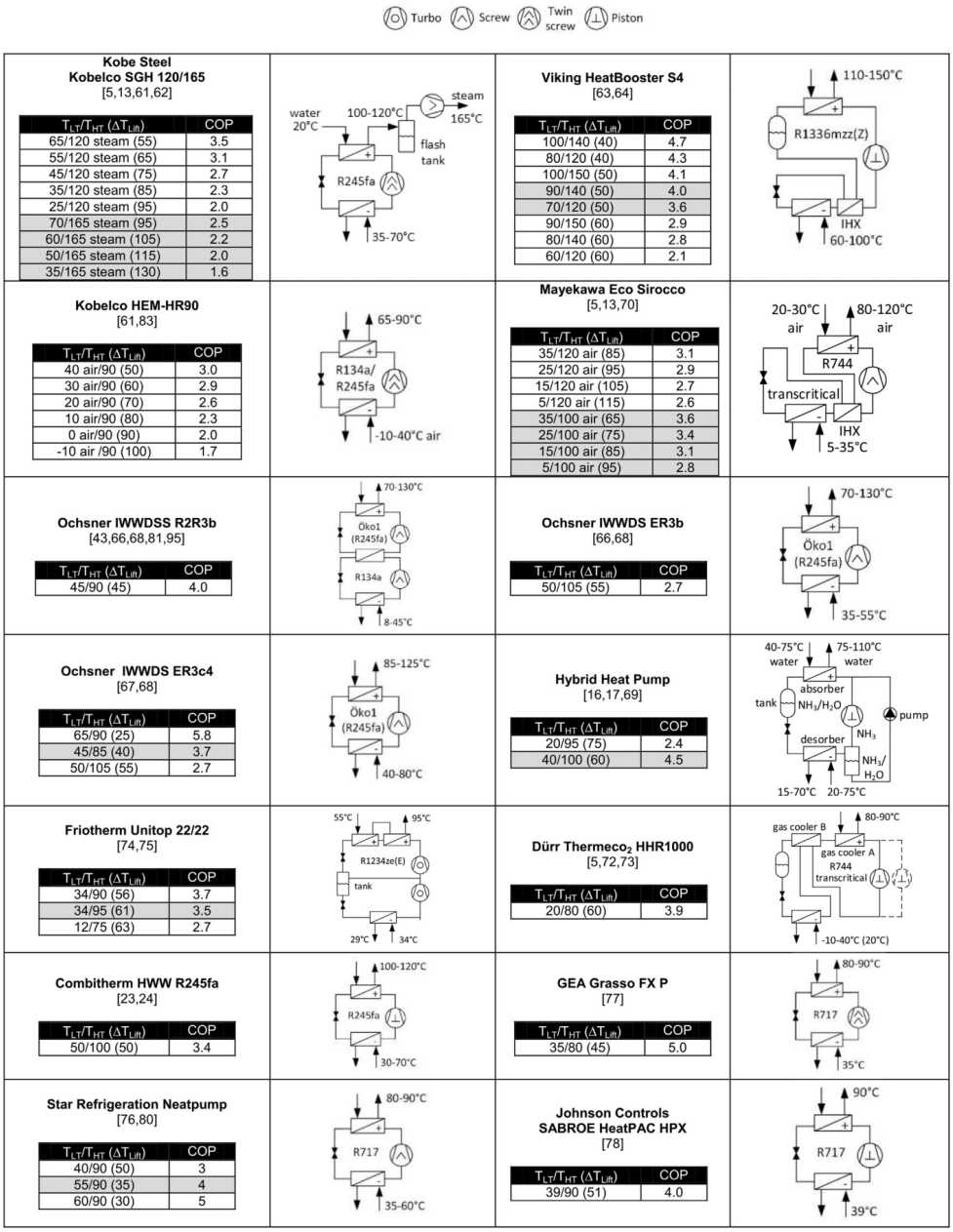


**Figure 3.2:** Commercially available high-temperature heat pumps, indicated with their source and sink temperatures, CoP and system setup [3].

## 3.2 Potential for HTHPs in industry

To determine the potential of heat pumps in high-temperature applications, a review of current industrial processes and waste heat streams is necessary. These determine the feasibility of a heat pump in terms of the temperatures, heat loads and CoP values. The lack of development of heat pumps for temperatures >160 °C is likely due to limited knowledge of potential applications [33]. Finding potential involves finding a process which needs heat at technically feasible temperatures. At the same time, a source of waste heat should be available which has temperature levels that allow efficient heat pump performance. The amount of heat available from waste fluid, augmented with the supplied compression energy, should be sufficient to supply the process heat demand. The process heat demand and waste heat supply should also be available simultaneously. Otherwise, a thermal buffer might be needed. Furthermore, the source and sink should both be at the same site, as long-distance heat transport is considered out of the scope of this research.

One consideration in the evaluation of the potential is that many plants have optimised their heat transfer network already with a pinch point analysis [12]. In these cases, many waste heat streams

are utilised already to provide process heat, leaving only a 'cold utility' and a 'hot utility'. The cold and hot utility is the extra amount of required cooling and heating respectively. A heat pump could be implemented between these two utilities. Depending on the amount of heating/cooling, the heat pump will be limited either by the cold utility or by the hot utility. If it is limited by the cold utility, extra heating by an external source is required at the hot utility. Equivalently, if the heat pump is limited by the hot utility, extra cooling by an external sink is required at the cold utility [28].

Another consideration is that many processes require very high temperatures over 400 °C, usually reached by a combustion process or by an electric arc furnace [29]. These temperatures are out of the scope of this research but heat pumps can still be beneficial in these cases by functioning as a preheater. The process fluid would then be preheated to a temperature efficiently achievable with a heat pump before its temperature is further increased by a combustion process or electric arc furnace. A heat pump is only useful if there is not already a waste heat source available to supply this heat. Preheating is however often already implemented in a heat transfer network.

These considerations open up a whole range of possibilities for HTHPs. It signifies that the optimal heat pump solution would be very site-specific. Information about energy flows and temperature levels at a specific site however remains mostly undisclosed. Nevertheless, the industrial sectors are analysed in search of heat pump potential. The first analysis is based on overall waste heat and process heat energy levels per industry and temperature range. Afterwards, an analysis is performed based on specific processes with their associated process and waste heat fluids.

### 3.2.1 Based on temperature and energy levels

In a study by McKenna & Norman (2010), the United Kingdom's energy-intensive industries were examined to identify the heat demands and waste heat sources between 2000 and 2004. This has been categorised into separate industry sectors and separate temperature bands. The industry sectors are aluminium, cement, ceramics, chemicals, food & drink, glass, gypsum, iron & steel, lime, pulp & paper, aero/auto and other industries. For the heat demands, the temperature bands are: <100 °C, 100-500 °C, 500-1000 °C, 1000-1500 °C and >1500 °C. The heat demand can be seen in Figure 3.3. The process heat demand in the 100-500 °C temperature range is approximately 13 % of the entire

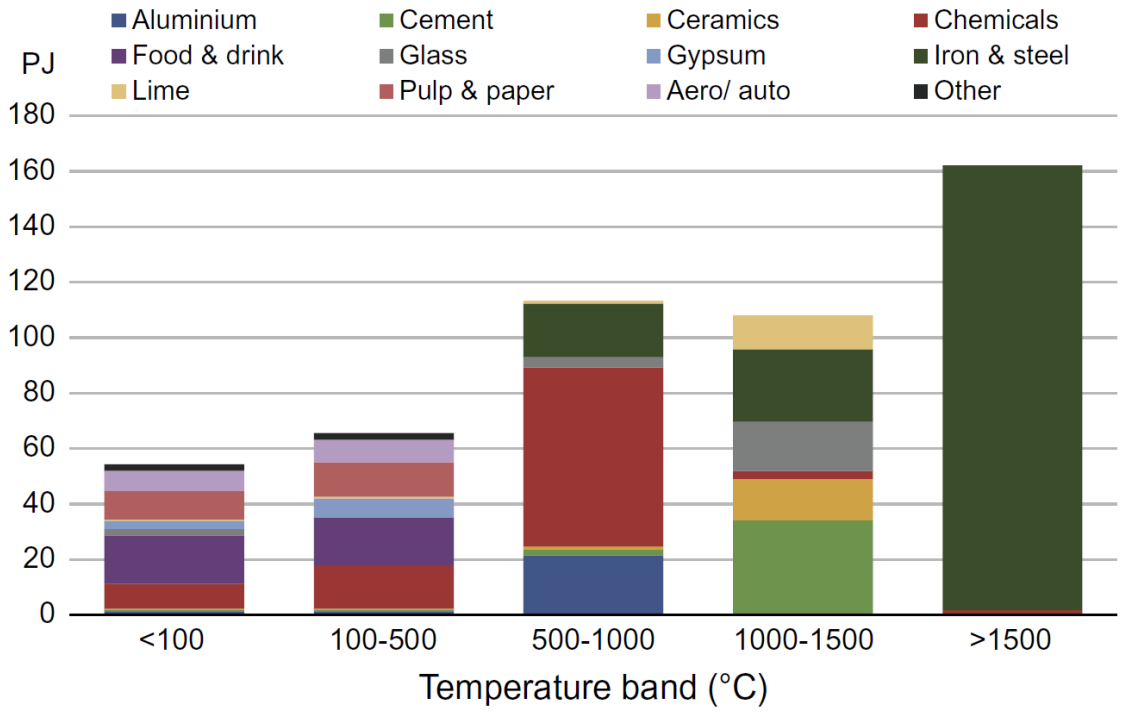


**Figure 3.3:** UK heat demand in the period 2000-2004 [17].

industrial heat demand in the UK. This heat is mostly divided between the pulp & paper, food & drink, gypsum, chemicals and aero/auto industries.

The waste heat sources were determined by analysing processes for their energy use, exhaust fractions (part of the input energy that is exhausted) and exhaust temperatures. This analysis gave estimates

of the amount of waste heat available and the corresponding temperatures. The results of these are shown in Figure 3.4. These values are the average values of a range between a high estimate and a low estimate. Most of this waste heat is situated in the 100-200 °C temperature range. Matches

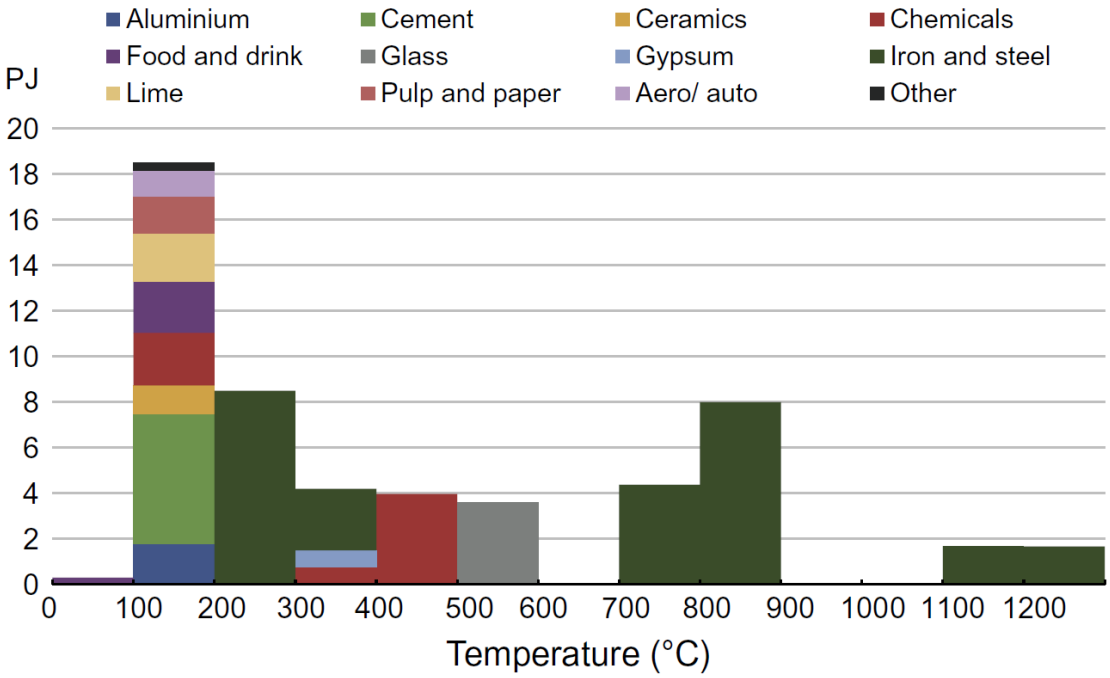


**Figure 3.4:** UK waste heat in the period 2000-2004 [17].

to the process heat demand can be made within the chemicals, food & drink, pulp & paper and aero/auto industries. However, the amount of waste heat is much smaller than the amount of heat consumed.

Continuing on the work of McKenna & Norman (2010), Hammond and Norman (2014) worked out the amount of waste heat that is technically feasible to recover based on the current heat recovery techniques. He considered: on-site heat recovery using heat exchangers, heat pumps, heat-to-chilling by using thermal heat pumps that utilize a heat source to achieve refrigeration, heat-to-electricity conversion and heat transportation by a heat network. He out-ruled any potential for heat pumps if the heat sink temperatures would be above 100 °C. This led to negligible potential for heat pumps, as there is comparatively little waste heat at temperatures below 100 °C to be used as a source.

The technologies that give the largest potential for heat recovery are on-site heat recovery and heat-to-electricity. On-site heat recovery can recover a significant part of the waste heat for the <100 °C demand. This is due to the largest part of the waste heat being situated in the 100-200 °C range. Heat at these temperatures can easily be recovered with heat exchangers for practically any process. For the demand in the range of 100-500 °C however, on-site heat recovery shows practically no potential. Only demand in the range of 500-1000 °C can again be supplied by recovered heat in heat exchangers. This means that there is a gap in waste heat recovery for the mid-range demand temperatures. A heat pump that can deliver heat at these temperatures might fill that gap. The waste heat that could be used for these heat pumps can be the waste heat currently allocated to heat-to-electricity potential. However, heat-to-electricity only becomes competitive for larger temperatures [17]. Heat pumps provide a significantly more efficient way to recover energy than heat-to-electricity when looking at the energy balance. Therefore, the potential exists that heat pumps will be the preferred solution.

If we assume that the 100-500 °C heat demand range can be reached by a heat pump, it becomes possible to utilize the 100-200 °C waste heat range, if the industries match. This is the case for the chemicals industry, the food and drink industry, the aero/auto industries and other industries. The iron & steel sector shows significant waste heat in the 200-300 °C range, however, their heat demand does not fall in the 100-500 °C.

In a study by Papapetrou et al. (2018), the heat consumption per industrial sector in the European Union was investigated. It used the results of Hammond & Norman (2014) for the 2000-2004 UK

industry and extrapolated these to EU energy levels in 2015. The results are shown in Figure 3.5a. In a follow-up study by Kosmadakis [29], these results were further broken down into more detailed temperature ranges, which are shown in Figure 3.5b. These results show that especially in the chemical industry, a large heat demand exists for the temperature range of 200-500 °C. This is followed by the paper industry, machinery and transport equipment.

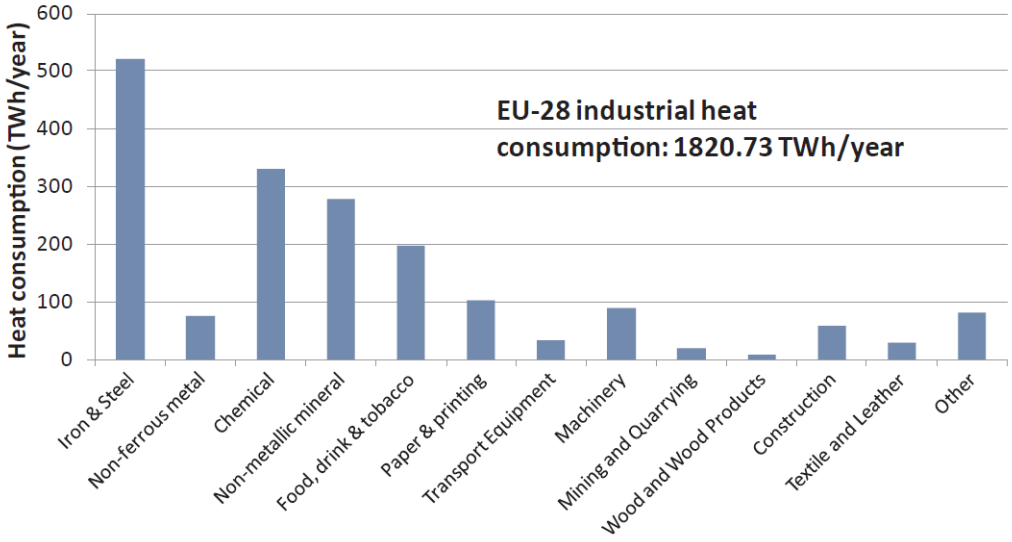


**(a)** EU heat consumption in 2015 per industry [10].

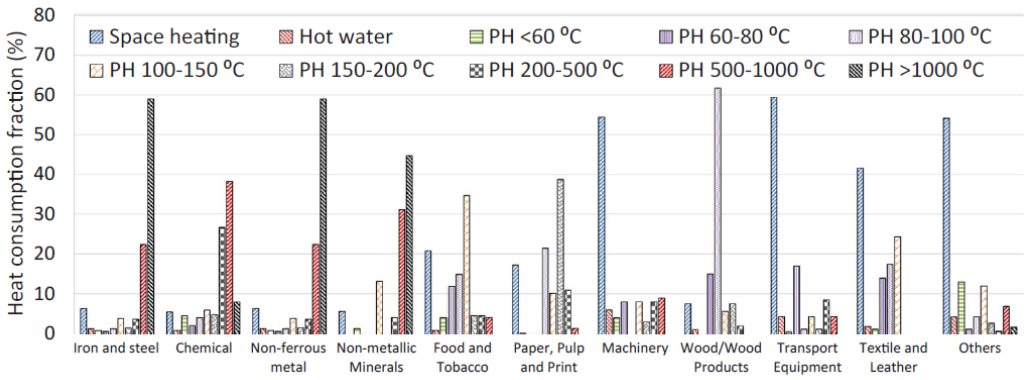


**(b)** Fractions of heat consumption per industry and per temperature range [29].

**Figure 3.5:** Total annual heat consumed in the European Union per industrial sector and per temperature range [39, 29].

Composing possible heat pump applications from this data is very hard to impossible, as it does not describe site-specific details concerning the arrangement of processes. It can only be used to derive an insight into relative heat pump necessity.

### 3.2.2 Based on specific processes

In a study carried out by Marina et al. (2021), a large data set was established to identify potential heat pump applications in the European Union. It lists different kinds of industrial processes with their required temperatures and heat demand, as well as accompanying waste heat streams with their respective temperatures and total heat content. On top of that, the process media are mentioned. The industrial sectors included are the paper, chemical, refinery and food industries. The processes which have a sink temperature above 200 °C are extracted and shown in Table 3.1. For the chemical industry, most chemicals are made with temperatures <200 °C. The oxy-alcohols lie only marginally outside this bound. The production of Phthalic anhydride requires temperatures of 220-240 °C, which is achieved using hot oil. This process produces waste heat streams of condensate at 200 °C. Moreover, the quantities of sink heat demand and source heat supply are comparable. This process is therefore promoted as a possible HTHP application [33]. The refinery industry has more processes

that are >200 °C. As can be seen, most processes currently use fuel-firing to achieve the required temperatures. The temperature lift can however not be too large as the CoP will become too low. In this regard, the refinery processes of catalytic cracking and hydrocracking seem to be the most promising potential for HTHP integration.

| **Process data** | | **Process heat** | | | **Waste heat** | | |
|---|---|---|---|---|---|---|---|
| **Industry** | **Process** | $\dot{Q}_H$[TJ/a] | $T_H$[°C] | **Medium** | $\dot{Q}_C$[TJ/a] | $T_C$[°C] | **Medium** |
| Chemical | Oxy-alcohols | 570 | 203 | Steam | 248 | 126-125 | Condensate |
| Chemical | Phthalic anhydride | 2508 | 220-240 | Hot oil | 2675 | 201-200 | Condensate |
| | | 2675 | 220-240 | Hot oil | 2842 | 201-200 | Condensate |
| Chemical | Propyleenglycol | 1127 | 203 | Steam | 1288 | 127-40 | Hot oil |
| Refinery | Catalytic cracking | 14489 | 210-217 | Waste heat | 24086 | 123-82 | Condensate |
| Refinery | Catalytic reforming | 22136 | 210-216 | Fuel | 12678 | 136-45 | Air |
| Refinery | Crude distillation | 160992 | 250-350 | Fuel | 80496 | 130-32 | Air |
| Refinery | Hydrocracking | 21672 | 330-345 | Fuel | 9288 | 210-170 | - |
| | | 13622 | 290-340 | Fuel | 12384 | 70-32 | Air |
| Refinery | Hydrotreating | 63809 | 310-330 | Fuel | 14180 | 140-30 | Air |
| Refinery | Thermal cracking | 37926 | 336-473 | Fuel | 19722 | 124-36 | Air |
| | | 4551 | 240-270 | Heat recovery | 1517 | 74-36 | Condensate |
| Refinery | Vacuum distillation | 108670 | 225-400 | Fuel | 25078 | 100-44 | Condensate |

**Table 3.1:** Industrial processes in the European Union showing the amount of heat, corresponding temperatures and the medium which contains this heat for both the process itself and the accompanying waste stream. From the original data, only the process with sink temperatures above 200 °C are selected [33].

## 3.3 Limitations to higher temperatures

Developing heat pumps for higher temperatures leads to increasing difficulties. These have prevented attempts to achieve temperatures sink temperatures above 200 °C. The limitations have been identified:

1. High compressor discharge temperatures that significantly overshoot the sink temperature level. This leads to material and sealing issues [7, 16].
2. High pressures required with conventional working fluids to reach the required sink temperature level [7]. It depends on the VHC whether pressure levels are problematic. If the VHC is low, the components can be small and high pressure can be handled more easily. $CO_2$ has a low VHC and systems can work with pressures reaching 150 °C. Water on the other hand has a high VHC and the size of the components limits the feasible operating pressure to around 25 bar [16, 3]. With transcritical cycles, one can implement superheating before compression to achieve the required sink temperature levels without needing very high pressures [16].
3. Generally, large temperature lifts are necessary for HTHP applications. This limits the efficiency of the system and the corresponding compression ratio may be too large for current compressor technology. Moreover, large overall compression ratios increase subsequent expansion losses [2].
4. Lubrication oil of the compressor, which degrades at higher temperatures. This first leads to decreased lubricity, oil tightness and eventually to chemical decomposition and coking [3]. Furthermore, the oil should be miscible with the refrigerant [2]. For temperatures above about 150 °C, oil becomes problematic to use [3].
5. Difficulty in finding suitable working fluids. Due to the long list of criteria for working fluids, compromises inevitably need to be made. This is in conjunction with the desired operating pressures, efficiency and equipment cost [2].
6. Lacking knowledge of market potential which prevents investments in HTHP technology for further development [3].

7. Large investment costs are necessary compared to acquiring heat from fossil fuels or direct electric heating [3].

## 3.4 Possible solutions to achieve higher temperatures

Several options to alleviate the limitations of Section 3.3 exist. Even though some are overlapping, possible solutions could be defined for each limitation:

1. Intercooling is an option to decrease the discharge temperature, while it could also improve efficiency. Despite that, it usually implies increased cost and complexity to the system [2]. Alternatively, liquid injection in the compressor is possible to cool the gas during compression [32, 24].
2. To decrease the required pressure level, working fluids can be selected with favourable thermodynamic properties. For subcritical cycles, a high critical temperature combined with a low critical pressure allows for high-temperature operation with low pressures. When high pressure levels are necessary, selecting a working fluid with a low VHC can allow small component sizes and therefore more ease with handling the high pressures. Moreover, a type of compressor can be selected that is especially capable of working with higher pressures.
3. To increase the efficiency of the system, advanced cycles like parallel compression and/or multistaging with intercooling can be used. Multistaging could also solve the issue of compression ratios being too large, yet possibly at the expense of efficiency, simplicity and costs. Apart from that, a compressor type can be selected with the largest possible isentropic efficiency. The choice of working fluid also influences the efficiency that can be reached for a certain temperature lift. Matching the working fluid temperature glides to that of the waste and process fluids is important to minimise irreversibilities. Matching inclined temperature glides can be achieved with trans- or supercritical systems, or with a zeotropic mixture of substances [24]. Another improvement is to use an expander in the place of the expansion valve, thereby recovering some of the energy in the return flow. Furthermore, the minimum temperature difference in the heat exchangers can be decreased, which improves efficiency but also increases heat exchanger size [32, 2].
4. One obvious solution is to find lubricants that fulfil the requirements of HTHPs. Another solution is to use oil-free compressors. These are however usually compromised on isentropic efficiency [2].
5. Comparing the available working fluids against each other for different types of system setups is an option to find good matches. Another option is to perform research into substances that have not yet been thermodynamically characterised.
6. Pursue market research projects to increase the incentive for technology development.
7. Perform a techno-economic evaluation to take equipment and maintenance costs into account to arrive at the most cost-effective product. This is however subject to constantly changing industry dynamics and policies. In the end, new technologies are usually more expensive than existing ones. To prevent limitations on innovation, the economic side of heat pumps has been mostly left out of the scope of the report.

# Chapter 4

# HP model: Design & Modelling Methodology

Answering the research questions involves finding solutions to the limitation posed in Section 3.3. For that purpose, a heat pump model is necessary which can simulate different working fluids for multiple cycle configurations in the temperature ranges of interest. Therefore, a modular heat pump model was developed which had the flexibility to simulate practically any type of heat pump. This section describes how these models were developed and what considerations and assumptions have been taken in the process. First, the fundamental structure is discussed Section 4.1 explaining which steps the model takes in which succession. Then, in Section 4.2 the inputs that the model takes are discussed together with how these lead to the initial conditions. In Section 4.3, the modelling of individual components is discussed and the corresponding equations are derived. The equations used to calculate the mass, heat and work flow rates are given in Section 4.4. Then in Section 4.5, it is discussed how the performance of the heat pump model is indicated and how these performance indicators are calculated. The components of a heat pump can be configured in different ways and the ones used in this research are discussed in Section 4.6. Lastly, in Section 4.7 it is shown how this model was integrated into a heat pump design tool that allows one to choose a process stream & a waste stream and fully configure a heat pump that optimally conforms to these streams.

## 4.1 Structure of the model

The structure of the model is shown in the process flow diagram of Figure 4.1. The model is designed to simulate a heat pump under steady-state conditions from a set of inputs defining the heat pump. The underlying working principle is that the inlet conditions of a component are used to calculate the outlet conditions. These outlet conditions then form the inlet conditions of the next component in the cycle. These conditions are the state properties temperature, pressure, specific enthalpy, specific entropy, specific flow exergy and relative mass flow rate. The relative mass flow rate is defined as the mass flow rate per unit of mass flow rate that flows through the evaporator.

**Calculate initial conditions** The initial conditions are calculated from the inputs. These inputs define the operating point of the heat pump, the working fluid, the setup and sequence of the components and the parameters of the components. These allow the model to calculate the outlet conditions of the evaporator and the condenser. Furthermore, the pressure levels for the entire heat pump are calculated. These are then fed to the model. The declaration of the inputs and the way these initial conditions are calculated is further explained in Section 4.2.

**Next component in the sequence** The model checks the component sequence to find out what the next component in the cycle is. If this component is the first in the sequence, the initial conditions are passed on as inlet conditions of this component. If this component is not the first, then the outlet conditions of the previous component are passed on as inlet conditions to this component. The first component is always the next component after the evaporator.

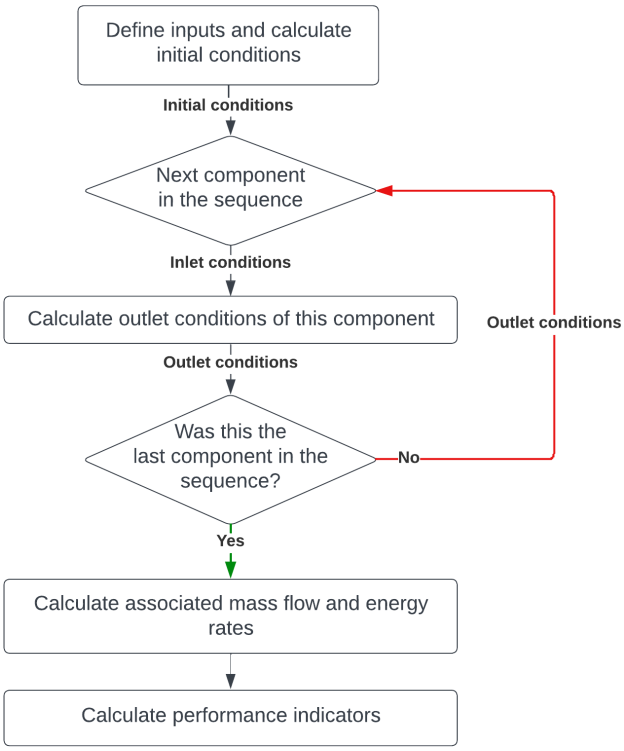


**Figure 4.1:** The process flow diagram of the heat pump model.

**Calculate outlet conditions of this component** The inlet conditions are used to calculate the outlet conditions of this component. The way the outlet conditions are calculated depends on the component and is explained in Section 4.3.

**Was this the last component in the sequence?** The model checks the component sequence to find out if the last component in the cycle has been calculated. If this is not the case, the outlet conditions of the previous component are sent back to the next component block. If the last component in the cycle has been calculated, the results are passed on to the energy and mass flow rate calculation block

**Calculate associated energy and mass flow rates** The results of the calculation are used together with the inputs to calculate the mass flow rates at each point in the cycle. These are then used to calculate for each component: the heat transfer rate, the power, the entropy production and the exergy destruction. The way these are calculated is explained in Section 4.4.

**Calculate performance indicators** The calculated energies can be used to calculate the parameters that define the efficiency and capacity of the heat pump. These are the Coefficient of Performance (CoP), the Volumetric Heat Capacity (VHC) and the exergy efficiency ($\eta_{ex}$). The way these are calculated is explained in Section 4.5.

The models are made in MatLab and the fluid properties are evaluated using REFPROP [20]. The working fluids that were used are listed in Chapter A together with some important characteristics. The fluids are referred to by the names in this list, which can be either a formula like C3CC6, an abbreviation like DMC or a shorter name like cyclohex. The equations of state that were used depend on the specific working fluid that was chosen. In each case, the default setting has been used.

## 4.2 Inputs and initial conditions

This section defines the inputs that the model uses and how these are used to calculate the initial conditions.

### 4.2.1 Definition of inputs

The following inputs can be supplied to the model:

1. **Sequence**: Different components can be arranged in various orders to make different configurations. The sequence defines the order in which the working fluid passes the components, starting from the first component after the evaporator. The sequence thereby also defines the configuration of the heat pump. All configurations contain one evaporator and one condenser, which are modelled as indirect-contact heat exchangers. Other components, which are shown in Section 4.3, can be added by inserting them in the sequence. The cycles used for the results are shown with their sequence in Section 4.6.
2. **Fluid**: The fluid input defines which fluid is to be used as the working fluid.
3. **Evaporator outlet temperature**: The evaporator outlet temperature ($T_{\mathrm{C},e}$) defines the desired temperature of the working fluid at the outlet of the evaporator.
4. **Evaporator pressure level**: This input defines the pressure of the working fluid in the evaporator ($p_{\mathrm{C}}$). This pressure can be set to the saturation pressure at a certain temperature $T_{\mathrm{C,sat}}$, which should be equal to or less than $T_{\mathrm{C},e}$. If $T_{\mathrm{C,sat}} = T_{\mathrm{C},e}$, then the evaporator delivers a fluid at a saturated or 2-phase state. If $T_{\mathrm{C,sat}} < T_{\mathrm{C},e}$, then the evaporator outlet is in a superheated state, with the difference between the temperatures being the degree of evaporator superheating: $\Delta T_{\mathrm{C,SH}} = T_{\mathrm{C},e} - T_{\mathrm{C,sat}}$. The evaporator pressure can however also be set above the critical pressure of the fluid. In that case, the fluid is not evaporating in the heat exchanger, nevertheless the name 'evaporator' is kept to avoid confusion. This situation implies the condenser will also have to be at supercritical conditions and thus a supercritical cycle is simulated.
5. **Evaporator outlet quality**: The evaporator outlet quality defines the quality of the vapour at the evaporator outlet. This input is used in case the evaporator pressure level is set to the saturation pressure at the temperature of the evaporator outlet, so $T_{\mathrm{C,sat}} = T_{\mathrm{C},e}$. It allows for the simulation of a less-than-saturated vapour exiting the evaporator. Such could be the case if not enough heat was transferred to the evaporator to fully evaporate the fluid, or if the vapour drags liquid droplets with it out of the outlet.
6. **Condenser outlet temperature**: The condenser outlet temperature ($T_{\mathrm{H},e}$) defines the desired temperature of the working fluid at the outlet of the condenser.
7. **Condenser pressure level**: This input defines the pressure of the working fluid in the condenser ($p_{\mathrm{H}}$). This pressure can be set to the saturation pressure at a certain temperature $T_{\mathrm{H,sat}}$, which should be equal to or greater than $T_{\mathrm{H},e}$. If $T_{\mathrm{H,sat}} = T_{\mathrm{H},e}$, then the condenser delivers a fluid at a saturated or 2-phase state. If $T_{\mathrm{H,sat}} > T_{\mathrm{H},e}$, then the condenser outlet is in a subcooled state, with the difference between the temperatures being the degree of condenser subcooling: $\Delta T_{\mathrm{H,SC}} = T_{\mathrm{H,sat}} - T_{\mathrm{H},e}$. The condenser pressure can however also be set above the critical pressure of the fluid. In that case, the fluid is not condensing in the heat exchanger, nevertheless the name 'condenser' is kept to avoid confusion. In this situation, the evaporator can be at subcritical or supercritical conditions. In the former case, a transcritical cycle is simulated, in the latter case a supercritical cycle.
8. **Condenser outlet quality**: The condenser outlet quality ($x_{\mathrm{H},e}$) defines the quality of the liquid at the condenser outlet. This input is used in case the condenser pressure level is set to the saturation pressure at the temperature of the condenser outlet, so $T_{\mathrm{H,sat}} = T_{\mathrm{H},e}$. It allows to simulate a less-than-saturated liquid exiting the condenser. Such could be the case if not enough heat was transferred away from the condenser to fully condense the fluid, or if the liquid drags vapour bubbles with it out of the outlet.
9. **Compressor isentropic efficiency**: The compressor isentropic efficiency $\eta_{\mathrm{CP}}$ defines the efficiency of the compressor compared to an ideal compressor, i.e. a compressor without irreversibilities. It is assumed that, if there are multiple compressors in one configuration, they all have the same isentropic efficiency.
10. **Expander isentropic efficiency**: The expander isentropic efficiency $\eta_{\mathrm{XP}}$ defines the efficiency of an expander compared to an ideal expander, i.e. an expander without irreversibilities. This setting is only needed when the cycle includes an expander. It is assumed that, if there

are multiple expanders in one configuration, they all have the same isentropic efficiency. Since this value is constant, it is assumed that it is independent of the compression ratio.

11. **ICHX setting**: If the configuration includes an indirect-contact heat exchanger, this input is used. It defines the amount of heat transfer happening in this heat exchanger. If the heat exchanger is one with a predefined heat load, as in Figure 4.2, then the amount of heat transfer $\dot{Q}_{\mathrm{HX}}$ needs to be specified. If the heat exchanger is of the type with two fluid streams, as in Figure 4.3, then either the change in temperature $\Delta T_{\mathrm{HX}}$ or the change specific enthalpy $\Delta h_{\mathrm{HX}}$ can be specified. Furthermore, it needs to be specified which of the two fluid streams this change should be applied to. This fluid stream is then the 'controlled stream' and the other fluid stream is the 'reacting stream'. The model will then make sure that the controlled stream attains the prescribed change in temperature or specific enthalpy in any way and that the reacting stream reacts to make up for this heat transfer. Also, the minimum temperature difference that is allowed to occur in the heat exchanger, $\Delta T_{\mathrm{HX,min}}$, needs to be specified. The model then checks if the temperature difference inside the exchanger does not drop below the specified minimum temperature difference.

12. **Waste heat supply or process heat demand**: This setting defines the rate at which waste heat energy is supplied, $\dot{Q}_{\mathrm{C}}$, or the rate at which process heat is demanded, $\dot{Q}_{\mathrm{H}}$. The former allows to define a set amount of waste heat, after which the model calculates how much process heat can be delivered. The latter allows to define a set amount of process heat, after which the model calculates how much waste heat is required. Irrespective of which is used, using the relative mass flow rate, the absolute mass flow rates at each point in the heat pump can be calculated. This input only defines the size and capacity of the heat pump system but does not influence the operating conditions or performance indicators. They are independent of system size and therefore apply for any heat load.

13. **Environmental temperature and pressure**: The environmental temperature $T_0$ and pressure $p_0$ are used for the reference state in the exergy analysis. The reference state can then be evaluated with:

$$h_0 = h\left(p = p_0, T = T_0\right) \qquad \& \qquad s_0 = s\left(p = p_0, T = T_0\right). \tag{4.1}$$

### 4.2.2 Calculation of initial conditions

With the evaporator and condenser pressure levels known, the overall pressure ratio can be calculated:

$$r_{\mathrm{cycle}} = \frac{p_{\mathrm{H}}}{p_{\mathrm{C}}}. \tag{4.2}$$

The sequence input is checked to retrieve the amount of compression stages $n_{\mathrm{com}}$ and the amount of expansion stages $n_{\mathrm{exp}}$. For multi-stage systems, the intermediate pressure levels are divided logarithmically between the stages such that each compression and expansion stage has the same pressure ratio. This results in the smallest possible pressure ratios and give optimum pressure levels according to Kiss & Ferreira (2017). The individual compression and expansion stage pressure ratios are then:

$$r_{\mathrm{com}} = \left(r_{\mathrm{cycle}}\right)^{\frac{1}{n_{\mathrm{com}}}} \qquad \& \qquad r_{\mathrm{exp}} = \left(r_{\mathrm{cycle}}\right)^{\frac{1}{n_{\mathrm{exp}}}}. \tag{4.3}$$

The evaporator outlet conditions can be calculated using the given inputs. If the evaporator pressure is set to the saturation pressure at $T_{\mathrm{C,sat}} = T_{\mathrm{C},e}$, then the specific enthalpy and entropy at the outlet are calculated using the pressure and the outlet quality:

$$h_{\mathrm{C},e} = h\left(p = p_{\mathrm{C}}, x = x_{\mathrm{C},e}\right) \qquad \& \qquad s_{\mathrm{C},e} = s\left(p = p_{\mathrm{C}}, x = x_{\mathrm{C},e}\right). \tag{4.4}$$

In any other case, then the specific enthalpy and entropy at the outlet are calculated using the pressure and the outlet temperature:

$$h_{\mathrm{C},e} = h\left(p = p_{\mathrm{C}}, T = T_{\mathrm{C},e}\right) \qquad \& \qquad s_{\mathrm{C},e} = s\left(p = p_{\mathrm{C}}, T = T_{\mathrm{C},e}\right). \tag{4.5}$$

The condenser outlet conditions are calculated with the same reasoning. If the pressure is set to the saturation pressure at $T_{\mathrm{H,sat}} = T_{\mathrm{H},e}$, then:

$$h_{\mathrm{H},e} = h\left(p = p_{\mathrm{H}}, x = x_{\mathrm{H},e}\right) \qquad \& \qquad s_{\mathrm{H},e} = s\left(p = p_{\mathrm{H}}, x = x_{\mathrm{H},e}\right), \tag{4.6}$$

else:

$$h_{\mathrm{H},e} = h\left(p = p_{\mathrm{H}}, T = T_{\mathrm{H},e}\right) \qquad \& \qquad s_{\mathrm{H},e} = s\left(p = p_{\mathrm{H}}, T = T_{\mathrm{H},e}\right). \tag{4.7}$$

The specific flow exergy can be calculated for both the evaporator and condenser outlet with the general formula:

$$e_{\mathrm{f}} = (h - h_0) - T_0\left(s - s_0\right). \tag{4.8}$$

## 4.3 Component models

The models make use of the fundamental thermodynamic laws derived at steady-state with the assumption that gravitational and kinetic effects can be neglected in all cases. With these conditions, the thermodynamic laws can be simplified before evaluating them for the different components. Using information and conventions from Moran et al. (2018), the mass, energy, entropy and exergy balances are retrieved:

1) Mass:
$$\sum_i \dot{m}_i = \sum_e \dot{m}_e \tag{4.9}$$

2) Energy:
$$\sum_j \dot{Q}_j - \sum_k \dot{W}_k = \sum_e \dot{m}_e h_e - \sum_i \dot{m}_i h_i \tag{4.10}$$

3) Entropy:
$$\sum_j \frac{\dot{Q}_j}{T_j} = \sum_e \dot{m}_e s_e - \sum_i \dot{m}_i s_i - \dot{\sigma}_{\mathrm{CV}} \tag{4.11}$$

4) Exergy:
$$\sum_j \left(1 - \frac{T_0}{T_j}\right) \dot{Q}_j - \sum_k \dot{W}_k = \sum_e \dot{m}_e e_{\mathrm{f},e} - \sum_i \dot{m}_i e_{\mathrm{f},i} + \dot{E}_{\mathrm{d}} \tag{4.12}$$

Here, $\dot{m}$ is the mass flow rate, $\dot{Q}$ is the heat flow rate into the system (if negative, heat flows out of the system), $\dot{W}$ is the work delivered by the system (if negative, work is supplied to the system), $h$ is the specific enthalpy, $T$ is the temperature of the surface at which the heat transfer takes place, $s$ is the specific entropy, $\dot{\sigma}_{\mathrm{CV}}$ is the entropy destruction rate, $e_{\mathrm{f}}$ is the specific flow exergy and $\dot{E}_{\mathrm{d}}$ is the exergy destruction rate. The subscripts $i$ and $e$ signify inlet and exit (outlet). The inlet conditions are always known properties in this model. The balances will be used to calculate the outlet conditions of the component. When two state properties are known, other state properties are evaluated using REFPROP 9.0 [20].

For all components, if the fluid is in the two-phase regime, the temperature $T$ is taken to be the saturation temperature. Otherwise, if the fluid is outside the two-phase regime, the temperature $T$ is approximated as the thermodynamically averaged temperature [35, 28, 55]:

$$T = \frac{T_e - T_i}{\ln \frac{T_e}{T_i}}. \tag{4.13}$$

The heat pumps modelled in this project consist of different types of heat exchangers, compressors, expansion valves and expanders. A brief description of how each component is modelled will be given here.

### 4.3.1 Heat exchangers

Heat exchangers allow heat to be transferred to and from a substance. All heat exchangers are assumed to have no pressure drop across them and are therefore isobaric components. Heat loss to the environment is neglected.

**Indirect-contact heat exchanger (ICHX) with predefined heat load** In this heat exchanger, a fluid is heated by a known amount of input heat energy $Q$. A diagram can be seen in Figure 4.2 where the system boundary is the rectangle. In this report, the condensers and evaporators are modelled like this type of heat exchanger. The thermodynamic balances of Equation (4.9)

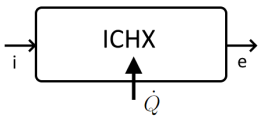


**Figure 4.2:** Indirect-contact heat exchanger with predefined heat load.

can be reduced to the following for this type of heat exchanger:

| | |
|---|---|
| 1) Mass: | $\dot{m}_i = \dot{m}_e = \dot{m}$ |
| 2) Energy: | $\dot{Q} = \dot{m}(h_e - h_i)$ |
| 3) Entropy: | $\frac{\dot{Q}}{T} = \dot{m}(s_e - s_i) - \dot{\sigma}_{\mathrm{CV}}$ |
| 4) Exergy: | $\left(1 - \frac{T_0}{T}\right)\dot{Q} = \dot{m}(e_{\mathrm{f},e} - e_{\mathrm{f},i}) + \dot{E}_{\mathrm{d}}$ |

Since the inlet enthalpy and relative mass flow rate are known, the outlet enthalpy can be calculated with:

$$h_e = h_i + \frac{\dot{Q}}{\dot{m}}. \tag{4.14}$$

With the outlet pressure also known ($p_e = p_i$), the other state properties can be evaluated with REFPROP. An ICHX with a predefined heat load can be called up with 'ICHX-Q' in the component sequence.

Alternatively, this heat exchanger can be used as an evaporator or condenser. The outlet state properties are in those cases already known from the initial conditions. A condenser or evaporator is called up with 'CD' or 'EV', respectively, in the component sequence.

It is possible that the fluid is highly superheated when entering the condenser and has a much larger temperature than the saturation temperature. In this project, it is assumed that the condenser can cope with this superheat in any case and that no special desuperheating is necessary.

**Indirect-contact heat exchanger (ICHX) with two fluid streams** This heat exchanger consists of two separated fluid streams, one colder than the other. The hotter fluid gives off its heat to the colder fluid without coming into contact with each other. This allows both streams to be at different pressures, and also to be substances of different kinds. A diagram can be seen in Figure 4.3. The system boundary is again the rectangle.

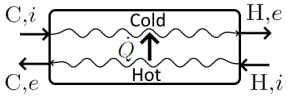


**Figure 4.3:** Indirect-contact heat exchanger with two fluid streams.

The thermodynamic balances of Equation (4.9) can be reduced to the following for this type of heat exchanger:

| | |
|---|---|
| 1) Mass: | $\dot{m}_{\mathrm{C},i} = \dot{m}_{\mathrm{C},e} = \dot{m}_C$ |
| | $\dot{m}_{\mathrm{H},i} = \dot{m}_{\mathrm{H},e} = \dot{m}_H$ |
| 2) Energy: | $0 = \dot{m}_{\mathrm{C}}(h_{\mathrm{C},e} - h_{\mathrm{C},i}) + \dot{m}_{\mathrm{H}}(h_{\mathrm{H},e} - h_{\mathrm{H},i})$ |
| 3) Entropy: | $0 = \dot{m}_{\mathrm{C}}(s_{\mathrm{C},e} - s_{\mathrm{C},i}) + \dot{m}_{\mathrm{H}}(s_{\mathrm{H},e} - s_{\mathrm{H},i}) - \dot{\sigma}_{\mathrm{CV}}$ |
| 4) Exergy: | $0 = \dot{m}_{\mathrm{C}}(e_{f\mathrm{C}e} - e_{f\mathrm{C}i}) + \dot{m}_{\mathrm{H}}(e_{f\mathrm{H}e} - e_{f\mathrm{H}i}) + \dot{E}_{\mathrm{d}}$ |

Which stream is the controlling stream and which is the reacting stream depends on the inputs. It can also differ whether the controlled stream is controlled by a temperature change or an enthalpy change. If the cold stream is the controlled stream and an enthalpy change $\Delta h_{\mathrm{HX}}$ has been specified, then:

$$h_{\mathrm{C},e} = h_{\mathrm{C},i} + \Delta h_{\mathrm{HX}}. \tag{4.15}$$

Alternatively, if a temperature change $\Delta T_{\mathrm{HX}}$ has been specified, then the outlet temperature of the cold stream is:

$$T_{\mathrm{C},e} = T_{\mathrm{C},i} + \Delta T_{\mathrm{HX}}. \tag{4.16}$$

The outlet enthalpy of the cold stream is then $h_{\mathrm{C},e} = h\left(p = p_{\mathrm{C}}; T = T_{\mathrm{C},e}\right)$.

In either case, the outlet enthalpy of the hot stream (the reacting stream) can then be calculated with:

$$h_{\mathrm{H},e} = h_{\mathrm{H},i} - \frac{m_{\mathrm{C}}}{m_{\mathrm{H}}}\left(h_{\mathrm{C},e} - h_{\mathrm{C},i}\right). \tag{4.17}$$

The remaining state properties can then be evaluated with REFPROP, as for each in/outlet the enthalpy and pressure are known. A controlling or reacting side ICHX is called up with 'ICHX$_{\mathrm{c}}$' or 'ICHX$_{\mathrm{r}}$', respectively, in the component sequence. When referring to the heat exchanger as a whole, just 'ICHX' is used.

**Direct-contact heat exchanger (DCHX)** This heat exchanger has two fluid streams which are allowed to mix and thereby exchange heat. The resulting single fluid stream leaves the heat exchanger, as seen in Figure 4.4. In general, the streams entering the heat exchanger are of the same substance. Moreover, the inlet and outlet pressures are all equal and perfect mixing is assumed.

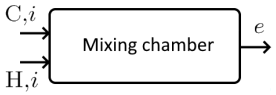


**Figure 4.4:** Schematic representation of direct-contact heat exchanger.

The thermodynamic balances of Equation (4.9) can be reduced to the following for this type of heat exchanger:

| | |
|---|---|
| 1) Mass: | $\dot{m}_e = \dot{m}_{\mathrm{C},i} + \dot{m}_{\mathrm{H},i}$ |
| 2) Energy: | $0 = \dot{m}_e h_e - \dot{m}_{\mathrm{C},i} h_{\mathrm{C},i} - \dot{m}_{\mathrm{H},i} h_{\mathrm{H},i}$ |
| 3) Entropy: | $0 = \dot{m}_e s_e - \dot{m}_{\mathrm{C},i} s_{\mathrm{C},i} - \dot{m}_{\mathrm{H},i} s_{\mathrm{H},i} - \dot{\sigma}_{\mathrm{CV}}$ |
| 4) Exergy: | $0 = \dot{m}_e e_{\mathrm{f},e} - \dot{m}_{\mathrm{C},i} e_{\mathrm{fC},i} - \dot{m}_{\mathrm{H},i} e_{\mathrm{fH},i} + \dot{E}_{\mathrm{d}}$ |

With the inlet states known, the outlet state can thus be calculated with:

$$h_e = \frac{\dot{m}_{\mathrm{C},i} h_{\mathrm{C},i} + \dot{m}_{\mathrm{H},i} h_{\mathrm{H},i}}{\dot{m}_{\mathrm{C},i} + \dot{m}_{\mathrm{H},i}}. \tag{4.18}$$

The other state properties can then be evaluated using REFPROP since the outlet enthalpy and the pressure are known. A DCHX is called up with 'DCHX' in the component sequence.

**Direct-contact heat exchanger with flash chamber (**DCHX$_{\mathrm{FC}}$**)** The direct-contact heat exchanger can also be combined with a flash chamber in which the vapour and liquid are separated from each other by gravity. It therefore has two outlets, one at the top for the vapour and one at the bottom for the liquid, as seen in Figure 4.5. The flash chamber is assumed to achieve perfect separation such that pure saturated vapour leaves from the top outlet while pure saturated liquid leaves from the bottom outlet.

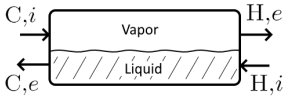


**Figure 4.5:** Schematic representation of a direct-contact heat exchanger combined with a flash chamber.

The thermodynamic balances of Equation (4.9) can be reduced to the following for this type of heat

exchanger:

| | |
|---|---|
| 1) Mass: | $\dot{m}_{\mathrm{C},e} + \dot{m}_{\mathrm{H},e} = \dot{m}_{\mathrm{C},i} + \dot{m}_{\mathrm{H},i}$ |
| 2) Energy: | $0 = \dot{m}_{\mathrm{C},e} h_{\mathrm{C},e} + \dot{m}_{\mathrm{H},e} h_{\mathrm{H},e} - \dot{m}_{\mathrm{C},i} h_{\mathrm{C},i} - \dot{m}_{\mathrm{H},i} h_{\mathrm{H},i}$ |
| 3) Entropy: | $0 = \dot{m}_{\mathrm{C},e} s_{\mathrm{C},e} + \dot{m}_{\mathrm{H},e} s_{\mathrm{H},e} - \dot{m}_{\mathrm{C},i} s_{\mathrm{C},i} - \dot{m}_{\mathrm{H},i} s_{\mathrm{H},i} - \dot{\sigma}_{\mathrm{CV}}$ |
| 4) Exergy: | $0 = \dot{m}_{\mathrm{C},e} e_{\mathrm{fC},e} + \dot{m}_{\mathrm{H},e} e_{\mathrm{fH},e} - \dot{m}_{\mathrm{C},i} e_{\mathrm{fC},i} - \dot{m}_{\mathrm{H},i} e_{\mathrm{fH},i} + \dot{E}_{\mathrm{d}}$ |

Due to the assumptions that pure saturated vapour and liquid leave from the outlets and that the entire heat exchanger is at the same pressure level $p_{\mathrm{HX}}$, the outlet enthalpies can be evaluated with REFPROP using:

$$h_{\mathrm{C},e} = h\left(p = p_{\mathrm{HX}}, x = 0\right) \qquad h_{\mathrm{H},e} = h\left(p = p_{\mathrm{HX}}, x = 1\right). \tag{4.19}$$

The other state properties can be evaluated equivalently. In many cases in heat pumps, the mass flow rates of this type of heat exchanger are equal in pairs. That is due to one outlet, after being routed through other components, usually coming back to one of the inlets. Taking Figure 2.13 as an example, the saturated vapour outlet 'He' comes back to the inlet '$\mathrm{C}, i$' after having passed through a compressor, the condenser and an expansion valve. Similarly, the saturated liquid outlet '$\mathrm{C}, e$' comes back to the inlet '$\mathrm{H}, i$'. Therefore:

$$\dot{m}_{\mathrm{H},e} = \dot{m}_{\mathrm{C},i} \qquad \& \qquad \dot{m}_{\mathrm{C},e} = \dot{m}_{\mathrm{H},i}. \tag{4.20}$$

Then, both mass flow rates can be related to each other using the thermodynamic balances:

$$\frac{\dot{m}_{\mathrm{H},e}}{\dot{m}_{\mathrm{H},i}} = \frac{\dot{m}_{\mathrm{C},i}}{\dot{m}_{\mathrm{C},e}} = \frac{h_{\mathrm{H},i} - h_{\mathrm{C},e}}{h_{\mathrm{H},e} - h_{\mathrm{C},i}}. \tag{4.21}$$

In the component sequence, this type of heat exchanger is separated into two parts. One is the 'Hot' side, which has the '$\mathrm{H}, i$' inlet and the '$\mathrm{H}, e$' outlet. The other is the 'Cold' side, which has the '$\mathrm{C}, i$' inlet and the '$\mathrm{C}, e$' outlet. A hot or cold side DCHX with a flash chamber is called up with '$\mathrm{DCHX_{FC,h}}$' or '$\mathrm{DCHX_{FC,c}}$', respectively, in the component sequence.

### 4.3.2 Machinery

This section describes the considerations and assumptions taken into account while modelling the mechanical components used in a heat pump. All components are assumed to operate adiabatically, without any heat transfer to or from the environment. The components are modelled with a certain isentropic efficiency, accounting for the irreversibilities in the process.

**Compressors and pumps** The compressors compress a gas (mostly dry gas but sometimes also wet) to an elevated pressure level, while pumps achieve the same for liquids. In Figure 4.6 a schematic representation is shown.

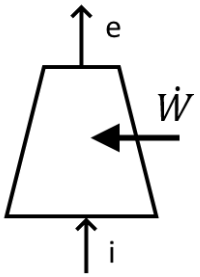


**Figure 4.6:** Schematic representation of a compressor.

The thermodynamic balances of Equation (4.9) can be reduced to the following for both the compressors and pumps:

| | |
|---|---|
| 1) Mass: | $\dot{m}_i = \dot{m}_e = \dot{m}$ |
| 2) Energy: | $\dot{W} = \dot{m}(h_i - h_e)$ |
| 3) Entropy: | $0 = \dot{m}(s_i - s_e) + \dot{\sigma}_{\mathrm{CV}}$ |
| 4) Exergy: | $\dot{W} = \dot{m}(e_{\mathrm{f},i} - e_{\mathrm{f},e}) - \dot{E}_{\mathrm{d}},$ |

The inlet pressure $p_i$ and the compression pressure ratio $r_{\text{com}}$ are known. The outlet pressure is thus: $p_e = r_{\text{com}} p_i$. Then, the outlet enthalpy is to be determined. To this end, the assumption is made that the compressor operates with a certain isentropic efficiency $\eta_{\text{CP}}$. The outlet enthalpy can then be calculated with:

$$h_e = h_i + \frac{h_{e,\text{s}} - h_i}{\eta_{\text{CP}}} \tag{4.22}$$

with isentropic outlet enthalpy: $h_{e,\text{s}} = h(p = p_e, s = s_i)$. The other state properties can then be evaluated with REFPROP since the outlet enthalpy and pressure are known. A compressor or pump is called up with 'CP' in the component sequence.

**Expanders** For expanders, a similar analysis as for the compressors and pump is conducted and their thermodynamic balances appear to be the same. They have an isentropic efficiency of $\eta_{\text{XP}}$, and their outlet enthalpy $h_e$ can be calculated with:

$$h_e = h_i + \eta_{\text{XP}}(h_{e,\text{s}} - h_i), \tag{4.23}$$

where $h_{e,\text{s}} = h(p = p_e, s = s_i)$ is the isentropic outlet enthalpy. The other state properties can now be evaluated in the same way as for the compressor. An expander is called up with 'XP' in the sequence.

### 4.3.3 Expansion valves

Expansion valves induce a pressure differential to the flow that passes it. They are assumed to operate adiabatically, so there is no heat transfer to or from the surroundings. They therefore operate isenthapically. A schematic representation is shown in Figure 4.7.


**Figure 4.7:** Schematic representation of an expansion valve.

The thermodynamic balances of Equation (4.9) can be reduced to the following:

| | |
|---|---|
| 1) Mass: | $\dot{m}_i = \dot{m}_e = \dot{m}$ |
| 2) Energy: | $h_i = h_e$ |
| 3) Entropy: | $0 = \dot{m}(s_e - s_i) - \dot{\sigma}_{\text{CV}}$ |
| 4) Exergy: | $0 = \dot{m}(e_{\text{f},e} - e_{\text{f},i}) + \dot{E}_{\text{d}}$ |

The inlet pressure $p_i$ and the expansion pressure ratio $r_{\text{exp}}$ are known. The outlet pressure is thus: $p_e = \frac{p_i}{r_{\text{exp}}}$. The other state properties can then be evaluated with REFPROP since the outlet enthalpy and pressure are known. An expansion valve is called up with 'XV' in the component sequence.

## 4.4 Calculation of energy and mass flow rates

Once the entire heat pump model is determined with a relative mass flow rate, the inlet and outlet enthalpies are known for each component and thus the absolute mass flow rates can be calculated. Subsequently, also the associated energy rates can be calculated.

### 4.4.1 Determination of absolute mass flow rates

If a waste heat supply $\dot{Q}_{\mathrm{C}}$ is given as an input, the absolute mass flow rate through the evaporator, $\dot{m}_{\mathrm{C}}$, can be calculated using the thermodynamic balances given for the indirect-contact heat exchanger with constant heat transfer:

$$\dot{m}_{\mathrm{C}} = \frac{\dot{Q}_{\mathrm{C}}}{h_{\mathrm{C},e} - h_{\mathrm{C},i}}. \tag{4.24}$$

To obtain the absolute mass flow rates at all points in the cycle, the relative mass flow rates should all be multiplied by $\dot{m}_{\mathrm{C}}$. If a process heat demand $\dot{Q}_{\mathrm{H}}$ is given as an input, the absolute mass flow rate through the condenser, $\dot{m}_{\mathrm{H}}$, can be calculated similarly:

$$\dot{m}_{\mathrm{H}} = \frac{\dot{Q}_{\mathrm{H}}}{h_{\mathrm{H},e} - h_{\mathrm{H},i}}. \tag{4.25}$$

To obtain the absolute mass flow rates at all points in the cycle, the relative mass flow rates should be multiplied by $\frac{\dot{m}_{\mathrm{H}}}{\dot{m}_{\mathrm{CD}}}$, where $\dot{m}_{\mathrm{CD}}$ is the relative mass flow rate through the condenser. The division by $\dot{m}_{\mathrm{CD}}$ is needed because of the definition of the relative mass flow rate, which is the mass flow rate per unit of mass flow rate through the evaporator.

### 4.4.2 Calculation of energy rates

The calculation of the energy rates is dependent on the component in question. The equations for the different components are shown here.

For evaporators, condensers or ICHXs with predefined heat loads, the heat transfer rates $\dot{Q}$ can be calculated with the general equation given the thermodynamic balances:

$$\dot{Q} = \dot{m}\left(h_e - h_i\right). \tag{4.26}$$

Then the entropy production and exergy destruction for these components can be calculated with

$$\dot{\sigma}_{\mathrm{CV}} = \dot{m}(s_e - s_i) - \frac{\dot{Q}}{T} \qquad \text{and} \qquad \dot{E}_{\mathrm{d}} = \left(1 - \frac{T_0}{T}\right)\dot{Q} - \dot{m}(e_{\mathrm{f},e} - e_{\mathrm{f},i}). \tag{4.27}$$

For the ICHX with two fluid streams, the DCHX without and with a flash chamber and the expansion valve, the entropy production can be calculated by subtracting the outlet entropies from inlet entropies, the general equation being:

$$\dot{\sigma}_{\mathrm{CV}} = \sum_e \dot{m}_e s_e - \sum_i \dot{m}_i s_i. \tag{4.28}$$

To obtain the exergy destructions for these components, the inlet flow exergies can be subtracted from the outlet flow exergies. The general equation is:

$$\dot{E}_{\mathrm{d}} = \sum_i \dot{m}_i e_{\mathrm{f},i} - \sum_e \dot{m}_e e_{\mathrm{f},e}. \tag{4.29}$$

The equations are fully written out for each component in Section 4.3.

For both the compressor and expander, the entropy productions and exergy destructions can be calculated with:

$$\dot{\sigma}_{\mathrm{CV}} = \dot{m}(s_e - s_i) \qquad \text{and} \qquad \dot{E}_{\mathrm{d}} = \dot{m}(e_{\mathrm{f},i} - e_{\mathrm{f},e}) - \dot{W}. \tag{4.30}$$

The total power input of the cycle, $\dot{W}_{\mathrm{cycle}}$, is calculated by summing all compressor powers and subtracting all expanders powers:

$$\dot{W}_{\mathrm{cycle}} = \sum_{k=1}^{n_{\mathrm{com}}} \dot{W}_{\mathrm{CP},k} - \sum_{k=1}^{n_{\mathrm{exp}}} \dot{W}_{\mathrm{exp},k}. \tag{4.31}$$

The total exergy destruction of the cycle, $\dot{E}_{\mathrm{d,cycle}}$ can be calculated by summing the exergy destructions of all components:

$$\dot{E}_{\mathrm{d,cycle}} = \sum \dot{E}_{\mathrm{d}}. \tag{4.32}$$

The total exergy input to the system, $\dot{E}_{\text{cycle},i}$, is the sum of the exergies that enter the system boundary. This is the heat transfer at the evaporator and the power supply at the compressor. It can be calculated with:

$$\dot{E}_{\text{cycle},i} = \left(1 - \frac{T_0}{\overline{T}_{\text{C}}}\right) \dot{Q}_{\text{C}} - W_{\text{cycle}}. \tag{4.33}$$

The useful exergy output of the system is the exergy that leaves the system at the condenser, which can be calculated with:

$$\dot{E}_{\text{cycle},e} = \left(1 - \frac{T_0}{\overline{T}_{\text{H}}}\right) \dot{Q}_{\text{H}}. \tag{4.34}$$

The temperatures $\overline{T}_{\text{C}}$ and $\overline{T}_{\text{H}}$ are the thermodynamically averaged temperatures in the evaporator and condenser. If the fluid is in the two-phase region in these heat exchangers, then these temperatures are the saturation temperatures. In any other case, these temperatures are calculated with Equation (4.13) [28, 55].

## 4.5 Calculation of performance indicators

With these inputs, the model can compute the most important performance indicators: the coefficient of performance, exergy efficiency, volumetric heating capacity and the pressure ratio.

**Coefficient of Performance** The CoP is the benchmark for the efficiency of a heat pump. It indicates the process heat transfer rate, $\dot{Q}_{\text{H}}$, per unit of power input, $\dot{W}_{\text{cycle}}$:

$$\text{CoP} = \frac{\dot{Q}_{\text{H}}}{\dot{W}_{\text{cycle}}}. \tag{4.35}$$

A higher CoP means that less energy is required. The theoretical maximum attainable CoP, $\text{CoP}_{\text{max}}$, also called the Carnot CoP [35], can be calculated with:

$$\text{CoP}_{\text{max}} = \frac{\overline{T}_{\text{H}}}{\overline{T}_{\text{H}} - \overline{T}_{\text{C}}}. \tag{4.36}$$

It is an economic question to assess whether the CoP is large enough that the reduced energy costs justify the larger capital cost and system complexity. Since this project is not focused on economic analysis, the threshold value of the smallest economically viable CoP is set to 1.5. This is based on the smallest CoP values found in Arpagaus et al., (2018) and Jiang et al. (2022), who provided an overview of existing industrial high-temperature heat pump systems.

An actual heat pump usually has a waste fluid running through the evaporator and a process fluid running through the condenser, which both have been disregarded in this analysis. Waste fluid and process fluids however always have a temperature difference to the working fluid. This difference makes the temperature lift between the waste and process fluid lower than the temperature lift of the working fluid. The overall CoP of an actual heat pump is therefore also lower than the CoP calculated here. How much lower depends on the temperature differences in the heat exchangers.

**Exergy efficiency** The exergy efficiency, $\eta_{\text{ex}}$, indicates how close the heat pump performs to the theoretical maximum. It relates the useful exergy output to the exergy input in the following ways [8]:

$$\eta_{\text{ex}} = \frac{\dot{E}_{\text{cycle},e}}{\dot{E}_{\text{cycle},i}} = 1 - \frac{\dot{E}_{\text{d,cycle}}}{\dot{W}_{\text{cycle}}} = \frac{\text{CoP}}{\text{CoP}_{\text{max}}}. \tag{4.37}$$

For the calculation of the exergy efficiency for a heat pump, the temperature of the reference state has to be set to the thermodynamically averaged evaporator temperature: $T_0 = \overline{T}_{\text{C}}$ [28]. As its value is rather used for informative purposes than for performance selection, no threshold value is specified.

**Volumetric heating capacity** The VHC is the benchmark for the size of a heat pump. It is an indication of the compressor size required to compress the fluid and is given in $\text{MJ/m}^3$. A higher VHC means that more energy can be delivered to the sink per unit of working fluid volume. In

other words, the higher the VHC is, the smaller the compressor can be [3]. The VHC is calculated with the process heat demand and the volumetric flow rate:

$$\text{VHC} = \frac{\dot{Q}_{\text{H}}}{\sum_{k=1}^{n_{com}} \dot{V}_{\text{CP}k,i}}. \tag{4.38}$$

where $\dot{V}_{\text{CP}k,i}$ is obtained from the mass flow rate and the density of the fluid at the inlet of compressor $k$:

$$\dot{V}_{\text{CP}k,i} = \frac{\dot{m}_{\text{CP}k}}{\rho_{\text{CP}k,i}}. \tag{4.39}$$

It depends on the application field and local parameters whether the VHC of a cycle is large enough. A lower practical limit of $1\,\text{MJ/m}^3$ was given by Arpagaus et al. (2018), which is used as the threshold value in the results.

**Compression pressure ratio** The compression pressure ratio, $r_{\text{com}}$, is a benchmark of how difficult it is to compress a fluid. The calculation is shown in Equation (4.3). Since most compressors have a limit on the pressure ratio that can be reached in a single stage, a larger pressure ratio means a more advanced and expensive compressor is required. Or even that multiple compressors or stages are required to reach the pressure ratio. The largest pressure ratio associated with conventional compressors is about 8 [2], which is therefore set as a threshold value in the results.

**Condenser pressure level** The pressure level of the working fluid on the sink side indicates the largest pressure in the system. Higher pressures mean the heat pump becomes more difficult and expensive to construct. The largest acceptable pressure is rather an economical question than a thermodynamic one. Since supercritical steam at pressures up to 300 bar is used in vapour power plants [35], it is assumed that supercritical steam pressures can be used in heat pumps as well. A pressure of 300 bar is therefore set as a threshold value.

**Evaporator pressure level** The pressure level of the working fluid on the source side indicates the smallest pressure in the system. If the pressure is sub-atmospheric, different types of sealing are needed to avoid air infiltration into the system. Therefore, if the pressure is too low, the heat pump becomes more difficult and expensive to construct. A lower limit was arbitrarily set to 0.5 bara by [11].

**Compressor discharge temperature** The discharge temperature of the compressor is an indication of the largest temperatures that occur in the system. For certain fluids, this temperature can reach very large values that lead to difficulties for the materials and components used in the heat pump. When there are multiple compressors in a configuration, only the largest discharge temperature is shown. If a compressor is lubricated, the temperature limit can be set to 180 °C to avoid thermal decomposition of the lubricant [37]. With oil-free compressors, this limitation is not present. No definite upper limit was however found in the literature. As this research however concerns sink temperature up to 400 °C, this was set as the threshold value.

## 4.6 Component configurations

There are many possible component configurations with an arbitrary number of compression stages. In this research, the number of stages will be limited to two. The configurations used in this research are listed below. The entries start with an identification code followed by a short description with a motivation for why this configuration was created. Lastly, the sequence which is used as input to the model is shown, with the accompanying diagrams shown in Figure 4.8 and Figure 4.9.

1. **1S-XV**: This is a single-stage cycle with an expansion valve, as shown in Figure 4.8a. It is referred to as the standard cycle and has the following sequence:

   CP - CD - XV - EV.

2. **1S-XP**: This is a single-stage cycle with an expander, as shown in Figure 4.8b with the expansion valve replaced by an expander. The expander is used to recover some of the potential energy in the pressurised flow coming from the condenser. It has the following sequence:

   CP - CD - XP - EV.

3. **1S-SH1**: This is a single-stage cycle with superheating of the compressor inlet using the condenser outlet, as shown in Figure 4.8c. The heat exchange is done with an ICHX. Except for supercritical cycles, the condenser outlet is always hotter than the evaporator outlet and this difference can be used to superheat the evaporator outlet. At the same time, the condenser outlet is subcooled. The superheat is beneficial to avoid liquid droplets entering the compressor and can also improve the CoP [59].

$$\text{ICHX}_\text{c} \text{ - CP - CD - } \text{ICHX}_\text{r} \text{ - XV - EV.}$$

4. **1S-SH2**: This is a single-stage cycle with superheating of the compressor inlet using the compressor outlet, as shown in Figure 4.8d. The heat exchange is again done with an ICHX. This cycle also superheats the compressor inlet to avoid liquid droplets entering the compressor. However, it only works if the compressor discharge temperature overshoots the condenser temperature so that the temperature difference can be utilised. The influence on the CoP will be compared to 1S-SH1. It has the following sequence:

$$\text{ICHX}_\text{c} \text{ - CP - } \text{ICHX}_\text{r} \text{ - CD - XV - EV.}$$

5. **2S-DCIC**: This is a double-stage cycle with intercooling using a direct-contact heat exchanger with a flash chamber ($\text{DCHX}_\text{FC}$) to cool the vapour from the first compressor before going into the second compressor, as shown in Figure 4.9a. This is achieved by mixing this vapour with the condenser outlet stream and separating the vapour and liquid, as explained in Section 2.2. Thereby, the cycle uses part of the energy otherwise wasted through the expansion valve and thus could potentially improve the CoP even for wet fluids. The two compressors both receive saturated vapour, but now at different mass flow rates. It has the following sequence:

$$\text{CP - } \text{DCHX}_\text{FC,h} \text{ - CP - CD - XV - } \text{DCHX}_\text{FC,c} \text{ - XV - EV.}$$

6. **2S-ICIC**: This is a double-stage cycle with intercooling using an ICHX with two fluid streams, as shown in Figure 4.9b. It uses an ICHX to cool the vapour from the first compressor before going into the second compressor. The fluid from the condenser flows through the expansion valve, after which it has cooled down to the temperature level of the condenser. The fluid from the first compressor is at a higher temperature, so this temperature difference can be utilised to cool the compressor outlet. The cooling stream partly evaporates in front of the compressor. This cycle is only useful if the temperature of the vapour from the first compressor overshoots the saturation temperature. If there is no overshoot, the intercooler would condense the vapour, leading to wet compression in the second compressor. It has the following sequence:

$$\text{CP - } \text{ICHX}_\text{c} \text{ - CP - CD - XV - } \text{ICHX}_\text{r} \text{ - EV.}$$

7. **2S-2SH-DCIC**: This is a double-stage cycle with intercooling using a DCHX and double superheating using two ICHXs, as shown in Figure 4.9c. This setup aims to combine the benefits of both intercooling and superheating. It has the following sequence:

$$\begin{aligned}\text{ICHX}_\text{c,1} \text{ - CP - } \text{DCHX}_\text{FC,h} \text{ - } \text{ICHX}_\text{c,2} \text{ - CP - CD} \\ \text{- } \text{ICHX}_\text{r,2} \text{ - XV - } \text{DCHX}_\text{FC,c} \text{ - } \text{ICHX}_\text{r,1} \text{ - XV - EV.}\end{aligned}$$

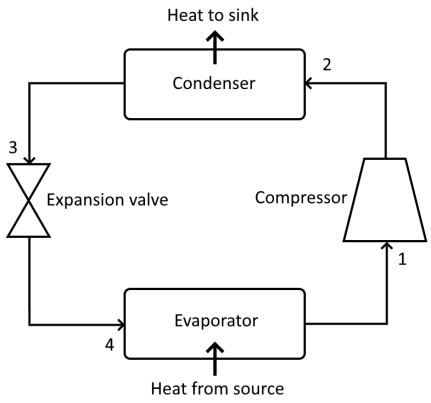


(a) 1S-XV

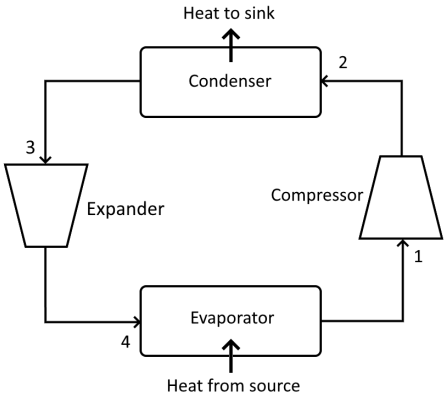


(b) 1S-XP

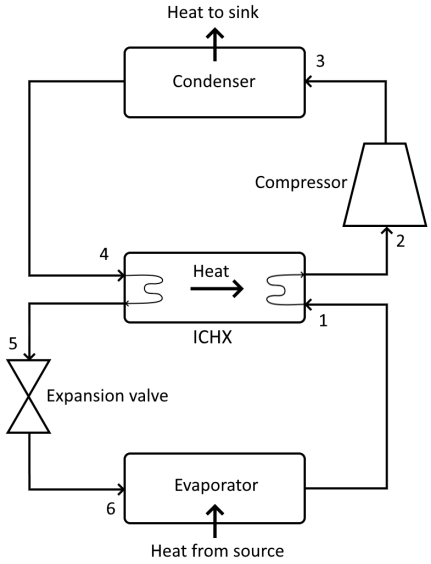


(c) 1S-SH1

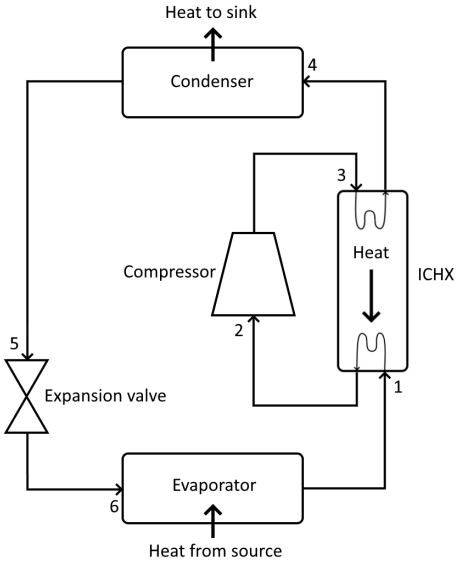


(d) 1S-SH2

**Figure 4.8:** Diagrams of single-stage cycles used in the model.

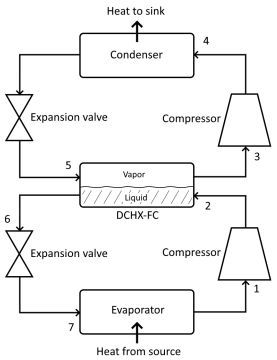


(a) 2S-DCIC

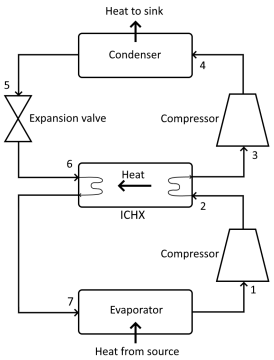


(b) 2S-ICIC

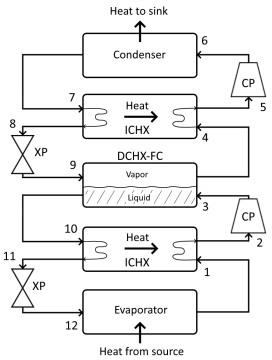


(c) 2S-2SH-DCIC

**Figure 4.9:** Diagrams of two-stage cycles used in the model.

## 4.7 Heat Pump design tool

To be able to conveniently design a heat pump when a certain waste heat supply and process heat demand are given, a heat pump design tool has been developed. This tool allows the user to define the waste and process fluids and visually tune a heat pump to the optimal configuration. The process fluid and its state can be defined with the following properties:

1. Type of fluid
2. Mass flow rate
3. Pressure
4. Inlet temperature
5. Outlet temperature or Process heat transfer rate $\dot{Q}_{\mathrm{H}}$

The latter option allows the user to either define the temperature that the process fluid should have at the outlet of the condenser, or define $\dot{Q}_{\mathrm{H}}$ directly. The user can then plot the states of the process fluid on T-s and p-h diagrams. The $\dot{Q}_{\mathrm{H}}$ is used as input to the heat pump model. Subsequently, the user can define a heat pump with the same inputs as in Section 4.2.1, after which the heat pump model simulates the cycle. The states are plotted in Ts- and p-h diagrams and the performance indicators are displayed. At this point, the necessary waste heat supply $\dot{Q}_{\mathrm{C}}$ is also known and the user can define a waste fluid with the following properties:

1. Type of fluid
2. Mass flow rate
3. Pressure
4. Inlet temperature

The tool calculates the states of the waste fluid and displays these on T-s and p-h diagrams as well.

To be able to tune the heat pump, the temperature profiles of the process fluid, the working fluid and the waste fluid in the evaporator and condenser are calculated and displayed in one graph. Furthermore, the temperature difference between the process fluid and the working fluid in the condenser, and between the waste fluid and the working fluid in the evaporator is calculated and displayed in another graph. With these graphs, the user can visually see whether the temperature profiles are possible and if no minimum temperature difference limits are violated. The heat pump can be optimised to minimise the temperature difference between the working fluid and the process/waste fluids.

It is also possible to control the heat pump model from the waste heat supply. In that case, the process is similar but allows the user to input an outlet temperature for the fluid or a waste heat demand $\dot{Q}_{\mathrm{C}}$. Then the heat pump is configured and after that the process fluid, which now adapts to the calculated $\dot{Q}_{\mathrm{H}}$

An example of a heat pump configuration in the heat pump design tool is shown in Figure 4.10. On the source side, a waste stream of hot air evaporates the working fluid benzene. In a single-stage cycle with superheat (**1S-SH1**), the benzene is pressurised to the pressure level of the sink. On the sink side, water is boiled at 18 bar. In the top one of the two rightmost diagrams, the temperature profiles in the evaporator and the condenser are shown. The heat pump has been tuned such that the temperature profiles reasonably match and the temperature difference between these profiles does not become lower than about 10 °C. These temperature differences are shown in the bottom right graph. In the top right, the performance indicators are shown. The inputs are shown on the left, with the top block being the process fluid inputs, the middle block the working fluid inputs and the bottom block the waste fluid inputs. The switch in the middle top allows to switch between a heat pump defined from the source or the sink side.

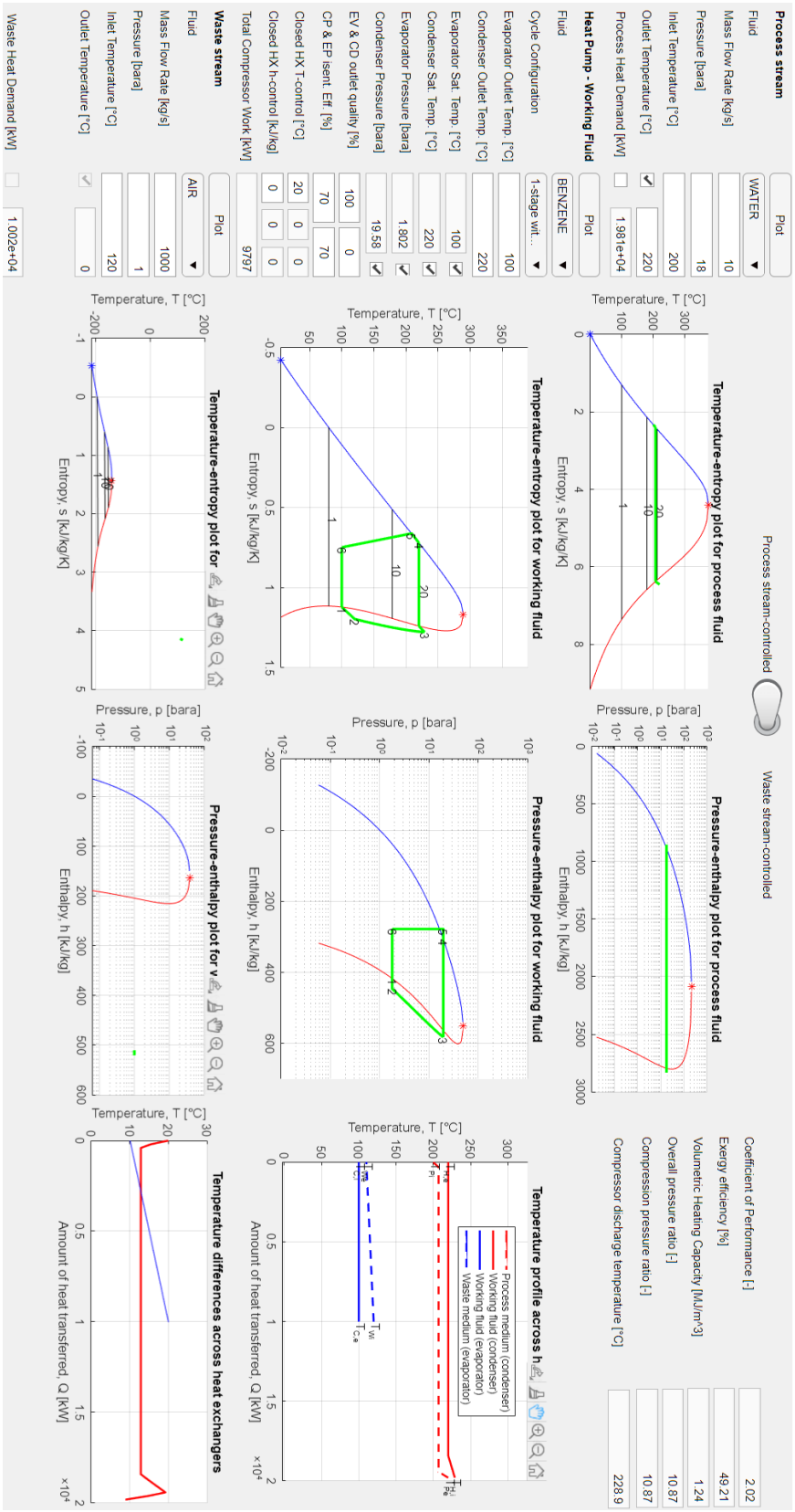


**Figure 4.10:** An example of a heat pump configuration in the heat pump design tool. On the source side, a waste stream of hot air evaporates the working fluid benzene. In a single-stage cycle with superheat (1S-SH1), the benzene is pressurised to the pressure level of the sink. On the sink side, water is boiled at 18 bar.

# Chapter 5

# HP Model: Results & Discussion

The goal of this investigation is to find out which fluids have the best performance and with which cycles this is achieved for certain operating conditions. To that end, the heat pump model is first validated in Section 5.1, using models from the literature. Afterwards, in Section 5.2, the model is simulated for two sets of operating conditions. This shows the benefits and merits of each fluid and provides the reader with information about which fluids could potentially be a suitable working fluid. Furthermore, the effect that superheating has on the fluids is shown. Then, the model is used to simulate different configurations per fluid. This allows the determination of the best configuration out of the ones defined in Section 4.6 for each fluid. The heat pump model is subsequently simulated for each fluid with its best configuration, for the two sets of operating conditions. The results are discussed and conclusions are drawn along the explanation of the results. A summary of the result and the conclusions that were drawn are given in Chapter 6, together with a general conclusion on the heat pump model.

## 5.1 Model validation

To validate the heat pump model, a few cases from the literature are simulated and the results are compared.

**First comparison** The first comparison is an example from Moran et al., (2015, p. 525-527). It concerns a **1S-XV** cycle using R134a as the working fluid. The T-s diagram is shown in Figure 5.1. It

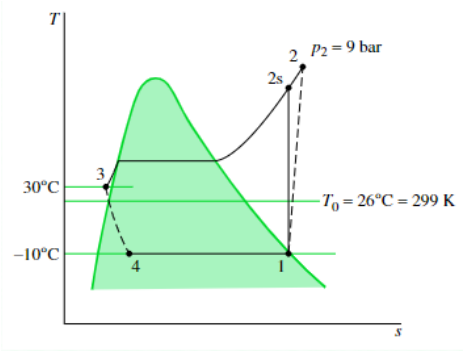


**Figure 5.1:** Example from [35]: Subcritical single-stage cycle without superheating using R134a as working fluid.

is seen that $T_{C,e} = -10\,°C$, $p_H = 9\,\text{bar}$ and $T_{H,e} = 30\,°C$. The evaporator pressure is the saturation pressure at $T_{C,e}$. The compressor isentropic efficiency is 80 % and the environment temperature is 26 °C. The example uses these inputs as a basis to calculate the compressor power $\dot{W}_{CP}$, the refrigeration capacity $\dot{Q}_C$, the refrigeration-based coefficient of performance $CoP_{refrigeration}$ and the rates of exergy destruction of the compressor and expansion valve, $\dot{E}_{d,CP}$ and $\dot{E}_{d,vl}$. As the main purpose of this cycle is refrigeration instead of heat pumping, the CoP is calculated as $\frac{\dot{Q}_C}{\dot{W}_{CP}}$. The heat pump model has been simulated with the same inputs. The results of the example and the

model are shown in Table 5.1. It is seen that the results of the model are in good agreement with the results from the example.

**Table 5.1:** Results from the example and the heat pump model for the single-stage cycle without superheating [35].

| **Case** | $\dot{W}_{\mathrm{CP}}$ [kW] | $\dot{Q}_{\mathrm{C}}$ [kW] | $\mathrm{CoP}_{\mathrm{refrigeration}}$ [-] | $\dot{E}_{\mathrm{d,CP}}$ [kW] | $\dot{E}_{\mathrm{d,vl}}$ [kW] |
|---|---|---|---|---|---|
| Example | 3.1 | 12.0 | 3.86 | 0.58 | 0.39 |
| Model | 3.1027 | 11.997 | 3.8667 | 0.58325 | 0.39493 |

**Second comparison** The second comparison is again a model from Moran et al., (2015,p. 542-543). Here, a **1S-XP** supercritical (Brayton) refrigeration cycle is simulated using air as the working fluid. The T-s diagram is shown in Figure 5.2. From the figure, the following inputs can be

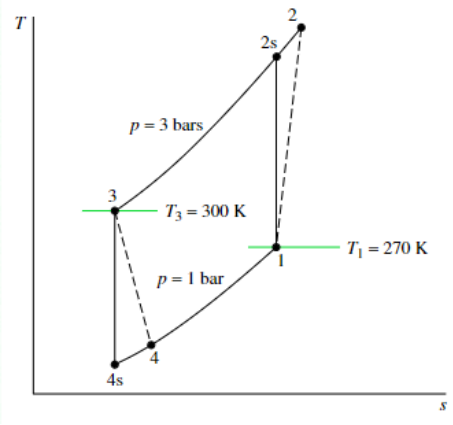


**Figure 5.2:** Example from [35]: Supercritical single-stage cycle with expander using air as the working fluid.

deduced: $p_{\mathrm{C}} = 1\,\mathrm{bar}$, $T_{\mathrm{C,e}} = -3.15\,^{\circ}\mathrm{C}$, $p_{\mathrm{H}} = 3\,\mathrm{bar}$ and $T_{\mathrm{H,e}} = 26.85\,^{\circ}\mathrm{C}$. The compressor isentropic efficiency is 80 %. The example uses these inputs as a basis to calculate the net power input to the cycle $\dot{W}_{\mathrm{cycle}}$, the refrigeration capacity $\dot{Q}_{\mathrm{C}}$ and the refrigeration-based coefficient of performance $\mathrm{CoP}_{\mathrm{refrigeration}}$. The net power input is the difference between the compressor and expander power: $\dot{W}_{\mathrm{cycle}} = \dot{W}_{\mathrm{CP}} - \dot{W}_{\mathrm{XP}}$. The heat pump model has been simulated with the same inputs. The results of the example and the model are shown in Table 5.2. It is seen that the results of the model are again in good agreement with the results from the example.

**Table 5.2:** Results from the example and the heat pump model for the supercritical Brayton refrigeration cycle [35].

| **Case** | $\dot{W}_{\mathrm{cycle}}$ [kW] | $\dot{Q}_{\mathrm{C}}$ [kW] | $\mathrm{CoP}_{\mathrm{refrigeration}}$ [-] |
|---|---|---|---|
| Example | 108.5 | 63.08 | 0.581 |
| Model | 108.35 | 63.228 | 0.5835 |

**Third comparison** The third comparison is a model from Cao et al. (2014), who simulated a **2S-DCIC** cycle, as in Figure 4.9a, using R152 as the working fluid. They simulated this cycle for an evaporator saturation temperature of $T_{\mathrm{C}} = 30\,^{\circ}\mathrm{C}$ and a condensation temperature in the range of 98-108 °C. For the comparison with the heat pump model, a condensation temperature of $T_{\mathrm{H}} = 100\,^{\circ}\mathrm{C}$ is selected. They model the evaporator such that the vapour at the exit has 3 °C of superheat. Likewise, the condenser is modelled such that the liquid at the exit has 5 °C of subcooling. The outlet temperatures of the evaporator and condenser become the saturation temperatures plus/minus the degree of superheating/subcooling, so $T_{\mathrm{C,e}} = 33\,^{\circ}\mathrm{C}$ and $T_{\mathrm{H,e}} = 95\,^{\circ}\mathrm{C}$.

The heat pump model requires the process heat demand $Q_{\mathrm{H}}$ as an input. However, in the model of Cao et al. (2014), heat flows are determined by the waste fluid flow in the evaporator. Here, waste water enters with 10 kg/s at 45 °C and leaves at 5 °C above the lowest working fluid temperature in the evaporator, which is 30 °C. The waste water, therefore, cools down to 35 °C. The waste heat supply can then be calculated: $\dot{Q}_{\mathrm{C}} = 420\,\mathrm{kW}$. Cao et al. (2014) calculated the CoP to be 3.75, which results in a process heat demand of $Q_{\mathrm{H}} = 573\,\mathrm{kW}$. Cao et al. (2014) use a correlation for the compressor isentropic efficiency based on the inlet and outlet pressures of the compressors. Next

to the CoP, other results from this model are the total power consumption $W_{\text{cycle}}$ and the exergy efficiency $\eta_{\text{ex}}$. The latter is calculated as:

$$\eta_{\text{ex}} = \frac{\dot{E}_{\text{d,e}}}{\dot{E}_{\text{d,i}}} \tag{5.1}$$

where $\dot{E}_{\text{d,e}}$ is the overall output exergy and $\dot{E}_{\text{d,i}}$ the overall input exergy, which are evaluated as:

$$\dot{E}_{\text{d,e}} = \dot{m}_{\text{P}} \left( e_{\text{f,P,e}} - e_{\text{f,P,i}} \right) \qquad \dot{E}_{\text{d,i}} = \dot{W}_{\text{cycle}} + \dot{m}_{\text{W}} \left( e_{\text{f,W,i}} - e_{\text{f,W,e}} \right). \tag{5.2}$$

The subscripts 'P' and 'W' indicate the product and waste streams, respectively. The heat pump model has been simulated with the same inputs. The results of the example and the model are shown in Table 5.3. The results of Cao et al. (2014) have been read from graphs and are therefore not perfectly accurate. Nevertheless, it is seen that the results of the model are in good agreement with the results from the literature.

**Table 5.3:** Results from the model of Cao et al. (2014) and the heat pump model for a 2-stage cycle with a direct-contact heat exchanger.

| **Case** | CoP [-] | $\dot{W}_{\text{cycle}}$ [kW] | $\eta_{\text{ex}}$ [%] |
|---|---|---|---|
| Cao et al. (2014) | 3.75 | 153 | 51.8 |
| Model | 3.7506 | 152.55 | 53.507 |

In conclusion, the heat pump model provides consistently similar results as models from other authors and thus the heat pump model is considered validated. It can now be used to assess the performance of different cycles and refrigerants.

## 5.2 Performance analysis

In this section, the heat pump model is simulated for different cases, fluids and configurations. The results display the heat pump performance, which is analysed and discussed. As became clear from Figure 3.4, the largest portion of waste heat is emitted at temperatures between 100-200 °C. At the same time, sufficient heat demand exists in the range of 100-500 °C. Therefore, it was decided to constrain the cases for which the model is simulated to the following two domains:

**Domain 1** An evaporator outlet temperature of $T_{\text{C},e} = 100\,°\text{C}$ and a condenser outlet temperature in the range of $T_{\text{H},e} = 150 - 300\,°\text{C}$. The evaporator and condenser pressure levels, $p_{\text{C}}$ and $p_{\text{H}}$, are the saturation pressures at these temperatures. Therefore, $T_{\text{C},e} = T_{\text{C}}$ & $T_{\text{H},e} = T_{\text{H}}$ and as such these temperatures are generally referred to as the source and sink temperature, respectively. The evaporator outlet quality is $x_{\text{C,e}} = 100\,\%$ and the condenser outlet quality is $x_{\text{H,e}} = 0\,\%$. This domain will show the potential of a vapour compression heat pump for the lower end of the high-temperature waste heat.

**Domain 2** An evaporator outlet temperature of $T_{\text{C},e} = 200\,°\text{C}$ and a condenser outlet temperature in the range of $T_{\text{H},e} = 250 - 400\,°\text{C}$. The evaporator and condenser pressure levels are again the saturation pressures at these temperatures. The evaporator outlet quality is $x_{\text{C,e}} = 100\,\%$ and the condenser outlet quality is $x_{\text{H,e}} = 0\,\%$. This domain will show the potential of a vapour compression heat pump for the higher end of the high-temperature waste heat.

The waste and product fluids are left out of consideration in these simulations. In other words, the minimum temperature difference is set to $\Delta T_{\text{min}} = 0$, assuming the unrealistic situation where no temperature difference is needed in the heat exchangers for the heat transfer. This is required since the tailoring of a heat pump to waste and process fluids is an optimisation problem. Though possible with the heat pump design tool shown in Section 4.7, this is a tedious and time-consuming process. An optimisation algorithm was however not developed. Nevertheless, this approach allows to qualitatively compare heat pump configurations and fluid for different temperature ranges without the added variability of waste and process fluids.

For all simulations, the compressor isentropic efficiency has been set to $\eta_{\text{CP}} = 70\,\%$, which is a value commonly used in theoretical calculations [3]. In case an expander is used, the same value is taken: $\eta_{\text{XP}} = 70\,\%$. The process heat demand is completely arbitrary and does, as stated, not influence the result. A value of $Q_{\text{H}} = 100\,\text{kW}$ is taken as it appears to be an average value in existing HTHPs [3].

For indirect-contact heat exchangers, a minimum temperature difference of 10 °C is set. This is on the safe side since many authors use a value of 5 °C [45, 3, 11]. The performance of the heat pumps is indicated using the performance indicators stated in Section 4.5. As was also mentioned in that section, the temperature of the reference state is set to the thermodynamically averaged evaporator temperature, $T_0 = \overline{T}_C$, which is just $T_{C,e}$ in this case because it is a subcritical cycle.

First, Section 5.2.1, different fluids will be simulated in a **1S-XV** configuration to compare their performance against each other. Being done for both domains, the results help to understand which fluids have the largest potential. In addition to this analysis, the effect of wet compression on the performance is elaborated in Section 5.2.2. It is also noticed that the lack of superheating severely limits the potential of many fluids. Therefore, the model is simulated with a **1S-SH1** configuration for different degrees of superheat in Section 5.2.3. Using the conclusions from these sections, some of the high-potential fluids will be simulated for the different configurations established in Section 4.6. These results are discussed in Section 5.2.4 and show which configurations have the best performance for which types of fluids. The results for the best fluids and configurations are then combined to show the best heat pump designs in Section 5.2.5.

### 5.2.1 Comparison of fluid performances in the standard cycle

The simplest configuration, **1S-XV**, has been chosen to initially show the performance of different fluids over the two domains. It will be referred to as the 'standard cycle'.

**Domain 1** All fluids are simulated for domain 1 and the ones with the best performance have been selected for display. The constraint for the selection in domain 1 is that at $T_H = 200\,°C$, the fluid must at least have a CoP of 1.5 and a VHC of $1\,MJ/m^3$. This constraint is in line with the threshold values defined in Section 4.5. Seven fluids passed this criterium, with 4 dry fluids (acetone, ethanol, methanol and water) and 3 wet fluids (benzene, cyclopen and DMC) The results for domain 1 are shown in Figure 5.3. The top left diagram shows the CoP for the range of sink temperatures, along with lines of constant exergy efficiency. It is seen that water has the largest CoP throughout the entire range of sink temperatures. Water is also the only fluid that can reach $T_H = 300\,°C$ from $T_C = 100\,°C$ in this cycle. Other fluids can only reach lower temperatures due to the critical temperature being lower than the sink temperature or due to the compressor compressing completely through the two-phase region, resulting in a liquid. This latter problem is only applicable to wet fluids and is the reason that many of these fluids can not be used without superheating (which is why the effect of superheating is discussed in Section 5.2.3). After water, the most efficient fluids are methanol and ethanol. However, they can only be used in this cycle up to about $T_H = 240\,°C$ (limited by critical temperature). All fluids but water show a large drop in exergy efficiency with increasing $T_H$. Water on the other hand sustains a relatively high efficiency of about $\eta_{ex} = 60\,\%$ at $T_H = 300\,°C$.

The top diagram shows the VHC for the range of sink temperatures. It is seen that methanol has a very much superior VHC value. The VHC of water is initially relatively low but, unlike all other fluids, shows a positive gradient and becomes larger than the other fluids for the higher sink temperatures.

The discharge temperature diagram clearly shows that water has a much larger temperature increase during compression than the other fluids. While all other fluids remain below the threshold value of 400 °C, water surpasses it already at about $T_H = 165\,°C$. Such temperatures require special materials and are therefore severely limiting the usage of water in heat pumps. These results clearly show that, for water, intercooling is a necessity. The other dry fluids have a much more modest temperature increase. For the wet fluids, the discharge temperature is equal to the saturation temperature due to wet compression and thus no overshoot is present. Such wet compression is only possible with certain compressor types, complicating the design of the heat pump

Regarding pressure levels, it is seen that none of the fluids have subatmospheric evaporator pressures, so there is no risk of air leaking into the system. All fluids have condenser pressures below the threshold value of 300 bar and the smallest condenser pressures are achieved by water, benzene and DMC. Water does however have the largest pressure ratio. That indicates that water is the most difficult to compress, which is in line with what was found in [11]. The pressure ratios all quickly surpass the threshold value of 8. For most cases, a dual-stage cycle (maximum pressure ratio of 64) is sufficient, but for the largest temperatures with water and methanol, triple-stage compression

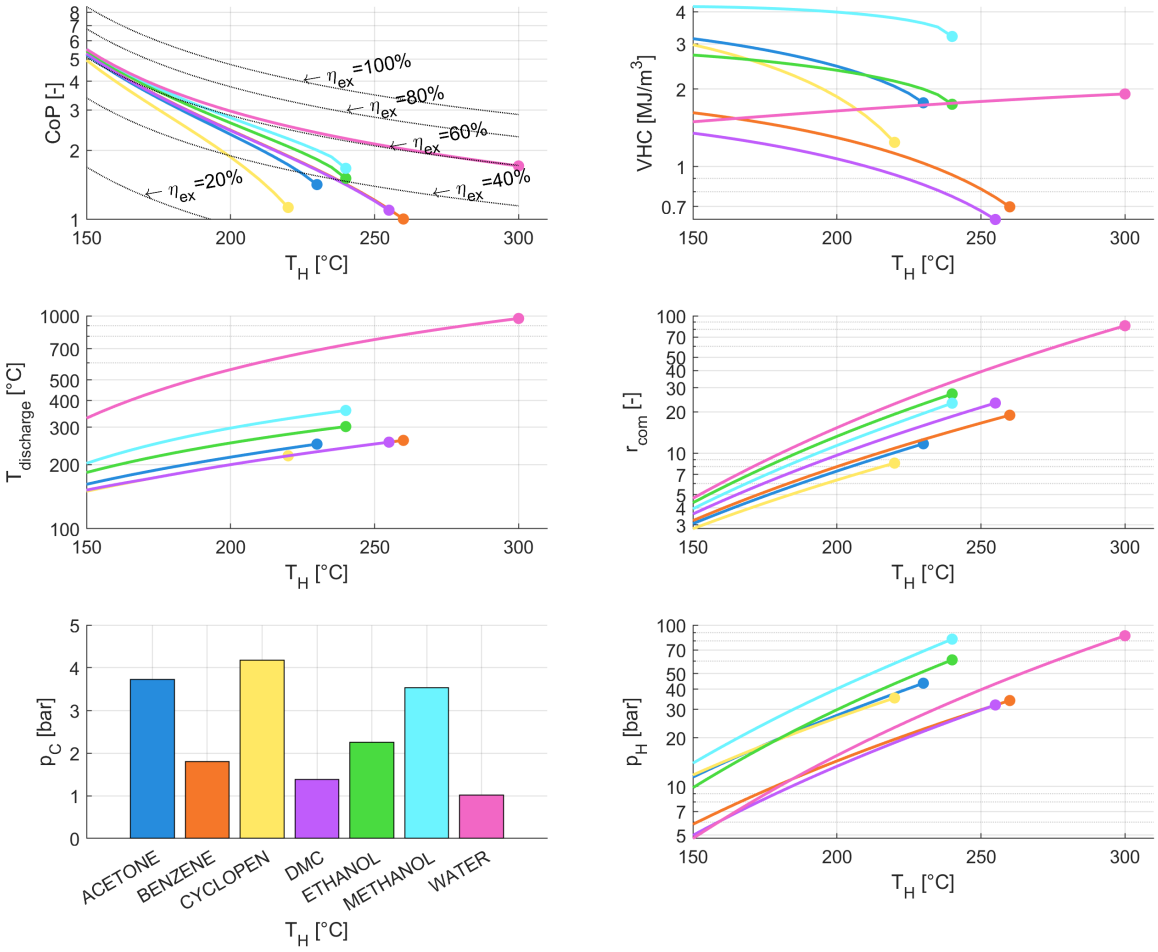


**Figure 5.3:** Performance figures for the configuration **1S-XV** over domain 1. Since the colours match, the bottom left diagram can be used as a legend.

might be needed. The diagrams of the pressure ratios seem to go hand in hand with those of the CoPs. That is, with higher CoP comes a higher pressure ratio.

From these results, it can be concluded that methanol is the most suitable working fluid, but only for sink temperatures up to 240 °C. It has the highest CoP apart from water and has a much larger VHC than the other fluids. Methanol however still poses some technical challenges for high temperature applications. It has the largest condenser pressure of the other fluids for every sink temperature. Another downside is that the compressor discharge temperature higher than the other fluids, although much lower than water. On top of that, methanol is toxic, has a GWP of 2 8 and is flammable. It has an auto-ignition temperature of 464 °C [9], which poses a threat in case of leakages. A close contender for methanol is ethanol, yet it has less performance with the same downsides. If the challenges of compressing water vapour are addressed, it would be a superior fluid to methanol. That is if a method to suppress the compressor discharge temperature is found along with a compression system that can handle the large pressure ratios, the higher efficiency of water combined with the lower sink pressure puts water at an advantage. This is further augmented by water being non-toxic, non-flammable and having a GWP of 1.

**Domain 2** For domain 2 again the best fluids have been selected and the results are shown in Figure 5.4. The constraint for the selection is that at $T_H = 250\,°C$, the fluid must at least have a CoP of 1.5 and a VHC of 1 MJ/m$^3$, which is again in line with the threshold values. Eleven fluids passed this criterium, with water being the only dry fluid. It can immediately be seen that the difference between water and the other fluids is significant. For the latter, the CoP quickly drops and only low sink temperatures are reached with useful CoP. Water on the other hand sustains an exergy efficiency of about 60 °C for most of the $T_H$-range and ends at a CoP just below 2 at about $T_H = 370\,°C$. The second-best fluid in terms of CoP is toluene.

Water also has the largest VHC by a considerable margin and remains relatively constant over the

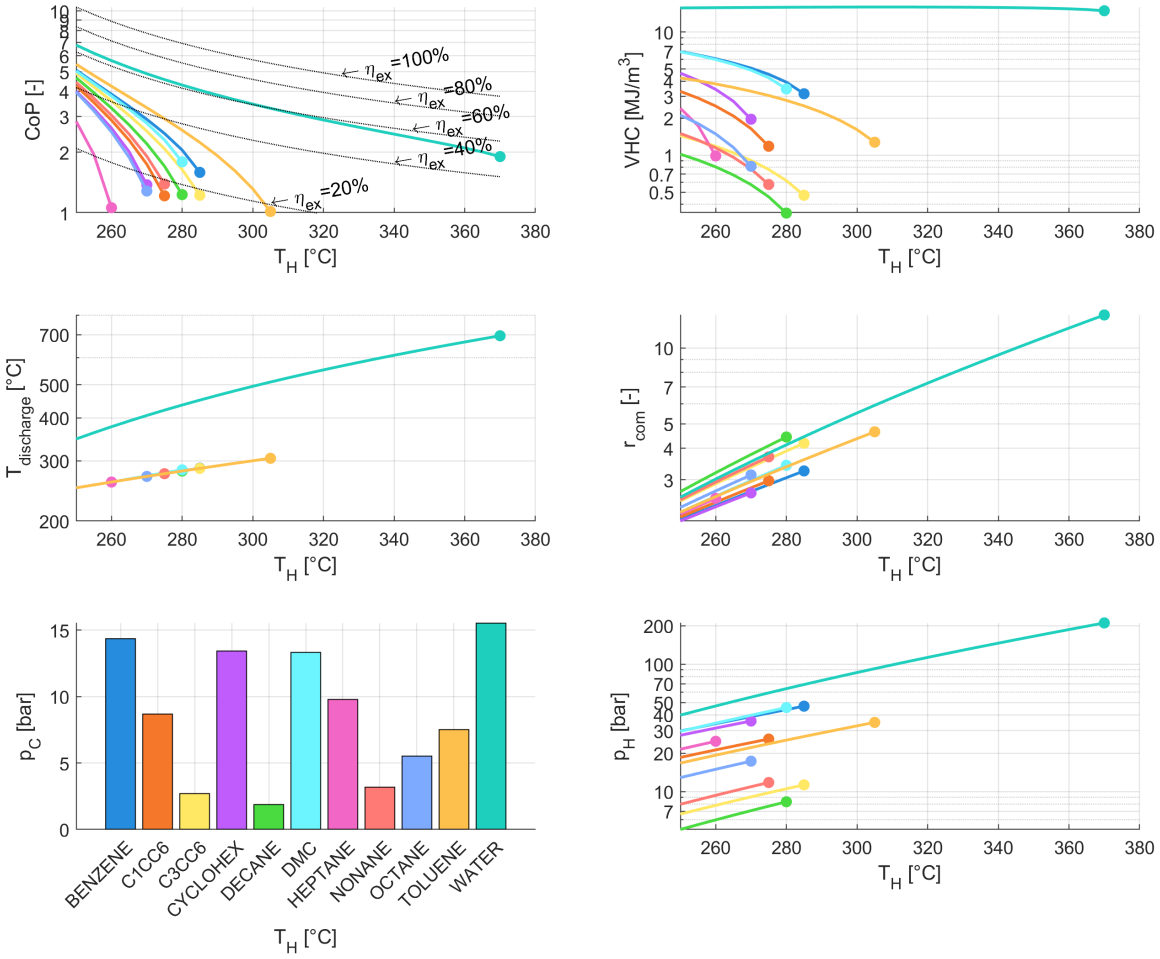


**Figure 5.4:** Performance figures for the configuration **1S-XV** over domain 2. Since the colours match, the bottom left diagram can be used as a legend.

entire domain. For the other fluids, the VHC quickly drops down to values that require very large compression equipment. The second-best fluids in terms of VHC are benzene and DMC, while toluene comes close to these.

The discharge temperature diagram again makes it clear that intercooling is a necessity for water. All other fluids exhibit complete wet compression.

Regarding pressures, no fluid is again below atmospheric conditions. Water however shows the largest pressures for both the evaporator and condenser compared to the other fluids, yet below the threshold value of 300 bar. The pressure ratio on the other hand is below 8 for most of the sink temperatures. Only for water, at the largest $T_H$ values, a dual-stage compressor might be necessary. Toluene is also more satisfactory than water in terms of evaporator pressure, condenser pressure and pressure ratio.

From these results, it can be concluded that none of these fluids is truly suited for this cycle. The CoP is uneconomically low for all fluids but water, while water has unacceptable temperatures and large pressures. For the lower sink temperatures, toluene is the most suitable working fluid, provided wet compression is possible. It has the largest CoP after water, acceptable VHC, no discharge temperature overshoot and a moderately low evaporator pressure, condenser pressure and pressure ratio. The downsides are however that toluene is flammable, irritant, poses a health hazard and has a GWP of 2.7 [27]. Even though water has a much better CoP and VHC, the technical challenges of a compressor that can handle the high temperatures, pressures and pressure ratios prevent it from being implemented. If these challenges could be solved, water can again be considered to be a superior fluid to toluene.

### 5.2.2 Exploiting wet compression for water

Assuming that wet compression is possible, the effect of wet compression with water is investigated. The advantage of wet compression is that the compression process happens (partly) in the two-phase region and thereby the temperature is fixed to the saturation temperature. Any heat generated during compression will evaporate liquid instead of increasing the temperature, preventing the large discharge temperature overshoot experienced with water. In the heat pump model, wet compression can be achieved by setting the evaporator outlet quality, $x_{\mathrm{CP},e}$, to lower than 100 % in the **1S-XV** cycle. This is only useful for dry fluids since wet fluids already compress in the two-phase region. To find out what effect $x_{\mathrm{CP},e}$ has on the CoP, the HP model has been simulated with a **1S-XV** cycle with $x_{\mathrm{CP},e}$ in the range of 50-100 % using water as the working fluid. The results for domain 1 and domain 2 are shown in Figure 5.5. The graphs show the points for which the CoP

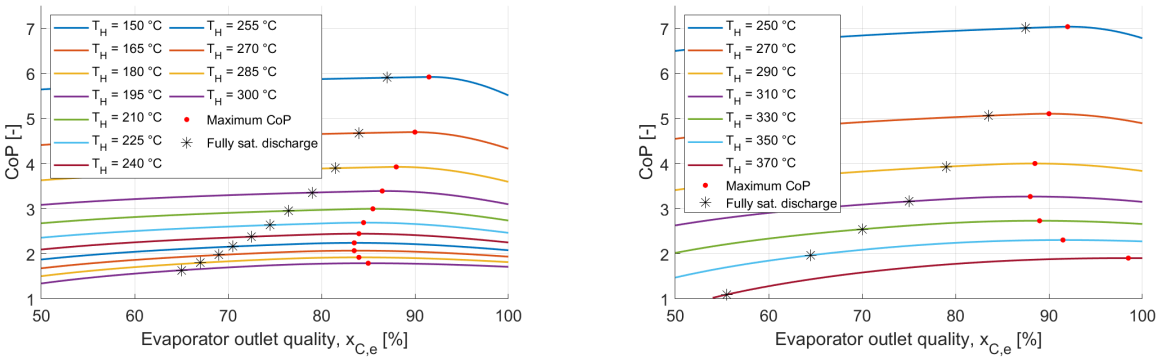


**(a)** Domain 1

**(b)** Domain 2

**Figure 5.5:** The CoP of the **1S-XV** cycle with water as working fluid where $x_{\mathrm{CP},e}$ has been varied in the range of 50-100 % for domain 1 and 2. The top graph, with the largest CoP values, corresponds to the lowest sink temperature.

becomes the largest for that sink temperature (red dots) and the points for which the discharge vapour is fully saturated (asterisks). That is, a larger quality results in the discharge vapour being superheated while a smaller quality would result in liquid still being present in the discharge. Since these points are not coincident, it does not hold that delivering saturated vapour results in the best CoP. Nevertheless, it can be seen that wet compression can improve the CoP compared to dry compression ($x_{\mathrm{CP},e} = 100\,\%$). However, for both domains, the best CoP is achieved at a higher quality than the quality for which the discharge vapour is saturated. Therefore, to reach the best efficiency, a superheated vapour is unavoidable. This data will be used in Section 5.2.4 to compare wet compression against the other cycles.

### 5.2.3 Superheating to prevent wet compression

One of the reasons that wet fluids could not be used up to large sink temperatures was that the compression process fully passes through the two-phase region, resulting in a subcooled liquid at the discharge. Then there is no more vapour left to condense, rendering the condenser useless. If the condenser outlet conditions are set such that saturated liquid is discharged, the heat pump cycle would even be invalid, as the working fluid would have to heat up in the condenser instead of cooling down. The condenser outlet conditions may be set to a subcooled liquid state such that the working fluid cools down in the condenser. An example of such a cycle is seen in Chapter B, which shows a very small exergy efficiency and is not considered any further.

Apart from a low efficiency, many types of compressors can not handle liquid droplets. If this is the case, then certainly wet fluids need superheating. However, some superheating (usually 5-10 °C) might also be necessary for dry fluids, as there is a risk that liquid droplets are entrained in the flow from the evaporator outlet to the compressor [61, 45]. Superheating can even improve the CoP for wet fluids [28, 2].

To show the effect of superheating on the performance of different fluids, the **1S-SH1** configuration is chosen. This cycle uses the condenser outlet, which is a saturated liquid at saturation temperature $T_{\mathrm{H}}$. The vapor coming from the evaporator outlet can therefore be superheated close to this temperature. There always needs to be a minimum temperature difference, which in this case is set to 10 °C. The source temperature is set to $T_{\mathrm{C}} = 100\,°\mathrm{C}$ and the sink temperature to $T_{\mathrm{H}} = 200\,°\mathrm{C}$. The model has been simulated for a range of superheat values from 0 °C to 90 °C. The results are

shown in Figure 5.6. Fluids for which the maximum VHC did not reach above 1 MJ/m$^3$ were not displayed.

The location of the dots on the line tells the reader what the minimum degree of superheat is for that fluid to avoid wet compression completely. As seen for the dry fluids (acetone, ethanol, methanol, R141B and water), no superheat is required while for a wet fluid like hexane, about up to 40 °C of superheat is necessary. As can be seen from these results, superheating increases the performance

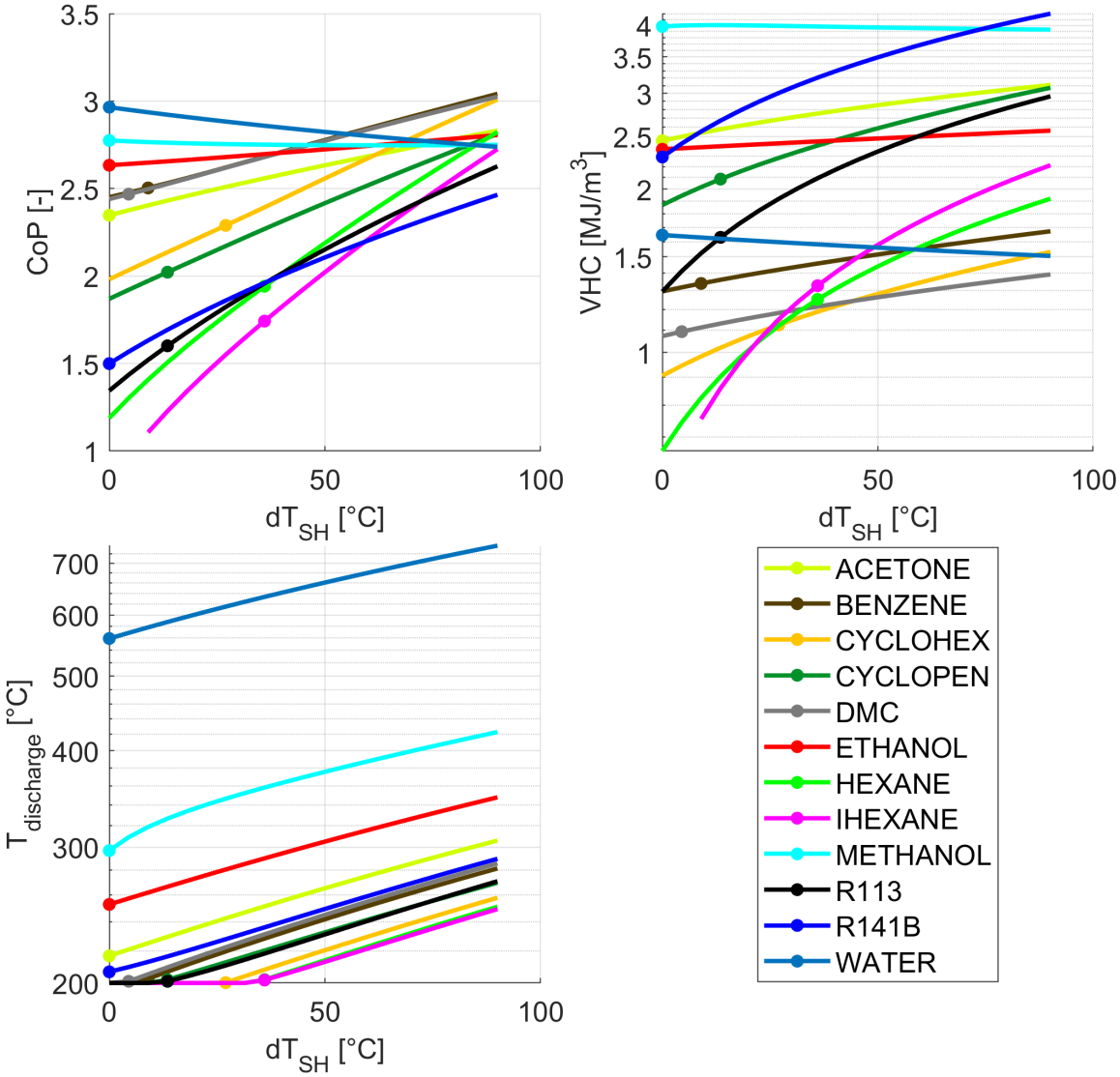


**Figure 5.6:** A single-stage heat pump with superheating using the condenser outlet for a degree of superheat in the range of 0-90 °C. The projection of the dots on the x-axis indicates the minimum superheat necessary to avoid wet compression completely.

of most fluids. For all fluids apart from water and methanol, the CoP increases considerably with increasing superheat. The reason for this can be explained using the p-h diagram of cyclohex. The cycle of cyclohex is shown in Figure 5.7 for a non-superheated case and a case with 60 °C superheat. By looking at the relative sizes of $\dot{Q}_{\mathrm{H}}$ and $\dot{W}$, it can be seen that for the non-superheated case, $\dot{W}$ is about half of $\dot{Q}_{\mathrm{H}}$, while for the case with 60 °C superheat, $\dot{W}$ is less than half of $\dot{Q}_{\mathrm{H}}$. These observations are supported by the CoP values, which are 1.98 without superheat and 2.67 with 60 °C superheat.

Since the CoP with water and methanol only decreases with more superheat and 5-10 °C is sufficient to prevent liquid in the compressor, the results for larger superheat values are essentially meaningless. For ethanol, the CoP increases marginally. However, the increase in discharge temperature does not justify this gain. Acetone shows a larger increase in CoP and a smaller discharge temperature, indicating the degree of superheat for this fluid would be a compromise. For the other fluids, the differences in discharge temperature are relatively small and are therefore not expected to have a

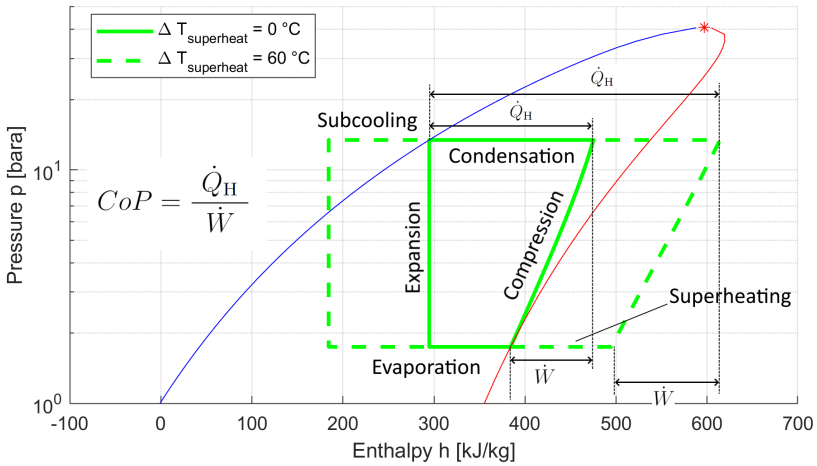


**Figure 5.7:** The p-h diagram of cyclohexane in a single-stage heat pump without superheating and with 60 °C superheating using the condenser outlet. Indicated are the specific heat delivered to the sink and the specific compression work.

**Table 5.4:** Safety and environmental classifications of selected fluids. The information was retrieved from [27] and [20].

| Fluid | GWP | ODP | Flammable | Irritant | Acute Toxic | Health hazard | Environmental hazard | ASHRAE 34 |
|---|---|---|---|---|---|---|---|---|
| Acetone | 0.5 | - | x | x | - | - | - | - |
| Benzene | - | - | x | x | - | x | - | - |
| C1CC6 | - | - | x | x | - | x | x | - |
| Cyclohex | - | - | x | x | - | x | x | - |
| Cyclopen | - | - | x | - | - | - | - | - |
| DMC | - | - | x | - | - | - | - | - |
| Ethanol | - | - | x | - | - | - | - | - |
| Heptane | - | - | x | x | - | x | x | - |
| Hexane | - | - | x | x | - | x | x | - |
| Ihexane | - | - | - | - | - | x | - | - |
| Methanol | 2.8 | - | x | - | x | x | - | - |
| MM | - | - | x | - | - | - | x | - |
| R113 | 6130 | 0.85 | - | x | - | - | x | A1 |
| R141B | 725 | 0.12 | - | x | - | - | - | - |
| Toluene | 2.7 | - | x | x | - | x | - | - |
| Water | - | - | - | - | - | - | - | A1 |

large influence in selecting between these fluids. Furthermore, it appears that for all fluids except water and methanol, the VHC increases with increasing superheat. Again, ethanol only marginally increases.

From these results, it can be concluded that methanol again appears to be a suitable fluid. At low superheat, it has a large CoP and VHCs, while the discharge temperature is not much larger than a wet fluid like benzene. Close contenders are ethanol and acetone which have a lower discharge temperature, though at the cost of CoP and VHC. In case the VHC is not significantly important compared to CoP, benzene at 90 °C superheat appears to be suited since it has an even larger CoP than water. The discharge temperature of benzene remains significantly below the threshold value. The safety and environmental aspects are summarised in Table 5.4. This shows that almost all fluids are flammable and many are irritant and pose health hazards. While benzene has these three traits, DMC is only flammable. Acetone is flammable and irritant, which is relatively safe compared to cyclohex and benzene, the latter being suspected to be carcinogenic [27].

Water is fully exempt from safety or environmental hazards. Without superheat, water has almost the largest CoP of the simulation and has a moderate VHC. These facts motivate the desire to find a method of water vapour compression which avoids unacceptable discharge temperatures.

### 5.2.4 Comparison of different configurations per fluid

With the knowledge of which fluids potentially have the best performance, different cycle configurations can be compared to obtain the best combination. To investigate the performance of different component configurations, the model is simulated for multiple configurations per fluid over domain

1. The results are compared based on percentual CoP and VHC improvement compared to the **1S-XV** cycle and on the discharge temperature.

As appeared in Fig. 5.6, a higher degree of superheat leads to a better CoP and VHC for all fluids except water and methanol. Therefore, the superheat in the **1S-SH1** and **1S-SH2** cycles was set to $(T_H - T_C) - 10$, which is the maximum possible while keeping a temperature difference of 10 °C in the heat exchanger. For the **2S-2SH-DCIC** cycle, it was assumed that the intermediate saturation temperature is approximately the average of the source and sink temperatures. The degree of superheat was therefore set to $(T_H - T_C)/2 - 10$ for both superheaters. A check was implemented to give an alert if the 10 °C minimum temperature difference was violated, which did not happen in any simulation. For methanol and water, the degree of superheating was set to a low value of 10 °C for all cycles containing a superheater. The degree of intercooling in the **2S-ICIC** cycle has been set such that the outlet temperature of the controlled stream is 10 °C above its saturation temperature, thereby prohibiting the presence of liquid droplets in the compressor inlet. For the wet fluids, the **2S-ICIC** was not simulated, as the fluid does not need intercooling in this cycle due to the wet compression. The **1S-XV** has been simulated with two levels of wet compression:

- Evaporator outlet quality set such that maximum efficiency is obtained (**1S-XV(wc-Eff)**)
- Evaporator outlet quality set such that saturated vapour is obtained (**1S-XV(wc-Sat)**)

This evaporator outlet quality data was obtained for water only. Nevertheless, it was also used for other fluids and though not optimised for these fluids, does provide a qualitative insight into the performance of a cycle with more or less wetness.

The cycles have been simulated for all fluids that appeared in Figure 5.6. It was noticed that all wet fluids have the same trend in the results. This trend is discussed using the results for benzene, which are shown in Figure 5.8. It is seen that the **2S-2SH-DCIC** cycle has the best improvement in CoP, though **1S-SH1** cycle is very close. In terms of VHC, the former cycle has a much larger improvement than the latter. The **2S-DCIC** cycle has a similar but smaller improvement in VHC compared to **2S-2SH-DCIC**. This confirms that direct-contact intercooling does improve the CoP but not as much as superheating does, while the inverse is true for the VHC. The performance of the **2S-2SH-DCIC** cycle in these aspects shows that the benefits of superheating and intercooling can be combined, at least for wet fluids.

Comparing both types of superheating cycles, **1S-SH1** and **1S-SH2**, it appears that the former is significantly better in terms of CoP and VHC, while equal in terms of discharge temperature.

The **1S-XV** and **1S-XP** cycles are coincident in VHC and discharge temperature, while the latter improves the CoP almost as much as the **2S-DCIC** cycle does. Even though the expander has to deal with wet expansion, which faces the same difficulties as wet compressions, it does show the improvements that might be possible.

The wet compression cycles also show a worse CoP compared to the standard cycle. This confirms that, at least for the wet fluids, the decrease in compression work is relatively less than the decrease in available enthalpy difference over the condenser. The VHCs also decrease compared to the standard cycle, so it can be concluded that such wet compression cycles are not desired with wet fluids.

The discharge temperature diagram shows that superheating leads to a significant temperature overshoot, though still below the threshold value of 400 °C. The superheat can be lowered to avoid this overshoot, however, as seen in Section 5.2.3, this will lower the CoP. The diagram also shows that the combination of superheating and intercooling results in an intermediate discharge temperature. It can thus be thought of as a compromise between preventing wet compression and avoiding large discharge temperatures.

For the other wet fluids that were simulated in this way, the general trend was equivalent to that of benzene, though with different absolute values. This trend can be summarised as:

- The best CoP was achieved by **2S-2SH-DCIC**, closely followed by **1S-SH1**
- The best VHC was also achieved by **2S-2SH-DCIC** and **2S-DCIC**, followed at a distance by **1S-SH1**
- The **2S-2SH-DCIC** achieves dry compression with moderate overshoot, while **1S-SH1** has an overshoot about twice as large. The other cycles end their compression in the two-phase region.

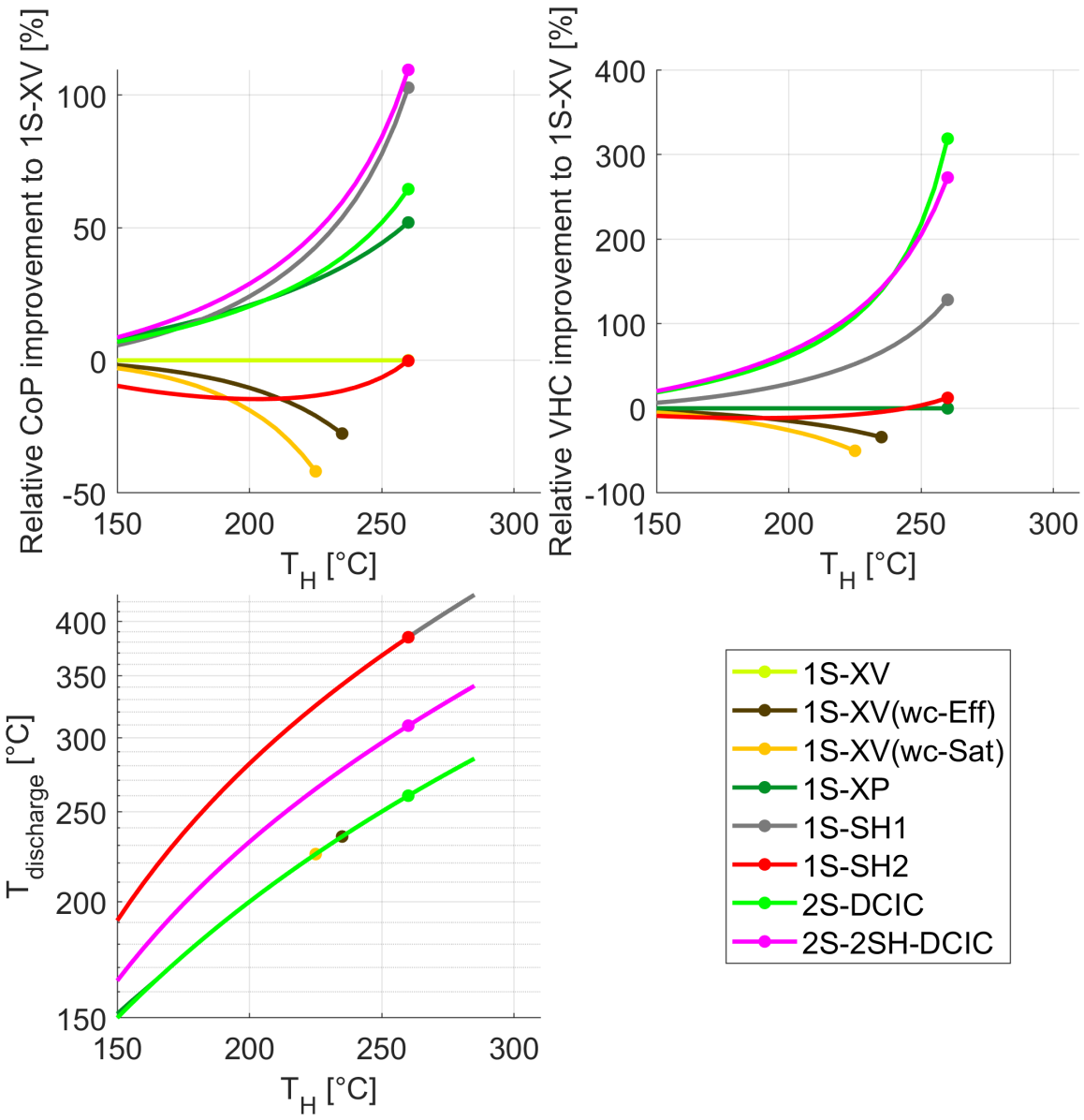


**Figure 5.8:** Comparison of different cycle configurations for benzene.

The fluids which have been simulated and follow the same trend include toluene, DMC, C1CC6, cyclohex, cyclopen and hexane. The respective diagrams can be seen in Chapter B. For these fluids, it can thus be concluded that **2S-2SH-DCIC** gives the most satisfactory results.

Fluids which follow different trends are water, methanol, ethanol and acetone. The comparison of configurations for water is shown in Figure 5.9. From the CoP diagram it appears that in general, the improvements possible with different cycles are much lower than what was possible with benzene. This is inherently connected with the already large CoP of water in the standard cycle. Nevertheless, improvements in CoP up to 10 % are possible with wet compression and intercooling cycles. Both the **1S-XV(wc-Eff)** and **1S-XV(wc-Sat)** can significantly improve the CoP for lower sink temperatures while the improvement diminishes for higher sink temperatures and even disappears for the latter cycle. The VHC of both these cycles also shows deterioration. Nevertheless, the discharge temperatures are the lowest compared to the other cycles.

Looking at the cycles with intercooling, it appears that in contrast to wet fluids, **2S-DCIC** performs better than **2S-2SH-DCIC** on all terrains. It has a larger CoP, while the VHC and discharge temperatures are, though similar, in favour of the former cycle. It is also seen that **2S-ICIC** performs significantly worse than **2S-DCIC** both on CoP and VHC. On discharge temperature, it is coincident with the **2S-2SH-DCIC** cycle and can therefore not be seen. This confirms that direct-contact intercooling is better than indirect-contact cooling. Comparing **2S-DCIC** to **1S-XV(wc-**

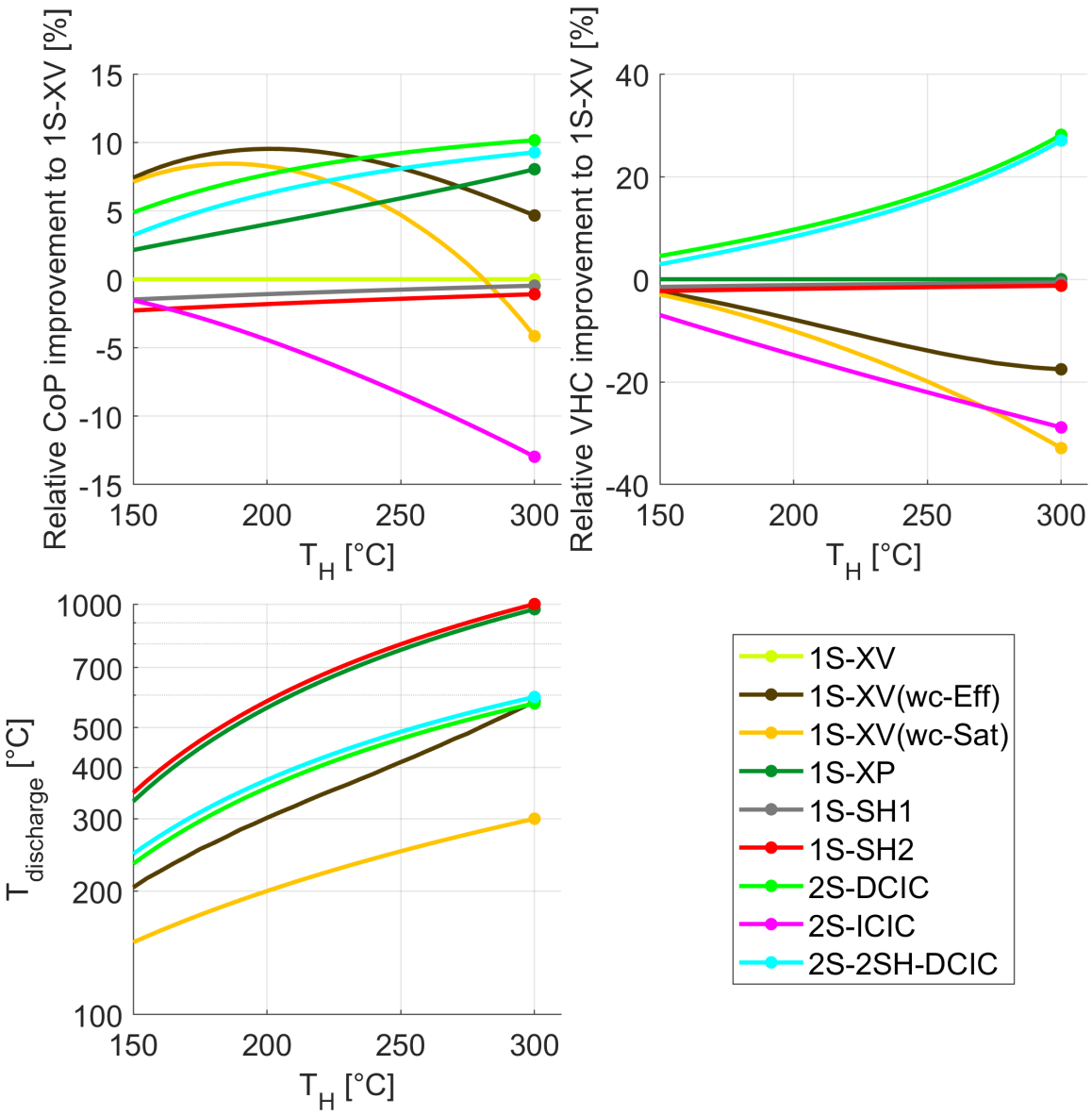


**Figure 5.9:** Comparison of different cycle configurations for water.

**Eff)** is difficult. The former scores better on VHC while the latter has a lower discharge temperature. The latter has a better CoP at low sink temperatures and is a simpler setup. Nevertheless, it requires technically challenging wet compression and at high sink temperatures, the CoP becomes less than **2S-DCIC**. Therefore, it was concluded that the **2S-DCIC** is the most suited.

The analysis for the fluids methanol, ethanol and acetone resulted in a slightly different conclusion. For methanol, it appeared that adding an expander to a single-stage cycle (**1S-XP**) results in a larger CoP improvement compared to the standard cycle than **2S-DCIC** gives. The latter has a better CoP than **2S-2SH-DCIC** for most of the sink temperature range and is very effective at keeping a low discharge temperature. On top of that, it has the largest VHC. Therefore, it is concluded that for methanol, **2S-DCIC** is the best configuration. For ethanol, it appeared that **2S-2SH-DCIC** has a slightly better CoP than **2S-DCIC** and comparable VHC. Since the discharge temperatures are relatively low, it was concluded that **2S-2SH-DCIC** is the best configuration for ethanol. The same was concluded for acetone. The respective diagrams can be seen in Chapter B.

### 5.2.5 Combination of best-performing cycles with the best fluids

From the previous section, it appeared that for most fluids, the **2S-2SH-DCIC** was the configuration with the best improvement compared to the standard cycle. Only for water and methanol, this was **2S-DCIC**. All fluids have been simulated again with their improved cycles over domains 1 and 2.

The results for domain 1 are shown in Figure 5.10 and for domain 2 in Figure 5.11. Again only the best fluids have been selected for display, with the following selection criteria:

- Domain 1: At $T_{\mathrm{H}} = 200\,^{\circ}\mathrm{C}$: CoP $> 3$ & VHC $> 1\,\mathrm{MJ/m^3}$
- Domain 2: At $T_{\mathrm{H}} = 250\,^{\circ}\mathrm{C}$: CoP $> 3$ & VHC $> 1\,\mathrm{MJ/m^3}$

The CoP limit was set larger than the threshold value to cut down on the number of fluids in the results display. This increased threshold was necessary because of the usage of the best configurations, which resulted in many fluids with a CoP larger than 1.5 at the stated $T_{\mathrm{H}}$.

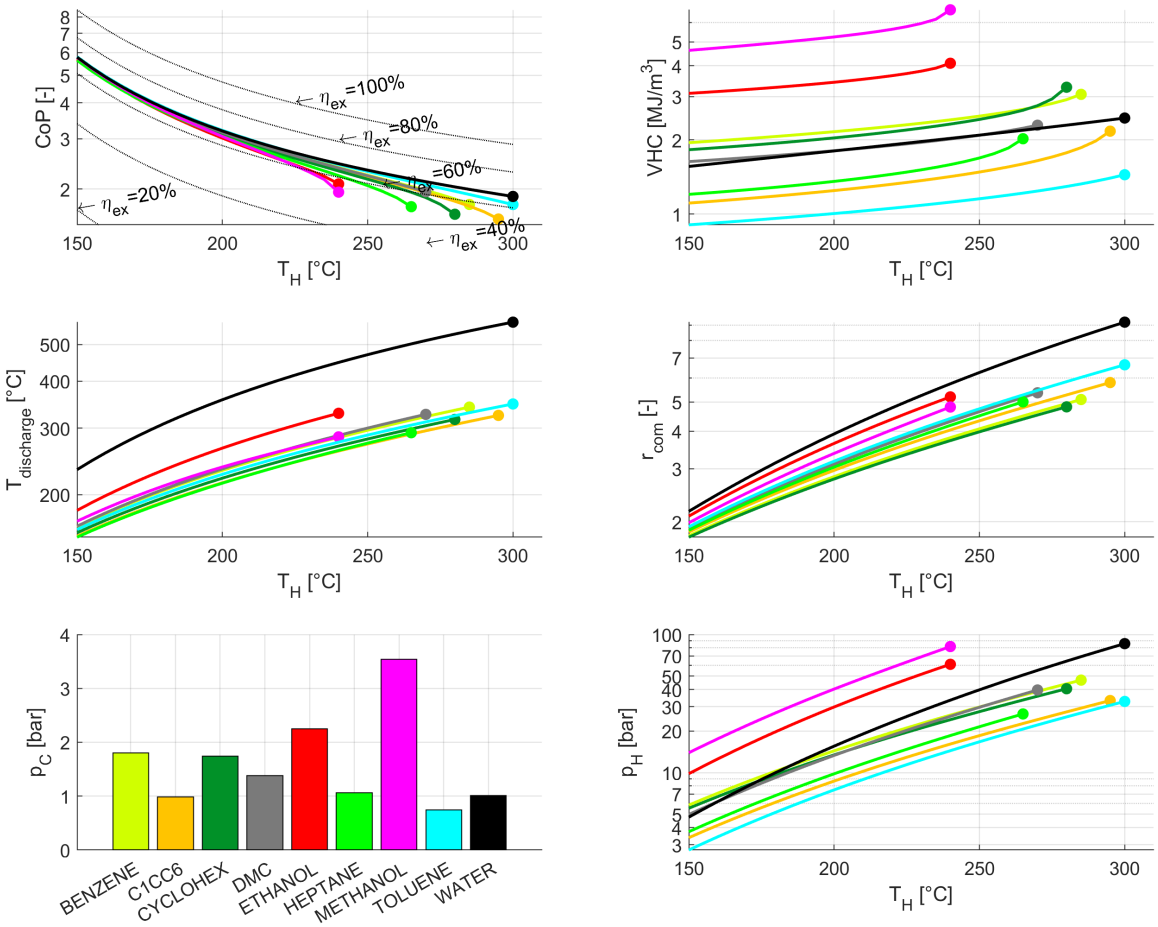


**Figure 5.10:** Performance figures for the different fluids using the configuration with the best improvement compared to **1S-XV** for domain 1. Since the colours match, the bottom left diagram can be used as a legend.

**Domain 1** From the results for domain 1, it appears that the CoP values are a lot less spread out compared to the results for **1S-XV** and that more fluids can be used up to a higher sink temperature. Nevertheless, water still has the best CoP values, can reach the largest sink temperatures and has average VHC. The discharge temperatures are lower than with the **1S-XV** cycle but still surpass the threshold value of 400 °C at about $T_{\mathrm{H}} = 220\,^{\circ}\mathrm{C}$. Benzene also has high a CoP and average VHC, while keeping the discharge temperatures below the threshold value. Due to the dual-stage compression, the pressure ratios of all fluids are lowered and do not surpass the threshold value of 8, except water for the largest sink temperatures.

The conclusion is therefore relatively comparable to the one for domain 1 of the **1S-XV** cycle, with benzene being the most suitable fluid to use. Again, if solutions can be found for the large discharge temperature, it would be a superior fluid due to the higher CoP and hazard-free characteristics.

**Domain 2** For this domain, the results look a bit different. In the CoP diagram, it is seen that over the entire $T_{\mathrm{H}}$ range, water has a better CoP by a considerable margin. Moreover, it is still the fluid that can reach the largest temperature lifts and sustains an exergy efficiency of about 60 % over this range. All other fluids have a quickly deteriorating exergy efficiency, where decane and C3CC6 can be considered edge cases. In terms of VHC, water is very much superior. The fluids

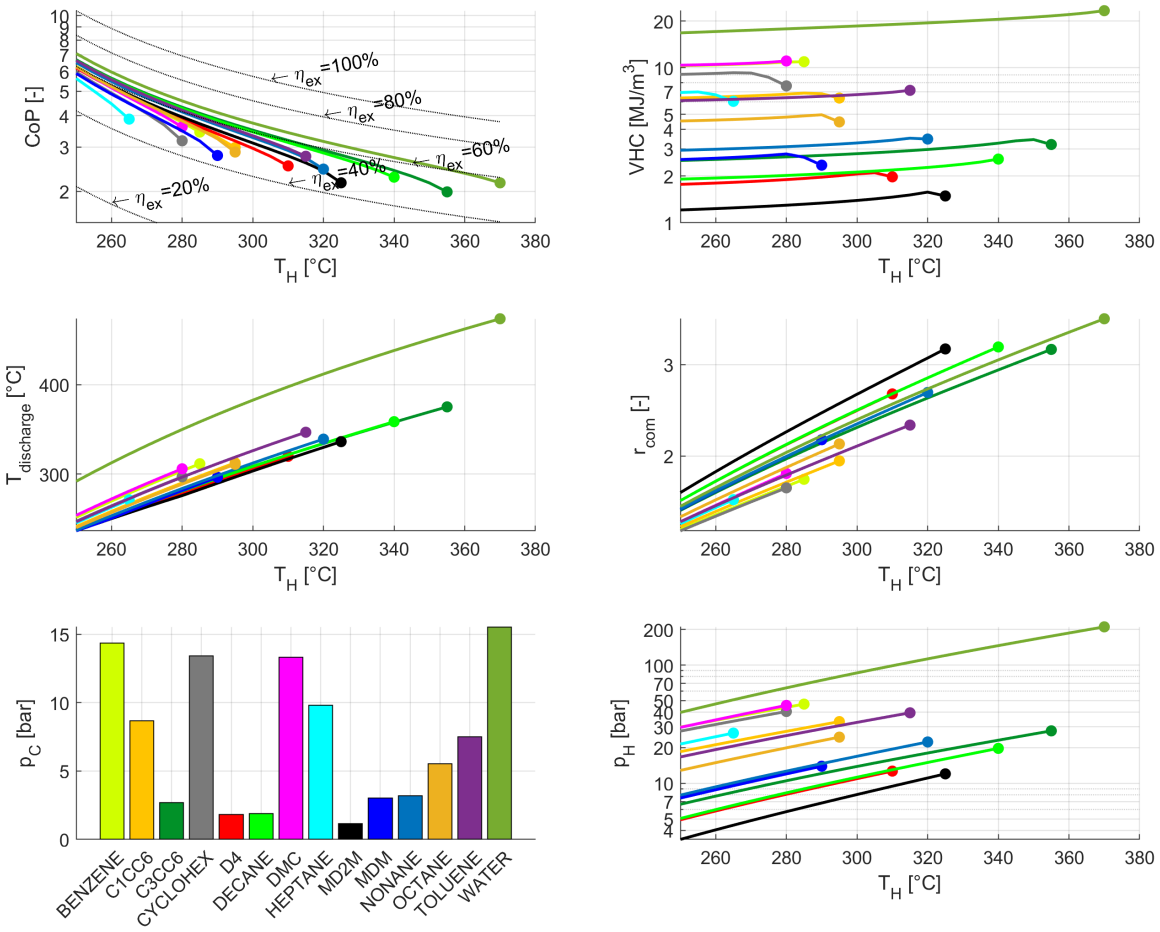


**Figure 5.11:** Performance figures for the different fluids using the configuration with the best improvement compared to **1S-XV** for domain 2. Since the colours match, the bottom left diagram can be used as a legend.

decane and C3CC6 have a VHC which is about a factor of 10 lower. Benzene and DMC also have relatively high VHC values, however, their use is limited to sink temperatures up to about only 270 °C. Regarding the discharge temperatures, water still has the same problem while all other fluids have similar results. The pressure ratios are however all largely below the threshold value. In conclusion, water is the most suitable fluid for domain 2, provided the discharge temperatures can be handled. If this can not be handled, C3CC6 would be the second-best alternative.

In this analysis, the condenser and evaporator have been modelled as indirect-constant heat exchangers with a constant heat load. In real heat pumps, however, there are process and waste fluids with distinct temperature profiles inside the condenser and evaporator. Because a minimum temperature difference is always required in these heat exchangers, the actual temperature lift and CoP of the heat pump are lower than what has been obtained in this chapter. However, since the characterisation of the process and waste fluids can vary wildly, it was decided to omit these from these simulations and focus on the working fluid solely. Moreover, this analysis only simulated subcritical cycles. This allowed a constant temperature profile in the condenser, setting the same bar for each fluid.

To obtain results for more realistic heat pumps, follow-up research would be necessary. A manual optimisation to find the optimum cycle configuration and fluid for a given case is possible using the heat pump design tool shown in Section 4.7. However, due to the vast number of possibilities and different variables, it can be very time-consuming and inefficient. A follow-up project could therefore be the development of an optimisation algorithm.

# Chapter 6

# HP Model: Summary & Conclusion

The heat pump model was first compared to three models from other authors. Consistent results were obtained, which led to the model being considered validated. Afterwards, the model was used to simulate various heat pump configurations for different fluids over two temperature domains. The results revealed which are the best configurations and which fluids have the best performance.

For the standard cycle in domain 1, **1S-XV**, it appeared that methanol was a good fluid to use because of its high CoP, VHC and only moderately high discharge temperature. However, it could only reach a sink temperature of 240 °C. Furthermore, the dangers of methanol were pointed out and it was realised that if the challenges regarding water vapour compression were solved, it would be a superior fluid. In domain 2, it appeared that no fluid came close to the CoP performance of water, however, the extreme discharge temperatures and large pressure ratios prevented water from being a suitable working fluid in this case. Toluene was the next best alternative, though it could only be used up to 305 °C.

With knowledge from the literature study, an investigation into the effect of wet compression with water as the working fluid was performed. This showed that wet compression can improve performance while lowering the discharge temperature. However, the best CoP was obtained with superheated vapour.

Because many of the simulated fluids are wet, most of the **1S-XV** cycles exhibit wet compression, which is challenging to achieve. To remedy this, the effect of superheating was investigated. It appeared that superheating could considerably increase the CoP while preventing wet compression. Despite this, it was concluded that methanol with minimal superheating still proved to be a favourable working fluid. Neglecting VHC, benzene would be a good fluid with high CoP and low discharge temperature. However, the safety and environmental issues of all fluids in the results were also pointed out and it was again realised that with water, none of these issues exist.

Subsequently, it was investigated which configurations of the ones developed in Section 4.6 give the best performance. It appeared that for all fluids except water and methanol, the **2S-2SH-DCIC** configuration gave the best results based on its good CoP and low discharge temperature. For water and methanol, it appeared that superheating did not improve the performance. Therefore, it was concluded that **2S-DCIC** would be the best cycle to use. For water, the standard cycle with wet compression appeared to give very favourable improvements. However, due to the reduced improvement at higher sink temperatures and the fact that wet compression is technologically challenging, this cycle was not preferred.

Using the **2S-DCIC** cycle for water and methanol and **2S-2SH-DCIC** for all other fluids, the two domains were simulated again. For both domains, it appeared that even with the improved configurations, no fluid could surpass the CoP performance of water. The discharge temperature of water was however still much higher than all other fluids. The first best-alternative fluids are benzene for domain 1 and C3CC6 for domain 2.

Drawing an overall conclusion from these results, a general trend is that water has the absolute best CoP performance. This is the case with a configuration setup that has fewer components

than those for the other fluids. Regarding VHC, water is average for the lower sink temperatures and becomes superior to the other fluids at higher sink temperatures. However, in most cases, the discharge temperature of water surpasses the threshold value, which is the main reason why water is challenging to use. Another challenge is the large pressure ratios. The alternative to water is benzene in domain 1 and C3CC6 in domain 2. Apart from the lower performance, these fluids have several associated safety and environmental hazards, making their usage dangerous. Water is, apart from being cheap and freely available, non-harmful and environmentally friendly. This makes water the ideal working fluid for a HTHP, provided the issues of high discharge temperatures and large pressure ratios can be solved.

In the next chapter, a compressor design is proposed which could solve these issues associated with water while keeping its beneficial characteristics.

# Chapter 7

# LPGC Model: Design & Modelling Methodology

In the previous chapter, it became clear that water is an attractive working fluid for a high-temperature heat pump. It attained the largest CoP relative to all other fluids, with a simpler cycle, while also being cheap, non-flammable, non-explosive, non-toxic and non-harmful to the environment. The main downside appeared to be the unacceptably large temperature increase during compression and the large pressure ratios. With multistage compression and intercooling, the discharge temperature and pressure ratio could be somewhat alleviated, yet at the expense of increased system complexity and cost. A method of water vapour compression is therefore desired which solves the problem of large discharge temperatures and pressure ratios. At the same time, this method should not compromise the heat pump to a great extent in terms of size, cost, or complexity.

It was seen that intercooling the vapour using a $\text{DCHX}_{\text{FC}}$ has a positive effect on the CoP. However, this intercooling can only be done between two compressor stages. To exploit this type of intercooling further, it is thus necessary to add more compressor stages. Since each stage requires an extra DCHX and another expansion device, system complexity increases quickly to uneconomic magnitudes.

Wet compression can be thought of as another way of intercooling, but then continuously. Due to the two-phase state of the vapour in the compressor, any heat generated with the compression will just evaporate more liquid. The temperature is thus fixed to the saturation temperature. This cycle also showed a large improvement in CoP compared to the standard cycle. Wet compression is however, as discussed in Section 2.3.2, troublesome with centrifugal compressors due to the damage that liquid droplets can do to the blades. A twin-screw compressor can be used for wet compression but requires oil for sealing. Oil-free twin-screw compressors are available, but are more susceptible to leakage and thus not suited for large pressure ratios [14]. The same problems are true for scroll and reciprocating compressors. The latter can however also be used with a liquid piston instead of a solid one, as noted in Section 2.3.2. This principle is known as Liquid Piston Gas Compression (LPGC).

To understand whether an LPGC would be a suitable compressor in heat pumps, it was decided to develop a detailed model simulating different effects that occur inside it. For this reason, background information about its working principle, characteristics, advantages and disadvantages was gathered, which is presented in Section 7.1. The information was used to develop a numerical model able to simulate the entire compression and discharge process. The structure, assumptions and calculations used in this model are described in Section 7.2. Then, in Section 7.3, the conditions which define the boundaries of the compression process are given. Finally, Section 7.4, discusses the limitations of the model that resulted from the implications in the modelling method.

## 7.1 Background information on LPGC

An LPGC can be thought of as a reciprocating piston-cylinder assembly, in which the solid piston is replaced by a rising liquid column. Using a pump, liquid can be forced into a gas-filled cylinder, called the compression chamber. A pool forms in the lower part of the chamber due to the higher density of the liquid compared to the gas. As the liquid is incompressible, the volume of the gas

has to decrease when there is no other exit in the chamber. The gas is therefore compressed to a higher pressure [30]. This section aims to show the advantages compared to other compressors (Section 7.1.1), explain the compression process (Section 7.1.2), describe how LPGC can be beneficial in heat pumps (Section 7.1.3) and finally, a summary of LPGC in literature is given (Section 7.1.4).

### 7.1.1 Advantages of LPGC

Unlike a solid piston, a liquid piston can take on any shape that is imposed on it [42]. This characteristic facilitates measures to increase the heat transfer from the gas, either by increasing the surface area of the chamber [43, 57] or by introducing (part) of the liquid as a spray [44, 30, 42]. The former can be done by dividing the compression chamber is multiple smaller compression chambers. The latter is done by diverting a fraction of the liquid and injecting it as finely dispersed droplets. The droplets have a large surface area for heat transfer [44]. This allows the gas temperature to remain low during compression, thereby also reducing the specific compression work. While spray injection is also possible in solid piston reciprocating compressors, a separate system is required to evacuate a surplus of injected liquid. If not addressed adequately, there is the risk of a hydraulic lock [43]. With LPGC, the droplets can conveniently fall into the liquid column [44].

Another advantage of LPGC is that compared to a solid piston, the sliding friction is replaced by viscous friction. Even though the friction forces were found to be of the same order magnitude, no oil is required as the operation is wear-free [57].

Furthermore, since any heating effects only happen in the compression chamber, the pump can operate at a constant low temperature. Therefore, a pump could be relatively cheap compared to a compressor. Depending on the type of pump, they could also be more efficient than a compressor. Typical hydraulic pump efficiencies are 80-90 % [34]. Due to the incompressibility of water, positive displacement pumps can reach large pressure ratios in one stage. On top of that, the flow rate is approximately linearly related to the pump speed, making simple control possible [18].

A disadvantage is that compression speed is limited by gravitational effects to prevent liquid separation and splashing [44]. Therefore, to achieve the required capacities, the LPGC system might require more floor space than ordinary compressors would. This downside could however be compensated by the fact that the compression chamber is easily scalable.

### 7.1.2 Compression process in LPGC

The different stages of the compression process in an LPGC are shown in Figure 7.1.

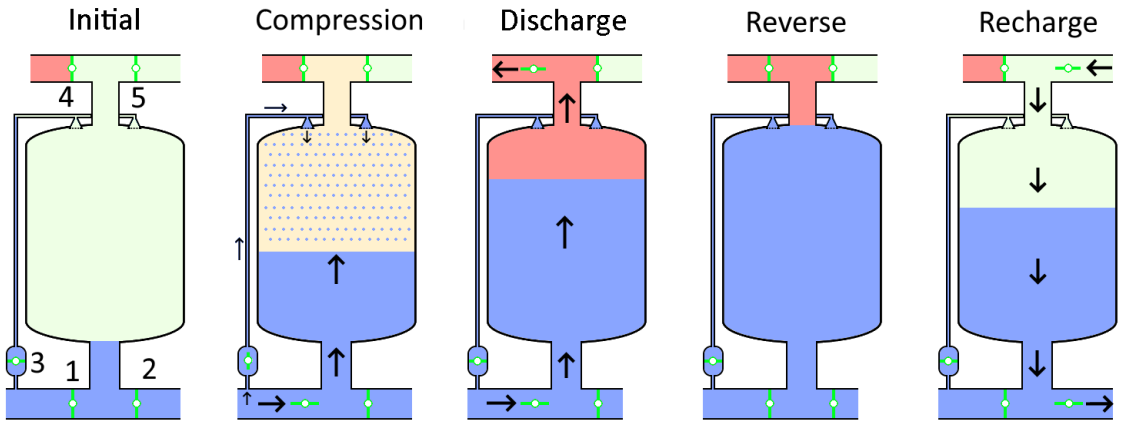


**Figure 7.1:** The separate stages that occur in the compression process of the LPGC. The blue colour indicates liquid, while the green, orange, and red colours describe low-pressure, medium-pressure, and high-pressure vapour respectively.

The system consists of a compression chamber that has in and outlets both at the top and at the bottom of the chamber. Spray nozzles are also situated at the top of the chamber. Furthermore, there are 5 valves, numbered in the drawing of the 'Initial' stage:

1. Liquid admission valve: controls the entrance of liquid into the chamber. The liquid comes from a pump and can therefore be forced into the compression chamber.
2. Liquid discharge valve: controls the release of liquid out of the chamber towards a liquid reservoir.
3. Spray valve: controls the amount of liquid towards the spray nozzles.
4. Vapour discharge valve: controls the release of vapour out of the chamber towards a high-pressure vapour reservoir.
5. Vapour admission valve: controls the entrance of vapour into the chamber towards a low-pressure vapour reservoir.

The orientation of the valves shows whether the fluid can flow in that stage or not, which is also indicated by the arrows. The stages of the cycle are:

- Initial: At this stage, the compression chamber contains only low-pressure vapour. All valves are closed and there is no flow. It is therefore only an instantaneous stage in the cycle
- Compression: In this stage, the liquid admission valve and spray valve are open. This allows liquid to enter from the bottom of the chamber forming a rising liquid column. As all other valves are closed, the vapour has no way out and thus the available volume for it decreases. Thereby the chamber pressure is increased. If the compression is assumed to be adiabatic, the temperature of the vapour increases rapidly. The spray valve allows some of the liquid to enter the compression chamber from the top. The spray nozzles inject the liquid as finely distributed small droplets right into the vapour space. This enables a large degree of heat transfer between the droplets and the vapour, thereby cooling the vapour.
- Discharge: In this stage, the vapour discharge valve is opened because the pressure in the chamber reached the desired value. The liquid admission valve is also still open and thus the liquid column keeps rising, thereby forcing the vapour out of the compression chamber. The spray valve is closed in this stage, as the vapour is not being compressed anymore. Adding more spray could lead to condensation of the vapour, which is undesirable.
- Reverse: At this stage, the compression chamber has been filled up with liquid. All valves are closed, so there is no more flow. It is therefore only an instantaneous stage in the cycle
- Release: In this stage, the liquid discharge valve is opened and the remaining high-pressure vapour forces the liquid out of the chamber. All other valves are closed.
- Recharge: In this stage, the pressure in the chamber is decreased to that of the low-pressure vapour. This allows the vapour admission valve to be opened, allowing new low-pressure vapour to enter the chamber. The vapour replaces the liquid, which keeps discharging from the chamber via the liquid discharge valve.

### 7.1.3 LPGC in heat pumps

A key characteristic of an LPGC in a vapour compression heat pump is that the liquid phase of the working fluid can be used to compress the vapour phase of this working fluid. So with the use of water as a working fluid, liquid water can be used to compress steam. Figure 7.2 shows a diagram of how an LPGC can be implemented in a vapour compression heat pump.

The system consists of the usual evaporator (1) and condenser (9), which are modelled as shell-and-tube heat exchangers. These heat exchangers also act as flash chambers, as visualised Figure 7.3. The waste and process heat streams flow through the tubes in the evaporator and condenser respectively. In the evaporator, the tubes are surrounded by saturated liquid water. As the waste heat stream gives up its heat, the water boils and the resulting steam gathers in the upper portion of the shell. Therefore steam can be drawn off from the top of the evaporator towards the vapour admission valve (2). This valve controls the admission of vapour into the compression chamber (6). From the bottom of the evaporator, liquid can be drawn off towards the pump (3). The pump is driven by a motor (4) and pumps liquid towards the compression chamber, governed by the liquid admission valve (5). A small fraction of the supplied liquid, controlled by the spray valve (7), is diverted to spray nozzles at the top of the chamber. The spray line is branched off before the liquid admission valve instead of after because of the pressure drop that the spray valves have. By controlling both valves, the amount of spray can be controlled.

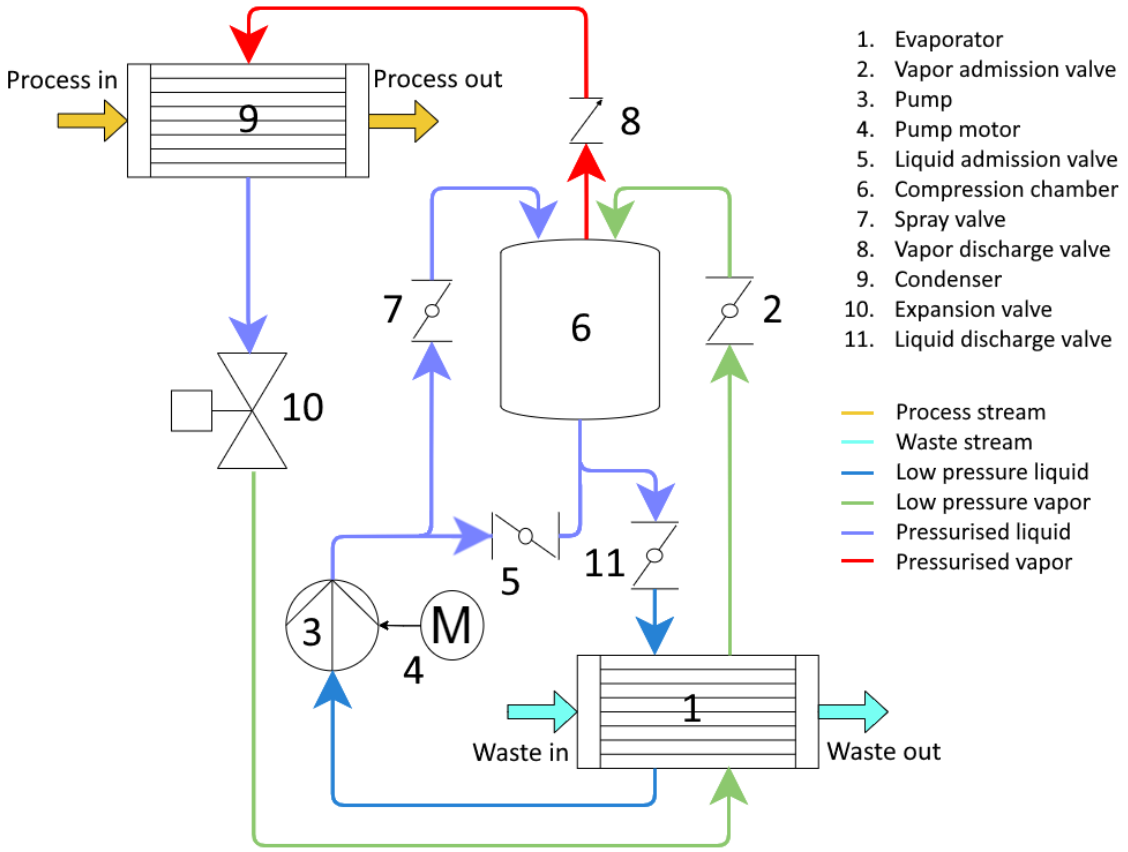


**Figure 7.2:** Diagram of a Liquid Piston Gas Compressor implemented in a vapour compression heat pump. The components are not drawn to size.

Once the pressure in the chamber reaches the desired discharge pressure, the discharge valve (8) opens, allowing the high-pressure steam to enter the condenser (9). In the condenser, the process stream flows through the tubes which are surrounded by the steam. The steam gives up its heat to the process fluid and thereby condenses. The condensate gathers at the lower portion of the condenser shell, where it can exit towards the expansion valve (10). This valve throttles the high-pressure condensate to the pressure of the evaporator, which the resulting stream subsequently enters. When the compression chamber is full of water, the liquid discharge valve (11) opens to allow the water back into the evaporator. This discharge is facilitated by the remaining pressure in the chamber and the higher position of the compression chamber to the evaporator so that the liquid naturally falls to the evaporator.

Depending on the pressures of the waste and process fluid it might not be desirable to have the working fluid outside the tubes in the evaporator and condenser. Generally, the fluid with the largest pressure is placed inside the tubes to minimise construction costs [58]. In that case, a separated flash chamber may be incorporated with an ordinary shell-and-tube heat exchanger.

Otherwise, the evaporator thus acts as both a heat exchanger and a liquid reservoir for the pumping liquid. A disadvantage of this system is its cyclic operation. With every cycle, there is an interval in which a lot of liquid is withdrawn from the evaporator, followed by an interval where a lot of liquid returns. The same goes for the vapour in the evaporator and condenser. The level of the liquid-vapour interface therefore changes during the process. The tubes in the evaporator should remain submerged in liquid to keep the same evaporating capacity. Similarly, the tubes in the condenser should remain submerged in vapour to keep the same condensing capacity. Furthermore, the pressure levels change during the inflow/outflow of liquid/vapour. The corresponding saturation temperature changes accordingly which undesirably deviates the process from the design point.

This problem can be dealt with by sizing the evaporator, condenser, and compression chamber such that the admission and discharge do not have a large influence on the surface levels in the heat

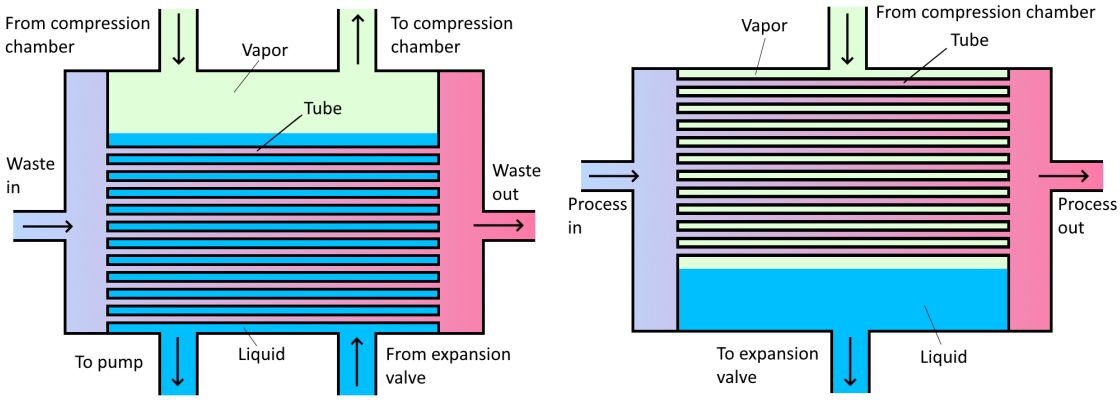


**(a)** Evaporator.

**(b)** Condenser.

**Figure 7.3:** The evaporator (a) and condenser (b) are shell-and-tube heat exchangers with extra space above and beneath the tubes respectively.

exchangers. This approach could however lead to largely oversized components. Another solution to this problem is having multiple smaller compression chambers in parallel to each other, but operating in different phases. The number of chambers can be chosen such that there is one chamber discharging to the condenser at all times, approaching a more continuous operation. Another reason for adding more compression chambers can be to increase the pumping capacity when increasing the chamber volume is not practical. Furthermore, a multitude of compression chambers allows the pump to run continuously instead of having to start and stop again and again.

During compression, the liquid column in the chamber likely heats up due to heat transfer from the compressed vapour. This heat is not wasted because once the release valve opens, the pressure is lowered and the liquid becomes supersaturated. A part of it therefore flashes to vapour either inside the compression chamber or in the evaporator.

### 7.1.4 LPGC in literature

Various projects in the literature investigated LPGC. Most of these use LPGC in Compressed Air Energy Storage (CAES) systems. Here, air is compressed and stored when there is a surplus of energy and expanded when there is an energy demand. With an ordinary compressor air significantly heats up, consuming considerably more work than isothermal compression would [42]. With LPGC, authors hope to achieve (near-) isothermal compression by the cooling which LPGC facilitates. This is either done by facilitating convection [40, 41], increasing the surface area of the compression chamber [57, 43], or by liquid spray injection [44, 30, 1, 42]

Van de Ven & Li (2009) made a numerical simulation which used water to compress air. Cooling was implemented by simulating an LPGC consisting of 1 up to 1.000.000 individual compression chambers. With more chambers, the ratio of wall area to volume was increased, giving more surface for heat transfer. The process was compared to an ordinary air compressor and it was found that the energy consumption of LPGC was 19 % lower than the ordinary compressor, while near-isothermal operation was achieved.

Qin & Loth (2013) made a numerical simulation of a liquid column of water in a compression chamber, moved up and down by a reciprocating piston in the same chamber, to compress air. Due to the gravitational effects, the acceleration of the liquid column is limited to prevent separation. Air was cooled by direct droplet spray injection and by pre-mixing of droplets in the air admission pipe. A detailed analysis considered individual droplet sizes, kinetics and evaporation effects. The compression process was assumed to be polytropic. Viscous losses in the compression were about 2% and therefore neglected. The vapour space was assumed to be adiabatic and the droplets were uniformly distributed through the chamber and had identical temperatures. The mean droplet diameters used were 10 µm, 20 µm, 50 µm and 100 µm. For each time step, the compression was calculated, followed by a heat balance to calculate the heat transfer to the droplets. The results showed that compression efficiency was improved from 71 % for adiabatic compression to 95 % with near-isothermal compression at high liquid mass loading. The optimum operation was achieved with direct injection of small droplets.

The work that referred LPGC to heat pumps was found in the work of Kowalski et al. (2022), who used propylene glycol to compress $CO_2$. In an experimental setup, a pump forced liquid into a compression chamber both as a column from the bottom and as spray from the top. Results showed that near-isothermal compression could be achieved and compression efficiency was improved by 17 % to 30 % compared to the adiabatic case. Even though the downsides of compressors in heat pumps motivated this research, no application to heat pumps was made.

## 7.2 LPGC Model

A numerical model of a Liquid Piston Gas Compressor with liquid spray injection has been made. In this model, the compression chamber is a cylindrical chamber with diameter $D$ and volume $V_C$, as seen in Figure 7.4. The model simulates the compression process from the 'Initial' stage until the 'Reverse' stage, referring to Figure 7.1. The release and recharge are not simulated as these are not relevant to the compression characteristics. Furthermore, the pressures in the evaporator and condenser are assumed to be constant and thus independent of the inflow/outflow of liquid/vapour. Also, it is assumed that deviations from thermodynamical equilibria can be neglected. As such the model is simulated as a quasi-equilibrium process.

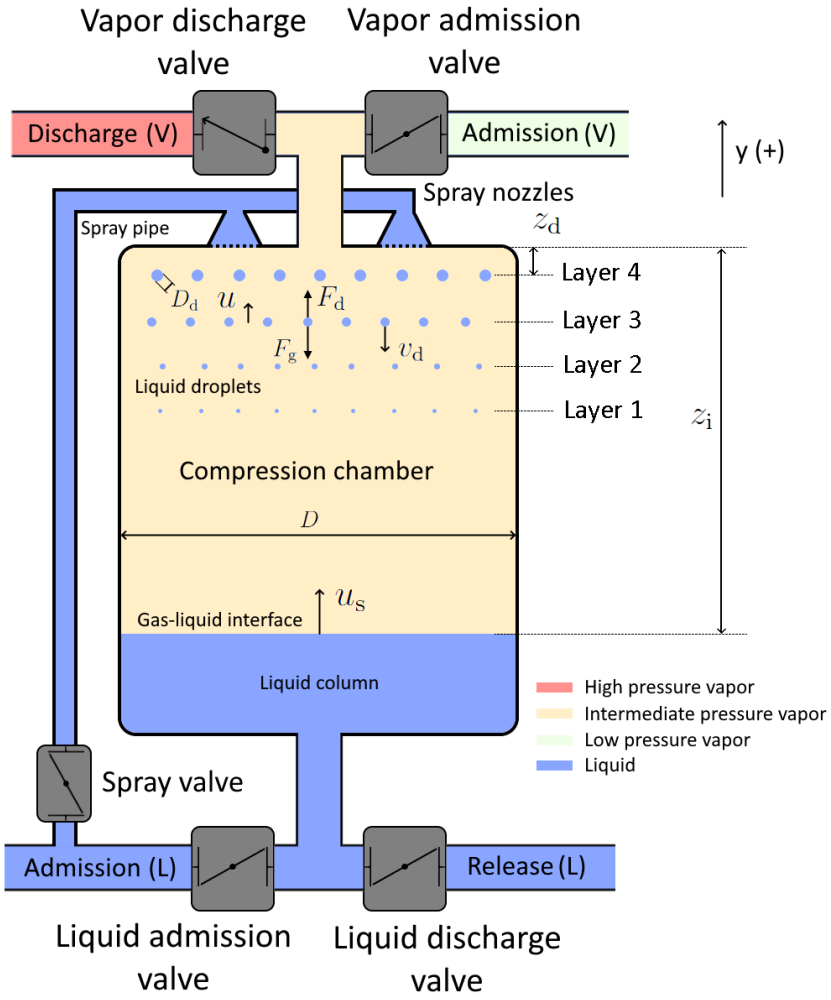


**Figure 7.4:** Schematic overview used for the model of the LPGC. It shows an instantaneous moment in the compressing part of the cycle. Four droplet layers have been injected.

In the initial state, $t = 0$, the chamber thus contains only saturated vapour at the pressure of the evaporator. The liquid column rises from the bottom to the top, thereby compressing the vapour. The admission of liquid stops when the chamber is filled, leaving a small clearance volume $V_{cl}$ in the discharge pipe. The clearance volume is defined as a percentage $f_{cl}$ of the chamber volume:

$$V_{cl} = f_{cl} V_C. \tag{7.1}$$

The final state of the simulation ($t = t_f$) is the point where the admission of liquid stops. The liquid mass flow rate, $\dot{m}_L$, is taken constant and thus the upwards velocity of the vapour-liquid surface, $u_s$, is also constant. The vapour space, which is taken as control volume (CV), is therefore gradually decreasing in volume. This vapour space is assumed to be adiabatic, so it does not exchange heat with the walls over the chamber, nor with the liquid column. The CV does have liquid droplets entering from the top and exiting at the bottom (droplets fall into the liquid column). A fraction $f_{LS}$ of the supply liquid is taken from the admission/release pipe and enters the chamber through the spray nozzles. This is the spray fraction. The mass flow rates of the liquid column (LC) and the liquid spray (LS) are therefore

$$\dot{m}_{LC} = (1 - f_{LS})\,\dot{m}_L \qquad \& \qquad \dot{m}_{LS} = f_{LS}\dot{m}_L \tag{7.2}$$

respectively. The velocity of the vapour-liquid surface is then

$$u_s = \frac{\dot{m}_{LC}}{\rho_L A_C}, \tag{7.3}$$

where $\rho_L$ is the liquid density and $A_C = \frac{1}{4}\pi D_C^2$ is the cross-sectional area of the chamber.

A new layer of droplets is assumed to enter the chamber in evenly spaced time intervals of $\Delta t_{LS}$. The droplets themselves are modelled as perfect spheres, which can be assumed for diameters lower than 400 µm [26]. Properties that describe droplets are denoted with a small 'd' subscript. Each layer is assumed to contain an equal amount of droplets. All droplets in one layer are assumed to be identical, so they always have the same diameter, vertical position, velocity etc. Therefore, some droplet properties describe the entire layer. The droplets are assumed to be perfectly distributed around the chamber from the moment they are injected. The droplet mass can then be calculated as:

$$m_d = \rho_L V_d \tag{7.4}$$

where $V_d$ is the droplet volume. The number of droplets injected each second is then:

$$\dot{n}_d = \frac{\dot{m}_{LS}}{m_d} \tag{7.5}$$

and number of droplets in each single layer is:

$$n_d = \dot{n}_d \Delta t_{LS}. \tag{7.6}$$

### 7.2.1 Structure of the model

The structure of this model is explained with the flow diagram shown in Figure 7.5. First, the inputs are defined and used to calculate the initial conditions of the LPGC, described further in Section 7.2.6. These are used to initiate a numerical model of the compression chamber with droplets sprayed into it. The steps that are taken with each step in time are:

- **Discharge pressure check**: it is checked whether the set discharge pressure was reached in the previous time step. If this has not been reached yet, the discharge valve is still closed and the model continues with adiabatic compression. Otherwise, if the discharge pressure has been reached, the discharge valve is open and the model continues with discharge property calculations.
- **Adiabatic compression**: due to the decreased volume of the vapour space, the pressure of the vapour increases. This increase is calculated with adiabatic process thermodynamics.
- **Reaching thermal equilibrium**: due to the difference in temperature between the droplets and the vapour, thermal energy will be exchanged. This will evaporate some of the droplets, thereby cooling the vapour. The pressure will be corrected for the changes in density and mass.
- **Discharge property calculation**: due to the discharge valve being open, the mass of the vapour decreases while the pressure stays constant. The remaining droplets in the chamber are
- **Calculating droplet kinematics**: the droplet masses might have changed by evaporation or by falling into the liquid column. Therefore, the forces on them have changed and thereby the path they take through the chamber.

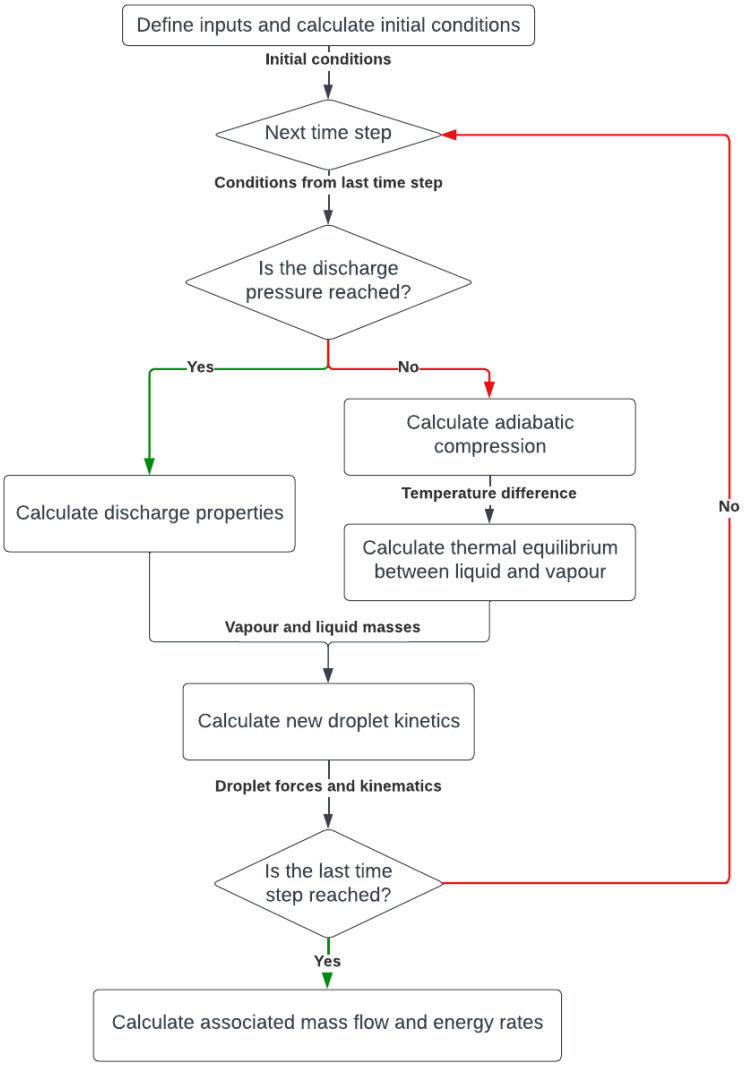


**Figure 7.5:** A flow diagram of the LPGC model showing the general sequence of actions that are taken.

This separated order of accounting for the different mechanics is similar to what Qin and Loth (2013) used. This process was validated in the same work using experimental data on channel flow developed in [25, 53].

When the last time step has been reached, the final mass and energy flow rates are calculated. These provide the specific work, compression efficiency and entropy production of the compression.

The length of a single time step in discrete form is $\Delta t$ so that:

$$t_j = t_{j-1} + \Delta t. \tag{7.7}$$

The first instant is at $j = 1$ and the simulation starts at $t = 0$, so $t_1 = 0$. The time step is derived from the final time and the number of steps $N$ of the simulation:

$$\Delta t = \frac{t_\mathrm{f}}{N}. \tag{7.8}$$

### 7.2.2 Adiabatic compression

The mass of the liquid column is that of the previous time step plus the part that has entered the chamber since.

$$m_{\mathrm{LC},j} = m_{\mathrm{LC},j-1} + \dot{m}_\mathrm{LC}\Delta t. \tag{7.9}$$

The volume of the liquid column is then $V_{\mathrm{LC},j} = \frac{m_{\mathrm{LC},j}}{\rho_{\mathrm{L},k}}$. The volume of the liquid present in the room as sprayed droplets is the sum of the volumes of all individual droplet layers:

$$V_{\mathrm{LS},j} = \sum_{k=1}^{N_{\mathrm{T},j}} \frac{m_{\mathrm{dT},k,j}}{\rho_{\mathrm{d},k,j}}, \tag{7.10}$$

where $m_{\mathrm{dT},k,j}$ is the total droplet mass of layer $k$, $\rho_{\mathrm{d},k,j}$ the droplet density of layer $k$ and $N_{\mathrm{T},j}$ the number of layers present in the chamber, all at time $t_j$.

Now, the volume left for the vapour can be calculated:

$$V_{\mathrm{V},j} = V_{\mathrm{C}} - V_{\mathrm{LC},j} - V_{\mathrm{LS},j}. \tag{7.11}$$

It is assumed that the relationship between pressure and volume can be described as a polytropic process, which was also used by Qin & Loth (2013) and Van de Ven & Li (2009). The pressure is then calculated using the polytropic process relation with the conditions of the previous time step:

$$p_j = p_{j-1} \left( \frac{V_{\mathrm{V},j-1}}{V_{\mathrm{V},j}} \right)^{\kappa_j}. \tag{7.12}$$

Here $\kappa_j$ is the polytropic index which is, for an isentropic (reversible and adiabatic) process, the ratio of specific heat capacities of the fluid [35, 49]. For the calculation, the heat capacities of the previous time step are used: $\kappa_j = \frac{c_{\mathrm{p},j-1}}{c_{\mathrm{V},j-1}}$. As the specific heats are recalculated every time step, the polytropic index dynamically follows the compression process.

The deviation of the isentropic process is quantified by the isentropic compression efficiency $\eta_{\mathrm{com}}$ [5, 2]:

$$h_{\mathrm{V},j} = h_{\mathrm{V},j-1} + \frac{h_{\mathrm{Vs},j} - h_{\mathrm{V},j-1}}{\eta_{\mathrm{com}}} \tag{7.13}$$

where $h_{\mathrm{Vs},j} = h\left(p = p_j, \rho = \rho_{\mathrm{V},j}\right)$ is the isentropic specific enthalpy evaluated at the current pressure $p_j$ and the current vapour density $\rho_{\mathrm{V},j} = \frac{m_{\mathrm{V},j}}{V_{\mathrm{V},j}}$. With the newly calculated vapour enthalpy and the current vapour density, which has not changed, the pressure corrected for the isentropic efficiency can be evaluated: $p_j = p\left(h = h_j, \rho = \rho_{\mathrm{V},j}\right)$.

### 7.2.3 Thermal equilibrium

Due to the assumption of a quasi-equilibrium process, it is assumed that the vapour and the droplets reach full thermal equilibrium with each time step. The thermal equilibrium is found by deriving the mass and energy balances of the vapour space. The total equilibrium mass is found by adding the droplet mass to the vapour mass $m_{\mathrm{V},j}$:

$$m_{\mathrm{eq},j} = m_{\mathrm{V},j} + m_{\mathrm{LS},j}. \tag{7.14}$$

The energy balance is:

$$m_{\mathrm{V},j} h_{\mathrm{V},j} + \sum_{k=1}^{N_{\mathrm{T},j}} m_{\mathrm{dT},k,j} h_{\mathrm{d},k,j} = m_{\mathrm{eq},j} h_{\mathrm{eq},j}. \tag{7.15}$$

Here $h_{\mathrm{V},j}$ is the vapour enthalpy, $m_{\mathrm{dT},k,j}$ the total droplet mass in layer $k$ and $h_{\mathrm{d},k,j}$ the enthalpy of the droplets in layer $k$, all at time $t_j$. From this equation the equilibrium enthalpy $h_{\mathrm{eq},j}$ can be calculated. The equilibrium volume is fixed and independent of the thermodynamics. It is the chamber volume minus the liquid column volume, $V_{\mathrm{eq},j} = V_{\mathrm{C}} - V_{\mathrm{LC},j}$, so that the equilibrium density is calculated with $\rho_{\mathrm{eq},j} = \frac{m_{\mathrm{eq},j}}{V_{\mathrm{eq},j}}$. With $h_{\mathrm{eq},j}$ and $\rho_{\mathrm{eq},j}$, two state points are known and the resulting pressure and quality $x_{\mathrm{eq},j}$ can be evaluated with RefProp. This pressure is therefore a correction to the previously calculated pressure and any variables that depend on it should be corrected as well.

The masses of the vapour and droplets remaining after the thermal equilibrium can be calculated with the quality:

$$m_{\mathrm{V},j} = x_{\mathrm{eq},j} m_{\mathrm{eq},j} \qquad \& \qquad m_{\mathrm{LS},j} = \left(1 - x_{\mathrm{eq},j}\right) m_{\mathrm{eq},j} \tag{7.16}$$

The total evaporated mass of droplets is then:

$$m_{\mathrm{evap,j}} = m_{\mathrm{LS},j-1} - m_{\mathrm{LS},j}. \tag{7.17}$$

To determine how this evaporation is distributed over all layers, the surface area of the droplets $A_{\mathrm{ds},j}$ before thermal equilibrium is used. The larger the surface area of the droplets in a layer, the larger the area available for heat transfer. Therefore it is assumed that more will evaporate from larger droplets. The surface distribution coefficient per layer, $n_{\mathrm{area},k,j}$, is thus the droplet surface area normalised by the total droplet surface area in the chamber:

$$n_{\mathrm{area},k,j} = \frac{A_{\mathrm{ds},k,j}}{\sum_{k=1}^{N_{\mathrm{T},j}} A_{\mathrm{ds},k,j}}. \tag{7.18}$$

The new liquid mass in layer $k$ can then be calculated with:

$$m_{\mathrm{dT},k,j} = m_{\mathrm{dT},k,j-1} - n_{\mathrm{area},k,j} m_{\mathrm{evap},j}. \tag{7.19}$$

Now that the mass of liquid droplets has been corrected, the volume of the liquid spray can be recalculated with Equation (7.10). This can be used to recalculate vapour volume with Equation (7.11) and then the vapour density can be calculated with:

$$\rho_{\mathrm{V},j} = \frac{m_{\mathrm{V},j}}{V_{\mathrm{V},j}}. \tag{7.20}$$

With the pressure and vapour density known, the other vapour state properties, $T_{\mathrm{V},j}$, $h_{\mathrm{V},j}$, $s_{\mathrm{V},j}$ and $\mu_{\mathrm{V},j}$, can be determined.

The liquid droplet state properties, $h_{\mathrm{d},j}$ and $\rho_{\mathrm{d},j}$ are determined by evaluating the saturated liquid state properties at the new higher pressure $p_j$. The liquid in the column is pumped to the new pressure and thus its specific enthalpy changes accordingly:

$$h_{\mathrm{L},j} = h_{\mathrm{C}} + \left(h_{\mathrm{Ls},j} - h_{\mathrm{C}}\right)/\eta_{\mathrm{PU}} \tag{7.21}$$

where $\eta_{\mathrm{PU}}$ is the isentropic efficiency of the pump and $h_{\mathrm{Ls},j}$ is the isentropic enthalpy evaluated from the new pressure and the liquid entropy of the evaporator. With the pressure and liquid enthalpy being known, the other liquid state properties, $T_{\mathrm{L},j}$, $h_{\mathrm{L},j}$, $s_{\mathrm{L},j}$ and $\mu_{\mathrm{L},j}$, can be determined.

### 7.2.4 Droplet kinematics

The droplets are modelled in 1D, so they only have vertical motion. They therefore do not move sideways and they do not interact with other droplets. In this section, most properties are evaluated at each time $j$ and for each layer $k$ separately, unless stated otherwise. For readability, however, the $j$ and $k$ notation has been dropped. The mass of an individual droplet is calculated by dividing the layer mass by the number of droplets: $m_{\mathrm{d}} = \frac{m_{\mathrm{dT}}}{n_{\mathrm{d}}}$. The droplet diameter, volume, frontal area and surface area can then be calculated:

$$D_{\mathrm{d}} = \left(\frac{6m_{\mathrm{d}}}{\pi\rho_{\mathrm{L}}}\right)^{\frac{1}{3}} \qquad V_{\mathrm{d}} = \frac{1}{6}\pi D_{\mathrm{d}}^3 \qquad A_{\mathrm{df}} = \frac{1}{4}\pi D_{\mathrm{d}}^2 \qquad A_{\mathrm{ds}} = \pi D_{\mathrm{d}}^2. \tag{7.22}$$

The only forces acting on the droplets are assumed to be the gravity $F_{\mathrm{g}}$ downwards and the drag $F_{\mathrm{D}}$ upwards. The buoyancy force is assumed to be negligible due to the density of steam being smaller than that of water by about a factor of 1000. The force balance then becomes:

$$\sum F = F_{\mathrm{D}} - F_{\mathrm{g}} = m_{\mathrm{d}}\dot{v}_{\mathrm{d}}. \tag{7.23}$$

Here, $v_{\mathrm{d}}$ is the velocity of the droplet and thus $\dot{v}_{\mathrm{d}}$ is its acceleration. The gravity is simply:

$$F_{\mathrm{g}} = m_{\mathrm{d}} g \tag{7.24}$$

where $g = 9.81\,\mathrm{m/s^2}$. The drag force is calculated with the general drag equation:

$$F_{\mathrm{D}} = \frac{1}{2} C_{\mathrm{D}} \rho_{\mathrm{V}} A_{\mathrm{d}} w_{\mathrm{d}}^2. \tag{7.25}$$

Here, $\rho_{\mathrm{V}}$ is the vapour density, and $w_{\mathrm{d}}$ is the relative velocity between the droplet and the vapour:

$$w_{\mathrm{d}} = u - v_{\mathrm{d}} \tag{7.26}$$

where $u$ is the vapour velocity at the position of the droplet, $z_\mathrm{d}$. The vapour velocity is zero at the top of the chamber, and $u_\mathrm{s}$ at the position of the vapour-liquid surface, $z_\mathrm{s}$. The vapour velocity may be assumed to be linearly distributed between these extremities [44], so that:

$$u = \frac{z_\mathrm{d}}{z_\mathrm{s}} u_\mathrm{s}. \tag{7.27}$$

The drag coefficient $C_\mathrm{D}$ is estimated with [36]:

$$C_\mathrm{D} = \frac{24}{\mathrm{Re}} + \frac{2.6\left(\frac{\mathrm{Re}}{5.0}\right)}{1+\left(\frac{\mathrm{Re}}{5.0}\right)^{1.52}} + \frac{0.411\left(\frac{\mathrm{Re}}{2.63\times10^5}\right)^{-7.94}}{1+\left(\frac{\mathrm{Re}}{2.63\times10^5}\right)^{-8.00}} + \frac{0.25\left(\frac{\mathrm{Re}}{10^6}\right)}{1+\left(\frac{\mathrm{Re}}{10^6}\right)} \tag{7.28}$$

where Re is the Reynolds number:

$$\mathrm{Re} = \frac{\rho_\mathrm{V} w_\mathrm{d} D_\mathrm{d}}{\mu_\mathrm{V}} \tag{7.29}$$

with $\mu_\mathrm{V}$ the dynamic viscosity of the vapour.

With the forces known, the acceleration can be computed. By integrating the acceleration, the velocity can be found. By integrating the velocity, the droplet position can be found. In the model, this is achieved with the Euler method [51]:

$$v_{\mathrm{dT},j} = v_{\mathrm{dT},j-1} + \dot{v}_{\mathrm{d},j}\Delta t, \tag{7.30}$$

$$z_{\mathrm{dT},j} = z_{\mathrm{dT},j-1} + v_{\mathrm{d},j}\Delta t. \tag{7.31}$$

The vapour-liquid surface position has increased as well:

$$z_{\mathrm{s},j} = z_{\mathrm{s},j-1} + u_\mathrm{s}\Delta t. \tag{7.32}$$

### 7.2.5 Calculation of energies and masses

The compression work is approximated by taking the sum of the differential amount of specific work done in each time step by the pump and multiplying it with the liquid mass flow rate through the pump:

$$W_\mathrm{CP} = \dot{m}_\mathrm{L} \sum_{j=1}^{N} \left(h_{\mathrm{L},j} - h_{\mathrm{L,C}}\right). \tag{7.33}$$

where $h_{\mathrm{L},j}$ is the enthalpy of the liquid after the pump at $t_j$ and $h_{\mathrm{L,C}}$ is the enthalpy of the liquid before the pump. The work can also be calculated by taking the integral of the differential pressure in the chamber over the vapour volume to obtain the work associated with the compression of the vapour by the liquid column and divide that by $\eta_\mathrm{PU}$ to account for the pump efficiency:

$$W_\mathrm{CP} = \frac{1}{\eta_\mathrm{PU}} \int (p - p_0)\,\mathrm{d}V. \tag{7.34}$$

In the model, the integral is approximated by a trapezoidal numerical integration using the 'trapz' function in MatLab.

To calculate the specific work, it is required to know the vapour mass discharged from the compression chamber. To that end, the vapour mass that will be left in the clearance volume should be subtracted from the vapour mass present at the instant the discharge valve opens:

$$m_\mathrm{V,discharged} = m_\mathrm{V,open} - m_\mathrm{cl}. \tag{7.35}$$

The specific work can then be calculated as:

$$w_\mathrm{CP} = \frac{W_\mathrm{CP}}{m_\mathrm{V,discharged}}. \tag{7.36}$$

### 7.2.6 Inputs & Initial conditions

The inputs that the LPGC model takes are largely analogous to the heat pump model. These are:

- Evaporator saturation temperature, $T_{\mathrm{C}}$
- Evaporator vapour quality, $x_{\mathrm{C}}$
- Condenser saturation temperature, $T_{\mathrm{H}}$
- Isentropic compression efficiency $\eta_{\mathrm{com}}$

Additional inputs to define the LPGC model are:

- Isentropic pump efficiency $\eta_{\mathrm{PU}}$
- Compression chamber volume, $V_{\mathrm{C}}$
- Compression chamber diameter, $D_{\mathrm{C}}$
- Clearance volume fraction, $f_{\mathrm{cl}}$
- Spray fraction, $f_{\mathrm{LS}}$
- Initial droplet diameter, $D_{\mathrm{d},1}$
- Initial droplet velocity, $v_{\mathrm{d},1}$
- Droplet layer time interval, $\Delta t_{\mathrm{LS}}$
- Number of simulations steps $N$

With these inputs, the initial conditions can be calculated. The initial thermodynamic state properties of temperature, density, specific enthalpy, specific entropy and dynamic viscosity can be determined for both the vapour and the liquid. These are $T_1$, $\rho_{\mathrm{L},1}$, $\rho_{\mathrm{V},1}$, $h_{\mathrm{L},1}$, $h_{\mathrm{V},1}$, $s_{\mathrm{L},1}$, $s_{\mathrm{V},1}$, $\mu_{\mathrm{L},1}$ and $\mu_{\mathrm{V},1}$

From the first instant, a layer of droplets is present at the top of the chamber. The initial mass of liquid droplets present is therefore:

$$m_{\mathrm{LS},1} = \dot{m}_{\mathrm{L}} \Delta t_{\mathrm{LS}}. \tag{7.37}$$

Apart from these droplets, the model starts with the chamber completely filled with this vapour from the evaporator. The initial mass of this vapour is:

$$m_{\mathrm{V},1} = \rho_{\mathrm{V},1} \left( V_{\mathrm{C}} - \frac{m_{\mathrm{LS},1}}{\rho_{\mathrm{L},1}} \right). \tag{7.38}$$

The entrance conditions of the liquid, determined above, define the state in which the liquid enters the chamber. The droplets enter the chamber with an initial diameter of $D_{\mathrm{d},1}$ and an initial velocity of $v_{\mathrm{d},1}$. During the simulation, however, the pressure increases and the vapour properties change. Therefore the properties with which the liquid enters the chamber also change and these are thus corrected accordingly. The initial droplet state properties $h_{\mathrm{d},1}$ and $\rho_{\mathrm{d},1}$ become that of the pumped liquid in the column calculated from Equation (7.21).

The initial vapour-liquid surface position is at the bottom of the compression chamber, so:

$$z_{\mathrm{s},1} = -\frac{V_{\mathrm{C}}}{\frac{1}{4}\pi D_{\mathrm{C}}^2}. \tag{7.39}$$

The initial droplet position is at the top of the compression chamber, so $z_{\mathrm{d},1} = 0$.

The simulation runs until the liquid column has filled the compression chamber volume up to the point where only the clearance volume is left for the vapour, thus:

$$V_{\mathrm{LC}} = V_{\mathrm{C}} - V_{\mathrm{cl}}. \tag{7.40}$$

The time at which this happens is needed before the simulation starts to set up the time vector. It is approximated by:

$$t_{\mathrm{f}} = \frac{V_{\mathrm{C}} - V_{\mathrm{cl}}}{\dot{V}_{\mathrm{L}}}, \tag{7.41}$$

where $\dot{V}_{\mathrm{L}}$ is the liquid volume flow rate calculated with the initial liquid density:

$$\dot{V}_{\mathrm{L}} = \frac{\dot{m}_{\mathrm{L}}}{\rho_{\mathrm{L},1}}. \tag{7.42}$$

This is valid under the assumption that the density of the liquid column remains approximately the same.

## 7.3 Boundary conditions

If the layer position has become lower than the vapour-liquid surface position, it has effectively encountered the liquid column. The layer mass will be removed from the liquid spray and added to the liquid column. These droplets will therefore not be able to exchange heat with the vapour anymore.

If the pressure in the chamber becomes larger than the condenser pressure, the discharge valve opens, allowing the vapour to discharge to the condenser. The liquid is still pumped into the chamber, thereby displacing the vapour out to the condenser. The pressure in the chamber however remains constant at the condenser pressure and thus no compression is taking place anymore. Because of this, the spray valve closes at the same time that the discharge valve opens to discontinue the injection of droplets in the chamber. If the injection continued, the pressure and quality of the vapour would rapidly decrease due to the injected droplets being colder than the vapour. Part of the vapour would condense to increase the droplet temperature to the saturation point. Some droplets would exit the chamber to the discharge pipe and end up in the condenser where they have no potential for heat transfer. The total liquid mass flow rate will however not change.

The distribution of the evaporated liquid mass over the layers by using the surface distribution $n_{\mathrm{area},k,j}$ may result in some layers being attributed an excess of evaporated mass, thereby resulting in a mathematically negative layer mass. To prevent this, the signs of the layer masses in $m_{\mathrm{dT},k,j}$ are checked and if any is negative, the distribution is recalculated with the mass distribution coefficient $n_{\mathrm{mass},k,j}$, where:

$$n_{\mathrm{mass},k,j} = \frac{m_{\mathrm{dT},k,j}}{\sum_{k=1}^{N_{\mathrm{T},j}} m_{\mathrm{dT},k,j}}. \tag{7.43}$$

The new liquid mass in layer $k$ at time $t_j$ can then be calculated with:

$$m_{\mathrm{dT},k,j} = m_{\mathrm{dT},k,j-1} - n_{\mathrm{mass},k,j} m_{\mathrm{evap},j}. \tag{7.44}$$

As such, negative mass is inherently prevented.

## 7.4 Limits to the model

As the model is not focused on representing an accurate CFD simulation, a large set of assumptions was used and the model is therefore highly simplified. Even though this approach is believed to be sufficient for the purpose of this model, some limitations are discussed here.

**Quasi-equilibrium process assumption** The first limitation is the assumption of a quasi-equilibrium process in which the droplets and vapour come into equilibrium with each other in every time step. This implies that with every $\Delta t$, any heat produced in the vapour is completely exchanged with the droplet. A more realistic model would calculate the heat transfer coefficient and subsequently the heat transfer to the droplets. The evaporator droplet mass could then be smaller than what is calculated in this mode. Qin & Loth (2014) employ such calculations, taking the evaporation effect into account as well. The evaporation of droplets causes a mass flux that changes the heat transfer coefficient. Connected to this limitation is that the model does not account for a possible reduction in drag force due to evaporation effects. This effect happens as the boundary layer near the droplet is different due to the vapour mass flux [44]. Furthermore, the model assumes that heat can always be transferred to the droplets, even if just one layer is present in the chamber. Even though more layers are added quickly, the first layers take a relatively large part of the heat in the initial stages. The influence that this behaviour has on the end result was not investigated.

**Adiabatic vapour space assumption** Another assumption was that the vapour space is fully adiabatic, which was also used by Qin & Loth (2014). Therefore, the model does not account for heat transfer between the liquid column and the vapour, even though there is a temperature difference between them. Furthermore, it assumes a perfectly flat vapour-liquid surface with no mixing. To quantify the heat transfer to the column relative to the droplets, the maximum droplet surface area was evaluated for the simulation that used the inputs Section 8.2.1. It appeared that the vapour-liquid surface area of the column was at least 23 % of the droplet surface area. Therefore, the column could play a significant part in cooling the vapour, which is not taken into account in the model. The same is true for the walls of the compression chamber. However, it is expected that they have a much smaller thermal mass compared to the liquid column.

**Step size assumption** In the results, the step size was arbitrarily set to a value which still showed similar performance as a much smaller step size. The droplets however have a characteristic response time $\tau_\mathrm{d}$. For Reynolds numbers smaller than 1, this time is:

$$\tau_\mathrm{d} = \frac{\rho_\mathrm{L} D_\mathrm{d}^2}{18\mu_\mathrm{V}}. \tag{7.45}$$

Due to the evaporation of the droplets and the associated reduction in droplet diameter, the characteristic time continuously decreases during the simulation. Once this characteristic time drops below the step size $\Delta t$, the particle kinetics become unstable. This behaviour expresses itself by a runaway effect where the calculated acceleration overcompensates the changes in the droplet characteristics. To prevent such events, the step size could be set so small that the characteristic time never becomes larger. This may however require an unnecessarily small step size. To suppress this effect at larger step sizes, the model checks if the acceleration surpasses a certain threshold value. When this is the case, the acceleration is set to 0. It is thereby assumed that the particle has reached its terminal velocity so that there would be no more acceleration anyway.

This simplification is intensively used in the model, since the $\tau_\mathrm{d}$ appeared to become significantly smaller than the step size. It was found by Qin & Loth (2014) that the step size should be set to $\Delta t = 0.02\tau_\mathrm{d}$ to be able to account for even the kinetics of even the smallest droplets. Since the purpose of this model is not to describe droplet dynamics accurately, this recommendation was dropped and the approach described above was utilised.

**Euler's method approximation** To compute the droplet velocities and accelerations, Euler's method was used. This method however results in an error increasing with time [51]. The step size should be set small enough such that the error remains insignificant. It was however not investigated whether the step size used in the results was small enough to fulfil this requirement. Nevertheless, since the step size was set to such a size that the results did not differ significantly with smaller step sizes, it is believed that the error remained small.

**Droplet collisions** It was assumed that droplets were perfectly distributed around the chamber and did not collide with each other or with the chamber walls. This assumption was also used in Qin & Loth (2014) and was taken on the basis that this model is not trying to accurately describe droplet behaviour.

**Compression speed** No considerations were made regarding the speed of compression. It was assumed that the vapour-liquid surface instantly reached its speed. In reality, however, pump and valve inertia do not allow instantaneous flow. Furthermore, gravitational effects limit the allowable acceleration of the surface to avoid separation. Besides that, the potential splashing of the vapour-liquid surface is not taken into account. Qin & Loth (2014) however assumed the same and used a limit of $0.5g$ for the acceleration of the vapour-liquid surface.

**Pumping simplifications** It was assumed that the pump outlet pressure was equal to the chamber pressure. However, in a real system, there is a pressure difference over the valves and spray nozzles. Therefore, the pump should work at a larger pressure ratio than the compression ratio of the heat pump. The magnitude of this pressure drop was not investigated, but Patil et al. (2020) experienced near-isothermal compression with an injection pressure of about 2 bar.

Another effect which is not considered for the pump is cavitation. Due to the pump receiving saturated liquid, cavitation is likely to happen [43]. In this project, it was assumed that the pump is cavitation resistant.

# Chapter 8

# LPGC Model: Results & Discussion

This section shows the results of compression processes simulated with the LPGC model. First, an attempt at validating the model is made in Section 8.1. Afterwards, the model is simulated for an example case. The inputs, initial conditions and results are shown in Section 8.2, which also discusses model behaviour. Lastly, the LPGC model is integrated into the heat model in Section 8.3. The influence of spray fraction on the performance is investigated and the best settings are used to compare a heat pump cycle with an LPGC using water against the best results of Chapter 5. The conclusion of these results is given in Chapter 9.

## 8.1 Model validation

Model validation is difficult because no literature has been found on liquid pistons using water to compress steam. The majority of the literature on LPGC concerns the compression of air with water. Some cases of different gases and different liquids have been found, but not with an identical liquid-gas pair. This characteristic is important since the evaporation of droplets that add to the vapour mass is an integral model dynamic. Furthermore, most of the literature is developed towards compressed air energy storage (CAES), for which isothermal compression is most desired. When applied to heat pumps, full isothermal compression is however obviously not desired. In contrast, it is important to prevent any condensation of the steam, as it reduces the amount of heat available for the compressor. Gearing the model to that found in literature, therefore, requires an unreasonable amount of adjustments and changes. The result would not represent the actual model anymore and could therefore not be used as validation.

Nevertheless, one way to test the model qualitatively is by setting the spray fraction to zero, resulting in a purely adiabatic compression. This compression can be compared to adiabatic compression literature. The work of Qin and Loth (2014) concerns an LPGC with water spray injection into an air-filled compression chamber. In the same compression chamber, a piston is placed with a fixed volume of liquid on top of it. With the piston moving up, the liquid column moves up and thus the air space is compressed. A numerical model was made that simulates droplets and their dynamics. The simulation was also run with the droplet mass loading set to zero. The starting pressure is $p_{\mathrm{C}} = 1.01\,\mathrm{bar}$ and a pressure ratio of $r_{\mathrm{com}} = 10$ was used. The discharge valve therefore opens at $p_{\mathrm{H}} = 10.1\,\mathrm{bar}$. The air in the chamber at the beginning of the compression process and the water used for the liquid piston both have a temperature of $20\,^{\circ}\mathrm{C}$. The polytropic index is taken to be the ratio of specific heat capacities of air. The exact value used is not explicitly given in the paper, but at the initial conditions, the value is $n = 1.402$ [20] so this value will be used in the validation. The compression chamber has a diameter $0.3\,\mathrm{m}$ and a length of $0.3\,\mathrm{m}$. The resulting compression curves are shown Figure 8.1a in terms of temperature, pressure and cumulative work against the piston travel. The red line represents the adiabatic case against which the LPGC model is compared. Figure 8.1b shows the results from the LPGC model when it is supplied with the same inputs. The discharge temperature, final work and piston travel at which the discharge valve opens can approximately be read from the graphs and compared to the values from the LPGC model. This comparison is shown in Table 8.1 where it is seen that the LPGC model closely approaches the

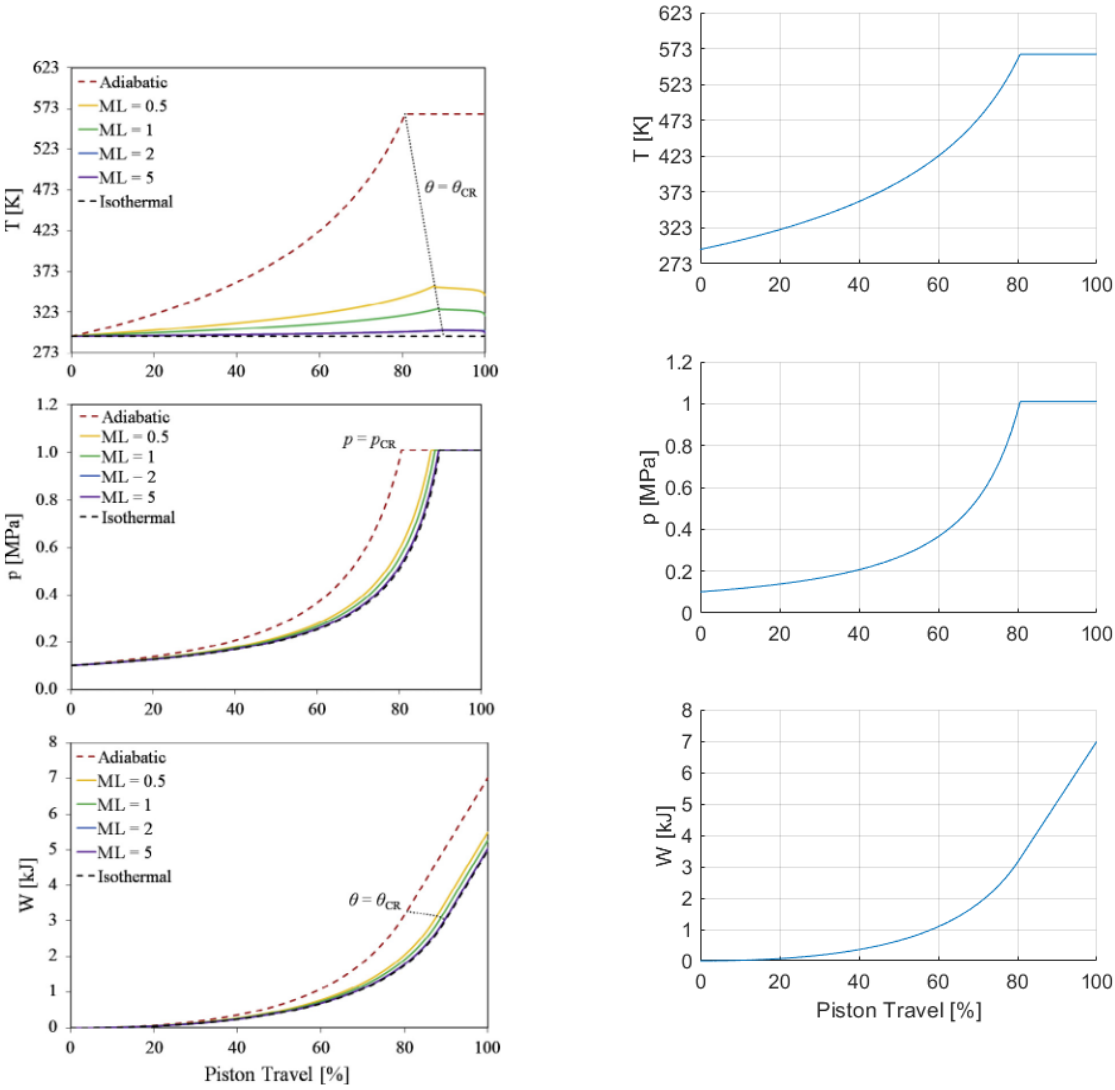


(a) Qin and Loth (2013) [44]

(b) LPGC model

**Figure 8.1:** Results of the model of Qin and Loth (2013) compared with the LPGC model for the same inputs [44].

model of Qin.

| | $T_{\text{discharge}}$ [K] | $W_{\text{final}}$ [kJ] | Piston travel [%] |
|---|---|---|---|
| Qin and Loth (2013) | 566.7 | 7.000 | 80.71 |
| LPGC model | 565.0 | 6.985 | 80.65 |
| Error [%] | 0.300 | 0.214 | 0.689 |

**Table 8.1:** Results of the model of Qin and Loth (2013) compared with the LPGC model for the same inputs [44].

With the adiabatic case validated, the compression process of the LPGC model can be trusted. The heat transfer and droplet kinetics are however yet to be validated. Nevertheless, as stated in Section 7.4, the purpose of the model is not to accurately describe droplet behaviour. Instead, it is hoped that the model can show the influence of the presence of liquid droplets on the thermodynamic properties of the vapour during the compression process. With that realisation, doubts about the validity of the droplet models can be somewhat alleviated.

## 8.2 Simulation of an example LPGC

An LPGC compressor is simulated to showcase and explain its behaviour. The inputs that are used for this example and the resulting initial conditions are first discussed in Section 8.2.1. Afterwards, the results of these inputs are shown in Section 8.2.2 together with a discussion of the behaviour.

### 8.2.1 Inputs

For the example simulation of this model, an evaporator pressure of $p_{\mathrm{C}} = 1\,\mathrm{bar}$ and a condenser pressure of $p_{\mathrm{H}} = 10\,\mathrm{bar}$ has been chosen arbitrarily. The isentropic compression efficiency is set equal to that of an ordinary compressor: $\eta_{\mathrm{com}} = 70\,\%$. The isentropic pump efficiency is set at $\eta_{\mathrm{PU}} = 80\,\%$ [34]. The gravitational acceleration is $g = 9.81\,\mathrm{m/s^2}$.

The geometry of the compression chamber and is chosen arbitrarily. It has a diameter of $D_{\mathrm{C}} = 0.5\,\mathrm{m}$ and a volume of $V_{\mathrm{C}} = 0.1\,\mathrm{m^3}$. The clearance volume is $f_{\mathrm{cl}} = 0.01\,\%$ of the chamber volume. The mass flow rate of the pumped liquid is set at $\dot{m}_{\mathrm{L}} = 10\,\mathrm{kg/s}$. This results in the chamber being full in about $9.5\,\mathrm{s}$.

The initial droplet diameter is chosen to be $D_{\mathrm{d},1} = 100\,\mu\mathrm{m}$ (one of the sizes used by Qin & Loth (2014)) and the initial velocity is arbitrarily set to $v_{\mathrm{d},1} = -0.1\,\mathrm{m/s}$. The number of steps is chosen to be 2000 , resulting in a time step of $\Delta t = 4.8\,\mathrm{ms}$. This step size showed no significant difference in the results compared to smaller step sizes. The interval between the injection of two layers of droplets is set at $Deltat_{\mathrm{LS}} = 20\,\mathrm{ms}$.

The fraction of liquid sprayed into the chamber, $f_{\mathrm{LS}}$ has been set such that the final quality of the vapour is approximately 1 such that there is no overshoot. In this case, the spray fraction needs to be $f_{\mathrm{LS}} = 0.00056$. With these inputs, the calculations that were necessary in advance of the simulation could be made and the results are shown in Table 8.2.

**Table 8.2:** The initial calculations, which are necessary for the simulation, calculated from the inputs.

| **Fluid properties** | **Quantity** | **Value** | **Unit** | **Source** |
|---|---|---|---|---|
| Initial temperature | $T_1$ | 99.6 | °C | Section 7.2.6 |
| Initial liquid specific enthalpy | $h_{\mathrm{L},1}$ | 417 | kg/kJ | Section 7.2.6 |
| Initial liquid specific entropy | $s_{\mathrm{L},1}$ | 1.30 | kg/kJ/K | Section 7.2.6 |
| Initial liquid density | $\rho_{\mathrm{L},1}$ | 959 | kg/m$^3$ | Section 7.2.6 |
| Initial liquid dynamic viscosity | $\mu_{\mathrm{L},1}$ | 2.83E-04 | Pa s | Section 7.2.6 |
| Initial vapour specific enthalpy | $h_{\mathrm{V},1}$ | 2.67E+03 | kg/kJ | Section 7.2.6 |
| Initial vapour specific entropy | $s_{\mathrm{V},1}$ | 7.36 | kg/kJ/K | Section 7.2.6 |
| Initial vapour density | $\rho_{\mathrm{V},1}$ | 0.590 | kg/m$^3$ | Section 7.2.6 |
| Initial vapour dynamic viscosity | $\mu_{\mathrm{V},1}$ | 1.22E-05 | Pa s | Section 7.2.6 |
| | | | | |
| **Initial calculations** | | | | |
| Initial mass of liquid droplets | $m_{\mathrm{LS},1}$ | 0.500 | kg | Equation (7.37) |
| Initial mass of vapour | $m_{\mathrm{V},1}$ | 0.0590 | kg | Equation (7.38) |
| Initial droplet volume | $V_{\mathrm{d},1}$ | 5.24E-13 | m$^3$ | Equation (7.22) |
| Initial droplet mass | $m_{\mathrm{d},1}$ | 5.02E-10 | kg | Equation (7.4) |
| Initial droplet frontal area | $A_{\mathrm{df},1}$ | 7.85E-09 | m$^2$ | Equation (7.22) |
| Initial droplet surface area | $A_{\mathrm{ds},1}$ | 3.14E-08 | m$^2$ | Equation (7.22) |
| Initial vapour-liquid surface position | $z_{\mathrm{s},1}$ | -0.509 | m | Equation (7.39) |
| Initial droplet position | $z_{\mathrm{d},1}$ | 0.000 | m | Section 7.2.6 |
| Initial layer mass | $m_{\mathrm{dT},1}$ | 1.35E-04 | kg | Equation (7.6) |
| Initial vapour velocity at droplet position | $u_1$ | 0.00 | m/s | Equation (7.27) |
| Initial relative velocity between droplet and vapour | $w_{\mathrm{d},1}$ | 0.10 | m/s | Equation (7.26) |
| Initial characteristic time scale | $\tau_{\mathrm{d},1}$ | 0.0436 | – | Equation (7.45) |
| Initial droplet Reynolds number | $\mathrm{Re}_{\mathrm{d},1}$ | 0.483 | - | Equation (7.29) |
| Initial droplet aerodynamic drag coefficient | $C_{\mathrm{d},1}$ | 50.1 | - | Equation (7.28) |
| Initial droplet drag force | $F_{\mathrm{d},1}$ | 1.16E-09 | N | Equation (7.25) |
| Initial droplet gravity force | $F_{\mathrm{g},1}$ | 4.92E-09 | N | Equation (7.24) |
| Initial droplet acceleration | $\dot{v}_{\mathrm{d},1}$ | -7.50 | m/s$^2$ | Equation (7.23) |
| | | | | |
| **General calculations** | | | | |
| Liquid column mass flow rate | $\dot{m}_{\mathrm{LC}}$ | 1.00E+01 | kg/s | Equation (7.2) |
| Liquid spray mass flow rate | $\dot{m}_{\mathrm{LS}}$ | 5.60E-03 | kg/s | Equation (7.2) |
| Liquid volume flow rate | $\dot{V}_{\mathrm{L}}$ | 0.0104 | m$^3$/s | Equation (7.42) |
| Clearance volume | $V_{\mathrm{cl}}$ | 1.00E-05 | m$^3$ | Equation (7.1) |
| Compression chamber cross-sectional area | $A_{\mathrm{C}}$ | 0.196 | m$^2$ | Equation (7.3) |
| Velocity of vapour-liquid surface | $u_{\mathrm{s}}$ | 0.053 | m/s | Equation (7.3) |
| Number of droplets injected every second | $\dot{n}_{\mathrm{d}}$ | 1.12E+07 | #/s | Equation (7.5) |
| Amount of droplets per layer | $n_{\mathrm{d}}$ | 2.23E+05 | # | Equation (7.6) |
| Time until chamber is completely full | $t_f$ | 9.49 | s | Equation (7.41) |
| Time step | $\mathrm{d}t$ | 0.00316 | s | Equation (7.8) |

### 8.2.2 Behavior analysis

With the inputs of Section 8.2.1, the model simulates a single compression process consisting of the compression and discharge stages. Figure 8.2 shows the chamber pressure and temperature evolution against time. In Figure 8.2a it can be seen how the chamber pressure changes between the evaporator (starting) pressure and condenser (final) pressure. Moreover, it shows the chamber pressure when the spray fraction is set to zero. This curve is equivalent to an ordinary adiabatic reciprocating compressor and is referred to as 'adiabatic'. In both cases, the pressure increases exponentially until the discharge pressure is reached and then remains at that pressure until the end of the cycle. It is seen that the LPGC pressure rises slower and reaches the discharge pressure at a later time. This is due to the vapour remaining at the saturated point and thus having a persistently higher density than the adiabatic compressor case. Therefore the same mass of vapour takes up less space and thus the pressure is lower.

In the adiabatic case, the vapour becomes highly superheated, causing the lower vapour density. As can be seen in Figure 8.2b, the adiabatic temperature ends up at about 360 °C, far above the condenser temperature of 180 °C. These results therefore show that the LPGC can effectively keep a low vapour temperature, which is one of the most important advantages.

The heat of compression, which causes the large temperature rise in the adiabatic compressor, is

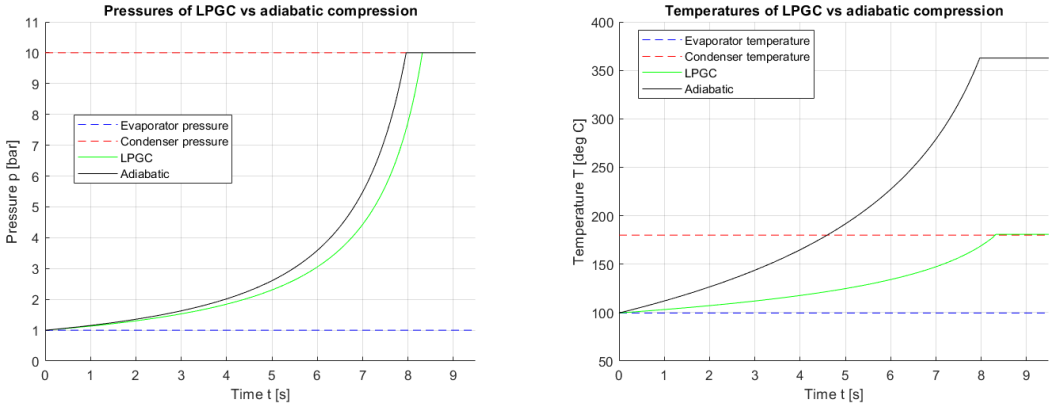


(a) (b)

**Figure 8.2:** Chamber pressure and temperature against time, with the evaporator and condenser properties also shown.

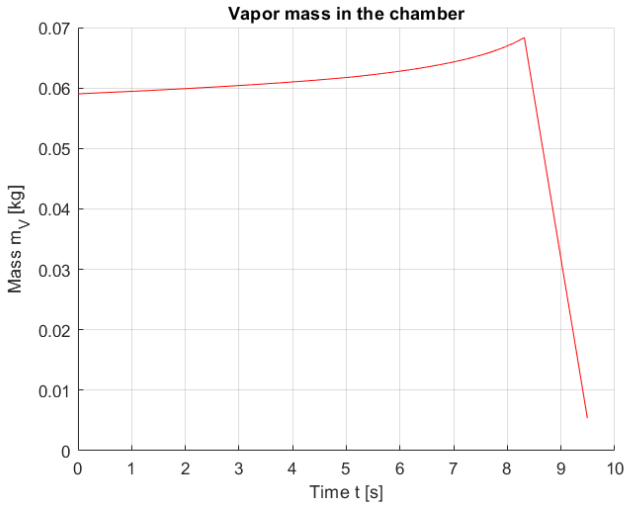


**Figure 8.3:** The vapour mass in the compression chamber. It increases during compression because of droplets evaporating. The sharp decrease is when the discharge valve opens.

completely devoted to evaporation in the LPGC. The mass of the vapour in the chamber therefore increases, which can be seen in Figure 8.3. From the initial vapour mass present, it exponentially increases until the discharge valve opens. After this, the vapour is steadily discharged from the chamber until the end of the discharge. At this point, the remaining vapour mass in the chamber corresponds to the leftover clearance volume. An increase in vapour mass should intuitively increase the chamber pressure since the available volume remains the same. However, as the pressure is lower than the adiabatic compression, this effect is weaker than the increase in density of the vapour due to the cooling effect.

The LPGC achieves this low-temperature compression with a significantly lower work input, which is another important advantage. The total work required is the area under the pressure-volume diagram, shown in Figure 8.4. The volume shown here is the liquid volume present in the chamber, which starts at zero and ends at the chamber volume minus the clearance volume. The area under the evaporator pressure line should be subtracted from the area under the p-V curves. It can already be seen that the LPGC has a lower area under the curve. The results of the work input $W$ are:

$$W_{\text{adiabatic}} = 29.4\,\text{kJ} \qquad \& \qquad W_{\text{LPGC}} = 26.6\,\text{kJ},$$

which is a 9.84 % improvement over the adiabatic compression. The advantage of LPGC is however even greater, as it delivers a greater mass of compressed vapour than the adiabatic compressor due to droplet evaporation. Dividing the work values above by the respective discharged vapour masses

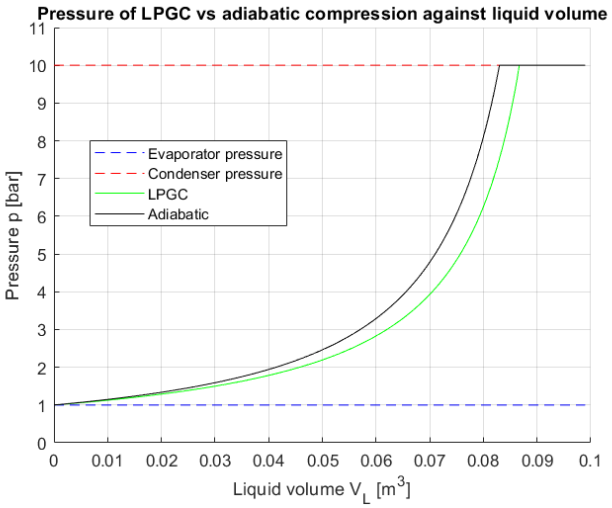


**Figure 8.4:** Pressure displayed against the liquid volume in the compression chamber, both for the LPGC and the adiabatic compressor. The area between these curves and the blue line (evaporator pressure) is the work of compression.

gives the specific work $w$:

$$w_{\text{adiabatic}} = \frac{W_{\text{adiabatic}}}{m_{\text{V},1}} = 499\,\text{kJ/kg} \qquad \& \qquad w_{\text{LPGC}} = \frac{W_{\text{LPGC}}}{m_{\text{V},open}} = 389\,\text{kJ/kg}. \tag{8.1}$$

This is a 22.1 % improvement of the LPGC over the adiabatic compression.

The evolution of the thermodynamic state properties of the vapour and liquid are shown in a T-s and p-h diagram in Figure 8.5. It shows how the properties of the vapour in the chamber and the liquid in the column change during the process. It also shows the combined vapour-liquid properties in magenta. Furthermore, adiabatic compression is shown in black. In both diagrams, it can be

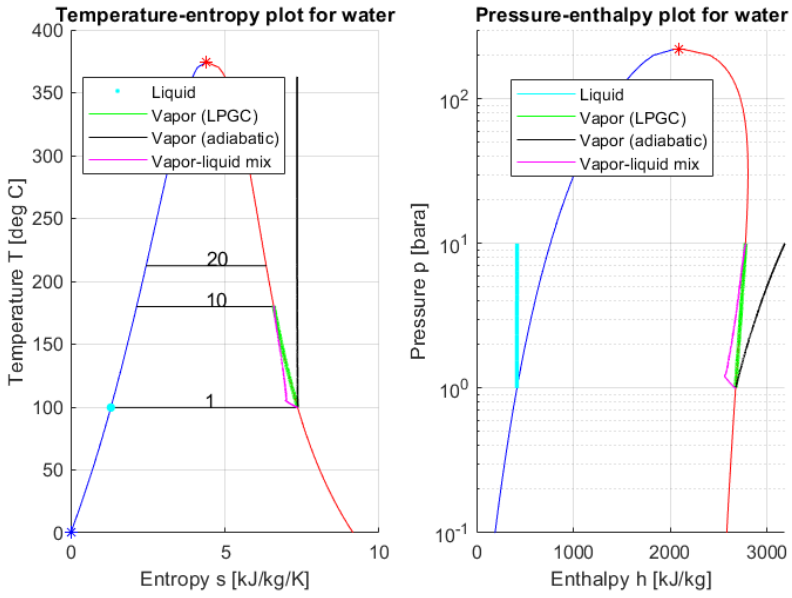


**Figure 8.5:** The temperature against specific entropy and pressure against specific enthalpy diagrams for this compression stage. The magenta line is the equilibrium quality which ends up at a quality of approximately 1. Furthermore, the adiabatic compression lines are shown in black.

seen that the LPGC vapour (green) is coincident with the saturated vapour line. In contrast, the adiabatically compressed vapour enters the superheated region. In the T-s diagram, it appears as if the specific entropy decreases, suggesting that the second law of thermodynamics is violated. To prove that this is not the case the entropy balance of the cycle is derived such that the entropy production can be calculated. The cycle is however not a steady state open or closed system, as there

is mass accumulation. To avoid the calculation of time-dependent terms, the system is interpreted as a theoretical closed system. Since mass can not enter or exit a closed system, all liquid and vapour that is present in the final state, already has to be present in the initial state. Figure 8.6 will be used for clarification.

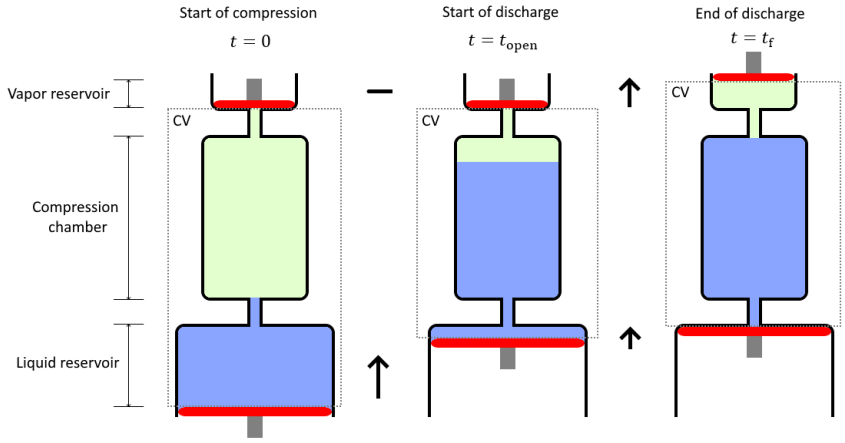


**Figure 8.6:** Illustration of the model used to determine the entropy production of the LPGC. This closed system representation is equivalent to the LPGC model.

The control volume (CV) encapsulates all liquid and vapour that is present both at the start and end of the cycle. It does change in volume to accommodate the increase in pressure. The liquid that will be pressed in the compression chamber, is initially in the liquid reservoir, which is equivalent to the liquid being in the evaporator. The red piston acts as the compressor, able to press the liquid into the compression chamber. As this happens, the vapour volume decreases and its pressure increases. When it reaches the discharge pressure, it can exit the compression chamber towards the vapour reservoir, which is equivalent to the condenser. There is also a red piston inside this chamber which can move to allow space for the vapour while maintaining its pressure. In this way, the cycle can be viewed as a closed system without compromising its dynamics.

The general equation of a closed-system entropy balance is [35]:

$$0 = \sum_j \frac{Q_j}{T_j} + \sum_i m_i s_i - \sum_f m_f s_f + \sigma_{\mathrm{CV}}, \tag{8.2}$$

where $\dot{Q}$ is the heat transfer across the system boundary, $T$ the temperature at the system boundary, $m$ the mass, $s$ the specific entropy and $\sigma_{\mathrm{CV}}$ the entropy production. The subscript $j$ signifies a certain system boundary, $i$ signifies the initial state and $f$ signifies the final state. Because the model is assumed adiabatic, there is no heat transfer across the system boundary. The equation can then be rewritten as:

$$\sigma_{\mathrm{CV}} = m_{\mathrm{L},f} s_{\mathrm{L},f} + m_{\mathrm{V},f} s_{\mathrm{V},f} - m_{\mathrm{L,i}} s_{\mathrm{L,i}} - m_{\mathrm{V,i}} s_{\mathrm{V,i}}. \tag{8.3}$$

In the initial state, this chamber is filled with liquid with a mass equal to the mass of the liquid column in the final state plus the mass of evaporated liquid:

$$m_{\mathrm{L,i}} = m_{\mathrm{LC,f}} + \left(m_{\mathrm{V,open}} - m_{\mathrm{V},1}\right). \tag{8.4}$$

where $m_{\mathrm{V,open}}$ is the mass of vapour at the instant the discharge valve opens. The initial vapour mass is just the mass of vapour that is present at the start of the simulation, $m_{\mathrm{V},1}$. The initial specific entropies of both the liquid and vapour are equal to those of the evaporator: $s_{\mathrm{L},i} = s_{\mathrm{L},1}$ & $s_{\mathrm{V},i} = s_{\mathrm{L},1}$.

In the final state, the mass of liquid is that of the liquid column, $m_{\mathrm{L},f} = m_{\mathrm{LC,f}}$. The mass of vapour in the final state is the same as what is present at the instant the discharge valve opens, $m_{\mathrm{V},f} = m_{\mathrm{V,open}}$. The specific entropies of the liquid and vapour in the final state are also equal to those at the instant the discharge valve opens since these properties do not change during discharge.

All values are thus known and the entropy production can be calculated. For this system, the result is:

$$\sigma_{\mathrm{CV}} = 94.9 \cdot 1303 + 0.07 \cdot 6587 - (94.9 + (0.07 - 0.06)) \cdot 1303 - 0.06 \cdot 7359 = 30\,\mathrm{kJ}. \tag{8.5}$$

This value being positive implies that the entropy of the system increased and therefore it does not violate the second law of thermodynamics.

Returning to the property diagrams, it is seen that the magenta line starts at the vapour saturation line, implying that there is no liquid in the vapour initially. As the droplets enter the chamber, however, the quality of the vapour-liquid equilibrium decreases while the pressure starts increasing. At one point, the line makes a sharp turn and starts approaching the vapour saturation line again. The evolution of the quality can be tracked more easily in Figure 8.7a, where the turn can also be seen. The positions of the individual droplet layers, which are shown in Figure 8.7b, are used to explain this sharp turn. In the latter figure, the green line is the position of the vapour-liquid surface,

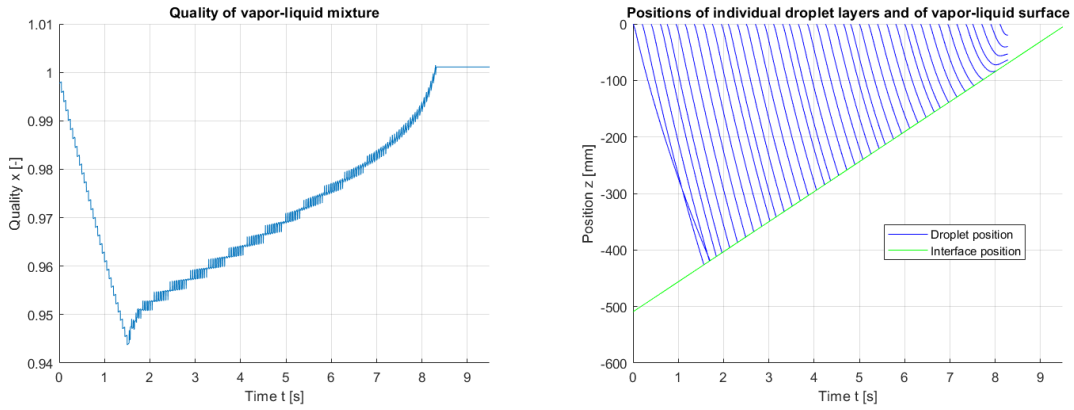


(a) (b)

**Figure 8.7:** Chamber pressure and temperature against time, with the evaporator and condenser properties also shown.

while each blue line is the position of an individual droplet layer. In total, there were 190 layers with this simulation, of which 50 are shown in this figure. It is seen that the vapour-liquid surface rises from the bottom while the droplets fall from the top. The droplet layers are injected in a consecutive manner which makes them behave differently. The first droplet layers are for example overtaken by droplet layers injected later in the process. This effect is due to a different degree of evaporation of these layers. The first layers take a relatively larger part in heat exchange with the vapour and therefore have evaporated relatively more than later layers. This makes the drag force comparatively more important, slowing the layer down more than later layers. When droplet layers encounter the vapour-liquid surface, they are absorbed in the liquid column. It can be seen that the first layers fall in the vapour-liquid surface at about 1.5 s. This coincides with the time at which the quality of the vapour-liquid equilibrium makes a sudden sharp turn. This sharp turn is therefore the result of the amount of liquid in the chamber steadily increasing until $t = 1.5\,\mathrm{s}$ after which addition and absorption of droplet layers cancel each other more or less out. From this point in time, the quality is influenced mainly by the evaporation. The degree of evaporation of the droplets depends on the heat of compression and the time they have in the chamber. Since the pressure and temperature increase exponentially during compression, the heat transfer to the droplets and with that the rate of evaporation should increase. However the further the vapour-liquid surface rises, the less time the droplets have in the chamber to evaporate. These two effects counteract each other and how this affects the degree of droplet evaporation can be seen in Figure 8.8. It can be seen that every layer starts with an equal mass, however follows a different evaporation path. Once a line stops, a layer has fallen on the vapour-liquid surface. If a layer reaches zero, it has fully evaporated. It can be seen that the first layers evaporate about half of their mass before encountering the surface. After about $t = 1.5\,\mathrm{s}$, there are so many droplets in the chamber that they do not evaporate so much before falling into the column. This is also due to the heat of compression being low in this phase (due to the exponential nature of the pressure increase). The further in the process, however, the more the droplets evaporate. This implies that the effect of increased heat of compression is much stronger than the shorter time the droplets have in the chamber. In the final phase before the discharge valve opens, the droplets fully evaporate even though they have a short time in the chamber.

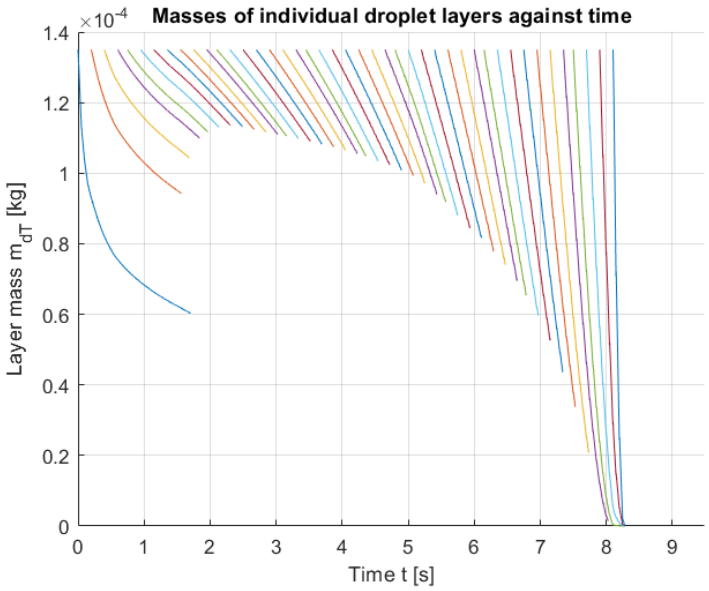


**Figure 8.8:** An overview of how different (not all) droplet layers lose their mass and when they enter the vapour-liquid surface.

A further remark can be made about the end state of the quality of the vapour-liquid equilibrium. The fraction of liquid sprayed, $f_{\mathrm{LS}}$, has been manually tuned such that the quality ends up at approximately 1. In this way, the vapour discharged from the chamber is as close as possible to saturated vapour, ensuring zero the compressor discharge temperature overshoot while not prematurely condensing vapour.

## 8.3 Application of LPGC to heat pumps

With the compression process explained, the LPGC is implemented into the heat pump model. To this end, the standard **1S-XV** cycle is taken and the 'CP' input in the sequence is replaced by 'LPGC'. The heat pump model then uses the LPGC for the compression process. Using the same inputs as Section 8.2.1, the resulting heat pump cycle is shown in Figure 8.9a. For comparison, a single-stage cycle with an adiabatic compressor acting between the same pressure levels is shown in Figure 8.9b.

The specific work calculated in Equation (8.1) can be used to obtain the CoP of this heat pump. When this is multiplied by the mass flow rate of the cycle, the compressor power is obtained: $\dot{W}_{\mathrm{LPGC}} = \dot{m} w_{\mathrm{LPGC}}$. The result is then:

$$\mathrm{CoP}_{\mathrm{adiabatic}} = 3.60 \qquad \& \qquad \mathrm{CoP}_{\mathrm{LPGC}} = 4.43,$$

which is a 23 % improvement of the LPGC over adiabatic compressor. The maximum CoP for this cycle is: $\mathrm{CoP}_{\mathrm{Max}} = 5.64$. The second law efficiencies are therefore:

$$\eta_{\mathrm{ex,adiabatic}} = 70.0\,\% \qquad \& \qquad \eta_{\mathrm{ex,LPGC}} = 78.1\,\%.$$

The volumetric heating capacities are:

$$\mathrm{VHC}_{\mathrm{adiabatic}} = 1.51\,\mathrm{MJ/m^3} \qquad \& \qquad \mathrm{VHC}_{\mathrm{LPGC}} = 1.21\,\mathrm{MJ/m^3},$$

which is a 20 % reduction, showing that the adiabatic compressor is at an advantage here. However, it is doubtful how useful this parameter is in comparing the compressor size in this case, as the type of compressor is very different.

It is desirable to find the relationship between the amount of spray injected in the chamber and the resulting CoP and the discharge temperature of the heat pump. Therefore, the LPGC model has been simulated for multiple spray fractions $f_{\mathrm{LS}}$ over a range of sink temperatures corresponding to domain 1 in Section 5.2. The suction pressure is thus the saturation pressure at $T_C = 100\,^{\circ}\mathrm{C}$ and the discharge pressure is the saturation pressure for the range $T_{\mathrm{H}} = 150 - 300\,^{\circ}\mathrm{C}$. The results are

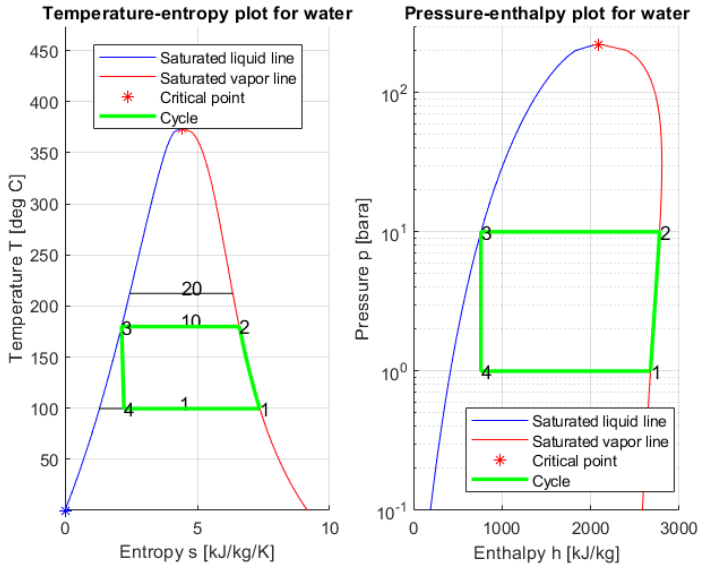


**(a)** LPGC

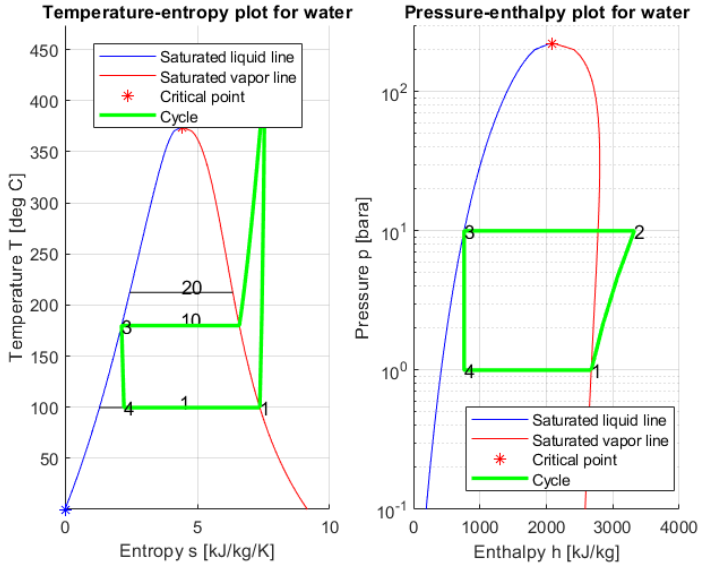


**(b)** Adiabatic

**Figure 8.9:** Property diagrams of a **1S-XV** heat pump cycle using (a) an LPGC compressor or (b) an ordinary adiabatic compressor.

shown in Figure 8.10. The different solid lines represent the CoP or the discharge temperature at certain spray fractions for different sink temperatures. In the CoP diagram, the order in the legend corresponds to the order in the diagram, so the upper line corresponds to $T_{\mathrm{H}} = 150\,^{\circ}\mathrm{C}$ and the bottom line to $T_{\mathrm{H}} = 300\,^{\circ}\mathrm{C}$. In the discharge temperature diagram, the order is inversed. The jiggly path of the lines is due to the limited number of $T_{\mathrm{H}}$ and $f_{\mathrm{LS}}$ values together with the intermittent nature of the spray injection. The spray fraction for which the maximum CoP is attained in the simulation is indicated with a black dot for each sink temperature. The spray fraction for which the discharge temperature becomes equal to the sink temperature is indicated with a blue dot for each sink temperature. The grey and cyan dashed lines represent curve fits to the black and blue points respectively. From the CoP diagram, two conclusions can be drawn. The first one is that for a higher sink temperature, a larger spray fraction is needed to obtain the maximum CoP. The second one is that the amount of spray necessary for the maximum CoP is not the same as the amount of spray necessary to achieve zero discharge temperature overshoot. The latter requires more spray to be injected, which implies that the maximum CoP is attained with a certain degree of overshoot and further more spray injection will only decrease the CoP. Therefore, the setting of $f_{\mathrm{LS}}$ will be a compromise between reaching the largest CoP and reducing the discharge temperature. The

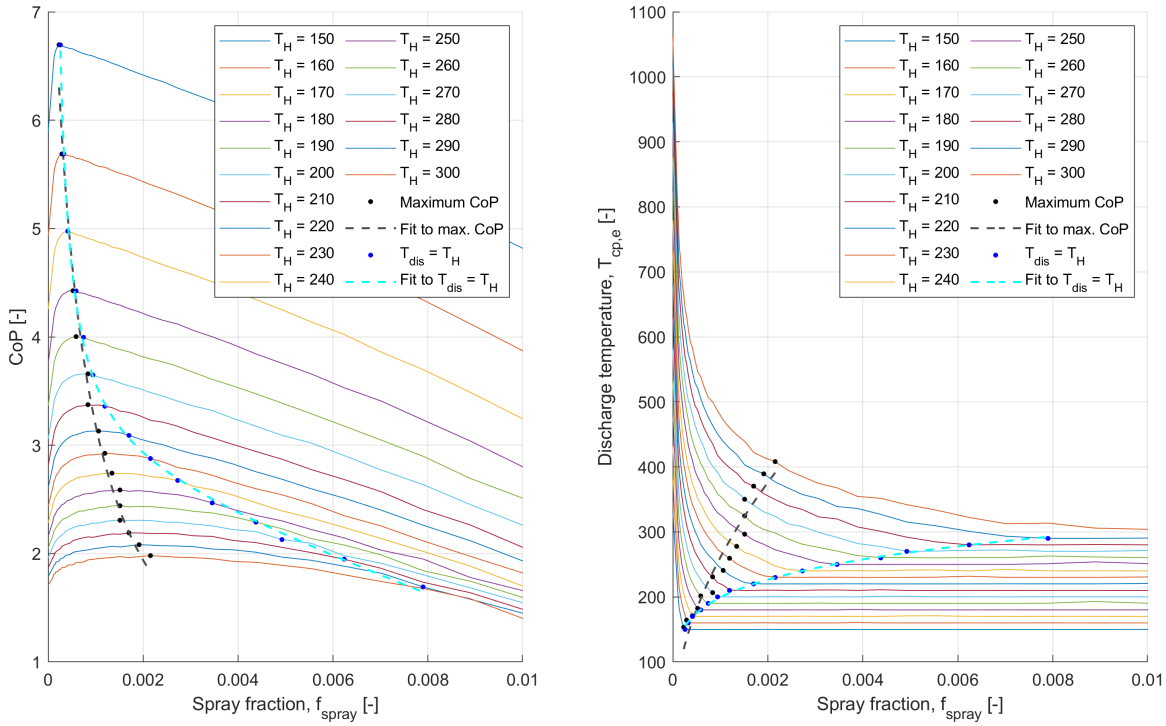


**Figure 8.10:** Diagrams showing the CoP and discharge temperatures for multiple sink temperatures in domain 1 over a range of spray fractions. The black dots are the spray fractions for which the CoP is maximum for that sink temperature. A grey fit curve passes through these points. The blue dots indicate the spray fractions for which the LPGC discharge is fully saturated vapour, with a cyan fit curve.

degree of overshoot that is evident at maximum CoP can be read from the discharge temperature diagram on the right. At the sink temperature of $T_{\mathrm{H}} = 300\,^{\circ}\mathrm{C}$, the discharge temperature is about $T_{\mathrm{H}} = 400\,^{\circ}\mathrm{C}$, thus the overshoot is about $100\,^{\circ}\mathrm{C}$.

It is also desirable to know the relationship between the sink temperature and the spray fractions that give maximum CoP and zero overshoot. This relation is displayed in Figure 8.11 together with fit curves. It can be seen that the relation between the sink temperature and spray fraction to obtain maximum CoP is linear. To achieve a discharge temperature equal to the saturation temperature, however, the amount of spray required increases exponentially.

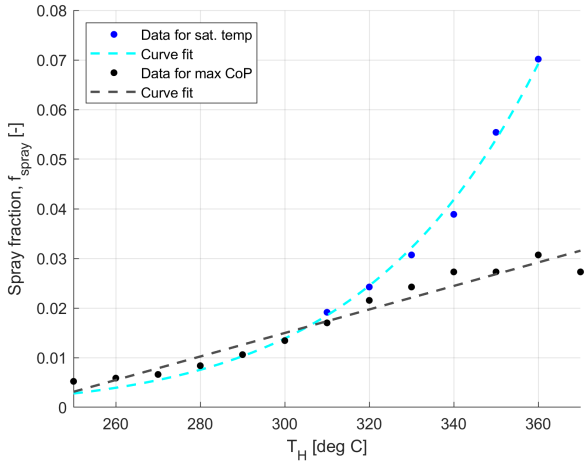


**Figure 8.11:** Diagram showing the spray fractions required for the sink temperatures in domain 1 to obtain the maximum CoP and fully saturated vapour.

This analysis was conducted in the same way for domain 2 and provided similar results. It was therefore concluded that the spray fraction is a compromise between the best CoP and the smallest discharge temperature. The fit curves were all derived using the 'fit' function in MatLab. The correlations for the curves with corresponding coefficients are given in Chapter C.

The relations allow the simulation of the LPGC model over a range of temperatures for the interesting limits of maximum CoP and zero discharge temperature overshoot. The performance of the LPGC model can then be compared to the cycles in Section 5.2.4. This comparison is done in the same way as Figure 5.9, with results for the relative CoP gain, the VHC and the discharge temperature plotted for water over domain 1. The results are shown in Figure 8.12. Only the configurations **1S-XV**, **1S-XV(wc)** and **2S-DCIC** are shown in this figure, as these appeared to be the best cycles for water. For the LPGC model, three settings of water spray fraction are shown: no spray (**1S-LPGC(dry)**), so much spray that the CoP is maximum (**1S-LPGC(Eff)**) and so much spray that the discharge temperature is equal to the saturation temperature (**1S-LPGC(Sat)**).

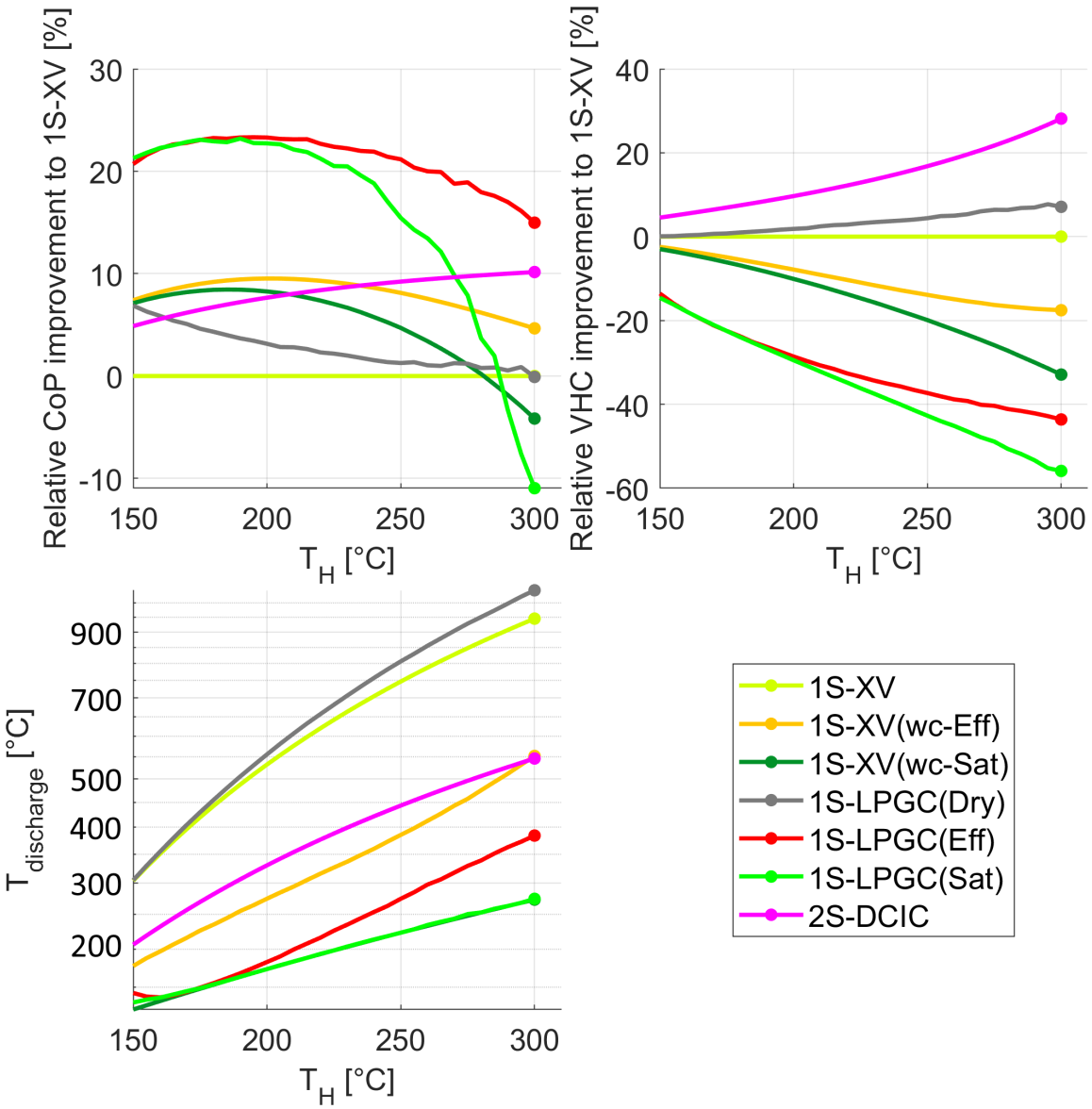


**Figure 8.12:** Comparison of different cycle configurations for water including LPGC with three different settings for the spray fraction: no spray (**1S-LPGC(dry)**), so much spray that the CoP is maximum ()1S-LPGC(Eff) and so much spray that the discharge temperature is equal to the saturation temperature (**1S-LPGC(Sat)**).

The jiggly shape of the performance lines for the LPGC models can again be explained by the intermittent nature of the spray injection, and the fact that a fit curve has been used which might not be very accurate. Nevertheless, the advantage of the LPGC is clear. For **1S-LPGC(Eff)**, the CoP is significantly larger than the other cycles over the entire domain. For the lower sink temperatures, **1S-LPGC(Sat)** is also much higher, however, the advantage quickly decreases for the higher sink temperatures until the CoP becomes even lower than that of the standard cycle. This behaviour is similar to what was observed for the **1S-XV(wc)** cycles. Also interesting to note is the behaviour of the LPGC model without spray (**1S-LPGC(dry)**) compared to the standard cycle. Even running dry, the LPGC appears to have a better performance. This difference can presumably

be attributed to the decoupling of the vapour compression and the pump itself. As was observed with the model validation, the LPGC running dry was in line with the literature, indicating that these results are correct.

Along with the significantly higher CoPs, the discharge temperature of **1S-LPGC(Eff)** is considerably lower than even **2S-DCIC**. For the lower sink temperatures, the discharge temperature is close to the saturation temperature. At the largest sink temperature, $T_{\mathrm{H}} = 300\,^{\circ}\mathrm{C}$, it is only about $100\,^{\circ}\mathrm{C}$ higher than the saturation temperature and about $180\,^{\circ}\mathrm{C}$ lower than the discharge temperature of **2S-DCIC**. For all temperatures, it remains below the threshold value of $400\,^{\circ}\mathrm{C}$. This discharge temperature can be further lowered by increasing the spray fraction, however at the expense of CoP.

Looking at the VHC diagram, it is seen that spray injection lowers the VHC compared to the other cycles. It is however again disputed if conclusions can be drawn from the VHC value due to the very different way of compressing. For the LPGC, it is calculated using the vapour inlet density. However, this disregards the density of the liquid spray also entering the chamber. On the contrary, for the **1S-XV(wc)** cycle, VHC is calculated with the average inlet density of the two-phase mixture at the inlet. Since this density is higher, the VHC of this cycle is inherently calculated to be larger than that of the LPGC. For the LPGC, it is not possible to determine a similar average inlet density because the liquid is added during the compression.

From these results, it can be concluded that **1S-LPGC(Eff)** allows a considerably increased performance for water compared to **2S-DCIC**. At the same time, the discharge temperature is significantly lowered to below the threshold. Therefore, **1S-LPGC(Eff)** replaces **2S-DCIC** as the best cycle for water. This conclusion might not be limited to water, but could also be applied to the other wet fluids. This possibility has however not been investigated in this research.

To compare the performance of water in an **1S-LPGC(Eff)** cycle to the other fluids using their best cycle, the same simulation as Section 5.2.5 has been performed. The results for domain 1 are shown in Figure 8.13.

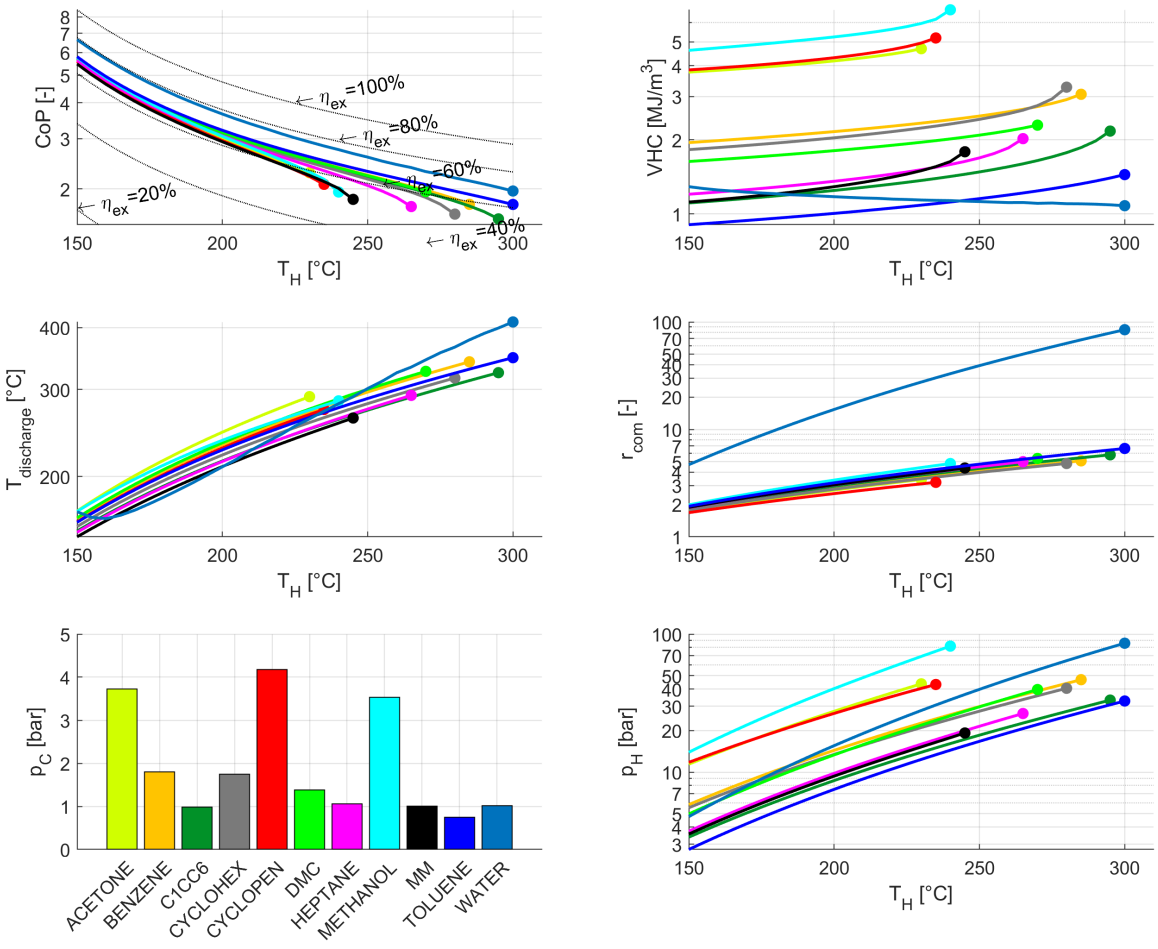


**Figure 8.13:** Performance figures for the different fluids using the configuration with the best improvement compared to **1S-XV** for domain 1.

**Domain 1** With an LPGC, water is clearly at a much higher level compared to the other fluids in terms of CoP. The CoP remains significantly higher than all other fluids over the entire domain. The discharge temperature remains one of the lowest for the lower sink temperatures and is only marginally larger than the other fluids for the higher sink temperatures. The VHC is on the lower end for the lower sink temperatures, while it becomes similar to the other fluids that can still be used at the higher sink temperatures. The pressure ratio is much larger than the other fluids due to being a single-stage compression cycle. For an LPGC however, the pressure ratio is not as problematic as with gas compressors due to liquid pumps usually being able to reach large pressure ratios.

**Domain 2** The results for domain 2 are shown in Figure 8.13. These results are similar in terms of the advantages of a water-LPGC relative to the other fluids. The difference in exergy efficiency between has become even larger, while the discharge temperature remains on the lower end for almost the entire range of temperatures. The threshold is only slightly surpassed by about 15 °C for the highest sink temperatures. The VHC is still the largest of all fluids despite the lower values calculated compared to the standard cycle. Therefore, it can be concluded that the water-LPGC heat pump outperforms all other fluids and configurations in both domains.

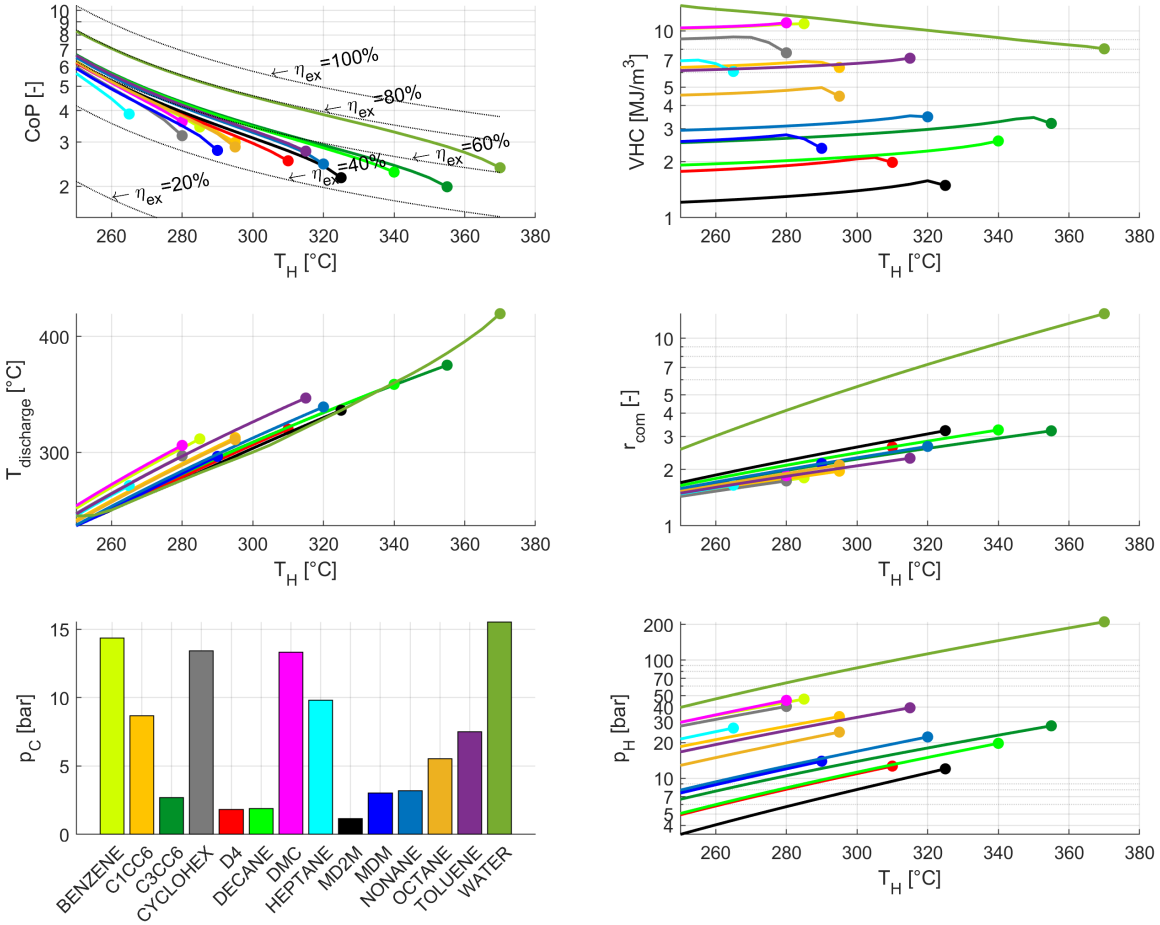


**Figure 8.14:** Performance figures for the different fluids using the configuration with the best improvement compared to **1S-XV** for domain 2. Since the colours match, the lower left diagram can be used as a legend.

The models for the heat pump and the LPGC have only been simulated for discharge pressures below the critical pressure of water. This is done to properly compare different fluids against each other by setting their source and sink temperatures equal. However, no restrictions have been identified that prohibit using an LPGC at supercritical pressures. Nevertheless, the LPGC model was not able to simulate this as it was built around liquid droplets, which can not be distinguished from vapour anymore at supercritical pressures.

# Chapter 9

# LPGC Model: Summary & Conclusion

The conclusions of Chapter 5 provided a starting point for the investigation of a compression method which would be suited for water. Not only did water have the best performance compared to other potential HTHP working fluids, but it was also the only hazard-free and environmentally friendly fluid. The disadvantages were a very large discharge temperature and large pressure ratios. By evaluating the different types of compressors, it appeared that a suitable solution would be the Liquid Piston Gas Compressor (LPGC).

The LPGC has many benefits compared to other compressors, the most important being the ability to use liquid spray injection for cooling while not requiring oil for lubrication or sealing. Moreover, in heat pumps using an LPGC, the liquid of the same cycle can be used to compress the vapour. This meant that the cooling of the vapour evaporated the sprayed liquid, adding to the mass of the vapour. To understand the evaporation of a spray of droplets during compression in an LPGC, a model was made that simulated this process.

First, an attempt was made to validate the model. However, due to the lack of comparable literature, the model could only be compared without spray injection. Moreover, the liquid compressed air instead of water vapour. Nevertheless, the results showed good agreement. It could however not be concluded that the model was completely validated.

Subsequently, the LPGC model was provided with an example case to test and show the dynamics. The model was set such that the discharge was saturated vapour. The results were compared to an ordinary adiabatic compressor without cooling. It was shown that the temperature could be kept to the saturation temperature while specific work was decreased by 22.1 %. From this, it could be concluded that the LPGC could provide a low-temperature fluid with more mass than the high-temperature discharge of an ordinary compressor without violating the first law of thermodynamics. From the T-s diagram, it appeared that the specific entropy decreased. To prove that the entropy production of the LPGC was positive, it was explained how a closed system approach was used to calculate this property. It was subsequently shown that the entropy production was indeed positive, so it could be concluded that the second law of thermodynamics was also not violated.

Then the droplet behaviour during compression was shown and explained. Since all effects could be logically explained by correlating different results, it could be concluded that the droplet model behaves as intuitively expected. The LPGC was then integrated into the standard heat pump cycle, which was compared to the same cycle using an ordinary adiabatic compressor. The CoP of the LPGC was increased by 23 %, while the VHC decreased by 20 %. The value of the VHC was however disputed due to the compression method being conceptually different. Nevertheless, it could be concluded that the LPGC in a heat pump would bring significant improvements

To determine what spray fractions would lead to the best performance, the heat pump model with LPGC was simulated for a range of spray fractions over the two domains, defined in Chapter 5. These results showed that the CoP could be maximised for certain spray fractions, which appeared to be smaller than the spray required for complete wet compression. It was therefore concluded that the spray fraction is a compromise between the best CoP and the smallest discharge temperature.

Using this data, the LPGC heat pump could be compared to the other configurations that were investigated in this project. These results showed that the setup geared for maximum efficiency resulted in a CoP improvement in the range of 15-25 % compared to the standard cycle, with the largest improvement reached for lower sink temperatures. The setup geared for saturated discharge vapour had a similar improvement for lower sink temperatures but deteriorated for higher temperatures. In terms of VHC, the LPGC was the worst. The significance of this performance indicator was, however, questioned for this kind of compressor. With the significantly lower discharge temperatures, it was concluded that the **1S-LPGC(Eff)** cycle is the best configuration for water.

With this knowledge, the **1S-LPGC(Eff)** cycle with water was compared to the results of the other fluids with their best configuration over the two domains. From these results, it was seen that the LPGC with water leads to significant improvements in efficiency compared to other fluids, while the discharge temperatures are similar and below the threshold value. Therefore, it can be concluded that a water-LPGC heat pump can suitably be used for upgrading industrial waste heat in the range of 100-200 °C to process heat in the range of 150-400 °C. This statement is the answer to the research question and is supported by the following facts:

- It allows the usage of water which is, compared to most other fluids, safe, environmentally friendly, widely available and cheap.
- The efficiencies considerably surpass that of all alternative fluids.
- The discharge temperatures are acceptably low.
- A simple single-stage heat pump cycle can be used, avoiding the added heat exchangers, compressors or expansion valves of multi-staged systems that the other fluids used.
- For the compression, a hydraulic pump can be used which can efficiently reach large pressure ratios in a single stage. Moreover, due to relatively low-temperature operation, it is a presumably inexpensive device.

# Bibliography


[1] Pinaki Acharya, Vikram Patil, and Paul Ro. "Experimental Investigation of Water Spray Cooling for Temperature Reduction in Liquid Piston Compressor". In: *International Compressor Engineering Conference* (Paper 2640 2018).

[2] Keri-Marie Adamson et al. "High-temperature and transcritical heat pump cycles and advancements: A review". In: *Renewable and Sustainable Energy Reviews* 167 (Oct. 2022), p. 112798. ISSN: 13640321. DOI: 10.1016/j.rser.2022.112798. URL: https://linkinghub.elsevier.com/retrieve/pii/S1364032122006827 (visited on 06/24/2023).

[3] Cordin Arpagaus et al. "High temperature heat pumps: Market overview, state of the art, research status, refrigerants, and application potentials". In: *Energy* 152 (June 2018), pp. 985–1010. ISSN: 03605442. DOI: 10.1016/j.energy.2018.03.166. URL: https://linkinghub.elsevier.com/retrieve/pii/S0360544218305759 (visited on 06/19/2023).

[4] ASHRAE and ANSI. *ASHRAE standard 34, designation and safety classification of refrigerants*. Atlanta, USA, 2016.

[5] Alireza Bahadori. "Gas Compressors". In: *Natural Gas Processing*. Elsevier, 2014, pp. 223–273. ISBN: 978-0-08-099971-5. DOI: 10.1016/B978-0-08-099971-5.00005-2. URL: https://linkinghub.elsevier.com/retrieve/pii/B9780080999715000052 (visited on 01/20/2024).

[6] Mohammad Bahrami, Ali A Hamidi, and Soheil Porkhial. "Investigation of the effect of organic working fluids on thermodynamic performance of combined cycle Stirling-ORC". In: *International Journal of Energy and Environmental Engineering* 4.1 (2013), p. 12. ISSN: 2251-6832. DOI: 10.1186/2251-6832-4-12. URL: http://www.journal-ijeee.com/content/4/1/12 (visited on 01/03/2024).

[7] Sarah Brückner et al. "Industrial waste heat recovery technologies: An economic analysis of heat transformation technologies". In: *Applied Energy* 151 (Aug. 2015), pp. 157–167. ISSN: 03062619. DOI: 10.1016/j.apenergy.2015.01.147. URL: https://linkinghub.elsevier.com/retrieve/pii/S0306261915004584 (visited on 06/25/2023).

[8] Paul Byrne and Redouane Ghoubali. "Exergy analysis of heat pumps for simultaneous heating and cooling". In: *Applied Thermal Engineering* 149 (Feb. 2019), pp. 414–424. ISSN: 13594311. DOI: 10.1016/j.applthermaleng.2018.12.069. URL: https://linkinghub.elsevier.com/retrieve/pii/S1359431118341723 (visited on 01/12/2024).

[9] CAMEO Chemicals. *Database of Hazardous Materials*. URL: https://cameochemicals.noaa.gov/.

[10] Eurostat. *Energy database*. 2016. URL: http://ec.europa.eu/eurostat/web/energy/.

[11] Guido Francesco Frate, Lorenzo Ferrari, and Umberto Desideri. "Analysis of suitability ranges of high temperature heat pump working fluids". In: *Applied Thermal Engineering* 150 (Mar. 2019), pp. 628–640. ISSN: 13594311. DOI: 10.1016/j.applthermaleng.2019.01.034. URL: https://linkinghub.elsevier.com/retrieve/pii/S1359431118353602 (visited on 01/03/2024).

[12] Nikunj Gangar, Sandro Macchietto, and Christos N. Markides. "Recovery and Utilization of Low-Grade Waste Heat in the Oil-Refining Industry Using Heat Engines and Heat Pumps: An International Technoeconomic Comparison". In: *Energies* 13.10 (May 18, 2020), p. 2560. ISSN: 1996-1073. DOI: 10.3390/en13102560. URL: https://www.mdpi.com/1996-1073/13/10/2560 (visited on 06/19/2023).

[13] Walter Grassi. *Heat Pumps*. Green Energy and Technology. Cham: Springer International Publishing, 2018. ISBN: 978-3-319-62198-2. DOI: 10.1007/978-3-319-62199-9. URL: http://link.springer.com/10.1007/978-3-319-62199-9 (visited on 06/25/2023).

[14] Arkadiusz Guzda. "Compressors in Heat Pumps". In: Vol 39 (No 2 June 2016), pp. 71–83. ISSN: bwmeta1.element.baztech-f44102e3-68f2-422b-86b6-68ed072c6a8d.

[15] Gábor Györke, Axel Groniewsky, and Attila Imre. "A Simple Method of Finding New Dry and Isentropic Working Fluids for Organic Rankine Cycle". In: *Energies* 12.3 (Feb. 1, 2019), p. 480. ISSN: 1996-1073. DOI: 10.3390/en12030480. URL: http://www.mdpi.com/1996-1073/12/3/480 (visited on 01/26/2024).

[16] Khalid Hamid et al. "Potential evaluation of integrated high temperature heat pumps: A review of recent advances". In: *Applied Thermal Engineering* 230 (July 2023), p. 120720. ISSN: 13594311. DOI: 10.1016/j.applthermaleng.2023.120720. URL: https://linkinghub.elsevier.com/retrieve/pii/S1359431123007494 (visited on 06/15/2023).

[17] G.P. Hammond and J.B. Norman. "Heat recovery opportunities in UK industry". In: *Applied Energy* 116 (Mar. 2014), pp. 387–397. ISSN: 03062619. DOI: 10.1016/j.apenergy.2013.11.008. URL: https://linkinghub.elsevier.com/retrieve/pii/S030626191300901X (visited on 06/21/2023).

[18] T.L. Henshaw et al. "Chapter 14: Fans, Pumps, and Compressors". In: *Marks' Standard Handbook for Mechanical Engineering*. Mcgraw Hill, 2017.

[19] Bin Hu, Di Wu, and R.Z. Wang. "Water vapor compression and its various applications". In: *Renewable and Sustainable Energy Reviews* 98 (Dec. 2018), pp. 92–107. ISSN: 13640321. DOI: 10.1016/j.rser.2018.08.050. URL: https://linkinghub.elsevier.com/retrieve/pii/S1364032118306348 (visited on 01/27/2024).

[20] Marcia Huber et al. *NIST Reference Fluid Thermodynamic and Transport Properties Database (REFPROP) Version 9 - SRD 23*. 2018. DOI: 10.18434/T4/1502528. URL: https://www.nist.gov/srd/refprop (visited on 05/26/2023).

[21] International Energy Agency. *Application of Industrial Heat Pumps*. HPP-AN35-1. 2014.

[22] Laure Itard. *Wet compression-resorption heat pump cycles: thermodynamic analysis and design*. Delft: Univ. of Technology, 1998. 305 pp. ISBN: 978-90-370-0165-5.

[23] Jonas K. Jensen et al. "On the development of high temperature ammonia–water hybrid absorption–compression heat pumps". In: *International Journal of Refrigeration* 58 (Oct. 2015), pp. 79–89. ISSN: 01407007. DOI: 10.1016/j.ijrefrig.2015.06.006. URL: https://linkinghub.elsevier.com/retrieve/pii/S0140700715001735 (visited on 06/25/2023).

[24] Jiatong Jiang et al. "A review and perspective on industry high-temperature heat pumps". In: *Renewable and Sustainable Energy Reviews* 161 (June 2022), p. 112106. ISSN: 13640321. DOI: 10.1016/j.rser.2022.112106. URL: https://linkinghub.elsevier.com/retrieve/pii/S1364032122000351 (visited on 06/15/2023).

[25] S.S. Kachhwaha, P.L. Dhar, and S.R. Kale. "Experimental studies and numerical simulation of evaporative cooling of air with a water spray—I. Horizontal parallel flow". In: *International Journal of Heat and Mass Transfer* 41.2 (Jan. 1998), pp. 447–464. ISSN: 00179310. DOI: 10.1016/S0017-9310(97)00133-6. URL: https://linkinghub.elsevier.com/retrieve/pii/S0017931097001336 (visited on 01/19/2024).

[26] James Kersey, Eric Loth, and Dennis Lankford. "Effect of Evaporating Droplets on Shock Waves". In: *AIAA Journal* 48.9 (Sept. 2010), pp. 1975–1986. ISSN: 0001-1452, 1533-385X. DOI: 10.2514/1.J050162. URL: https://arc.aiaa.org/doi/10.2514/1.J050162 (visited on 11/27/2023).

[27] Sunghwan Kim et al. "PubChem 2023 update". In: *Nucleic Acids Research* 51 (D1 Jan. 6, 2023), pp. D1373–D1380. ISSN: 0305-1048, 1362-4962. DOI: 10.1093/nar/gkac956. URL: https://academic.oup.com/nar/article/51/D1/D1373/6777787 (visited on 01/07/2024).

[28] Anton Alexandru Kiss and Carlos A. Infante Ferreira. *Heat pumps in chemical process industry*. Boca Raton, FL: CRC Press, Taylor & Francis Group, an Informa business, 2017. 422 pp. ISBN: 978-1-4987-1895-0.

[29] George Kosmadakis. "Estimating the potential of industrial (high-temperature) heat pumps for exploiting waste heat in EU industries". In: *Applied Thermal Engineering* 156 (June 2019), pp. 287–298. ISSN: 13594311. DOI: 10.1016/j.applthermaleng.2019.04.082. URL: https://linkinghub.elsevier.com/retrieve/pii/S1359431118376087 (visited on 06/19/2023).

[30] Steve Kowalski et al. "Initial Design and Experimental Results of a Novel Near-Isothermal Compressor for Heat Pump Applications". In: (Jan. 7, 2022). URL: https://www.osti.gov/servlets/purl/1885330.

[31] Mikkel E. Larsen, ed. *Refrigeration: theory, technology, and applications*. Hauppauge, N.Y: Nova Science Publishers, 2011. 555 pp. ISBN: 978-1-61668-930-8.

[32] Renato M. Lazzarin. "Heat pumps in industry—I. Equipment". In: *Heat Recovery Systems and CHP* 14.6 (Nov. 1994), pp. 581–597. ISSN: 08904332. DOI: 10.1016/0890-4332(94)90029-9. URL: https://linkinghub.elsevier.com/retrieve/pii/0890433294900299 (visited on 06/22/2023).

[33] A. Marina et al. “An estimation of the European industrial heat pump market potential”. In: *Renewable and Sustainable Energy Reviews* 139 (Apr. 2021), p. 110545. ISSN: 13640321. DOI: 10.1016/j.rser.2020.110545. URL: https://linkinghub.elsevier.com/retrieve/pii/S1364032120308297 (visited on 06/17/2023).

[34] Mobil Serv. *Hydraulic efficiency*. 2018. URL: chrome-extension://oemmndcbldboiebfnladdacbdfmadadm/https://www.mobil.com/lubricants/-/media/project/wep/shared/mobil-row-lubesus1-us/lubricant-expertise/resources/hydraulic-fluid-efficiency/tech-topic-hydraulic-efficiency-3.pdf.

[35] Michael J. Moran et al. *Principles of engineering thermodynamics*. Eighth edition, SI version. OCLC: 908412182. Singapore: Wiley, 2015. ISBN: 978-1-118-96088-2.

[36] Faith Morrison. “Data Correlation for Drag Coefficient for Sphere”. In: (11), p. 2.

[37] Torben Ommen et al. “Technical and economic working domains of industrial heat pumps: Part 1 – Single stage vapour compression heat pumps”. In: *International Journal of Refrigeration* 55 (July 2015), pp. 168–182. ISSN: 01407007. DOI: 10.1016/j.ijrefrig.2015.02.012. URL: https://linkinghub.elsevier.com/retrieve/pii/S0140700715000444 (visited on 01/04/2024).

[38] Gerald Ondrey. “High-temperature heat pump promises significant energy savings”. In: (June 1, 2021). URL: https://www.chemengonline.com/heat-pump/.

[39] Michael Papapetrou et al. “Industrial waste heat: Estimation of the technically available resource in the EU per industrial sector, temperature level and country”. In: *Applied Thermal Engineering* 138 (June 2018), pp. 207–216. ISSN: 13594311. DOI: 10.1016/j.applthermaleng.2018.04.043. URL: https://linkinghub.elsevier.com/retrieve/pii/S1359431117347919 (visited on 06/19/2023).

[40] Joong-kyoo Park et al. “Analysis and Proof-of-Concept Experiment of Liquid-Piston Compression for Ocean Compressed Air Energy Storage (OCAES) System”. In: Marine Energy Technology Symposium (Apr. 2014).

[41] Vikram C. Patil, Pinaki Acharya, and Paul I. Ro. “Experimental investigation of heat transfer in liquid piston compressor”. In: *Applied Thermal Engineering* 146 (Jan. 2019), pp. 169–179. ISSN: 13594311. DOI: 10.1016/j.applthermaleng.2018.09.121. URL: https://linkinghub.elsevier.com/retrieve/pii/S1359431118333027 (visited on 01/28/2024).

[42] Vikram C. Patil, Pinaki Acharya, and Paul I. Ro. “Experimental investigation of water spray injection in liquid piston for near-isothermal compression”. In: *Applied Energy* 259 (Feb. 2020), p. 114182. ISSN: 03062619. DOI: 10.1016/j.apenergy.2019.114182. URL: https://linkinghub.elsevier.com/retrieve/pii/S0306261919318690 (visited on 01/18/2024).

[43] Cecil Piya. “Liquid Piston Gas Compression”. Bachelor thesis. Worcester: Worcester Polytechnic Institute, 2009.

[44] Chao Qin and Eric Loth. “Liquid piston compression efficiency with droplet heat transfer”. In: *Applied Energy* 114 (Feb. 2014), pp. 539–550. ISSN: 03062619. DOI: 10.1016/j.apenergy.2013.10.005. URL: https://linkinghub.elsevier.com/retrieve/pii/S0306261913008258 (visited on 11/15/2023).

[45] Florian Reissner. “Development of a Novel High Temperature Heat Pump System”. Doctoral Thesis. Erlangen-Nürnberg: Friedrich-Alexander-Universität, Nov. 3, 2015. URL: urn:nbn:de:bvb:29-opus4-67152.

[46] Jahar Sarkar. “Ejector enhanced vapor compression refrigeration and heat pump systems—A review”. In: *Renewable and Sustainable Energy Reviews* 16.9 (Dec. 2012), pp. 6647–6659. ISSN: 13640321. DOI: 10.1016/j.rser.2012.08.007. URL: https://linkinghub.elsevier.com/retrieve/pii/S1364032112004765 (visited on 01/26/2024).

[47] Elisabeth Schröder et al. “Study on Heat Transfer in Heat Exchangers for a New Supercritical Organic Rankine Cycle”. In: *Heat Transfer Engineering* 35.18 (Dec. 12, 2014), pp. 1505–1519. ISSN: 0145-7632, 1521-0537. DOI: 10.1080/01457632.2014.897558. URL: http://www.tandfonline.com/doi/abs/10.1080/01457632.2014.897558 (visited on 06/25/2023).

[48] I. K. Shatalov, Yu. A. Antipov, and K. G. Dubentsov. “Use of the Lorenz Cycle in Heat Pumps”. In: *Chemical and Petroleum Engineering* 53.11 (Mar. 2018), pp. 716–719. ISSN: 0009-2355, 1573-8329. DOI: 10.1007/s10556-018-0410-6. URL: http://link.springer.com/10.1007/s10556-018-0410-6 (visited on 06/25/2023).

[49] David A. Simpson. “Gas Compression”. In: *Practical Onshore Gas Field Engineering*. Elsevier, 2017, pp. 513–571. ISBN: 978-0-12-813022-3. DOI: 10.1016/B978-0-12-813022-3.00008-0. URL: https://linkinghub.elsevier.com/retrieve/pii/B9780128130223000080 (visited on 01/19/2024).

[50] Wichean Singmai, Kasemsil Onthong, and Tongchana Thongtip. "Experimental Investigation of the Improvement Potential of a Heat Pump Equipped with a Two-Phase Ejector". In: *Energies* 16.16 (Aug. 9, 2023), p. 5889. ISSN: 1996-1073. DOI: 10.3390/en16165889. URL: https://www.mdpi.com/1996-1073/16/16/5889 (visited on 01/26/2024).

[51] James Stewart. *Calculus*. EIghth edition. OCLC: ocn892432745. Boston, MA, USA: Cengage Learning, 2016. 1 p. ISBN: 978-1-285-74062-1.

[52] Jian Sun et al. "A Review of Super-High-Temperature Heat Pumps over 100 °C". In: *Energies* 16.12 (June 8, 2023), p. 4591. ISSN: 1996-1073. DOI: 10.3390/en16124591. URL: https://www.mdpi.com/1996-1073/16/12/4591 (visited on 01/26/2024).

[53] R. Sureshkumar, S.R. Kale, and P.L. Dhar. "Heat and mass transfer processes between a water spray and ambient air – II. Simulations". In: *Applied Thermal Engineering* 28.5 (Apr. 2008), pp. 361–371. ISSN: 13594311. DOI: 10.1016/j.applthermaleng.2007.09.015. URL: https://linkinghub.elsevier.com/retrieve/pii/S1359431107003134 (visited on 01/19/2024).

[54] Arvind Thekdi and Sachin U. Nimbalkar. *Industrial Waste Heat Recovery - Potential Applications, Available Technologies and Crosscutting R&D Opportunities*. ORNL/TM–2014/622, 1185778. Jan. 1, 2015, ORNL/TM–2014/622, 1185778. DOI: 10.2172/1185778. URL: http://www.osti.gov/servlets/purl/1185778/ (visited on 06/19/2023).

[55] S. Touber. *Thermische machines – Een compressie warmtepomp*. 1996.

[56] D.M. Van De Bor, C.A. Infante Ferreira, and Anton A. Kiss. "Low grade waste heat recovery using heat pumps and power cycles". In: *Energy* 89 (Sept. 2015), pp. 864–873. ISSN: 03605442. DOI: 10.1016/j.energy.2015.06.030. URL: https://linkinghub.elsevier.com/retrieve/pii/S0360544215007860 (visited on 06/19/2023).

[57] James D. Van De Ven and Perry Y. Li. "Liquid piston gas compression". In: *Applied Energy* 86.10 (Oct. 2009), pp. 2183–2191. ISSN: 03062619. DOI: 10.1016/j.apenergy.2008.12.001. URL: https://linkinghub.elsevier.com/retrieve/pii/S0306261908003218 (visited on 01/27/2024).

[58] VDI e. V., ed. *VDI Heat Atlas*. Berlin, Heidelberg: Springer Berlin Heidelberg, 2010. ISBN: 978-3-540-77876-9. DOI: 10.1007/978-3-540-77877-6. URL: https://link.springer.com/10.1007/978-3-540-77877-6 (visited on 01/28/2024).

[59] Di Wu and Bin Hu. "Performance analysis of water refrigerant heat pump with different configurations for high-temperature application". In: *Frontiers in Energy Research* 11 (Nov. 6, 2023), p. 1257865. ISSN: 2296-598X. DOI: 10.3389/fenrg.2023.1257865. URL: https://www.frontiersin.org/articles/10.3389/fenrg.2023.1257865/full (visited on 01/09/2024).

[60] Wei Wu et al. "A novel distributed energy system using high-temperature proton exchange membrane fuel cell integrated with hybrid-energy heat pump". In: *Energy Conversion and Management* 235 (May 2021), p. 113990. ISSN: 01968904. DOI: 10.1016/j.enconman.2021.113990. URL: https://linkinghub.elsevier.com/retrieve/pii/S0196890421001667 (visited on 06/25/2023).

[61] Benjamin Zühlsdorf, Jonas Kjær Jensen, and Brian Elmegaard. "Heat pump working fluid selection—economic and thermodynamic comparison of criteria and boundary conditions". In: *International Journal of Refrigeration* 98 (Feb. 2019), pp. 500–513. ISSN: 01407007. DOI: 10.1016/j.ijrefrig.2018.11.034. URL: https://linkinghub.elsevier.com/retrieve/pii/S0140700718304870 (visited on 06/14/2023).

# Appendix A

# Information on working fluids

This list of working fluids was obtained from [20].

**Table A.1:** List of all pure fluids available in RefProp with their corresponding name, chemical formula, molar mass $M$, normal boiling point temperature $T_b$, critical temperature $T_C$, critical pressure $p_C$, GWP, ODP and ASHRAE 34 Safety Classification (if determined) [20].

| Reference | Short name | Formula | $M$[g/mol] | $T_b$[°C] | $T_C$[°C] | $p_C$[bar] | GWP | ODP | Class |
|---|---|---|---|---|---|---|---|---|---|
| 13BUTADIENE | 1,3-Butadiene | C4H6 | 54.1 | -4.5 | 152.0 | 43.1 | | | |
| 1BUTYNE | 1-Butyne | C4H6 | 54.1 | 8.1 | 158.9 | 41.4 | | | |
| 1PENTENE | 1-Pentene | C5H10 | 70.1 | 30.0 | 192.6 | 36.0 | | | |
| 22DIMETHYLBUTANE | 2,2-Dimethylbutane | C6H14 | 86.2 | 49.7 | 216.9 | 31.4 | | | |
| 23DIMETHYLBUTANE | 2,3-Dimethylbutane | C6H14 | 86.2 | 58.0 | 227.5 | 31.6 | | | |
| 3METHYLPENTANE | 3-Methylpentane | C6H14 | 86.2 | 63.2 | 232.9 | 31.8 | | | |
| acetone | Acetone | C3H6O | 58.1 | 56.1 | 235.0 | 46.9 | 0.5 | | |
| acetylene | Acetylene | C2H2 | 26.0 | -84.9 | 35.2 | 59.9 | | | |
| ammonia | Ammonia | NH3 | 17.0 | -33.3 | 132.4 | 113.6 | | | B2L |
| argon | Argon | Ar | 39.9 | -185.8 | -122.5 | 48.6 | | | A1 |
| benzene | Benzene | C6H6 | 78.1 | 80.1 | 288.9 | 49.1 | | | |
| butane | Butane | C4H10 | 58.1 | -0.5 | 152.0 | 38.0 | 4 | | A3 |
| 1BUTENE | Butene | C4H8 | 56.1 | -6.3 | 146.1 | 40.1 | | | |
| CO2 | Carbon dioxide | CO2 | 44.0 | -78.5 | 31.0 | 73.8 | 1 | | A1 |
| CO | Carbon monoxide | CO | 28.0 | -191.5 | -140.3 | 34.9 | | | |
| COS | Carbonyl sulfide | COS | 60.1 | -50.2 | 105.6 | 63.7 | | | |
| chlorine | Chlorine | Cl2 | 70.9 | -34.0 | 143.7 | 76.4 | | | |
| chlorobenzene | Chlorobenzene | C6H5Cl | 112.6 | 132.1 | 359.2 | 45.2 | | | |
| C2BUTENE | cis-Butene | C4H8 | 56.1 | 3.7 | 162.6 | 42.3 | | | |
| cyclobutene | Cyclobutene | C4H6 | 54.1 | 2.6 | 174.9 | 51.5 | | | |
| CYCLOHEX | Cyclohexane | C6H12 | 84.2 | 80.7 | 280.5 | 40.8 | | | |
| CYCLOPEN | Cyclopentane | C5H10 | 70.1 | 49.3 | 238.6 | 45.8 | | | |
| CYCLOPRO | Cyclopropane | C3H6 | 42.1 | -31.5 | 125.2 | 55.8 | | | |
| D4 | D4 | C8H24O4Si4 | 296.6 | 175.7 | 313.4 | 13.5 | | | |
| D5 | D5 | C10H30O5Si5 | 370.8 | 210.9 | 345.2 | 10.9 | | | |
| D6 | D6 | C12H36Si6O6 | 444.9 | 245.0 | 372.6 | 9.6 | | | |
| DEA | DEA | C4H11NO2 | 105.1 | 268.1 | 463.4 | 49.5 | | | |
| decane | Decane | C10H22 | 142.3 | 174.1 | 344.6 | 21.0 | | | |
| D2 | Deuterium | D2 | 4.0 | -249.5 | -234.8 | 16.8 | | | |
| R150 | Dichloroethane | C2H4Cl2 | 99.0 | 83.5 | 288.5 | 52.3 | | | |
| DEE | Diethyl ether | C4H10O | 74.1 | 34.5 | 193.6 | 37.2 | | | |
| DMC | Dimethyl carbonate | C3H6O3 | 90.1 | 90.1 | 283.9 | 49.1 | | | |
| DME | Dimethyl ether | C2H6O | 46.1 | -24.8 | 127.2 | 53.4 | 1 | | A3 |
| C22 | Docosane | C22H46 | 310.6 | 368.1 | 519.1 | 11.7 | | | |
| C12 | Dodecane | C12H26 | 170.3 | 216.3 | 385.0 | 18.2 | | | |
| ethane | Ethane | C2H6 | 30.1 | -88.6 | 32.2 | 48.7 | 5.5 | | A3 |
| ethanol | Ethanol | C2H6O | 46.1 | 78.4 | 241.6 | 62.7 | | | |
| EGLYCOL | Ethylene glycol | C2H6O2 | 62.1 | 197.2 | 445.9 | 105.1 | | | |
| EBENZENE | Ethylbenzene | C8H10 | 106.2 | 136.2 | 344.0 | 36.2 | | | |
| ethylene | Ethylene | C2H4 | 28.1 | -103.8 | 9.2 | 50.4 | 3.7 | | A3 |
| ETHYLENEOXIDE | Ethylene oxide | C2H4O | 44.1 | 10.5 | 195.8 | 73.0 | | | |
| fluorine | Fluorine | F2 | 38.0 | -188.1 | -128.7 | 51.7 | | | |
| D2O | Heavy water | D2O | 20.0 | 101.4 | 370.7 | 216.6 | | | |
| helium | Helium | He | 4.0 | -268.9 | -268.0 | 2.3 | | | A1 |
| heptane | Heptane | C7H16 | 100.2 | 98.4 | 267.1 | 27.4 | | | |
| C16 | Hexadecane | C16H34 | 226.4 | 286.8 | 449.0 | 14.8 | | | |
| hexane | Hexane | C6H14 | 86.2 | 68.7 | 234.7 | 30.4 | | | |
| HYDROGEN | Hydrogen (normal) | H2 | 2.0 | -252.8 | -240.0 | 13.0 | | | A3 |
| HCL | Hydrogen chloride | HCl | 36.5 | -85.0 | 51.5 | 83.1 | | | |
| H2S | Hydrogen sulfide | H2S | 34.1 | -60.3 | 100.0 | 90.0 | | | |
| ISOBUTAN | Isobutane | C4H10 | 58.1 | -11.7 | 134.7 | 36.3 | | | A3 |
| IBUTENE | Isobutene | C4H8 | 56.1 | -7.0 | 144.9 | 40.1 | | | |
| IHEXANE | Isohexane | C6H14 | 86.2 | 60.2 | 224.6 | 30.4 | | | |
| IOCTANE | Isooctane | C8H18 | 114.2 | 99.2 | 270.9 | 25.7 | | | |
| IPENTANE | Isopentane | C5H12 | 72.1 | 27.8 | 187.2 | 33.8 | | | A3 |
| krypton | Krypton | Kr | 83.8 | -153.4 | -63.7 | 55.3 | | | |
| MD2M | MD2M | C10H30Si4O3 | 310.7 | 194.4 | 326.3 | 11.4 | | | |
| MD3M | MD3M | C12H36Si5O4 | 384.8 | 229.9 | 355.8 | 9.6 | | | |
| MD4M | MD4M | C14H42O5Si6 | 459.0 | 259.8 | 380.1 | 8.4 | | | |
| MDM | MDM | C8H24O2Si3 | 236.5 | 152.5 | 292.2 | 14.4 | | | |
| MEA | MEA | C2H7NO | 61.1 | 170.4 | 398.3 | 81.3 | | | |
| methane | Methane | CH4 | 16.0 | -161.5 | -82.6 | 46.0 | 25 | | A3 |
| methanol | Methanol | CH4O | 32.0 | 64.5 | 240.2 | 82.2 | 2.8 | | |
| MLINOLEA | Methyl linoleate | C19H34O2 | 294.5 | 355.7 | 525.9 | 13.4 | | | |
| MLINOLEN | Methyl linolenate | C19H32O2 | 292.5 | 356.0 | 498.9 | 13.7 | | | |
| MOLEATE | Methyl oleate | C19H36O2 | 296.5 | 354.0 | 508.9 | 12.5 | | | |
| MPALMITA | Methyl palmitate | C17H34O2 | 270.5 | 329.1 | 481.9 | 13.5 | | | |
| MSTEARAT | Methyl stearate | C19H38O2 | 298.5 | 356.4 | 501.9 | 12.4 | | | |
| C1CC6 | Methylcyclohexane | C7H14 | 98.2 | 100.9 | 299.1 | 34.7 | | | |
| MM | MM | C6H18OSi2 | 162.4 | 100.5 | 245.6 | 19.3 | | | |
| MXYLENE | m-Xylene | C8H10 | 106.2 | 139.1 | 343.7 | 35.3 | | | |
| neon | Neon | Ne | 20.2 | -246.1 | -228.8 | 26.6 | | | A1 |
| NEOPENTN | Neopentane | C5H12 | 72.1 | 9.5 | 160.6 | 32.0 | | | |
| nitrogen | Nitrogen | N2 | 28.0 | -195.8 | -147.0 | 34.0 | | | A1 |
| NF3 | Nitrogen trifluoride | F3N | 71.0 | -129.0 | -39.2 | 44.6 | | | |
| N2O | Nitrous oxide | N2O | 44.0 | -88.5 | 36.4 | 72.5 | 298 | | |
| nonane | Nonane | C9H20 | 128.3 | 150.8 | 321.4 | 22.8 | | | |

**Table A.1 continued from previous page**

| Reference | Short name | Formula | $M$[g/mol] | $T_b$[°C] | $T_C$[°C] | $p_C$[bar] | GWP | ODP | Class |
|---|---|---|---|---|---|---|---|---|---|
| NOVEC649 | Novec 649, 1230 | C6F12O | 316.0 | 49.1 | 168.7 | 18.7 | | | |
| octane | Octane | C8H18 | 114.2 | 125.6 | 295.6 | 24.8 | | | |
| ORTHOHYD | Orthohydrogen | H2 | 2.0 | -252.8 | -239.9 | 13.1 | | | A3 |
| oxygen | Oxygen | O2 | 32.0 | -183.0 | -118.6 | 50.4 | | | |
| OXYLENE | o-Xylene | C8H10 | 106.2 | 144.4 | 357.1 | 37.4 | | | |
| PARAHYD | Parahydrogen | H2 | 2.0 | -252.9 | -240.2 | 12.9 | | | A3 |
| pentane | Pentane | C5H12 | 72.1 | 36.1 | 196.6 | 33.7 | | | A3 |
| C4F10 | Perfluorobutane | C4F10 | 238.0 | -2.0 | 113.2 | 23.2 | | | |
| C6F14 | Perfluorohexane | C6F14 | 338.0 | 57.1 | 174.9 | 17.4 | | | |
| C5F12 | Perfluoropentane | C5F12 | 288.0 | 29.3 | 147.9 | 20.6 | | | |
| propadiene | Propadiene | C3H4 | 40.1 | -32.3 | 124.9 | 52.2 | | | |
| propane | Propane | C3H8 | 44.1 | -42.1 | 96.7 | 42.5 | 3.3 | | A3 |
| C3CC6 | Propylcyclohexane | C9H18 | 126.2 | 156.7 | 357.7 | 28.6 | | | |
| PROPYLEN | Propylene | C3H6 | 42.1 | -47.6 | 91.1 | 45.6 | 1.8 | | A3 |
| PROPYLENEOXIDE | Propylene oxide | C3H6O | 58.1 | 34.1 | 215.0 | 54.4 | | | |
| propyne | Propyne | C3H4 | 40.1 | -23.2 | 129.2 | 56.3 | | | |
| PXYLENE | p-Xylene | C8H10 | 106.2 | 138.3 | 343.0 | 35.3 | | | |
| R11 | R11 | CCl3F | 137.4 | 23.7 | 198.0 | 44.1 | 4750 | 1 | A1 |
| R1123 | R1123 | C2HF3 | 82.0 | -59.1 | 58.6 | 45.4 | 1 | | |
| R113 | R113 | C2Cl3F3 | 187.4 | 47.6 | 214.1 | 33.9 | 6130 | 0.85 | A1 |
| R114 | R114 | C2Cl2F4 | 170.9 | 3.6 | 145.7 | 32.6 | 10000 | 0.58 | A1 |
| R115 | R115 | C2ClF5 | 154.5 | -39.2 | 80.0 | 31.3 | 7370 | 0.57 | A1 |
| R116 | R116 | C2F6 | 138.0 | -78.1 | 19.9 | 30.5 | 12200 | | A1 |
| R12 | R12 | CCl2F2 | 120.9 | -29.8 | 112.0 | 41.4 | 10900 | 0.82 | A1 |
| R1216 | R1216 | C3F6 | 150.0 | -30.3 | 85.8 | 31.5 | | | |
| R1224YDZ | R1224yd(Z) | C3HClF4 | 148.5 | 14.6 | 155.5 | 33.4 | 1 | | |
| R123 | R123 | C2HCl2F3 | 152.9 | 27.8 | 183.7 | 36.6 | 77 | 0.01 | B1 |
| R1233ZDE | R1233zd(E) | C3H2ClF3 | 130.5 | 18.3 | 166.5 | 36.2 | 1 | | A1 |
| R1234yf | R1234yf | C3F4H2 | 114.0 | -29.5 | 94.7 | 33.8 | | | A2L |
| R1234ZEE | R1234ze(E) | C3F4H2 | 114.0 | -19.0 | 109.4 | 36.3 | 6 | | A2L |
| R1234ZEZ | R1234ze(Z) | C3F4H2 | 114.0 | 9.7 | 150.1 | 35.3 | | | |
| R124 | R124 | C2HClF4 | 136.5 | -12.0 | 122.3 | 36.2 | 609 | 0.02 | A1 |
| R1243zf | R1243zf | C3H3F3 | 96.1 | -25.4 | 103.8 | 35.2 | | | |
| R125 | R125 | C2HF5 | 120.0 | -48.1 | 66.0 | 36.2 | 3500 | | A1 |
| R13 | R13 | CClF3 | 104.5 | -81.5 | 28.9 | 38.8 | 14400 | 1 | A1 |
| R1336MZZZ | R1336mzz(Z) | C4H2F6 | 164.1 | 33.5 | 171.4 | 29.0 | 2 | | A1 |
| R134a | R134a | C2H2F4 | 102.0 | -26.1 | 101.1 | 40.6 | 1430 | | A1 |
| CF3I | R13I1 | CF3I | 195.9 | -21.9 | 123.3 | 39.5 | | | |
| R14 | R14 | CF4 | 88.0 | -128.1 | -45.6 | 37.5 | 7390 | | A1 |
| R141b | R141b | C2H3Cl2F | 116.9 | 32.1 | 204.4 | 42.1 | 725 | 0.12 | |
| R142b | R142b | C2H3ClF2 | 100.5 | -9.1 | 137.1 | 40.6 | 2310 | 0.06 | A2 |
| R143a | R143a | C2H3F3 | 84.0 | -47.2 | 72.7 | 37.6 | 4470 | | A2L |
| R152a | R152a | C2H4F2 | 66.1 | -24.0 | 113.3 | 45.2 | 124 | | A2 |
| R161 | R161 | C2H5F | 48.1 | -37.5 | 102.1 | 50.5 | | | |
| R21 | R21 | CHCl2F | 102.9 | 8.9 | 178.3 | 51.8 | 151 | 0.04 | B1 |
| R218 | R218 | C3F8 | 188.0 | -36.8 | 71.9 | 26.4 | 8830 | | A1 |
| R22 | R22 | CHClF2 | 86.5 | -40.8 | 96.1 | 49.9 | 1810 | 0.04 | A1 |
| R227ea | R227ea | C3HF7 | 170.0 | -16.3 | 101.8 | 29.3 | 3220 | | A1 |
| R23 | R23 | CHF3 | 70.0 | -82.0 | 26.1 | 48.3 | 14800 | | A1 |
| R236ea | R236ea | C3H2F6 | 152.0 | 6.2 | 139.3 | 34.2 | 1410 | | |
| R236fa | R236fa | C3H2F6 | 152.0 | -1.5 | 124.9 | 32.0 | 9810 | | A1 |
| R245ca | R245ca | C3H3F5 | 134.0 | 25.3 | 174.4 | 39.4 | 726 | | |
| R245fa | R245fa | C3H3F5 | 134.0 | 15.0 | 153.9 | 36.5 | 1030 | | B1 |
| R32 | R32 | CH2F2 | 52.0 | -51.7 | 78.1 | 57.8 | 675 | | A2L |
| R365mfc | R365mfc | C4H5F5 | 148.1 | 40.2 | 186.9 | 32.7 | 794 | | |
| R40 | R40 | CH3Cl | 50.5 | -24.0 | 143.2 | 66.9 | | | B2 |
| R41 | R41 | CH3F | 34.0 | -78.3 | 44.1 | 59.0 | 107 | | |
| RC318 | RC318 | C4F8 | 200.0 | -6.0 | 115.2 | 27.8 | 10300 | | A1 |
| RE143a | RE143a | C2H3F3O | 100.0 | -23.6 | 104.8 | 36.4 | | | |
| RE245cb2 | RE245cb2 | C3H3F5O | 150.0 | 5.6 | 133.7 | 28.9 | | | |
| RE245fa2 | RE245fa2 | C3H3F5O | 150.0 | 29.3 | 171.7 | 34.3 | | | |
| RE347MCC | RE347mcc (HFE-7000) | C4H3F7O | 200.1 | 34.2 | 164.6 | 24.8 | | | |
| SO2 | Sulfur dioxide | O2S | 64.1 | -10.0 | 157.5 | 78.9 | | | B1 |
| SF6 | Sulfur hexafluoride | SF6 | 146.1 | -68.3 | 45.6 | 37.5 | | | |
| toluene | Toluene | C7H8 | 92.1 | 110.6 | 318.6 | 41.3 | 2.7 | | |
| T2BUTENE | trans-Butene | C4H8 | 56.1 | 0.9 | 155.5 | 40.3 | | | |
| C11 | Undecane | C11H24 | 156.3 | 195.8 | 365.7 | 19.9 | | | |
| VINYLCHLORIDE | Vinyl chloride | C2H3Cl | 62.5 | -13.7 | 151.8 | 55.9 | | | |
| water | Water | H2O | 18.0 | 100.0 | 373.9 | 220.6 | | | A1 |
| xenon | Xenon | Xe | 131.3 | -108.1 | 16.6 | 58.4 | | | |

# Appendix B

# Comparisons & Examples of heat pump cycles

In this appendix, extra comparisons and examples of cycles are shown.

## B.1 Standard cycle with compression completely passing through the two-phase region

A **1S-XV** cycle using a dry fluid could be set to work between two pressure levels such that the compressor discharges subcooled liquid. Such a cycle is theoretically possible and would be practically possible if a compressor can handle the compression of a vapour which condenses to liquid in the process. An example of such a cycle is given here, which uses the following inputs:

- Fluid: C12
- Sequence: CP - CD - XV - EV
- Evaporator outlet temperature: $T_{\mathrm{C},e} = 200\,^{\circ}\mathrm{C}$
- Evaporator pressure level: $p_{\mathrm{C}} = p_{\mathrm{C,sat}}\,(T = T_{\mathrm{C},e})$
- Evaporator outlet quality: $x_{\mathrm{C},e} = 100\,\%$
- Condenser outlet temperature: $T_{\mathrm{H},e} = 250\,^{\circ}\mathrm{C}$
- Condenser pressure level: $p_{\mathrm{H}} = 6\,\mathrm{bar}$
- Compressor isentropic efficiency: $\eta_{\mathrm{CP}} = 70\,\%$

All other inputs were not applicable. The T-s and p-h diagrams of this cycle are shown in Figure B.1. The performance indicators are:

- CoP = 3.968
- $\eta_{\mathrm{ex}} = 37.9\,\%$
- VHC = $0.48\,\mathrm{MJ/m^3}$
- $p_{\mathrm{C}} = 0.68\,\mathrm{bar}$
- $p_{\mathrm{H}} = 6.00\,\mathrm{bar}$
- $r_{\mathrm{com}} = 8.87\,\mathrm{bar}$
- $T_{\mathrm{dis}} = 298.1$

## B.2 Comparison of cycle configurations for extra fluids

This section shows the comparison of cycle configurations for other fluids than benzene and water, augmenting the statements made in Section 5.2.4. The fluids included here are:

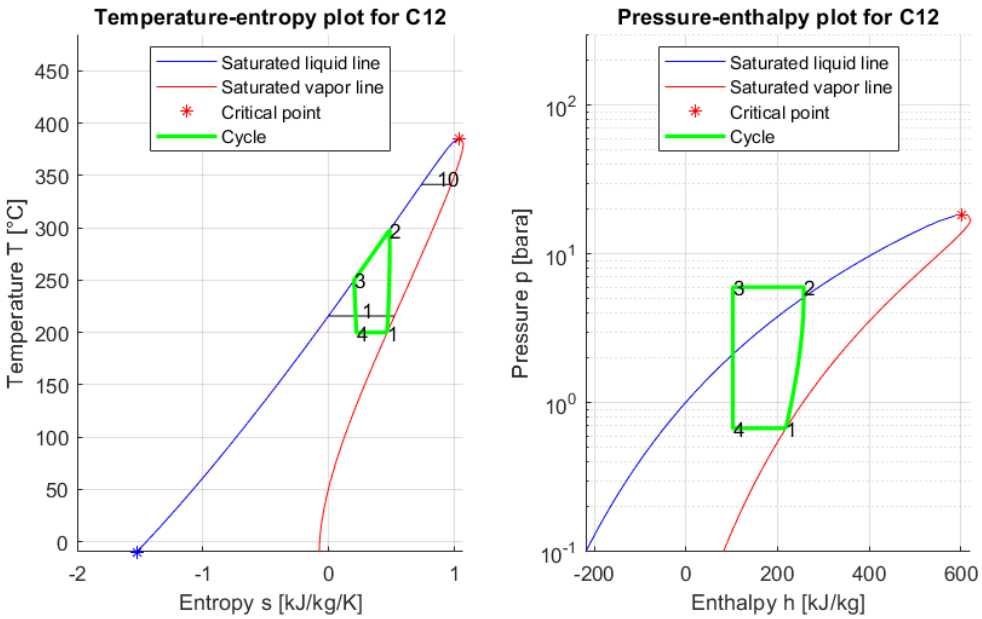


**Figure B.1:** Example of a standard cycle with compression completely passing through the two-phase region.

1. Methanol
2. Ethanol
3. Acetone
4. Cyclohex
5. Toluene
6. DMC
7. Hexane
8. C1CC6
9. Cyclopen

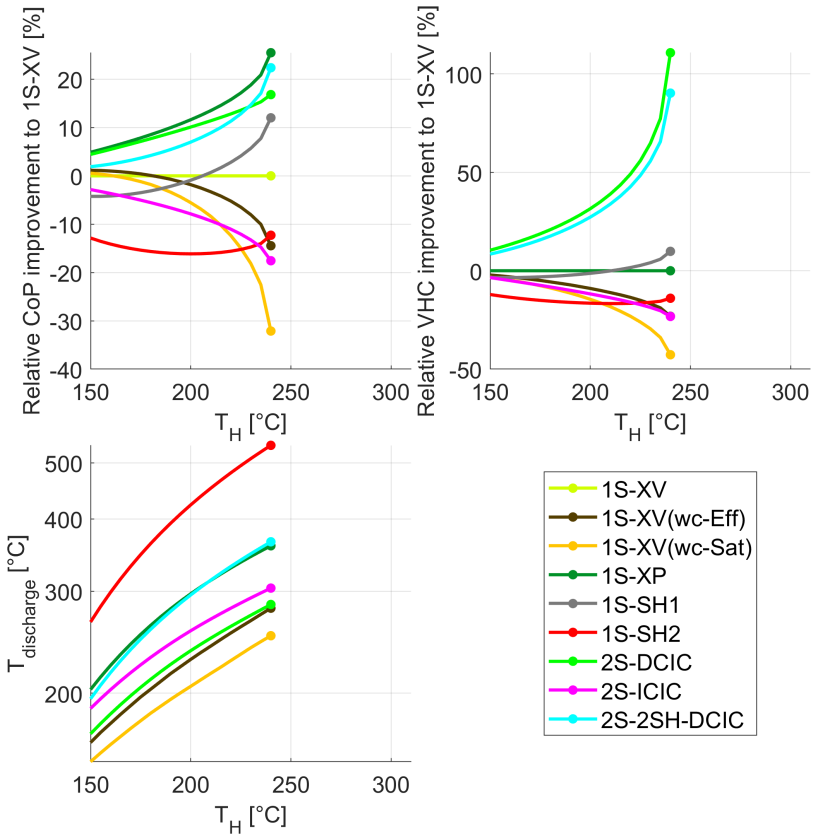


**Figure B.2:** Comparison of different cycle configurations for methanol.

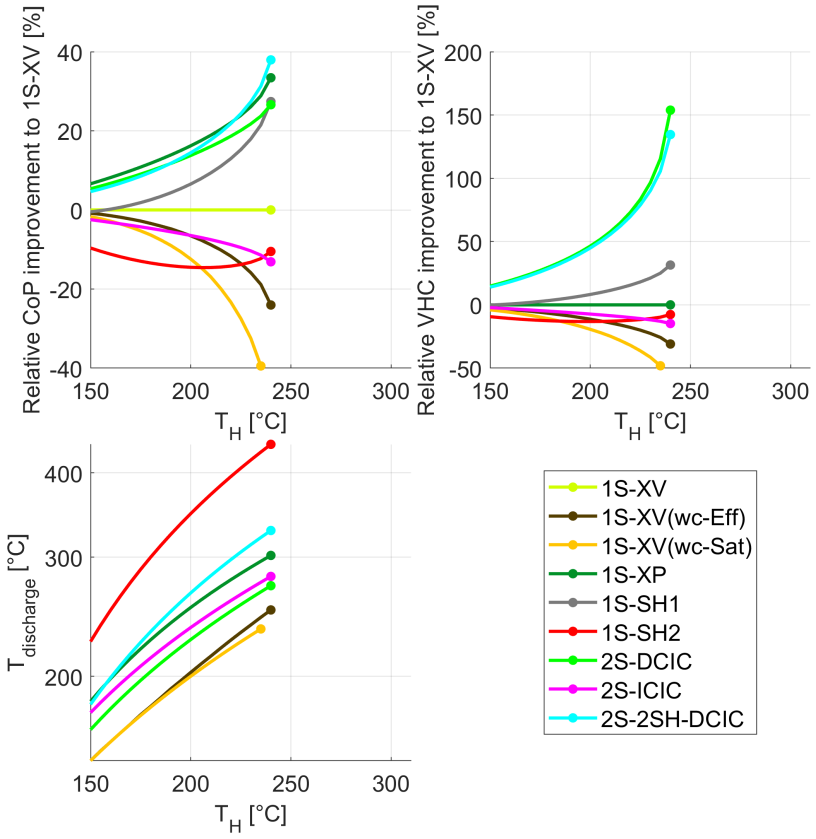


**Figure B.3:** Comparison of different cycle configurations for ethanol.

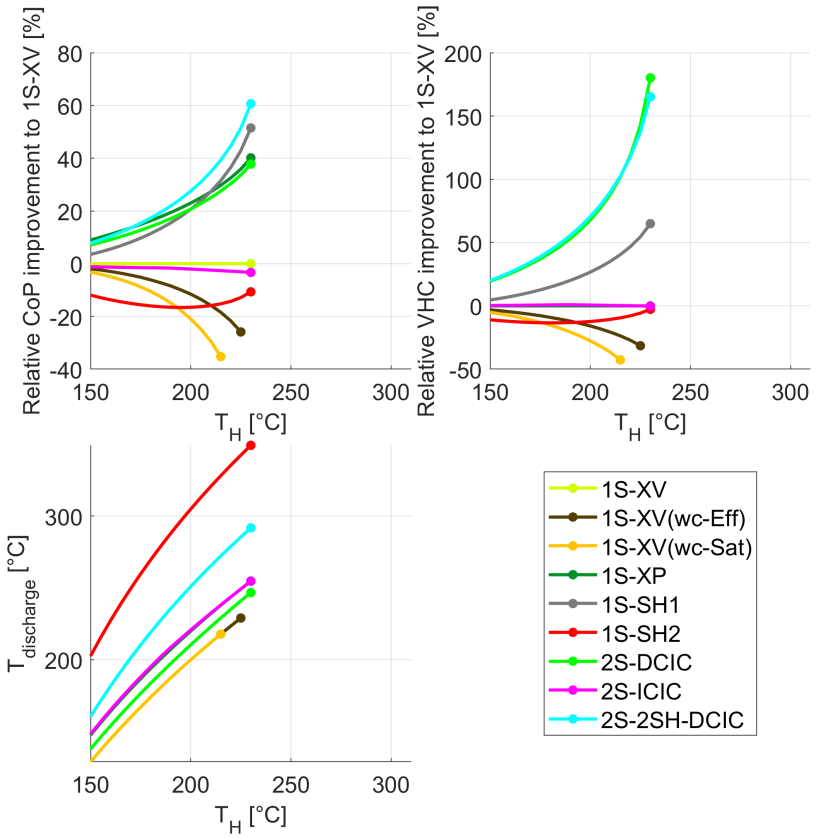


**Figure B.4:** Comparison of different cycle configurations for acetone.

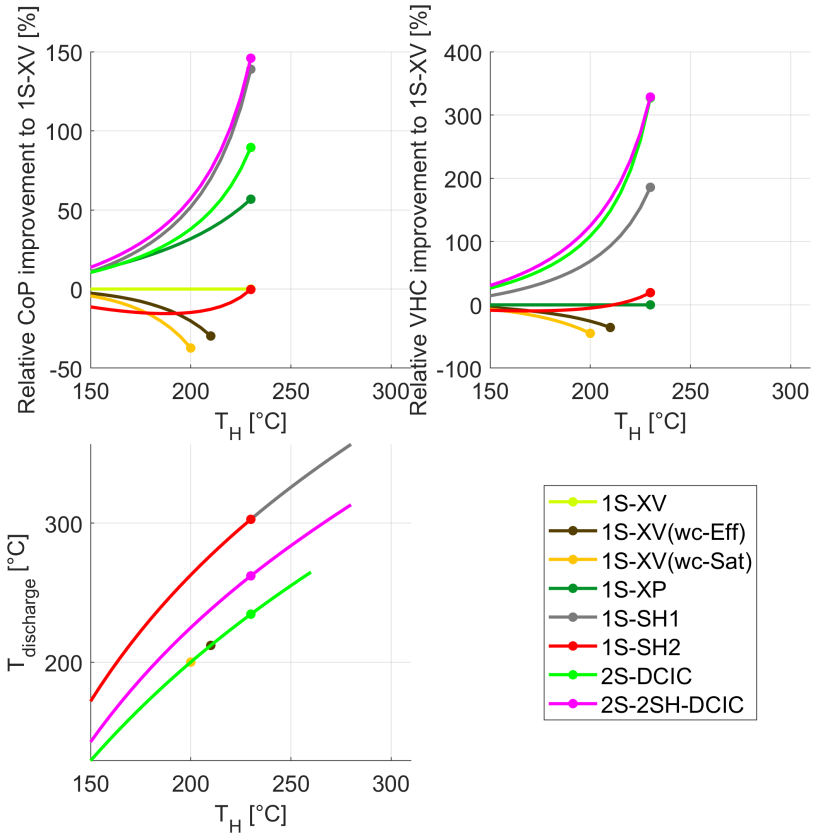


**Figure B.5:** Comparison of different cycle configurations for cyclohex.

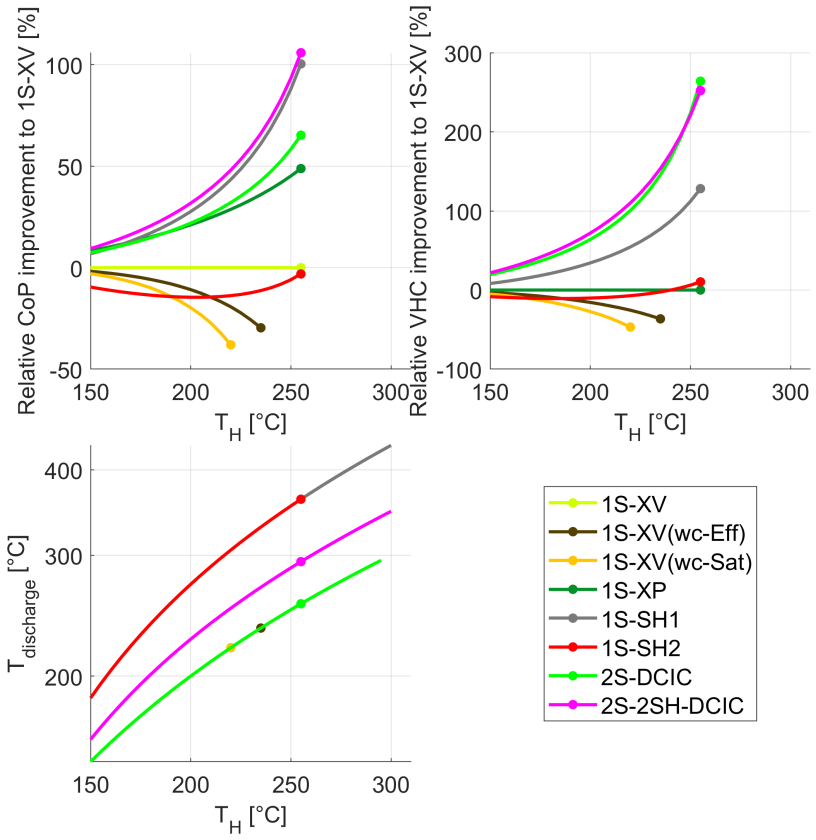


**Figure B.6:** Comparison of different cycle configurations for toluene.

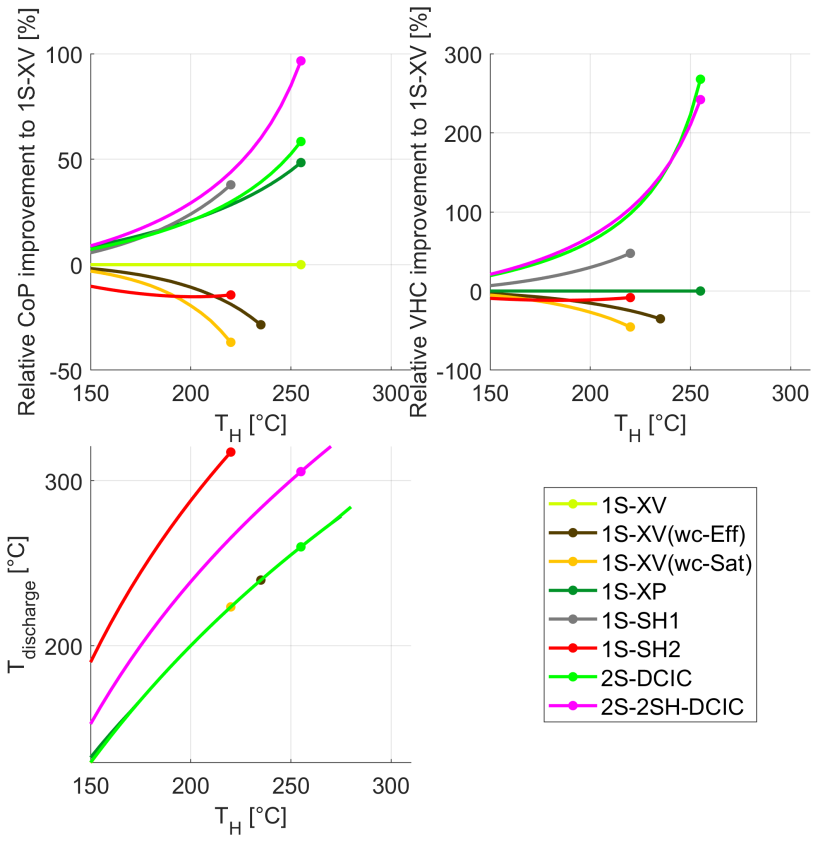


**Figure B.7:** Comparison of different cycle configurations for DMC.

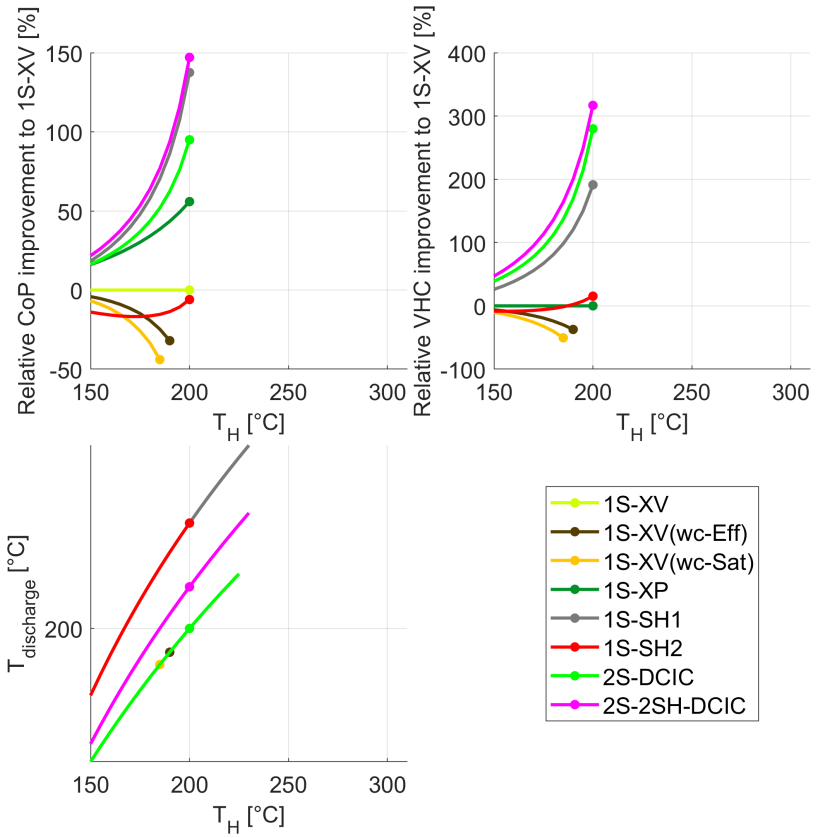


**Figure B.8:** Comparison of different cycle configurations for hexane.

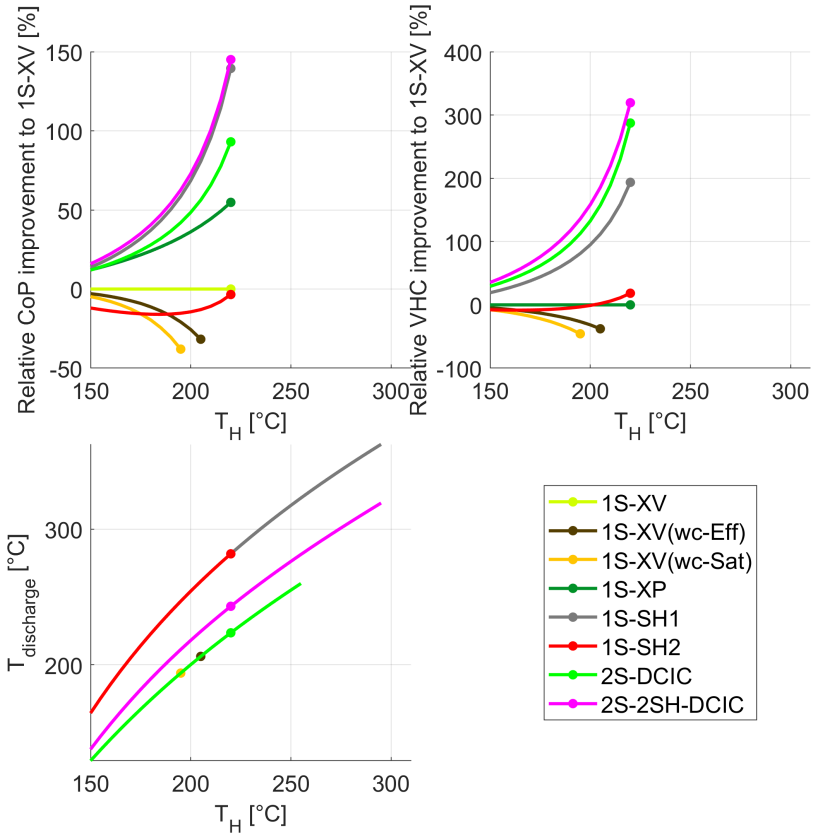


**Figure B.9:** Comparison of different cycle configurations for C1CC6.

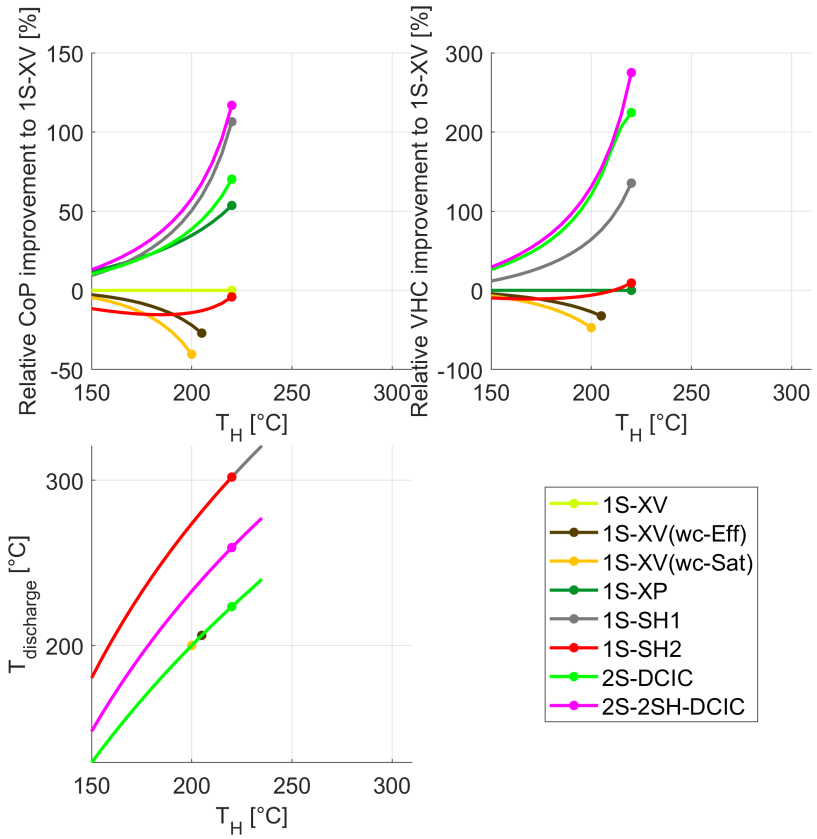


**Figure B.10:** Comparison of different cycle configurations for cyclopen.

# Appendix C

# Correlations for fit curves

In this appendix, the fit correlations and coefficients for the fit curves over the two domains are given.

## C.1 Domain 1

The fit curves in the CoP diagram of Figure 8.10 use the following relation, where $f$ represents the spray fraction:

$$CoP = \frac{p_1 f^2 + p_2 f + p_3}{q_1 f^2 + q_2 f + q_3}. \tag{C.1}$$

The constants for these fits are:

- To find the maximum CoP from the spray fraction:

| | | |
|---|---|---|
| $p_1 = 0$ | $p_2 = 0$ | $p_3 = 120.3$ |
| $q_1 = 0$ | $q_2 = 2424e + 04$ | $q_3 = 13.55$ |

- To find the CoP for which the discharge temperature will be equal to the saturation temperature:

| | | |
|---|---|---|
| $p_1 = -159.3$ | $p_2 = 2.789$ | $p_3 = 8.64e - 4$ |
| $q_1 = 0$ | $q_2 = 1$ | $q_3 = -2.071e - 05$ |

The fit curves in the discharge temperature diagram of Figure 8.10 use the following relation to obtain the temperature (in °C):

$$T_{\mathrm{CP},e} = a f^b \tag{C.2}$$

The constants for these fits are:

- To find the discharge temperature for which the CoP will be maximum:

$$a = 1e + 04 \qquad b = 0.528$$

- To find the discharge temperature from the spray fraction:

$$a = 717.5 \qquad b = 0.1855$$

The fit curves in Figure 8.11 are characterised by the following:

- The curve fit for which the CoP will be maximum:

$$f = aT_{\mathrm{H}} + b \qquad \text{with} \qquad a = 1.244e - 05 \qquad \& \qquad b = -0.001698.$$

- The curve fit for which the discharge will be saturated vapour:

$$f = aT_{\mathrm{H}}^b \qquad \text{with} \qquad a = 2.349e - 16 \qquad \& \qquad b = 5.489.$$

## C.2 Domain 2

For domain 2, the diagrams showing the CoP and $T_{\text{discharge}}$ for different spray fractions is shown in Figure C.1

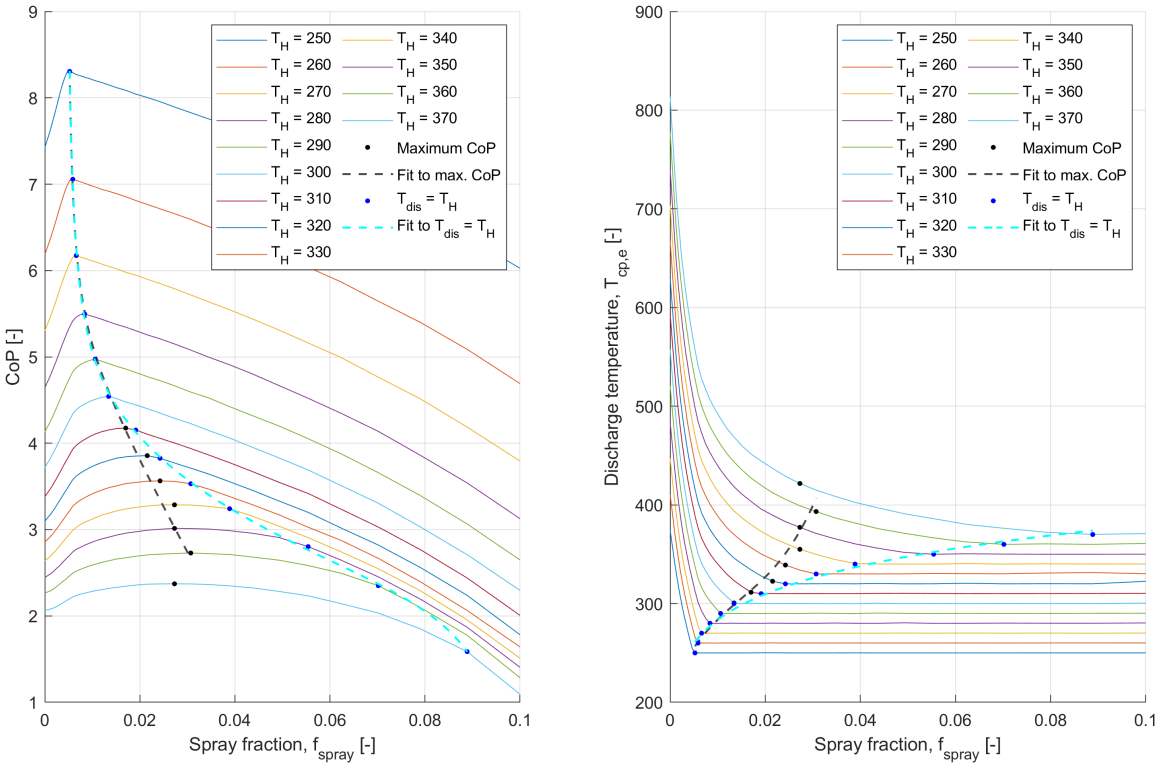


**Figure C.1:** Diagrams showing the CoP and discharge temperatures for multiple sink temperatures in domain 2 over a range of spray fractions.

The fit curves in the CoP diagram of Figure C.1 use the following relation, where $f$ represents the spray fraction:

$$CoP = \frac{p_1 f^5 + p_2 f^4 + p_3 f^3 + p_4 f^2 + p_5 f + p_6}{q_1 f^5 + q_2 f^4 + q_3 f^3 + q_4 f^2 + q_5 f + q_6}. \tag{C.3}$$

The constants for these fits are:

- To find the maximum CoP from the spray fraction:

$$\begin{array}{lllll} p_1 = 0 & p_2 = 0 & p_3 = -99.02 & p_4 = 6.012 & p_5 = -0.2073 \\ q_1 = 0 & q_2 = 0 & q_3 = 0 & q_4 = 1 & q_5 = -4.267e-3 \end{array}$$

- To find the CoP for which the discharge is saturated vapour:

$$\begin{array}{lllll} p_1 = 0.6447 & p_2 = -6.264 & p_3 = -22.91 & p_4 = -8.11 & p_5 = 1.048 \\ q_1 = 6.833 & q_2 = -34.51 & q_3 = 1.628 & q_4 = 0.2008 & q_5 = -8.117e-4 \end{array}$$

The fit curves in the discharge temperature diagram of Figure C.1 are characterised by the following relations to obtain the discharge temperature (in °C):

- To find the discharge temperature for which the CoP will be maximum:

$$\begin{array}{lll} T_{\text{CP},e} = p1 f^3 + p2 f^2 + p3 f + p4 & & \text{with:} \\ p1 = 9.425e+06 & & p2 = -4.203e+05 \\ p3 = 1.033e+04 & & p4 = 213. \end{array}$$

- To find the discharge temperature from the spray fraction:

$$T_{\text{CP},e} = a f^b \qquad \text{with:} \qquad a = 508.4 \qquad b = 0.1268.$$

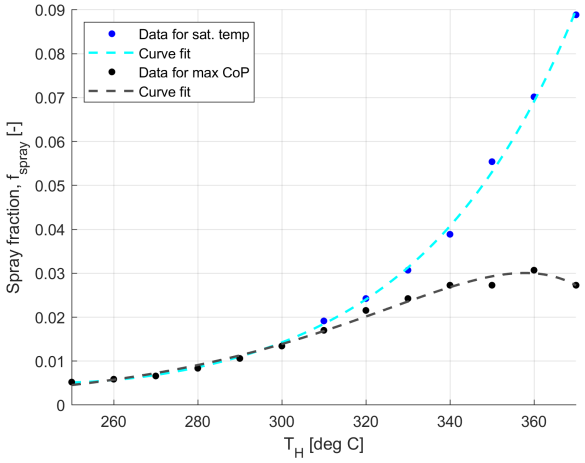


**Figure C.2:** Diagram showing the spray fractions required for the sink temperatures in domain 1 to obtain the maximum CoP and fully saturated vapour.

Figure C.2 shows the spray fractions for which the CoP is maximum and for which the discharge is fully saturated vapour over domain 2.

The fit curves in Figure C.2 are characterised by the following equation:

$$f = ae^{b*T_{\mathrm{H}}} + ce^{d*T_{\mathrm{H}}} \tag{C.4}$$

The coefficients are:

- The curve fit for which the CoP will be maximum:

$$a = -2.307e-6 \qquad b = 0.0328 \qquad c = 7.718e-6 \qquad d = 0.0297.$$

- The curve fit for which the discharge will be saturated vapour:

$$a = 2227 \qquad b = -0.05725 \qquad c = 5.142e-06 \qquad d = 0.02641.$$